Investigation of the Visco-elastic Behaviour of Watersoluble Cellulosic Derivatives in Uniaxial Elongation

Dissertation

zur Erlangung des Doktorgrades

des Fachbereiches Chemie

der Universität Hamburg

vorgelegt von

JAN PHILIP PLOG

aus Lüneburg

Hamburg 2005

Publications/ Talks

C. Clasen, J.P. Plog, W.-M.Kulicke, M. Owens, C. Macosko, L.E. Scriven, M. Verani, G.H. McKinley

"How dilute are dilute solutions in extensional flows ?"

In preparation

J.P. Plog, C. Clasen, W.-M. Kulicke

"Influence of the concentration, molar mass and molar mass distribution on the elongational behaviour of polymer solutions"

VDI Workshop "Rheology",

Dortmund, 28.02.-01.03. 2005

J.P. Plog, W.-M. Kulicke, C. Clasen

"Influence of the Molar Mass Distribution on the Elongational Behaviour of Polymer Solutions in Capillary Break-up, Case Study: Elongational Behaviour of blended Cellulose Ethers",

Applied Rheology 15 (2005), 28-37

C. Clasen, M. Verani, J.P. Plog, G.H. McKinley, W.-M. Kulicke

"Effects of Polymer Concentration and Molecular Weight on the Dynamics of viscoelastocapillary Breakup",

XIVth International Congress on Rheology (ICR 2004)

Seoul (Korea), 22.-27. 8. 2004

Proceedings of the XIVth International Congress on Rheology, RE33, p. 1-3

(electronic version)

ISBN 89-950057-5-0

M. Laschet, J.P. Plog, C. Clasen, W.-M. Kulicke

"Examination of the flow behaviour of HEC and hmHEC solutions using structure-property-relationships and rheo-optical methods",

Colloid and Polymer Science 282 (2004), 373-380

DOI 10.1007/s00396-003-0949-3

ISSN 00396-003-0949-0

C. Clasen, J.P. Plog, W.-M. Kulicke

"Rheology of water soluble cellulosic derivatives",

4th International Symposium "Materials from renewable Resources"

Erfurt, 11.-12. 9. 2003

Proceedings of the 4th International Symposium "Materials from renewable Resources", S4-16, p. 1-13 (electronic version)

Posterpresentations

J.P. Plog, C. Clasen, M. Knarr, W.-M. Kulicke

"Characterization of time- and thermogradient dependent gelation of aqueous polysaccharide solutions with rheo-mechanical and rheo-optical techniques"

XIVth International Congress on Rheology 2004 (ICR 2004)

Seoul (Korea), 22.-27. 8. 2004

Proceedings of the XIVth International Congress on Rheology, FB 19, p. 1-3

(electronic version)

ISBN 89-950057-5-0

J.P. Plog, M. Knarr, C. Clasen, W.-M. Kulicke

„Charakterisierung der Viskoelastizität und Gelbildung nativer Rohstoffe via rheo-mechanischer und rheo-optischer Methoden"

XXVI. Hamburger Makromolekulares Symposium 2003

Hamburg, 8.-9. 9. 2003

Proceedings of the XXVI. Hamburger Makromolekulares Symposium 2003, p. 42-43

ISBN 3-00-012171-4

M. Knarr, J.P. Plog, W.-M. Kulicke

„Rheo-mechanical and rheo-optical description of the solution characteristics of semi-dilute and concentrated hydrocolloid solutions"

6th European Conference on Rheology (EuroRheo 2002)

Erlangen, 1.-6. 9. 2002

Proceedings of the 6th European Conference on Rheology, p. 635-636

Zusammenfassung

Die fortlaufende Erhaltung konstanter Fließeigenschaften eines für ein spezielles Anwendungsprofil maßgeschneiderten Cellulosederivates ist eine tägliche Herausforderung der Cellulose verarbeitenden Industrie. Diese Problematik besteht, da Cellulose als nachwachsender Rohstoff bedingt durch unterschiedliche Wachstumsbedingungen und Umwelteinflüsse eine variierende Molmasse bzw. Molmassenverteilung aufweist. Um die Produkteigenschaften konstant zu halten, ist es eine übliche Vorgehensweise in der chemischen Reaktionstechnik die umzusetzende Cellulose aus verschiedenen Proben abzumischen, um den Einfluß der Molmasse bzw. der Molmassenverteilung (MMD, *molar mass distribution*) der einzelnen Cellulosechargen zu minimieren. Obwohl durch dieses Verfahren eine annähernd konstante Ruhescherviskosität η_0 gewährleistet werden kann, sind die Zusammenhänge in „realen" Fließfeldern komplexer. Dort sind durch verschiedene, dem Scherfließen überlagerte Dehnfelder Fließanomalien wie z.B. Schmelzenbruch oder Fadenzug zu beobachten, weshalb den Dehnviskositäten- und spannungen in der technischen Applikation eine besondere Bedeutung zukommt. Da Fließphänomene wie der Fadenzug oberflächenspannungsgesteuerte Prozesse sind, bei denen nur jeweils die längsten Relaxationsmoden τ_0 eines Polymers angesprochen werden, ist die genaue Kenntnis der Molmassenverteilung von gravierender Bedeutung. Bedingt dadurch, dass die längsten Relaxationsmoden eines Polymers mit zunehmender Molmassenverteilungsbreite bei konstanter gewichtsmittlerer Molmasse ansteigen, ist eine enge Verteilung für eine Optimierung des Fadenzugverhaltens zu gewährleisten. Da die absolute Bestimmung der Molmassenverteilung mittels Lichtstreuung eine sehr kosten- und arbeitsintensive polymeranalytische Methode ist, war es das Hauptziel der hier in dieser Arbeit vorgestellten Forschungsbemühungen zu untersuchen, ob die Molmassenverteilung mit den rheologischen Materialfunktionen korreliert werden kann.

Der *erste Teil* dieser Arbeit behandelt die Rheologie des Polymerstandards Polystyrol (PS) gelöst in Diethylphthalat (DEP) und Styrololigomeren. Dieses bereits in vergangenen Arbeiten gut charakterisierte Polymer [1] wurde herangezogen, um die Möglichkeiten, aber auch die experimentellen Grenzen der relativ neuen Methode des *capillary break-up* mit dem uniaxialen Dehnrheometer CaBER in Hinblick auf ihre Empfindlichkeit gegenüber der Molmasse bzw. ihrer Verteilung, der Konzentration und der Lösungsmittelgüte zu überprüfen.

Zunächst wurde die Konzentrations- und Molmassenabhängigkeit der Materialfunktionen des stationären Scherfließens (Scherviskosität η, längste Relaxationszeit τ_0 und Steigung der Fließkurve n) und der dynamischen Oszillation (G' und G'') untersucht. Um die visko-elastischen Eigenschaften dieses Polymer-Lösungsmittel-Systems quantitativ zu erfassen, wurden die Struktur-Eigenschafts-Beziehungen des Scherfließens für Polystyrol in DEP aufgestellt.

$\eta_0 - [\eta] - c$	$\eta_0 /(Pa \cdot s) = 1.10 \cdot 10^{-2} \left(c \cdot [\eta] + 0.368 \cdot c \cdot [\eta]^2 + 8.46 \cdot 10^{-3} \cdot c \cdot [\eta]^{4.82} + 1 \right)$
$\tau_0 - [\eta] - c$	$\tau_0 / s = 1.29 \cdot 10^{-10} \cdot c^{-2.423} \cdot \left(\left(c \cdot [\eta] \right)^2 + 0.368 \cdot \left(c \cdot [\eta] \right)^3 + 8.46 \cdot 10^{-3} \cdot \left(c \cdot [\eta] \right)^{5.82} \right)$
$n - [\eta] - c$	$n = -0.82 + 0.65 \cdot 10^{0.079 \cdot c[\eta]}$

Mit diesen Struktur-Eigenschafts-Beziehungen ist es möglich die Fließkurve eines beliebigen Polystyrols in DEP theoretisch als eine Funktion von Konzentration c und Staudinger Index $[\eta]$ zu berechnen. Um den Staudinger Index $[\eta]$ in die gewichtsmittlere Molmasse M_w zu überführen, wurde die bislang unbekannte Kuhn-Mark-Houwink-Sakurada Beziehung für Polymer-Lösungsmittel System bestimmt:

$$[\eta] = 8.23 \cdot 10^{-3} \cdot M_w^{0.702} \ [ml/g]$$

Für dieselben Polystyrole gelöst in DEP, wurden dann über einen weiten Konzentrationsbereich die dehnrheologischen Materialfunktionen des *capillary break-up* bestimmt. Die transienten Dehnviskosiät η_E zeigten im Newtonischen Fließbereich die nach dem Trouton-Verhältnis für uniaxiale Dehnfelder erwarteten dreifachen Wert der Ruhescherviskosität des Scherfließens η_0, im instationären Fließbereich wurden dann aufgrund der *coil-stretch-transition* Dehnviskositäten in der Größenordnung von bis zum 100-fachen von η_0 bestimmt. Die längsten Relaxationszeiten τ_0 stiegen für die verschiedenen Molmassen im untersuchten Konzentrationsbereich um zwei Größenordnungen.

Da die Konzentrationsabhängigkeit der längsten Relaxationszeit τ_0 von ultrahochverdünnten Polymerlösungen in letzter Zeit in der Literatur kontrovers diskutiert worden ist, wurden zusätzlich noch eine Reihe von Polystyrollösungen in hoher Verdünnung (Polystyrol in Styrololigomeren, sog. Bogerfluide) untersucht, da in DEP bei Konzentrationen im ppm Bereich keine sinnvollen Ergebnisse aufgrund von nicht mehr detektierbaren Relaxationszeiten erhalten wurden. Es konnte gezeigt werden, dass die längste Relaxationszeit τ_0 auch noch unterhalb einer konservativen Definition der kritischen Konzentration c^* mit sinkender Konzentration abnimmt. Diese Abnahme endet erst unterhalb einer neu definierten kritischen Konzentration für uniaxiale Dehnströmungen $c^\S$:

$$c^\S > \frac{3}{2} \frac{1}{[\eta] \cdot L^2} \zeta(3\nu)$$

Dieses ist die kleinste Konzentration, bei der sich das Polymer noch im uniaxialen Dehnströmfeld elastisch bemerkbar macht. Es konnte im Gegensatz zur aktuellen Interpretation von experimentellen CaBER-Ergebnissen durch numerische Kalkulationen gezeigt werden, dass unterhalb dieser kritischen Konzentration die längste Relaxationszeit τ_0 mit der Zimm-Relaxationszeit τ_z übereinstimmt und nicht unterhalb dieses theoretischen Wertes fällt.

Um den Einfluß der Molmassenverteilung auf das rheologische Fließverhalten zu erfassen bzw. die längste Relaxationszeit über definierte Moden der Molmassenverteilung zu bschreiben, wurden verschiedene Polystyrole definiert abgemischt, sodass die gewichtsmittlere Molmasse M_w der Abmischungen konstant $5.8 \cdot 10^6$ g/mol betrug, während sich die Molmassenverteilungen und die dazugehörigen Polydispersitäten M_w/M_n in einem Fenster von 1.0 bis 1.84 bewegten. Während Scherexperimente diese Unterschiede in der Molmassenverteilungsbreite nicht auflösen konnten, zeigten sich in der uniaxialen Dehnung gravierende Unterschiede in den längsten Relaxationszeiten für die untersuchten Polystyrolabmischungen. Die so erhaltenen Relaxationszeiten konnten, normiert über die längste Relaxationszeit der monodispersen Probe, über definierte Moden der Molmassenverteilung, das z+2-Mittel M_{z+2} und das Gewichtsmittel M_w beschrieben werden:

$$\frac{\tau_0}{\tau_{0,M}} = \left(\frac{M_{z+2}}{M_w^1}\right)^{1.22}$$

Der *zweite Teil* der Arbeit behandelt die Rheologie der Cellulosederivate Methylhydroxyethylcellulose (MHEC) und hydrophob modifizierter Hydroxyethylcellulose (hmHEC). Auch diese beiden Hydrokolloide wurden im Hinblick auf den Einfluß der Molmassenverteilung auf das Fließverhalten vollständig rheologisch charakterisiert.

Hierfür wurde zuerst die Konzentrations- sowie Molmassenabhängigkeit der Materialfunktionen des stationären Scherfließens und der dynamischen Oszillation in den Lösungsmitteln Wasser und Natronlauge (2 Gew.%) quantitativ bestimmt. Da die hier untersuchten MHECs aus verschiedenen Cellulosen abgemischt wurden, galt es auch hier vor allem den Einfluß der Molmassenverteilung auf das rheologische Fließverhalten aufzuklären. Es zeigte sich, dass die uniaxiale Dehnung die einzige Methode war, die die Unterschiede in der Molmassenverteilung quantitativ in Form von unterschiedlichen Relaxationszeiten τ erfassen konnte. Desweiteren wurde gefunden, dass das für die Polystyrole erhaltene Skalierungsgesetz zur Korrelation der unterschiedlichen Moden der Molmassenverteilung mit den längsten Relaxationszeiten auch auf die Methylhydroxyethylcellulosen übertragbar war. Die Ergebnisse der uniaxialen Dehnung konnten zudem direkt mit den zuvor mittels einer kombinierten Anlage aus SEC/MALLS/DRI (Größenausschlußchromatographie, Vielwinkellaserlichtstreuung und Differentialrefraktometer) bestimmten absoluten Molmasssenverteilungen der untersuchten MHECs korreliert werden. Zusätzlich dazu zeigte sich die uniaxiale Dehnung als wirksames Instrument zur empfindlichen Bestimmung der nicht molekular dispers gelösten Anteile der untersuchten Cellulosederivate (MHEC und hmHEC) in Lösung. Die für die unzentrifugierten Lösungen der Hydrokolloide erheblich längeren Abrisszeiten (obwohl auch diese zum großen Teil optisch transparent waren) konnten direkt mit der Wiederfindungsrate der Lichtstreuung korreliert werden.

Abstract

One of the major problems in cellulosic industry is to maintain a constant flow profile of a respective special product, tailored for a decisive application, because cellulose as a biopolymer shows a pronounced variation in its molar mass or its molar mass distribution due to varying growing conditions. To keep the product properties constant, it is common use to blend the raw cellulose, which is to be chemically converted to its final form, from different cellulose pulps. This blending results in a minimisation of the influence of the molar mass or the molar mass distributions (MMD) of the single cellulose pulp. Although this procedure ensures almost constant zero-shear rate viscosities η_0, interellations in "real" flow fields are more complex than that. In complex flow fields simple shear is superposed by different kinds of elongational stresses resulting in flow anomalies like filament formation or die swell, therefore elongational viscosities or – stresses are particularly important. As flow phenomena like filament formation are surface tension controlled processes, only the longest modes of relaxation τ_0 of a polymer are excited. Since the longest relaxation time increases with the broadness of the MMD at a constant weight-average molar mass the distribution has to be kept narrow for optimization of the filament formation behaviour. As light scattering methods are very expensive and labour-intensive, the main aim of this work is therefore to examine the possibility of a correlation of the MMD of a polymer with the rheological or better elongational material functions.

The *first part* of this work is dealing with the rheology of the polymer standard polystyrene dissolved in diethylphthalate (DEP) and styrene oligomere. This already in former works well characterized polymer [1] was consulted to record the possibilities of the relatively new method of capillary break-up with the uniaxial elongational rheometer CaBER in regards of its sensitivity to the molar mass or its distribution, concentration and quality of the solvent.

First of the concentration- and molar mass dependence of the material functions of steady shear flow (shear viscosity η, longest relaxation time τ_0 and slope of the flow curve n), and oscillatory shear (G' and G'') were investigated. To quantify the visco-elasticity of the system polystyrene (PS) in diethylphthalate (DEP) the structure-property-relationships of shear flow were established.

$\eta_0 - [\eta] - c$	$\eta_0 / (Pa \cdot s) = 1.10 \cdot 10^{-2} \left(c \cdot [\eta] + 0.368 \cdot c \cdot [\eta]^2 + 8.46 \cdot 10^{-3} \cdot c \cdot [\eta]^{4.82} + 1 \right)$
$\tau_0 - [\eta] - c$	$\tau_0 / s = 1.29 \cdot 10^{-10} \cdot c^{-2.423} \cdot \left(\left(c \cdot [\eta] \right)^2 + 0.368 \cdot \left(c \cdot [\eta] \right)^3 + 8.46 \cdot 10^{-3} \cdot \left(c \cdot [\eta] \right)^{5.82} \right)$
$n - [\eta] - c$	$n = -0.82 + 0.65 \cdot 10^{0.079 \cdot c[\eta]}$

With these structure-property-relationships one is able to describe the complete flow curve of polystyrene in diethylphthalate theoretically as a function of the concentration and the intrinsic viscosity $[\eta]$. To transfer these intrinsic viscosities $[\eta]$ to the weight-average molar mass M_w, the Kuhn-Mark-Houwink-Sakurada relationship was established via viscosimetry for this polymer-solvent-system:

$$\left[\eta\right]=8.23\cdot10^{-3}\cdot M_w^{0.702} \ [\text{ml/g}]$$

For the same polystyrenes dissolved in DEP the elongational material functions were then determined over a wide range of concentrations in capillary break-up experiments. The transient elongational viscosity η_E reflected the Trouton ratio of uniaxial elongation in the Newtonian flow regime, resulting in trice the value of the zero-shear viscosity η_0 of steady shear. In the non-Newtonian flow regime transient elongational viscosities around a hundredfold the values of η_0 were determined according to the coil-stretch-transition. The longest relaxation times τ_0 rose about to orders of magnitude for the different molar masses in the investigated concentration range. As the concentration dependence of the longest relaxation times τ_0 of ultradilute solutions was discussed rather controversely in literature recently, polystyrene Boger fluids (polystyrene in styrene oligomer) at very high dilution were also investigated, since at concentrations in the ppm regime no reasonable data could be obtained for the polystyrene solutions in DEP as the relaxation processes were not detectable anymore in capillary break-up. It could be shown that the relaxation times τ_0 show even below the most conservative definition of the critical concentration c^* a strong decrease with a decreasing concentration. This decrease of relaxation times ends below a concentration $c^\S$:

$$c^\S > \frac{3}{2}\frac{1}{\left[\eta\right]\cdot L^2}\zeta(3\nu)$$

This is the lowest concentration for an observable polymer contribution to a capillary break-up experiment. It could be shown in contrast to the current interpretation, that below this concentration the longest relaxation times τ_0 are equal to the Zimm relaxation times τ_z and do not fall below that theoretical value.

To analyse the influence of the MMD in order to describe the longest relaxation time of the polymers in uniaxial elongation via integral mean values of the molar mass distribution, defined polystyrene blends in diethylphthalate were then prepared. This was done in a fashion that the weight-average molar masses M_w were kept constant at 5.8 Mg/mol with different MMDs varying in its polydispersity indices M_w/M_n from approx. 1.0 to 1.84. Whereas the methods steady shear flow and oscillatory shear where not able to detect these differences in the MMD even qualitatively, uniaxial elongation in capillary break-up yielded different longest relaxation times τ_0 for the investigated blends. These longest relaxation times, reduced by the relaxation times of the mono disperse sample could be scaled via the z+2-average and the weight-average molar mass:

$$\frac{\tau_0}{\tau_{0,M}}=\left(\frac{M_{z+2}}{M_w^1}\right)^{1.22}$$

The *second part* of this work is dealing with the rheology of the cellulosic derivatives methylhydroxyethyl cellulose (MHEC) and hydrophobically modified hydroxyethyl cellulose (hmHEC). These two hydrocolloids were also characterized rheologically in regards to the influence of the MMD on the flow behaviour.

As for the polystyrenes, first of all the concentration- and molar mass dependence of the material functions of steady shear flow and oscillatory shear were quantified in the solvents water and aqueous 2 wt% sodium hydroxide. As the investigated MHEC samples were blended from different cellulose pulps, the influence of the MMD had to be clarified. Again only uniaxial elongation proved to be the right tool to correlate the rheological

behaviour in terms of the determined longest relaxation times τ_0. It could be shown that the scaling law determined for the polystyrene blends could be directly assigned to the here investigated commercially available, blended celluloseethers.

The results of uniaxial elongation could then be correlated directly with the absolute molar mass distributions obtained via means of SEC/MALLS/DRI (size-exclusion-chromatography, multi-angle laser light scattering and differential refractometer).

In addition to this, uniaxial elongation in capillary break-up proved to be a method allowing for a very sensitive detection of non molecularly dispersed fractions of the investigated native cellulosic derivatives (MHEC and hmHEC), because the non centrifuged sample solutions (even though they mostly appeared optically transparent) showed pronounced longer break-up times than the uncentrifuged ones.

Table of content

1 Introduction

Cellulosic derivatives, as one of the most important representatives of watersoluble biopolymers in technical application ($2.5 \cdot 10^5$ t/a production in Germany alone [2]), show a more than complex rheological flow behaviour. Since most cellulosic derivatives are watersoluble biopolymers there is a whole variety of problems that can occur in technical application, but more to that later. Despite the possibility of handling problems, cellulosic derivatives are constantly gaining in importance in a time of a globally growing energy and resource demand, especially with increasing ecological awareness of the consumer. From the about 6 billion tons of renewable resources, that is about 3 % of the annualy produced biomass, only a tiny amount is used for chemical industry [3, 4]. This *tiny amount* still makes about 10 % of the annual resource demand of chemical industry on the whole [4]. A reason for this growing interest is found not only in the almost limitless availability of cellulose itself and the biological compatibility but particularly in the large number of various cellulosic derivatives that can be synthesized to fulfil the most diverse tasks in the process of *rheological modelling* of a special product. This chemical and rheological versatility is obtained rather easily via etherification and esterification with various agents.

Cellulosic derivatives find use in a large range of technical applications [5, 6]. The most important fields at this point are building materials [5, 6] where they are used as thickening- and water retention agents in mortars and plasters, foods [7, 8] as thickening and gelation agents as well as pharmaceuticals and cosmetics [9, 10], where they are used as superabsorbing- and stabilizing agents and paints as thickening and in some cases associative thickening agents [11].

The good solubility in water, which is usually aimed for, has the disadvantage of pronounced problems arising with the molecular characterization in comparison to organic solvents. This is a result of the distinctive hydrogen-bonds (and other energetic Van der Waals interactions like Coulomb interactions) that more than often prevent the single cellulose molecules from being solved molecular dispersely. Besides the problems with dissolving the respective polymer, the characterization of the molecular structure in aqueous solvents is more than difficult. In the last few years many studies have been done on this issue [12], as well on the rheo-mechanical detectable flow behaviour in as well steady shear- as oscillatory shear fields [1, 10, 12, 13] as on the topic of rheo-optical detection of flow phenomena incorporating associating structures [14-16]. In addition to this the flow behaviour of cellulosic derivatives in elongational flows was also investigated recently [17].

For polymeranalytics, the studies published for example in this working group are as extensive, for example on NMR-spectroscopy and ultrasonic degradation to get information on how the substituents are distributed along the polymer backbone [18-20]. Like afore said the molar mass and the particle size or its distributions play a major role in technical application, so there was a quiet a lot of research invested on that issue via light scattering methods with different means of fractionation [21-24]. Another very simple and easy accessible analytical method to obtain information on the molecular structure of the single polymer coil is viscosimetry [25].

Besides the topic of the solution structure another major problem with cellulosic derivatives in comparison to synthezised polymers like polyolefines is that maintaining

constant visco-elastic properties of a respective cellulosic derivative designed for a decisive application is not a trivial task. This problem occurs since cellulose as a biopolymer naturally shows a pronounced variation in its molar mass or its MMD in dependence from origin and growing conditions of the respective sample. To circumvent this problem and maintain a constant flow profile, it is common use in cellulose processing industry to blend the raw sample, which is to be chemically converted to its final form, from different cellulose pulps. This blending results in a minimisation of the influence of the molar mass or the MMD of the single cellulose pulp, ensuring almost constant zero-shear rate viscosities η_0, independently of the respective origin and growing conditions of the employed cellulose.

Although this procedure ensures almost constant zero-shear rate viscosities η_0, interellations in *real* flow fields are far more complex than that. As in these complex flow fields simple shear is usually superposed by different kinds of elongational stresses, knowledge of the elongational viscosities or – stresses are particularly important.

As elongational induced flow phenomena like filament formation are surface tension controlled processes, only the longest mode of relaxation τ_0 of a polymer is excited. Since the longest relaxation time of a polymer increases with the broadness of the MMD at a constant weight-average molar mass, knowledge of the molar mass distribution is of great importance. As light scattering methods for determination of the absolute molar mass or its distribution are very expensive and labour-intensive, the main aim of this work is therefore to examine the possibility of a correlation of the MMD of a polymer with the rheological or better elongational material functions.

However, being the most complicated flow field to set up, it was not until recently that the first easy to handle commercial elongational rheometer for polymer solutions entered the market. With the CaBER (capillary break-up extensional rheometer) elongational rheometer the determination of a longest relaxation time as a characteristic viscoelastic parameter has recently gained much attention mainly because of the simplicity of this approach. Following the derivation of Entov and Hinch [26], the elastic thinning of a polymer solution filament in a CaBER like experiment can be described by an exponential decrease in time. The longest relaxation time τ_0 of the polymers undergoing a molecular unravelling in the uniaxial flow can then be easily determined. The validity of this approach and its consistency with other determination methods have been shown in several publications for a range of different polymers, molar masses and concentrations in dilute to semi dilute solutions [27-33]. In these cases, the exponential decay of the filament could be observed over sufficiently long times.

The capillary break-up experiment provides a convenient means for probing chain-chain interactions as a function of polymer concentration through measurements of the characteristic time-scale of the fluid in a strong extensional flow and several investigations of the transient elongational behaviour of a range of different polymers and molar masses [28, 30-33] in semi dilute to dilute solutions have been reported.

This work focuses on the one hand on a detailed investigation of the capillary break-up dynamics and relaxation times of semi-dilute to ultradilute polymer solutions. This is to be investigated via the polymer standard polystyrene dissolved in different solvents (diethylphthalate and styrene oligomer). However, in order to quantitatively analyze the dynamics of the capillary break-up process in very dilute solutions it was first of all necessary to answer the question of how much stress is carried by the polymer and how much by the solvent. In other words, under what physical conditions does a coil-stretch transition on the

molecular scale occur and affect the resulting macroscopic fluid dynamics. Since the deformation rate is not constant in these surface tension driven flows in dependence of the concentration, a satisfactory description of the occurrence of coil-stretch transition in this evolving flow field requires more than a simple definition of a critical concentration.

On the other hand, like afore said, the pronounced sensitivity of uniaxial elongation in capillary break-up is to be exploited in a fashion that the longest relaxation times obtained for the investigated polymer solutions are to be correlated with the molar mass or the molar mass distribution of the polymer. This problem specification is to be met at first via defined blends of polystyrene standards of varying molar masses dissolved in diethylphthalate. These blends are to be prepared in a way that the polydispersity M_w/M_n of the MMD varies, whereas the weight-average molar mass M_w is to be kept constant. The elongational material functions and especially the longest mode of relaxation τ_0 is then to be directly correlated with different mean values of the MMD.

After acquisition of the possibilities and the threshold conditions of the relatively new method of capillary break-up, outlined via the standard system polystyrene in DEP and styrene oligomer, it is to be investigated if the same principles can be transferred to the elongational behaviour of the celllulosic derivatives MHEC and hmHEC. In addition to this, the influence of the non-molecularly dispersed fraction of the cellulosic solutions on the elongational behaviour is to be investigated.

Polymers in solution are used in a broad range of molar masses in a multitude of applications. Ultra high molecular polyelectrolytes (polycations) are used as flocculation agents for wastewater treatment. Here, the electrostatic interactions of the polymer and the solid particles in the solution are used [34, 35]. The use of either polycations with a high molar mass or a combined use of polycations and polyanions depends on the separation problem [36]. Other polymers with high molar masses are being used for the drag reduction in aqueous solutions [1], e.g. poly(ethylene oxide) (PEO) to increase the range of fire extinguishing systems and oil-soluble vinyl copolymers or poly(isobutene) (PIB) in oil pipelines [37]. Other application areas include the use of sodium poly(acrylamide-co-acrylate) (PAAm/AAcNa) in enhanced oil recovery (polymer flooding) [38]. Even bodily biopolymers with a high molar mass, such as the hyaluronic acid in the synovial fluid of the knee joint provide, for example, the right lubrication [39, 40]. Polymers with a very low molar mass, such as poly(acrylic acids) are used as encrustation inhibitors. Other low molar mass polymers such as poly(methylmethacrylate) or styrene-isoprene- or styrene-butadiene copolymers with molar masses of $1 \cdot 10^4$-$2 \cdot 10^4$ g/mol are utilized to improve the viscosity index (VI) of motor oils [41]. Biopolymers from renewable sources find many areas of use in solution. An example is hydroxyethyl starch (HES) with a range of the molar mass of $M = 7 \cdot 10^4$-$3 \cdot 10^5$ g/mol for the use in medical applications as blood plasma expander [19, 42]. In this case, the colloid osmotic pressure of the polymer is used to propagate the flow of tissue water into the veins. Fig. 1 shows the broad range of molar masses in which polymers in solution find applications.
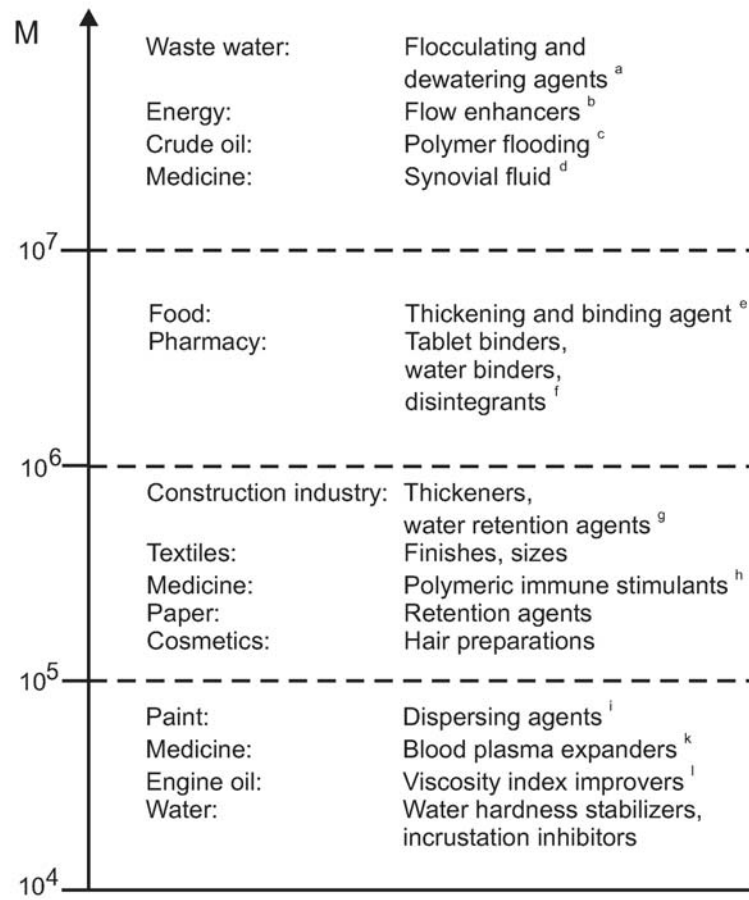
Figure 1: Application areas of polymers in regards of the molar mass.

2 Investigated Polymers

2.1 Polystyrene standards (PS)

The investigated polystyrenes are narrowly distributed standard systems, which allow for an exact correlation of the determined visco-elastic material functions with the molecular parameters such as the molar mass and the intrinsic viscosity. Polystyrene exhibits a slightly expanded coil structure and does not tend to form aggregates in the used solvents, so that it is suited very well for reproducable rheological measurements for calibration. Polystyrene was investigated in this work in the solvents toluene, diethylphthalate and styrene oligomers.

The molecular structural parameters of the investigated polystyrenes were already characterized in detail in former works in this research group [43-46]. The molecular structural parameters of our investigated polystyrenes are shown in Tab. 1.

Table 1: Intrinsic viscosities [η] and critical concentration of investigated polystyrene standards in toluene and weight average molar masses M_w with polydispersity index M_w/M_n.

Standard [+]	No.	[η] cm³/g	$c^*_{[\eta]}$ wt%	M_w Mg/mol	M_w/M_n -
0.956	1	230	$1.2 \cdot 10^{-2}$	1.0	1.00-1.05
1.8	1b	483	$5.5 \cdot 10^{-3}$	2.8	1.00-1.05
3.848	2	592	$4.3 \cdot 10^{-3}$	3.7	1.00-1.05
7.11	3	810	$3.0 \cdot 10^{-3}$	5.8	1.00-1.05
11.4	4	1124	$2.2 \cdot 10^{-3}$	9.1	1.00-1.05
13.2	5	1054	$2.3 \cdot 10^{-3}$	8.2	1.00-1.05
16.8	5b	1176	$2.1 \cdot 10^{-3}$	9.5	1.20
20.0	5c	987	$2.5 \cdot 10^{-3}$	7.5	1.20
23.6	6	822	$3.0 \cdot 10^{-3}$	5.9	1.30

[+] Molar masses provided by manufacturers in Mg/mol (see chapter 8.2 for details)

2.2 Methylhydroxyethyl cellulose (MHEC)

Methylhydroxyethyl cellulose is a mixed cellulose ether and one of the most common cellulosic derivatives that finds use in a vast field of technical applications. Synthesis is usually achieved, as for the here investigated samples, via Williamson eherification in a slurry process [47-49], leading to a structure shown schematically in Fig. 2.

With R = -CH_3 or
$-(CH_2CH_2O)_nH$
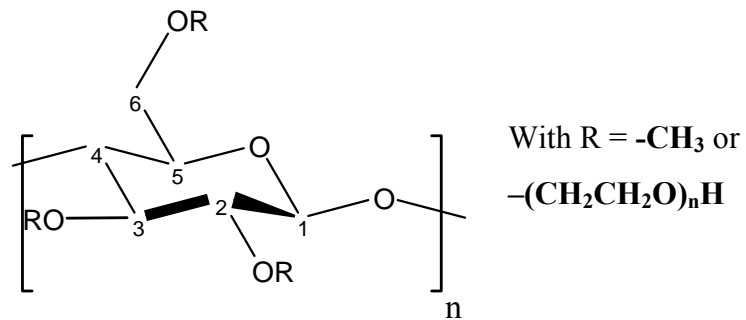
Figure 2: Anhydro glucose unit (AGU) of methylhydroxyethyl cellulose.

Multiple substitution is an important issue for cellulosic derivatives that incorporate modifications with terminal hydroxyl group, in this case a hydroxyethyl group. The *degree of substituition* (DS), that varies from 0-3 (for the three protons per AGU that can be substituted), is not a sufficient means of characterization. The so-called *molar degree of substitution* (MS) has to be taken into account, a value that incorporates multiple substitution and usually varies from 1-5 [48]. The molecular structural parameters of our MHECs are shown together with the blending composition in the Tables 2 and 3.

The main application of MHEC can be found in building industry as thickener or agent for water retention in plasters, mortars and tile adhesives, as shown schematically in Fig. 3.

Figure 3: MHEC as thickener and water retention agent in plasters.

Table 2: Blending composition, DS and MS of investigated MHECs.

MHEC	Pulp 1 1738[+]	Pulp 2 925[+]	Pulp 3 356[+]	DS	MS
1st Batch					
1	37.5	25	37.5	1.64	0.25
2	25	50	25	1.65	0.24
3	12.5	75	12.5	1.65	0.26
4	-	100	-	1.68	0.19
5	50	-	50	1.67	0.30
2nd Batch					
6	37.5	25	37.5	1.78	0.31
7	25	50	25	1.75	0.30
8	12.5	75	12.5	1.79	0.31
9	-	100	-	1.80	0.29
10	50	-	50	1.76	0.33

[+] Intrinsic viscosities of the native cellulose samples (provided by manufacturer)

Table 3: Molecular structural parameters of the investigated MHECs 1-10.

MHEC	$[\eta]$ cm^3/g	$c^*_{[\eta]}$ wt%	M_w Kg/mol	M_w/M_n	c^*_{LS} wt.%	Recovery Rate wt%	R_G nm
1st batch							
1	853	0.29	327	2.3	0.0069	94	85
2	926	0.27	335	2.6	0.0079	98	82
3	790	0.32	307	2.3	0.0095	99	75
4	947	0.26	297	2.1	0.01	99	71
5	876	0.29	360	2.9	0.006	92	91
2nd batch							
6	691	0.36	323	2.9	0.0051	79	83
7	547	0.46	294	2.5	0.0087	70	72
8	689	0.36	298	2.7	0.0093	87	75
9	676	0.37	299	2.3	0.01	87	76
10	604	0.41	341	3.5	0.0059	74	90

2.3 Hydrophobically modified hydroxyethyl cellulose (hmHEC)

Hydrophobically modified hydroxyethyl cellulose (hmHEC) is a cellulosic derivative, that is used as an associative thickener agent [50, 51], mainly in water soluble paints. Another field of application is drag reduction. The anhydro glucose unit (AGU) of hmHEC is shown in Fig. 4.
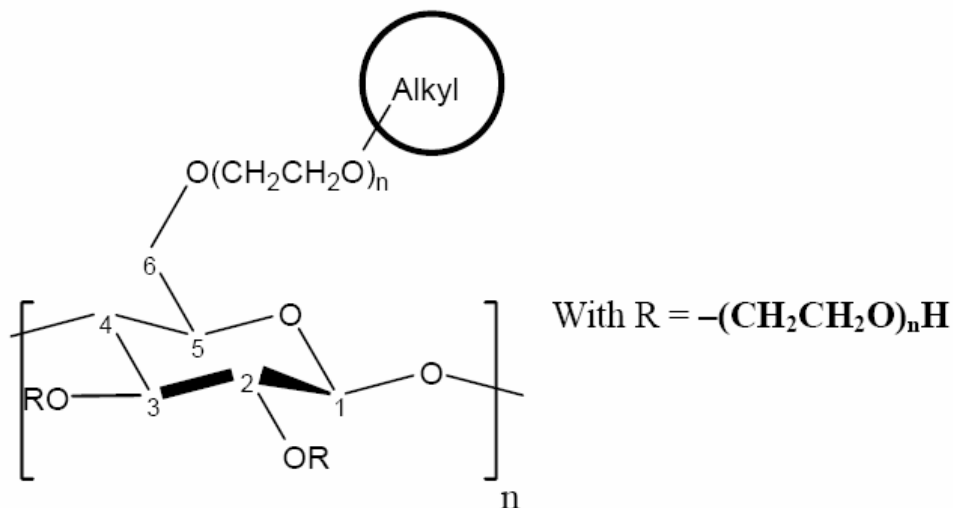
Figure 4: Anhydro glucose unit (AGU) of hmHEC.

The alkyl substituent, highlighted with the circle in Fig. 4 (with approx. 10 to 24 C-atoms), is introduced via Williamson etherification into the cellulosic backbone [52]. Because of steric hindrance, the alkylhalogenide substitutes only the proton of the hydroxyethyl group in position 6. The degree of substitution (DS) is around 0.02-0.04 for the most typical, commercially availabel hmHECs, which means that only every 50th-25th AGU carries a hydrophobic modification. The molecular structural parameters of our investigated hmHECs are shown in Table 4.

Figure 5: To scale (in regards of hydrophobic sidechains compared to the backbone of the polymer) schematic depiction of a hmHEC coil.

However, this tiny amount of hydrophobic sidechains (see Fig. 5 for a to scale schematic depiction of a hmHEC coil) enables the polymer to show a pronounced shear thickening behaviour, especially when surfactants are added to the solution, that support the build-up of micellar structures together with the hydrophobic sidechains (see Fig. 6). The water soluability of this polymer is decreasing with increasing DS and lenght of the hydrophobic modification [14].
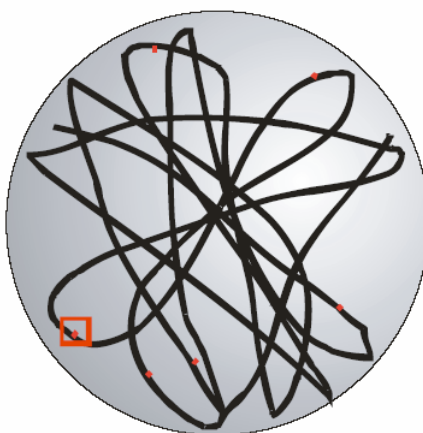
The effect of associative thickening derives from the transition from intra- to inter-molecular micellar structures (see Fig. 6). The hydrophobic modifications form intramolecular micelles under equilibrium conditions. These intra-molecular micelles are degraded in shear flow, so that the hydrophobic chains are free to form inter-moelcular micelles [14] that lead to shear thickening behaviour. This explicit behaviour, which is referred to as dilatancy is shown experimentally in chapter 6.2.1.
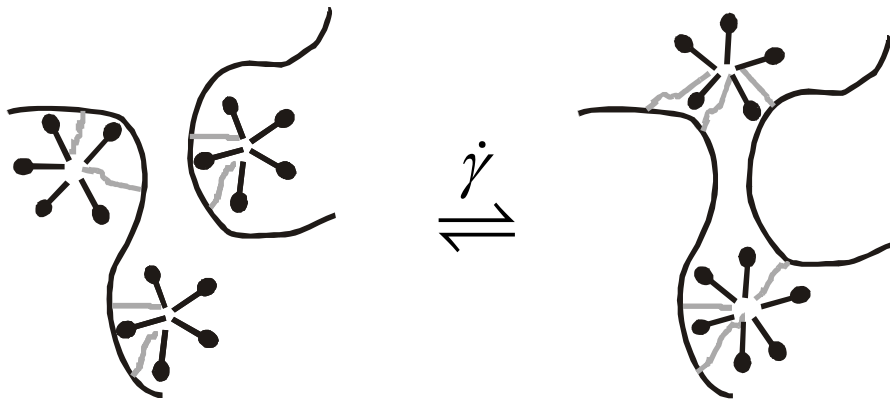
Figure 6: Shear induced transition from intra- to intermolecular micellar structures formed by the hydrophobic sidechains of hmHEC together with surfactants.

Table 4: Molecular structural parameters of the investigated hmHECs 1 and 2.

Sample	$[\eta]$ cm^3/g	$c^*_{[\eta]}$ wt%	M_w Kg/mol	M_w/M_n	c^*_{LS} wt%	Recovery Rate wt%	R_G nm
hmHEC 1	712	0.35	277	2.6	0.042	45	68
hmHEC 2	403	0.62	262	1.3	0.040	47	56

3 Polymeranalytical Methods

3.1 Viscosimetry

Viscosimetry is one of the basic analytical methods for examining the structure and the properties of polymer fluids. Many different polymers from varying production processes are utilized in solution in diverse applications. Furthermore, it is possible, by varying the molar mass of one and the same polymer system, to specifically tailor the properties of the polymer to the area of use. Polymers are chain- or thread-shaped molecules that take on a coil-like structure in dilute solutions. Even though the molecule continuously changes its form under the influence of statistic thermodynamic movement, it fills out a constant spherical space in solution over a time average. In principle, a molecule can also take the shape of compact aggregated spherical particles (glycogen, globular proteins), or in the case of ionic polymers take on a linear rod-like structure, since through the same charges on the chain repelling forces are in effect.

Theoretical approaches to determine solution structures of neutral polymers act on the assumption of the pseudo ideal state. Here the solvation forces from the solvent and the aggregation forces of the chain segments are in an equilibrium where the coil appears to be unaffected by forces. This pseudo ideal state is called the theta state. Theta conditions exist when the exponent a of the $[\eta]$-M-relationship has the value $a = 0.5$, for sufficiently long chains to show long range interactions, and even more important at the same time the value of the second virial coefficient is $A_2 = 0$. Accordingly, a pseudo ideal solvent is called theta solvent and the corresponding temperature is called theta temperature. As Flory showed in his Nobel price lecture [53], the theta state can be described mathematically exactly from the chemical structure of the chain.

Real polymer solutions mostly do not occur in the theta state. Both, the undisturbed dimensions of the polymer coils and other thermodynamical states of the coil can be experimentally determined with the help of viscosimetry.

For all polymer solutions a characterization of the molar mass and the flow properties has to be made in order to tailor the properties to the area of use as shown in Fig. 1. Practically the determination of the molar mass and the solution structure is done using viscosimetry. The solution structure, or to be more precise, the solution conformation of a polymer is the constant volume requirement of the coiled thread-like molecule over the time average. The description of the dimensions of the coil is made in practice by using the intrinsic viscosity $[\eta]$ that represents a measure for the effective experimentally observed density of the thread-like molecule in solution. Within a theta solvent, the polymer thread can be viewed as infinitely thin for all practical reasons (see Fig. 7).
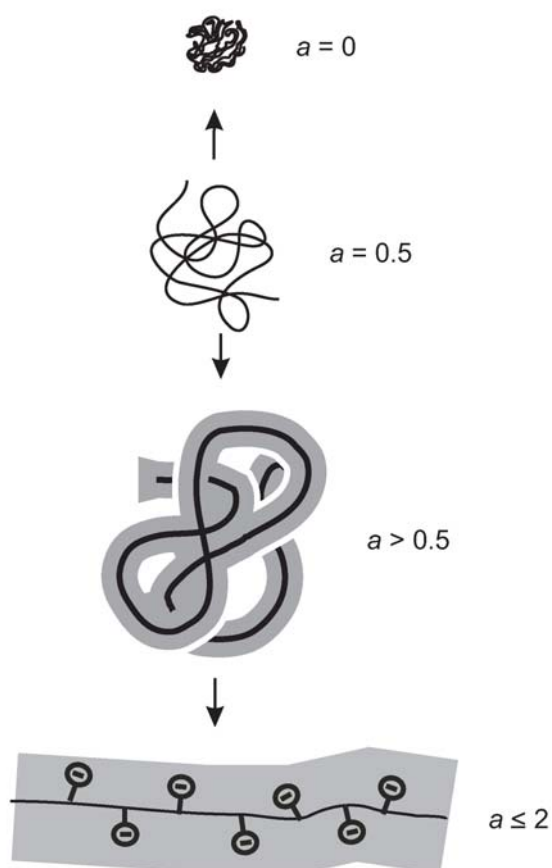
Figure 7: Influence of the coil shape on the exponent a of the [η]-M-relationship.

In a so-called "good" solvent the hydrodynamic interactions around the polymer chain increases, the thread appears to become thicker, and the volume requirement increases (see Fig. 7). The volume requirement also increases with an increasing molar mass and the accompanying elongation of the polymer chain. The effect of this increased volume requirement on the flow behavior of the solution can be measured directly using viscosimetry.

Since the viscosity of a polymer solution is not only dependent on the molar mass, but also on the concentration, the solvent, the type and composition of the polymer solution fraction, the temperature and the pressure. The measurement of the viscosity therefore is not only for the practical and simple determination of a single product trait. Besides a simple single-point measurement and the quality control, viscosimetry allows for a much deeper insight into the flow properties of a polymer solution. The increase of the internal friction of a solution (the "viscosity") can be described using well-defined laws of physics by assuming the polymer to require a volume fraction of the solution, depending on the molecular dimensions of the single coil, the rigidity of the chain, the intermolecular interactions of the polymer coils. Furthermore, direct information about the solution structure can be obtained using an [η]-M-relationship (Kuhn-Mark-Houwink-Sakurada-relationship).

For practical reasons, it is especially relevant to be able to directly determine the molar mass M of a polymer from the [η]-M-relationship using only simple viscosimetry. But often it is enough to be able to perform a single-point measurement with viscosimetry in order to

verify the product properties for the daily incoming and outgoing goods control. Relevant application areas are listed in Fig. 1.

The viscosity enhancing properties of a polymer coil due to an increasing internal friction caused by assumed spherical shaped, rigid particles (that the coils can be represented by as suggested by Einstein) can be described via a Taylor-series:

$$\eta_{sp} = B_1 \cdot \phi + B_2 \cdot \phi^2 + B_3 \cdot \phi^3 + ... \qquad \text{(Eq. 1)}$$

Here the fraction of the polymer in solution is given by the volume fraction ϕ:

$$\phi = \frac{V_{\text{polymer}}}{V_{\text{solution}}} \qquad \text{(Eq. 2)}$$

Fortunately, all higher powers in Eq. 1 can be disregarded for an ideal state of dilution! According to Einstein, the polymer coils are assumed to be perfectly inelastic and behave like hard spheres. Therefore, the following simple (and experimentally confirmed) relationship is obtained:

$$\eta_{sp} = 2.5 \cdot \phi \qquad \text{(Eq. 3)}$$

The volume of the polymer coils V_{polymer} can be described via the ratio of the mass m_{polymer} of the polymer to its density ρ_{equ}. This density ρ_{equ} does not correspond to the density in the dry state, but with the density of the polymer in solution, where solvent molecules surround the polymer chain.

$$\phi = \frac{V_{\text{polymer}}}{V_{\text{solution}}} = \frac{\left(\dfrac{m_{\text{polymer}}}{\rho_{\text{equ}}}\right)}{V_{\text{solution}}} = \frac{c}{\rho_{\text{equ}}} \qquad \text{(Eq. 4)}$$

With this, the specific viscosity for a truly dilute solution is:

$$\eta_{sp} = 2.5 \cdot \frac{c}{\rho_{\text{equ}}} \qquad \text{(Eq. 5)}$$

Therefore the specific viscosity depends not only on the concentration but also on the density in solution and therefore on the molecular dimensions in solution according to Eq. 5. In order to obtain the true viscosity enhancing properties of a specific polymer, the reduced viscosity η_{red} is introduced:

$$\eta_{\text{red}} = \frac{\eta_{sp}}{c} = \frac{2.5}{\rho_{\text{equ}}} \qquad \text{(Eq. 6)}$$

This reduced viscosity only depends on the density in solution and the concentration. The concentration dependence of the reduced viscosity is given by folllwing term:

$$\eta_{\text{red}} = \frac{\eta_{sp}}{c} = [\eta] + B_2 \cdot [\eta]^2 \cdot c \qquad \text{(Eq. 7)}$$

The unit of the reduced viscosity is defined via the used concentration unit, which is usually [g ml^{-1}] for viscosimetric measurements. With this, the unit for the reduced viscosity is [ml g^{-1}].

However, also the reduced viscosity is not independent of the concentration if we lwave the truly dilute state. Even though viscosimetric measurements are performed below the critical concentration c^*, where the single polymer coils start to interpenetrate, the truly dilute state is roughly reached at $c^*/100$ and therefore below the experimental range of visossimetric measurements and small polymer interactions (that are decreasing with a decreasing concentration) have to be considered. The true viscosity enhancing properties of a polymer is therefore the reduced viscosity extrapolated to c→0:

$$[\eta] = \lim_{\substack{c \to 0 \\ \dot{\gamma} \to 0}} \eta_{\text{red}}$$

(Eq. 8)

According to the IUPAC nomenclature, the intrinsic viscosity should be named limiting viscosity number but this denomination is not widely used yet. As shown in Eq. 8, another condition for the determination of the intrinsic viscosity is that the shear rate has to be $\dot{\gamma} \to 0$.

The intrinsic viscosity $[\eta]$ has the same unit, $[\text{ml g}^{-1}]$, as the reduced viscosity η_{red}. For a better understanding, the intrinsic viscosity can be considered as a measure for the volume demand of the single polymer coil in ideally diluted solution. The intrinsic viscosity is proportional to the reciprocal density of the polymer coil in solution according to Eq. 5 and 6 and therefore directly related to the polymer dimensions.

Determination of the intrinsic viscosity can then be achieved by incorporating the first higher order term of Eq. 1 leading to Eq.7 for the reduced viscosity. Substitution of B_2 in Eq.7 leads to the Huggins virial equation [54], which yields the intrinsic viscosity via extrapolation of the reduced viscosity to zero:

$$\frac{\eta_{sp}}{c} = [\eta] + K_H [\eta]^2 c$$

(Eq. 9)

The slope $K_H [\eta]^2$ can be directly correlated with the second virial coefficient A_2, describing the intermolecular interactions between polymer and solvent.

The intrinsic viscosity $[\eta]$ represents the most relevant variable to describe the viscous behavior of a polymer solution and most viscosimetric measurements have the aim of its determination.

The knowledge of the dimensions of a single polymer coil allows for the calculation of the solution volume filled with polymer. A matter of particular interest is the polymer concentration where the solution is completely filled with polymer coils and the coils start to interpenetrate as shown in Fig. 8. The intrinsic viscosities and the resulting critical concentrations of the investigated polymers are listed in Tables 1-4.
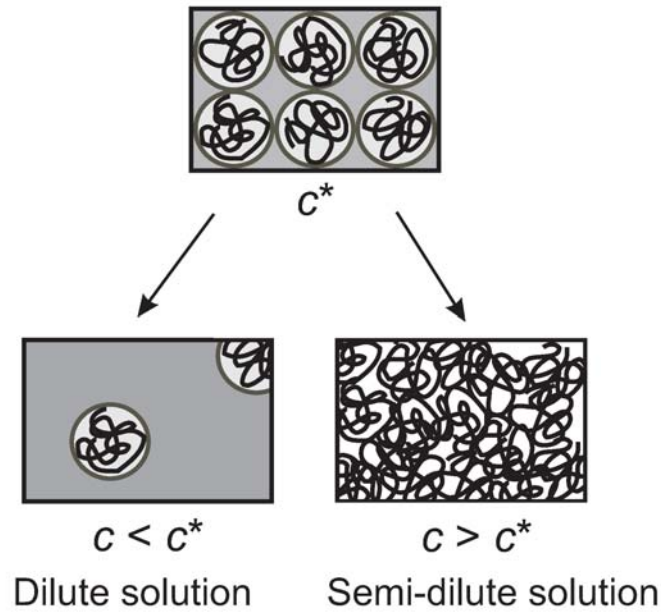
Figure 8: Definition of the critical concentration c*.

This concentration is denoted as the critical concentration c^*. The critical concentration marks the transition from a dilute to a semi-concentrated solution. This transition is accompanied by great changes in the flow properties of a polymer solution. At concentrations above c^* the flow behavior is dominated by the intermolecular interactions of the polymer coils whereas below c^* mainly the polymer-solvent interactions determine the flow properties. Nearly all technical applications of polymer solutions require concentrations equal to or above c^*. For example, the blood plasma volume expander hydroxyethyl starch (HES) is used at the critical concentration to obtain a maximum polymer concentration without a superproportional increase of the viscosity.

The critical concentration is reached for a volume fraction ϕ of the polymer of one. In this case, Eq. 3 yields:

$$V_{solution} = V_{polymer} = \frac{m_{polymer}}{\rho_{equ}}$$

(Eq. 10)

With Eq. 5 the critical concentration of the viscosimetry $c^*_{[\eta]}$ is obtained:

$$c^*_{[\eta]} = \frac{m_{polymer}}{V_{solution}} = \rho_{equ} = \frac{2.5}{[\eta]}$$

(Eq. 11)

Therefore the critical concentration $c^*_{[\eta]}$ is proportional to the reciprocal intrinsic viscosity. The factor of 2.5 assumes that the polymer coils behave like hard spheres in solution. Viscosimetric measurements for the determination of the intrinsic viscosity have to be performed in dilute solutions at concentrations clearly below c^* to assure that terms of $(O)^2$ and higher in Eq. 1 can be neglected.

The intrinsic viscosity $[\eta]$ of a polymer in a certain solvent can also be empirically correlated with the molar mass M:

$$[\eta] = K_{[\eta]} \cdot M^a \qquad\qquad\qquad\qquad\qquad\qquad\qquad\text{(Eq. 12)}$$

In the literature, this dependence is referred to as the *[η]-M-relationship* or the *Kuhn-Mark-Houwink-Sakurada-relationship* (KMHS-relationship). $K_{[\eta]}$ and *a* are constant for a given solvent and temperature.

The exponent *a* is a measure for the solvent quality and therefore for the solution structure of the dissolved polymer. The knowledge of $K_{[\eta]}$ and *a* allows for an easy determination of the molar mass of a polymer by measuring the intrinsic viscosity. The determination of the molar mass from Eq. 12 yields the viscosity average molar mass M_η. The values of M_η lie between the number average molar mass M_n and the weight average molar mass M_w (see Fig. 9). The parameters of K and *a* can be obtained from molecular theory for the limiting cases of theta or good solvents as shown in chapter 4.1. However, the exact determination of these parameters for a given polymer-solvent-system requires viscosimetry.

3.2 Determination of the molar mass and the molar mass distribution

The solution structure and the visco-elastic properties of polymers in solution are mainly dominated by the molar mass and the molar mass distribution. Particularly the formation of entanglements between the single polymer coils that occur above a critical molar mass has a great influence on the flow- and visco-elastic properties of a polymer solution (see chapter 4.4.1 and 4.4.2).

Cellulosic derivatives that are of native origin do not show a uniform degree of polymerization but a distribution in its molar mass. Subject to where the origin of the resource is and how the climatic backround is, the molar mass and its distribution vary. However, one has to keep in mind that the molar mass distribution is not symmetric but usually asymmetric because of the influencing parameters listed above. A typical distribution for native cellulose derivatives is shown in Fig. 9 [25].
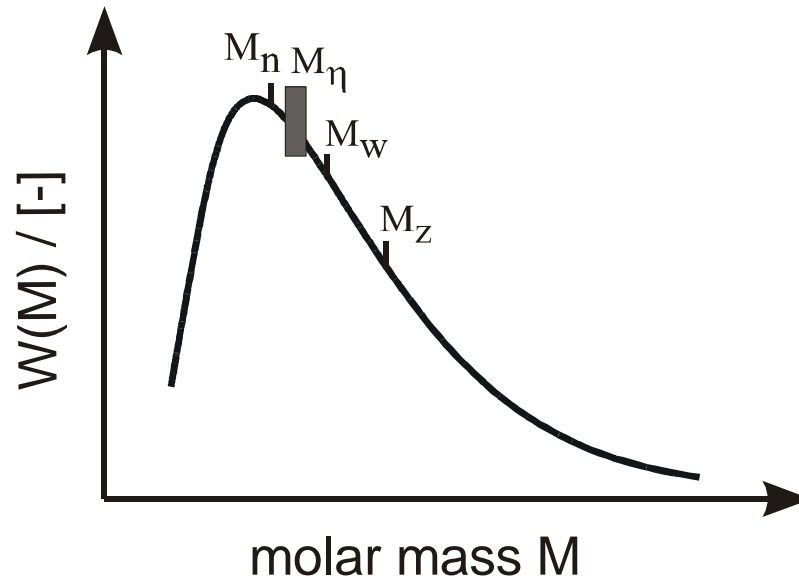
Figure 9: Schematic depiction of the molar mass distribution of a native cellulose derivative with the mean moments of the distribution M_n, $M_{[\eta]}$, M_w und M_z.

The exact determination of the absolute distribution of the molar mass is experimentally very complicated to achieve, so that usually different mean values of the molar mass distribution are consulted to characterize a polymer

The most commonly used mean values of the molar mass distribution are the number-average molar mass M_n ($\beta = 0$), weight-average molar mass M_w ($\beta = 1$) and the centrifuge-average molar mass M_z ($\beta = 2$). The exact definitions of these modes are given in Eq. 13.

$$M_x = \frac{\sum_i n_i \cdot M_i^{\beta+1}}{\sum_i n_i \cdot M_i^{\beta}}$$

(Eq. 13)

Another mean value is the viscosity-average molar $M_{[\eta]}$ which is accesible via viscosimetric measurements. It can be calculated according to Eq. 14. For allmost every polymer, $M_{[\eta]}$ is an intermediate value between M_n and M_w.

$$M_{[\eta]} = \left(\frac{\sum_i n_i \cdot M_i^{1+a}}{\sum_i n_i \cdot M_i} \right)^{\frac{1}{a}}$$

(Eq. 14)

The ratio of M_w and M_n, M_w / M_n is a measure for the width of the distribution and is called the polydispersity.

However, often the degree of polymerization P is given instead of the molar mass of a polymer. It can be directly related to the molar mass of the single repeating unit. In Table 5 the different mean values of the molar mass are summarized together with the corresponding analytical method of determination.

Table 5: Different mean values of the molar mass and the corresponding analytical method for determination.

	Method	Mean Value
Relative	*Viscosimetry*	$M_{[\eta]}$
	Size-Exclusion-Chromatography (SEC)	M_{SEC}
Absolute	*Osmosis*	M_n
	Light-Scattering	M_w
	Ultracentrifugation	M_z

The relative methods for determination of the molar mass still need some kind of calibration with a substance of known chemical structure and molar mass. Viscosimetry belongs to the relative methods and was discussed in detail in chapter 3.1. Another relative method is the size-exclusion chromatography which will be discussed in detail in the following section. The advantage of the so called absolute methods is that no information on the chemical and physical structure is needed to determine the molar mass. Examples for these absolute methods are the membrane osmosis, ultracentrifugation and light scattering [55].

3.2.1   Light Scattering

Elastic light scattering is divided into Rayleigh-, Debye- and Mie-scattering in dependence on the size of the interacting particle. For Rayleigh-scattering the interacting particle can be understood as a uniform scattering center with an isotropic scattered light distribution [56]. From a particle size on that is one twentieth of the wavelenght λ of the used lightsource ($d \geq \lambda / 20$) the scattering centres within the molecule dissapear and the intensity of the scattered light decreases with increasing scattering angle. The single molecule can not be understood as a single scattering center anymore which is referred to as Debye-scattering [57]. Is the particle size in the range of the wavelenght of the used light, not only destructive- but also constructive interference between the scattering centers is the result. The scattered light distribution shows maxima and minima around the scattering center. Mie showed for the first time that even this problem could be solved for spherical particles [58].

In the area of validity of the Rayleigh and Debye approximation Eq. 15 is the central equation for analysis of the light scattering measurements.

$$\frac{K \cdot c}{R_\vartheta} = \frac{1}{M_w \cdot P_\vartheta}$$

(Eq. 15)

with

$$K = \frac{4 \cdot \pi^2 \cdot n_0^2}{N_A \cdot \lambda_0^4} \left(\frac{\delta n}{\delta c} \right)_{p,T,\lambda}^2$$

(Eq. 16)

and

$$R_\vartheta = \frac{I_\vartheta}{I_0} \cdot \frac{h^2}{V_S}$$

(Eq. 17)

The intensity of the scattered light I_ϑ is refered to as the reduced variable R_ϑ, that is standardized on the intensity of the primary light beam I_0 and the distance h of the detector from the scattering volume V_S. The scattering function P_ϑ gives the dependence of the intensity of the scattered light from the scattering angle ϑ and the radius of gyration R_G.

The scattering function can be described independently of the geometry of the particles via a virial function. In this case analysis of the light scattering experiment is carried out via the following equation that gives the weight-average molar mass via the ordinate interception and the radius of gyration R_G via the slope

$$\frac{K \cdot c}{R_\vartheta} = \frac{1}{M_w} + \frac{16 \cdot \pi^2 \cdot n_0^2}{3 \cdot M \cdot \lambda_0^2} \cdot R_G^2 \cdot \sin^2 \left(\frac{\vartheta}{2} \right) + ...$$

(Eq. 18)

3.2.2   Size Exclusion Chromatography (SEC)

To determine the absolute distribution of the molar mass of a polymer, fractionation of the sample in single slices with monodispersely distributed molar mass is essential. In the last years size-exclusion chromatography (SEC) was established as a powerful tool of fractionation of polymer samples.

Advantages of this method are the very small amounts of sample needed (mg-range), the braod range of molar masses that can be fractioned (10^3-10^7 g·mol^{-1}) and the short period of analysis (1-2 h) [59].

Fractionation of the sample results from the hydrodynamic volume of the single molecule and is shown in Fig. 10. When the polymer solution flows through the column the single polymer coils can diffuse in every part of the matrix that offers enough space for them. Small molecules can diffuse deeper into the pores of the matrix and stay therefore longer on the column, they elute later than the bigger molecules. Molecules that are bigger than the biggest pores in the matrix eluate first, they are not kept back at all. Via this size-exclusion the upper limit of this method is set. In the past crosslinked polystyrenes where used as matrix material, nowadays they got replaced by polysaccharides like dextrane, agarose or cellulose [60].
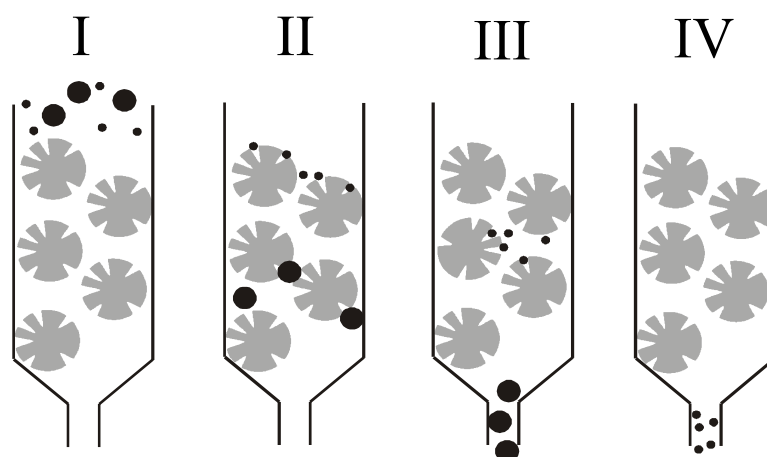
Figure 10: Schematic depiction of the fractionation principle of a SEC column via the hydrodynamic radius of the particles.

The applicableness of SEC as fractionation method is limited to molecularly dispersed polymer solutions. Polymers that tend to structure build-up in solution and the formation of aggregates may complicate the analysis, because the filling matrix of the columns induces an elongational flow field that may lead to degradation of the sample. In addition to this, ionic interactions (absorption phenomena) are a great issue, so that polyelectrolytes can not be characterized with this method [61].

3.2.3   Combined Methods of SEC/MALLS/DRI

The disadvantage of the relative methods for determination of the molar mass and the molar mass distribution, like mentioned before, is that one has to have the right polymer standard systems for callibration. Via coupling of the SEC with a concentration detector and a light scattering device one comes to an absolute method [22].

The principle of this coupling of SEC, multi-angle-laser-light-scattering (MALLS) and differential refractometer (DRI) is shown in Fig. 11. The assignment of a multi-angle-laser-light photometer has the advantage that via the dependece of the scattered light from the angle the primary beam reaches the sample, information on the radius of gyration can be obtained as can be seen in Eq. 18.

For determination of the molar mass and the radius of gyration for every fraction of the sample the concentration and the intensity of the scattered light is measured simultaneously at different angles for every slice made by the SEC (see Fig. 11 A). The values for $K{\cdot}c/R_{\vartheta}$ are then plotted in a 1D Zimm-plot versus $\sin^2(\vartheta/2)$. Extrapolation of the data to $\vartheta = 0$ gives the reciprocal value of the weight-average molar mass M_w via the ordinate section for every fraction, via the slope one can determine the radius of gyration R_G (see Fig. 11 B). Via this method one can determine the molar mass and the particle size depending on the volume of elution (see Fig. 11 C).
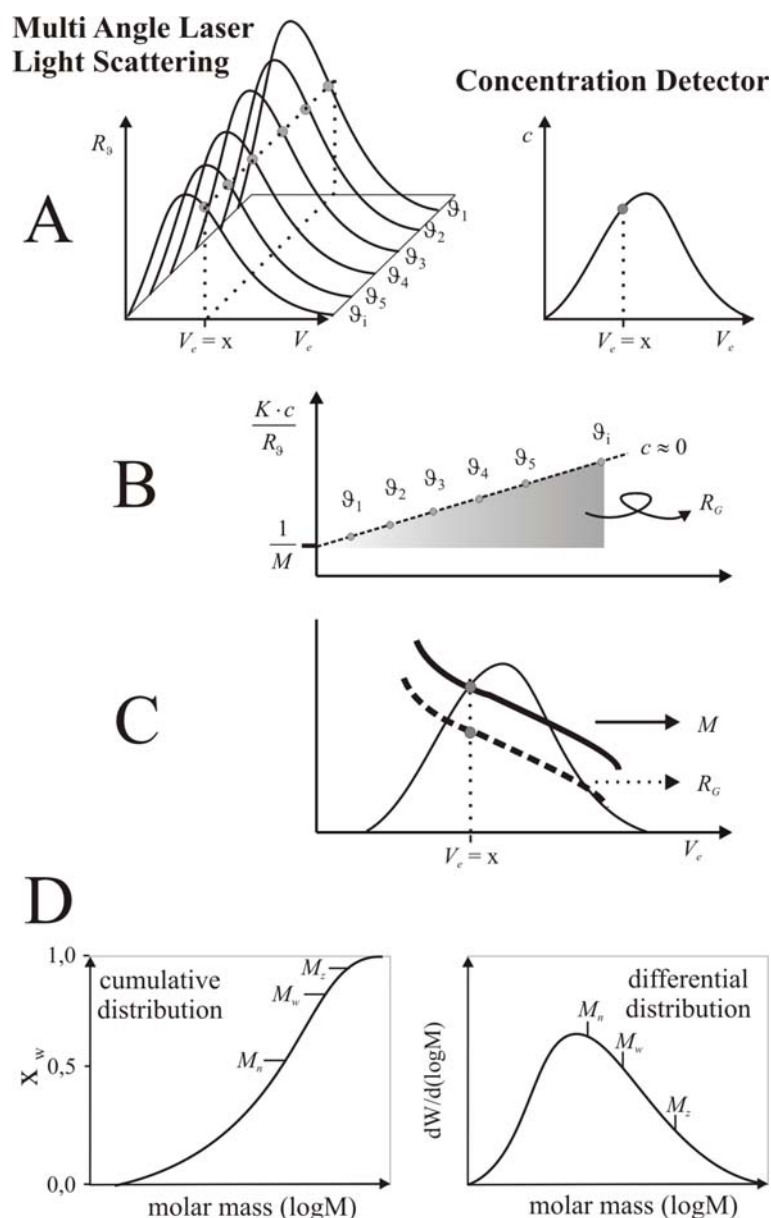
Figure 11: Determination of the absolute molar mass and molar mass distribution as well as the radius of gyration via SEC/MALLS/DRI.

Are the volumes of elution for each single fraction small enough, one can assume that the single fractions are monodispers in matters of the molar mass. Via the single molar masses M_i and the corresponding concentrations c_i the mean values of the molar mass M_n, M_w and M_z of the polydisperse sample can be evaluated according to Eq. 13. The mean values of the radius of gyration can be determined analogous. Plotting of the absolute molar mass distribution can be done as well cumulativly as differentially (see Fig. 11 D).

Like already described in chapter 3.1 it is possible to evaluate the critical concentration c^* of viscosimetry via the intrinsic viscosity (see Eq. 11). Via light scattering experiments one can evaluate another critical concentration via the weight-average molar mass M_w, the radius of gyration R_G and the Avogardo-constant N_A [62].

$$c_{LS}^* = \frac{M_w}{\frac{4}{3} \cdot \pi \cdot N_A \cdot R_G^3}$$

(Eq. 19)

This critical concentration of light scattering c_{LS}^* describes, in contrast to the critical concentration of viscosimetry $c_{[\eta]}^*$, the real conditions in solution, because the evaluation is not based on a simple model, like the solid spheres are in the Einstein-approximation (see Eq. 3) for the polymer coils.

The radius of gyration R_G of a polymer in a certain solvent can also be correlated with the molar mass M in analogy to Eq. 12 (see chapter 3.1):

$$R_G = K_{R_G} \cdot M^\nu$$

(Eq. 20)

The exponent ν is referred to as the excluded volume factor. It can be correlated with the exponent a from the Mark-Houwink-relationship (Eq. 12) as follows:

$$a = 3\nu - 1$$

(Eq. 21)

For theta conditions both exponents show the same value of 0.5, in thermodynamically better solvents the factors differ from each other.

The light-scattering measurements for this work were carried out on a device shown schematically in Fig. 12. Results fort he systems investigated are given in Tables 3 and 4.
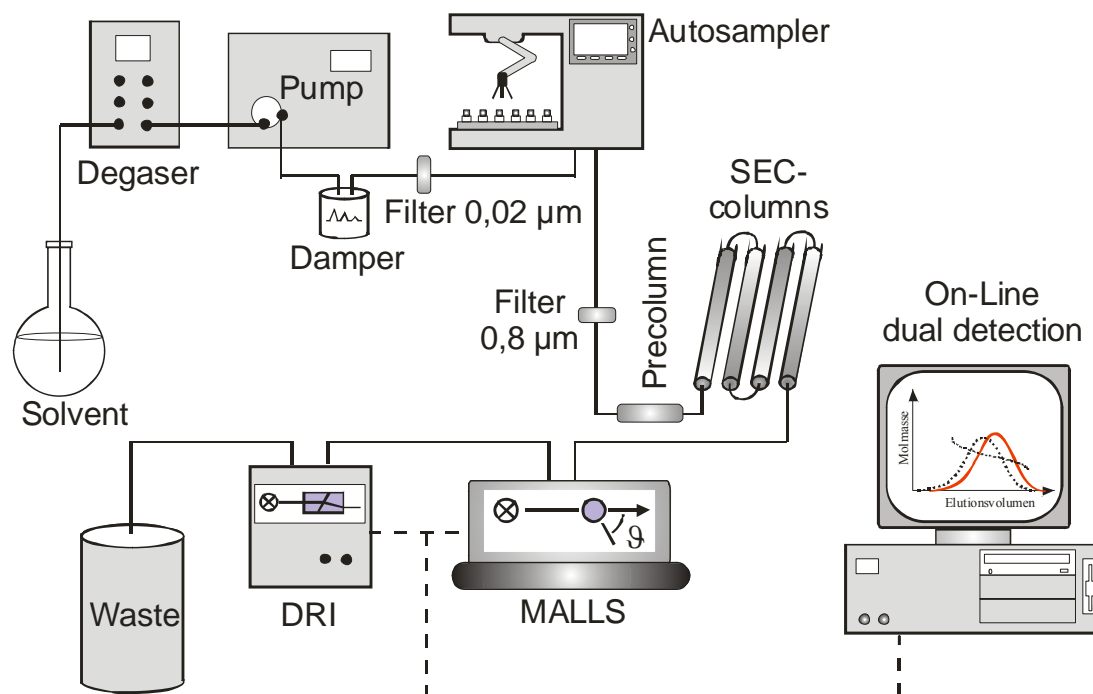

Figure 12: Combined means of SEC/MALLS/DRI for determination of molar mass and coil size, as well as their distributions.

3.3 Rheology

The basic principle of rheology (derives from the greek *rheos* = river) is the correlation of the deformation of a fluid with the occuring stresses, in particularly during flowing processes. As in polymer solutions flowing processes are very complex, a closer description of the resulting deformations and stresses is to follow.

Whereas the viscosity of fluids like oil or water remains constant, independently from the nature and velocity of the applied deformation, polymer solutions of all kinds show very sophisticated flow properties. Polymer solutions and polymer melts show as well a deformation dependent viscosity as elasticity induced flow anomalies like the Weissenberg-effect[63] and die swell [64].

To clarify the visco-elastic properties of a polymer solution, rheology offers three different measurement methods, steady shear, small amplitude oscillatory shear (SAOS) and elongational flow shown in Fig. 13 in form of the *rheological circle* [65]. The detection of the deformation induced stress can be actively achieved via mechanical transducers or passsivly from optical detection of the polymer conformation and application of the so-called stress-optical rule.
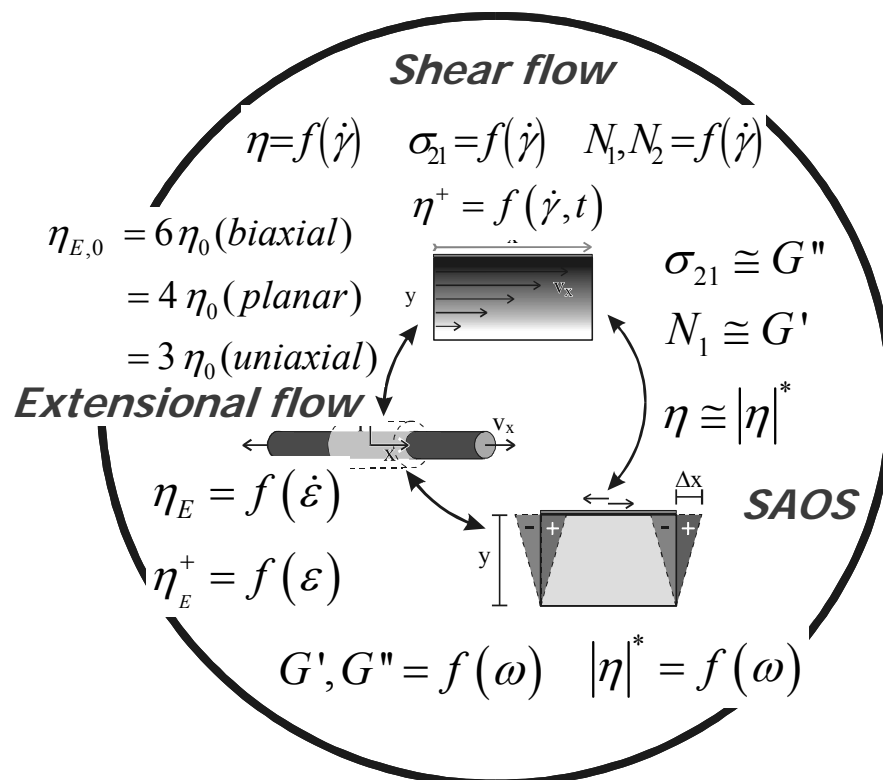

Figure 13: Rheological Circle [65].

All three experimental means shown in Fig. 13 are essential to determine the visco-elastic properties of a polymer fluid quantitatively in all different flow conditions.

3.3.1   Steady shear flow

The most commonly used rheological method for characterization of polymer fluids is the steady shear flow. Fig. 14 shows a schematic depiction of steady shear between two parallel plates. The upper plate is moved parallel to its surface with the stress σ_{21}, while the lower plate is fixed with a velocity of $v = 0$. Under stationary conditions, a laminar flow profile is build up in the fluid with a gradient in deformation $\dot{\gamma}$. The stress σ_{21} that acts on the moving plate is called shear stress, the gradient in deformation $\dot{\gamma}$ is called shear rate [66].
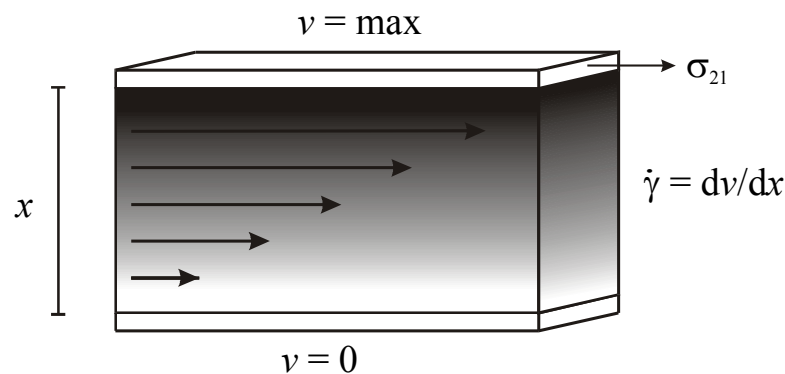

$v = \max$

σ_{21}

$\dot{\gamma} = dv/dx$

x

$v = 0$

Figure 14: Schematic depiction of steady shear flow between to parallel plates.

In a laminar flow profile, the shear stress is directly proportional to the shear rate, with a factor of proportionality η that is called shear viscosity. The one dimensional mathematical definition was found by Newton and is therefore called Newtons law of viscosity.

$$\sigma_{21} = \eta \cdot \dot{\gamma} \qquad \qquad \text{(Eq. 22)}$$

For so-called Newtonian fluids like water and oil, the shear viscosity is a shear independent material constant. However, for non-Newtonian fluids like polymer solutions or polymer melts this linear correlation is only valid for small shear rates. Above a so-called critical shear rate $\dot{\gamma}_{crit.}$ the steady state shear viscosity (zero-shear viscosity) is left and the shear viscosity becomes a function of the deformation rate. A decreasing shear viscosity with increasing shear rate, which is the commonly observed response of nearly all polymer fluids, is referred to as shear thinning behaviour. The inverse response, an increasing shear viscosity with increasing shear rate is referred to as shear thickening behaviour (dilatancy) and is observed for example for associative thickeners like hydrophobicaly modified hydroxyethylcellulose (hmHEC, see chapter 2.3 and 6.2.1, for further information also see [14]). However, in comparison to Newtonian fluids non-newtonian fluids do not dissipate the whole deformation energy via viscous flow, but store a part of it elastically. In this case these fluids are usually referred to as visco-elastic.

To completely describe the visco-elastic properties of a polymer fluid, the shear stress is not enough, because it reflects only the viscous behaviour. In Fig. 15 the complete state of deformation in a shear field is shown schematically.
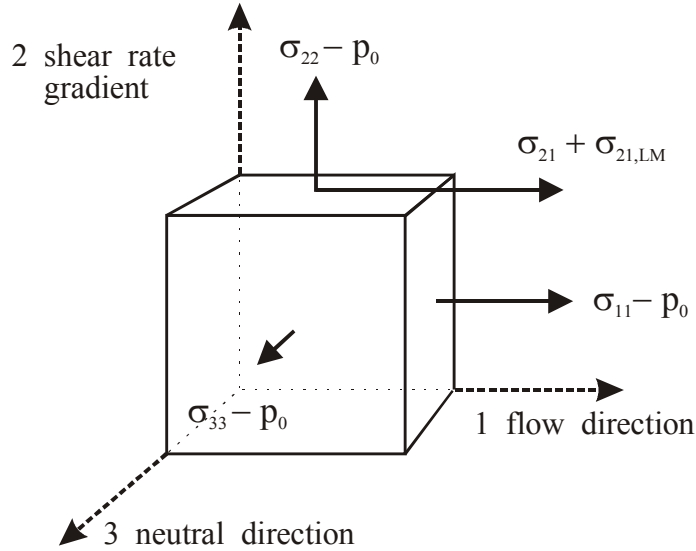
Figure 15: Schematic depiction of the state of deformation in a shear field.

The deformation of the fluid can be described via the *velocity gradient tensor* **L**:

$$\mathbf{L} = \begin{bmatrix} \dfrac{\partial v_x}{\partial x} & \dfrac{\partial v_x}{\partial y} & \dfrac{\partial v_x}{\partial z} \\[2mm] \dfrac{\partial v_y}{\partial x} & \dfrac{\partial v_y}{\partial y} & \dfrac{\partial v_y}{\partial z} \\[2mm] \dfrac{\partial v_z}{\partial x} & \dfrac{\partial v_z}{\partial y} & \dfrac{\partial v_z}{\partial z} \end{bmatrix}$$

(Eq. 23)

L can be very complex in a real flow field were different kinds of deformations may bear on the fluid. Therefore rheology aims for the investigation of simple flow fileds that can be covered completely with simple mathenatics. For simple shear for example **L** becomes:

$$\mathbf{L} = \begin{bmatrix} 0 & \dot{\gamma} & 0 \\ 0 & 0 & 0 \\ 0 & 0 & 0 \end{bmatrix}$$

(Eq. 24)

As **L** is not symmetrical, a rotational share results. To get rid of rotation the sum of **L** with its transpose $\mathbf{L}^T$ is established:

$$\mathbf{L} + \mathbf{L}^T = \begin{bmatrix} 0 & \dot{\gamma} & 0 \\ 0 & 0 & 0 \\ 0 & 0 & 0 \end{bmatrix} + \begin{bmatrix} 0 & 0 & 0 \\ \dot{\gamma} & 0 & 0 \\ 0 & 0 & 0 \end{bmatrix} = \begin{bmatrix} 0 & \dot{\gamma} & 0 \\ \dot{\gamma} & 0 & 0 \\ 0 & 0 & 0 \end{bmatrix} = 2\mathbf{D}$$

This new tensor 2 **D** is called the *rate of deformation tensor*. For the complete state of stress the elastic components σ_{ii} (*normal forces*) that act on the polymer coil in direction of the face normals have to be considered. The coordinate system is given by the flow direction (direction 1), the direction of the shear rate gradient (direction 2) and the neutral direction (direction 3). With the aid of tensor notation an arbitrary stress tensor σ_{ij} can be described by the following three addends [66]:

$$\boldsymbol{\sigma}_{abs} = -p \cdot \mathbf{I} + \eta_S \cdot 2\mathbf{D} + \boldsymbol{\sigma}_p$$

$$= -p \cdot \begin{bmatrix} 1 & 0 & 0 \\ 0 & 1 & 0 \\ 0 & 0 & 1 \end{bmatrix} + \eta_S \begin{bmatrix} 0 & \dot{\gamma} & 0 \\ \dot{\gamma} & 0 & 0 \\ 0 & 0 & 0 \end{bmatrix} + \begin{bmatrix} \sigma_{p,11} & \sigma_{p,12} & 0 \\ \sigma_{p,21} & \sigma_{p,22} & 0 \\ 0 & 0 & \sigma_{p,33} \end{bmatrix} \qquad \text{(Eq. 25)}$$

where $\mathbf{I}$ is the *identity tesor*. The first term of Eq. 25 includes the hydrostatic pressure p_o that acts compressing on the polymer fluid. The second term describes the state of stress of the solvent and the third term describes the state of stress of the polymer. Besides the shear stresses (σ_{12} and σ_{21}) the normal stresses (σ_{11}, σ_{22} & σ_{33}) , that result because the deformed coil wants to relax back in the entropically favored conformation, have to be considered. However, the absolute values of the normal stresses still incorporate the hydrostatic pressure. For this reason the normal stresses are converted to normal stress differences, resulting in four material functions altogether (see Eqs. 26-29) that allow for a precise description of the flow behaviour in steady shear [65].

$$\sigma_{12} = \sigma_{21} = f_1(\dot{\gamma}) \qquad \text{(Eq. 26)}$$

$$\sigma_{abs,\,11} - \sigma_{abs,\,22} = N_1 = f_2(\dot{\gamma}) \qquad \text{(Eq. 27)}$$

$$\sigma_{abs,\,22} - \sigma_{abs,\,33} = N_2 = f_3(\dot{\gamma}) \qquad \text{(Eq. 28)}$$

$$\sigma_{abs,\,11} - \sigma_{abs,\,33} = N_3 = f_4(\dot{\gamma}) \qquad \text{(Eq. 29)}$$

3.3.2 Small amplitude oscillatory shear (SAOS)

Another rheological method to determine the visco-elastic properties of a fluid is the small amplitude oscillatory shear. Here the response of a fluid (shear stress σ_{21}) is determined depending on a sinusoidal small amplitude deformation γ (see Fig. 16). An advantage of this method is that shear-sensitive structures like gelating systems can be characterized free of destruction, because over the whole measuring range the amplitude is kept very small, so that the so-called linear visco-elastic regime is not left.

For a Newtonian fluid the phase difference δ becomes the maximum value of 90°, because the sample acts purely viscous, whereas a purely elastic fluid (Hookean fluid) does not show any phase difference at all ($\delta = 0°$).
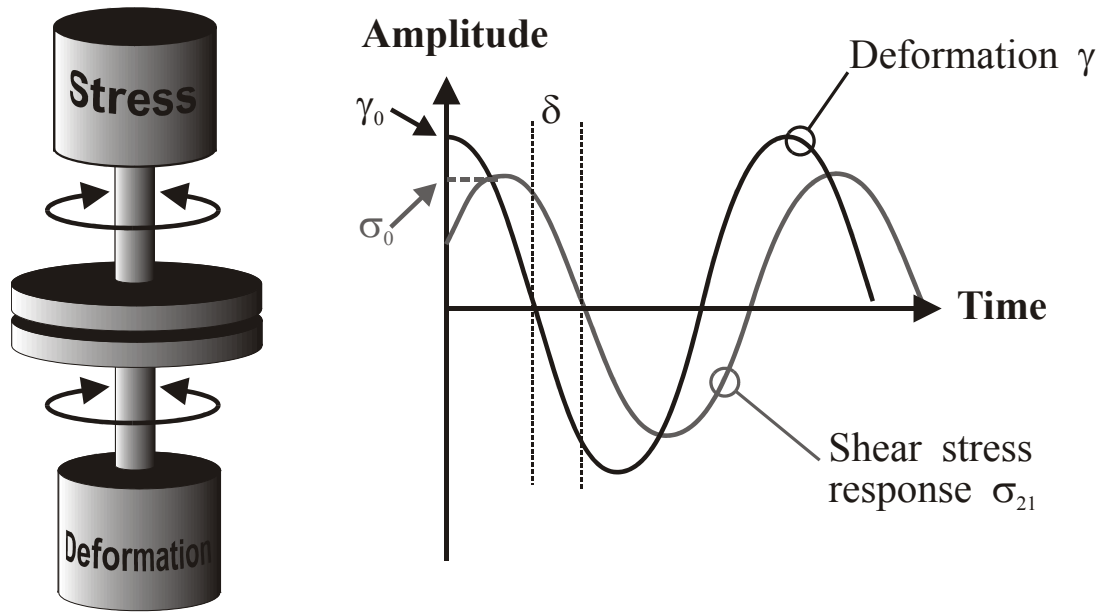
Figure 16: Schematic depiction of SAOS experiment with progression of deformation γ, shear stress σ₂₁ (response) and phase difference δ for visco-elastic fluids.

The constant of proportionality between the induced deformation and the responding shear stress is the elastic modulus G according to the Hookean law for a purely elastic solid:

$$\sigma_{21} = G \cdot \gamma \tag{Eq. 30}$$

For visco-elastic fluids the value of the phase difference lies somewhere between the maxima ($0 < \delta < 90°$), so that analog to the Hookean law a complex shear modulus G^* can be defined that describes the ratio of maximum shear stress σ_o to the maximum amplitude of deformation γ_0 incorporating the phase difference δ:

$$G^* = \frac{\sigma_0}{\gamma_0} \cdot e^{i \cdot \delta} \tag{Eq. 31}$$

By means of Eulers correlation [67] this complex shear modulus can be splitted a real part G' that is refered to as the storage modulus and an complex part G'' that is refered to as the loss modulus.

$$G^* = G' + i \cdot G'' \tag{Eq. 32}$$

The storage modulus counts for the part of the inserted energy that is stored elastically, whereas the loss modulus counts for the energy that is dissipated irreversiblely via viscous flow.

$$G' = \frac{\sigma_0}{\gamma_0} \cdot \cos \delta \tag{Eq. 33}$$

$$G'' = \frac{\sigma_0}{\gamma_0} \cdot \sin \delta \tag{Eq. 34}$$

The ratio of storage- and loss modulus the so-called loss factor *tan δ* gives a direct measure if the viscous or the elastic components of the polymer fluid outweights:

$$\tan \delta = \frac{G''}{G'}$$

(Eq. 35)

Analog to the Newtonian law (see Eq. 22) a complex viscosity η^* can be defined, that again splits up in a real and a complex part. As the complex part can not be measured the absolute value of the complex viscosity $|\eta^*|$ is used instead [68]

$$|\eta^*| = \frac{\sqrt{G'^2 + G''^2}}{\omega} = \sqrt{\eta'^2 + \eta''^2}$$

(Eq. 36)

The progression of storage- and loss moduli (see Fig. 17) with the frequency allows for an interpretation of the solution structure.

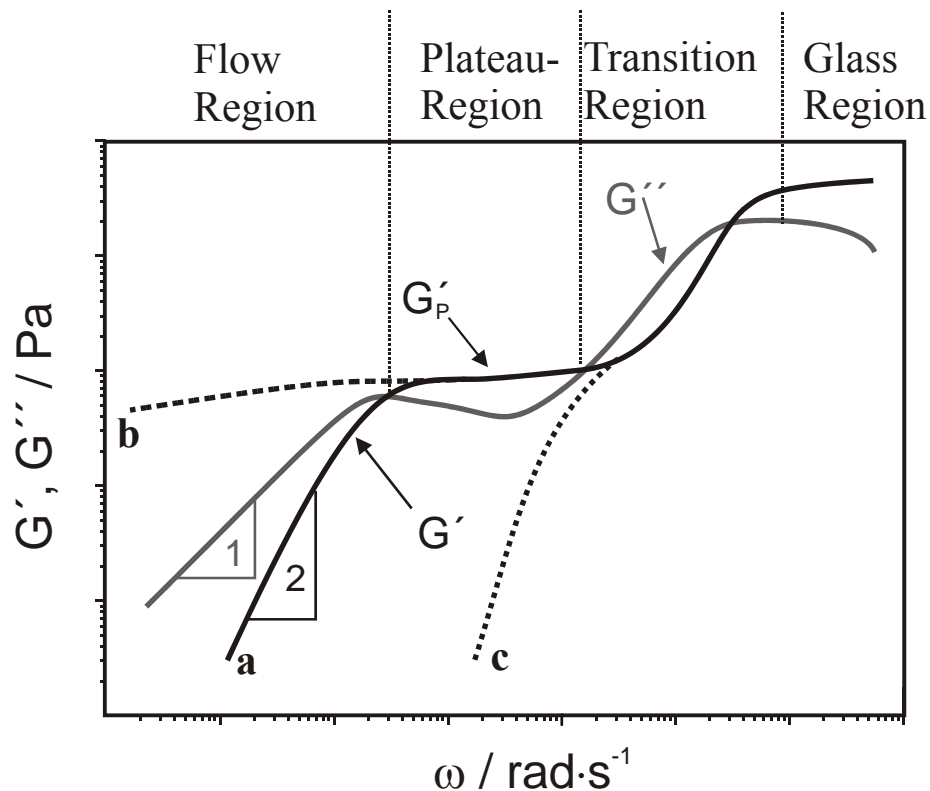*Figure 17: Schematic depiction of the progression of the storage modulus G' and the loss modulus G'' with the angular frequency ω for different solution structures (a: temporary network, b: permanent network, c: no network).*

For temporary networks like high molecular weight polymers in solution, that form intermolecular entanglements, trend (a) is characteristic and can be devided qualitatively in four different regions. In the range of the so-called *flow region*, the values of the loss modulus G'' lie above the values of the storage modulus G'. At these low frequencies the viscous behaviour of the polymer solution dominates, because the single polymer coils are still able to slide of each other, so that the inserted energy is dissipated.

With increasing frequency the polymer chains are not able to relax completely anymore, a temporary network results. The moduli discharge into a *plateau region* where almost no dependece of the moduli from the frequency can be observed, because the inserted energy is stored between the entanglements of the temporary network. With further increasing frequency not even the single chain segments are able to follow the deformation anymore. In

this *transition region* the bonds between the single atoms are distorted and the moduli are rising again. This increase finally ends in the *glass region*, where even the single atoms are not able to follow the high velocity of deformation anymore, the modes of motion are completely frozen [69].

3.3.3   Elongational Rheology

For most of the technical applications in polymer processing, the elongational behaviour of polymer solutions and melts is of the utmost importance, because elongational flow fields play a superior role. For a Newtonian liquid, the viscosity measured in a shearing flow can be used to predict the stress in other types of deformation. This, in general, is not so for complex fluids. In a *steady elongational flow*, for example, the rheological behaviour of a complex fluid, especially one in which there are long polymer molecules, is often very different from that in *shear*. An elongational flow is one in which fluid elements are stretched or extended without being rotated or sheared.
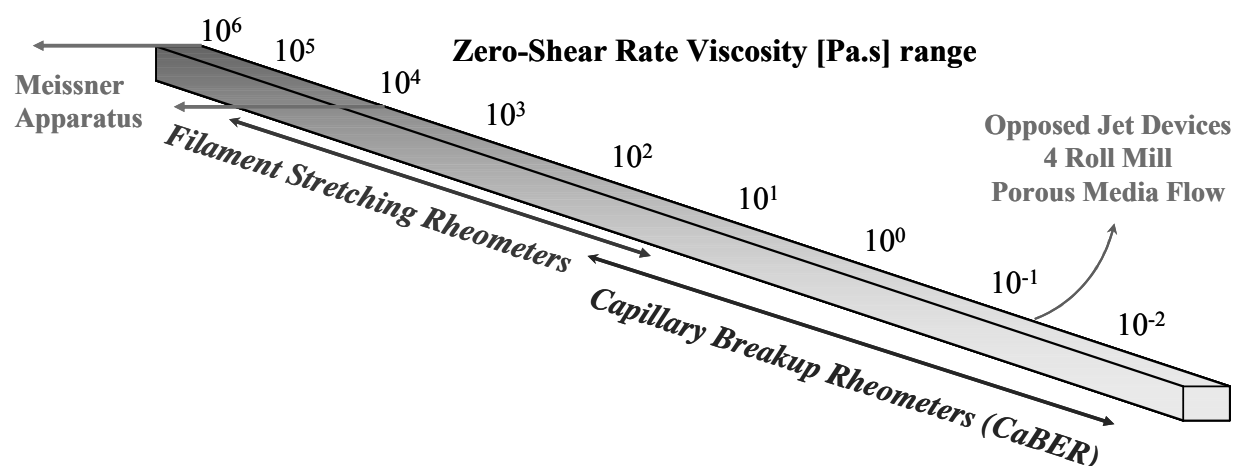

Figure 18: Schematic depiction of the available techniques for measuring the elongational viscosity in regards to the zero-shear viscosity of the fluid to be investigated.

In the past several approaches have been done to determine the elongational viscosity of highly concentrated polymer solutions and polymer melts (see Fig. 18), such as the "fano flow" [70], the "triple jet" [71] or pressure drop in sudden contractions [72], the "opposing jets" introduced by Fuller [73] have been used in several variants to extract material functions for biplanar elongational flows [74-76]. However, a comparison of these experimental techniques in the project M1 [77] showed that severe problems in the quantitative correlation of the material functions determined with the opposed jet device [78] demanded other investigation methods for elongational flows of polymer solutions.

Rheo-optical measurements of the conformation of polymer coils in solution in axis-symmetric geometries [79, 80] and 2- and 4-roller mills [81-84] allowed a passive way of determining the state of stress in strong elongational flows, however only in the range of applicability of the stress optical rule [85].

The flow through porous media finally provided a suitable method for the investigation of dilute solutions in extension [38, 59, 86, 87], however, since these geometries do not provide a uniform elongational flow field, their use for a quantitative investigation of dilute solutions is limited.

A first mechanical detection of the transient state of stress of a polymer solution in a defined uniaxial flow field could be obtained in filament stretching setups by Sridhar et al. [88, 89]. A comparison of different approaches of this type of experiment [32] showed for the first time the possibility of a quantitative determination of material functions in elongational flow in a purely uniaxial flow field. A recent overview of filament stretching rheometry is given in [90]. However, filament stretching setups are complex and expensive. Recent investigation of jet break-up [91] and drop pinch-off [92, 93] as well as the groundbreaking work of Entov and Co-workers [26, 31, 94, 95] have demonstrated the capability of a capillarity driven uniaxial elongation for the determination of transient elongational material functions. The development and testing of kinetic models [96-98] as well as the technical realisation [28, 97-99] enabled an accessible and affordable investigation of polymer solution in elongational flow with this capillary break-up elongational rheometry.

Especially for dilute solutions a distinction between the dynamics of capillary break-up experiment and of a filament stretching experiment, as carried out by Gupta et al. [100], is necessary, since most reported filament stretching experiments had to be carried out at Deborah numbers $De \gg 1$ whereas the capillary break-up of filaments chooses a natural Deborah number of $De = 2/3$ according to the theoretical analysis of Entov and Hinch [26] and backed up by several experimental observations [33].

The capillary break-up experiment provides a convenient means for probing chain-chain interactions as a function of polymer concentration through measurements of the characteristic time-scale of the fluid in a strong elongational flow and several investigations of the transient elongational behaviour of a range of different polymers and molar masses [28, 30-33] in semi dilute to dilute solutions have been reported. Because all elongational experiments in this work were achieved on a capillary breakup elongational rheometer (CaBER[1] by ThermoHaake, the first commercially available elongational rheometer, see Fig. 19), only the theoretical backround for uniaxial deformation is to be discussed in the following section.

Figure 19: Front view of the capillary break-up elongational rheometer (CaBER) and the endplates between which the actual stretching takes place.

3.3.3.1   Uniaxial deformation in CaBER like experiments

The uniaxial deformation ε of a fluid cylinder equals the elongation of the cylinder ΔL based on its initial lenght L (see Fig.):

$$\varepsilon = \frac{\Delta L}{L}$$

(Eq. 37)

The deformation rate $\dot{\varepsilon}$ is the temporal derivation of the deformation:

$$\dot{\varepsilon} = \frac{d\frac{\Delta L}{L}}{dt} = \frac{1}{L} \cdot \frac{dL}{dt}$$

(Eq. 38)

with $\dot{\varepsilon} = \frac{d\left(\ln\frac{L}{L_0}\right)}{dt}$ it comes to following expression for the time dependent lenght of the fluid cylinder:

$$L = L_0 e^{\dot{\varepsilon}t}$$

(Eq. 39)

With constant deformation rate, the lenght of the fluid cylinder increases exponentially! A so-called *Hencky strain* can then be defined to account for this correlation:

$$\varepsilon = \int_0^t \dot{\varepsilon}\,dt = \int_0^t \frac{d\left(\ln\frac{L}{L_0}\right)}{dt}\,dt = \ln\frac{L}{L_0}$$

(Eq. 40)

With a constant cylinder volume:

$$V = const = A(t) \cdot L(t) = \pi \cdot \left(\frac{D(t)}{2} \right)^2 \cdot L(t) \tag{Eq. 41}$$

one comes to following expression for the elongation:

$$\frac{L}{L_0} = \frac{V \cdot \pi \cdot \left(\frac{D_0}{2} \right)^2}{V \cdot \pi \cdot \left(\frac{D}{2} \right)^2} = \left(\frac{D_0}{D} \right)^2 \tag{Eq. 42}$$

so that applies for the deformation rate:

$$\dot{\varepsilon} = \frac{d \left(\ln \frac{L}{L_0} \right)}{dt} = \frac{d \left(\ln \left(\frac{D_0}{D} \right)^2 \right)}{dt} = \frac{-2}{D} \frac{dD}{dt} \tag{Eq. 43}$$

and analog for the Hencky strain:

$$\varepsilon = -2 \ln \frac{D}{D_0} = 2 \ln \frac{D_0}{D} \tag{Eq. 44}$$

integrated in analogy to the elongation, one comes to the temporal evolution of the diameter with constant deformation rate:

$$D = D_0 e^{-\left(\frac{\dot{\varepsilon}t}{2} \right)} \tag{Eq. 45}$$

3.3.3.2 Real fluid cylinder in capillary breakup experiments

In comparison to the ideal case described above the real fluid cylinder is exposed to gravity. To quantify this effect, the *Bond number* gives the ratio from hydrostatic pressure to surface tension, here already related to the CaBER experiment:

$$Bo = \frac{\rho \cdot g \cdot L_0}{\frac{2\sigma}{D_0}} \tag{Eq. 46}$$

For values $\gg 1$ the gravitational influence becomes pronounced and the fluid cylinder is highly deformed before the experiment starts (see Fig. 20). If the worst comes to the worst, the sample even can not be filled into the device.

Figure 20: „Sagging" fluid cylinder in the CaBER for Bo >> 1.

Another important aspect of the CaBER experiment is that the initial deformation of the fluid (with rapid stretching between the endplates) is not influenced by surface tension or viscosity of the fluid but only by fluid inertia (inertia controlled). The filament rapidly forms an hourglass-like shape between the endplates (see Fig. 21).
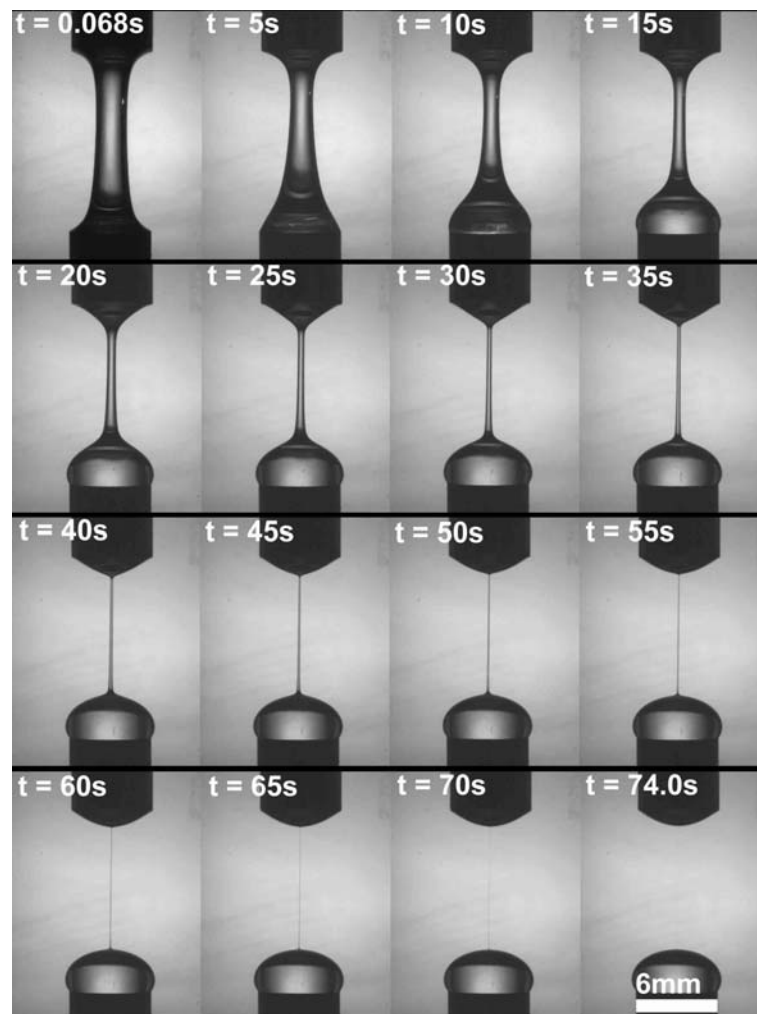

Figure 21: Filament shape after separation of the endplates ("hourglass") and filament evolution with time for a polystyrene Boger fluid.

The diameter of the hourglass right after stretching D_1 can be evaluated via the ratio of the initial aspect ratio (Λ_0) and final aspect ratio (Λ_f) an the initial diameter D_0 according to *reversed squeeze flow theory* (Spiegelberg et al. [101]):

$$D_1 = D_0 \left(\frac{\Lambda_0}{\Lambda_f} \right)^{\frac{4}{3}} \qquad \text{(Eq. 47)}$$

with the aspect ratio being $\Lambda = \dfrac{L}{R} = \dfrac{2L}{D}$.

However, the determination of the initial diameter D_0 is not easy, because it depends strongly on the filling and is therefore not automatically equal to the diameter of the plates.

Another result of the initial deformation because of rapid separation is the build-up of a polymer stress before the actual CaBER experiment (surface tension controlled contraction of the filament) even starts. This initial stress of the polymer is of some importance for the following considerations.

3.3.3.3 Newtonian fluids in capillary break-up

The behaviour of a Newtonian fluid in a CaBER experiment is fairly simple. The „effective" surface tension γ/R acts vertically to the surface of the fluid filament and squeezes it together. The occuring stress σ_s (suffix s means solvent) results in a deformation rate $\dot{\varepsilon}$ that depends on the elongational viscosity η_e of the fluid:

$$\sigma_s = \frac{\gamma}{\left(\dfrac{D}{2} \right)} = 3\eta_s \cdot \dot{\varepsilon} \qquad \text{(Eq. 48)}$$

The elongational viscosity has according to the *Trouton Ratio* [102] the triple value of the shear viscosity $\eta_e = 3\eta_s$.

Combining Eqs. 43 and 48 gives:

$$\gamma = -3\eta_s \cdot \frac{dD}{dt} \qquad \text{(Eq. 49)}$$

The temporal evolution of the filament diameter can the be obtained via integration of this expression:

$$D = D_0 - \frac{\gamma}{3\eta_s} t \qquad \text{(Eq. 50)}$$

The filament diameter decreases linear with time for a Newtonian liquid. Experimentally, the slope obtained is not the predicted $-\dfrac{\gamma}{3\eta_s}$ (Eq. 50), but a more flat one.

With considerations involving the longitudinal stresses in the filament (see [98] for a detailed analysis) one comes to a slightly extended expression of Eq. 50:

$$D = D_0 - (2X - 1)\frac{\gamma}{3\eta_s}t \qquad\qquad (Eq.\ 51)$$

The value of X depends strongly on the nature of the investigated polymer fluid. For the polymer systems investigated in this work the best value is X = 0.7127, found by Papageorgiou for standard Newtonian fluids in CaBER experiments [103].

3.3.3.4 Visco-elastic fluids in capillary break-up

For polymer solutions Eq.48, describing the elongational stress of a Newtonian fluid with the stress component of the polymer σ_p:

$$\frac{\gamma}{\left(\frac{D}{2}\right)} = 3\eta_s \cdot \dot{\varepsilon} + \Delta\sigma_p \qquad\qquad (Eq.\ 52)$$

The surface tension $\gamma/(D/2)$ is therefore not only used to deform the solvent ($3\eta_s\dot{\varepsilon}$), but also the polymer coil $\Delta\sigma_p$. Eq. 52 derives from the tensor expression for the complete elongational stress condition:

$$\boldsymbol{\sigma}_{abs} = -p\mathbf{I} + \boldsymbol{\sigma}_s + \boldsymbol{\sigma}_p = -p\mathbf{I} + \eta_s 2\mathbf{D} + \boldsymbol{\sigma}_p \qquad\qquad (Eq.\ 53)$$

or

$$\begin{bmatrix} 0 & 0 & 0 \\ 0 & -\gamma\!\!\left/\!\!\left(\frac{D}{2}\right)\right. & 0 \\ 0 & 0 & -\gamma\!\!\left/\!\!\left(\frac{D}{2}\right)\right. \end{bmatrix} = -p\begin{bmatrix} 1 & 0 & 0 \\ 0 & 1 & 0 \\ 0 & 0 & 1 \end{bmatrix} + \eta_s\begin{bmatrix} 2\dot{\varepsilon} & 0 & 0 \\ 0 & -\dot{\varepsilon} & 0 \\ 0 & 0 & -\dot{\varepsilon} \end{bmatrix} +$$

$$\begin{bmatrix} \sigma_{p,11} & 0 & 0 \\ 0 & \sigma_{p,22} & 0 \\ 0 & 0 & \sigma_{p,33} \end{bmatrix} \qquad\qquad (Eq.\ 54)$$

Summing up the single stress contributions of the polymer and resolving gives:

$$\frac{\gamma}{\left(\frac{D}{2}\right)} = 3\eta_s\dot{\varepsilon} + \left(\sigma_{p,11} - \sigma_{p,22}\right) \qquad\qquad (Eq.\ 55)$$

with $\sigma_{p,11} - \sigma_{p,22} = \Delta\sigma_p$, the first normal stress difference of elongational rheology. In the following the longitudinal stress $\sigma_{p,11}$ is referred to as $\sigma_{p,zz}$ and the radial stress $\sigma_{p,22} = \sigma_{p,33}$ is referred to as $\sigma_{p,rr}$.

According to Entov and Hinch [26] the normal stress difference of elongation can be directly correlated with the conformational tensor $\mathbf{A}$, the conformations the coil takes in the different space directions:

$$\Delta \sigma_p = \sigma_{p,zz} - \sigma_{p,rr} = \sum_{i=1}^{N_{modes}} g_i \cdot f_i \cdot \left(A_{11,i} - A_{22,i} \right)$$ (Eq. 56)

As the relaxation behaviour of a polymer coil depends not only on the longest mode, but on the different modes of relaxation N_{modes} refers to the number of modes of relaxation that are accounted for; g_i refers to the elastic modulus of the respective mode and f_i the FENE factor (see chapter 4.3.2 for details) of the respective mode that is to be evaluated as follows:

$$f_i = \frac{1}{1 - \dfrac{tr\mathbf{A}_i}{L_i^2}}$$ (Eq. 57)

whereas L_i is the finite extensibility of the respective mode. The respective elastic moduli g_i can be evaluated according to the Zimm theory (see chapter 4.1.3) and are considered as constant for the different modes of relaxation:

$$g_i \equiv G \equiv nk_BT$$ (Eq. 58)

with n = particle density, k_B = Boltzmann constant and τ_Z = Zimm relaxation time.

The finite extensibility L^2 can be determined via the Kuhn chain model [104], which is a simple approach to convert molecular information from a real hydrocarbon macromolecule into the parameters describing a polymer chain of statistically equvalent freely-rotating rigid rods:

$$L^2 = 3N_K$$ (Eq. 59)

Where N is the *Kuhn step size*, a value that relates the mean square size of the coil at equilibrium conditions $\left\langle Q_{eq}^2 \right\rangle_0$ (the subscript 0 on the root mean square size indicates that the unperturbed chain is regarded to) to the mean square size of the coil at maximal aspect ratio $\left\langle Q_{max}^2 \right\rangle$:

$$N_K = \frac{\left\langle Q_{max}^2 \right\rangle}{\left\langle Q_{eq}^2 \right\rangle_0}$$ (Eq. 60)

The value of N can be directly correlated with the weight-average molar mass of a polymer M_w, the molar mass of a single monomer M_u:

$$N_K = \frac{4M_w}{3M_u \cdot C_\infty}$$ (Eq. 61)

with C_∞ being the so-called characteristic ratio of the polymer:

$$C_\infty = \frac{\left\langle Q_{eq}^2 \right\rangle_0}{Nb^2}$$ (Eq. 62)

with N being the number of bonds and b being the bond length.

This model can be expanded in a manner that the thermodynamical quality of the solvent has an effect on the coil expansion at equilibrium conditions:

$$L^2 = 3N_K^{2(1-\upsilon)}$$ (Eq. 63)

where υ is the excluded volume coefficient.

Coming back to the conformation **A** of a polymer coil. This is to be understood as a measure for the shape and the orientation of the coil. The end-to-end distance of a polymer coil can be described via a vector $\vec{Q}$:

$$\vec{Q} = \begin{pmatrix} x_1 \\ x_2 \\ x_3 \end{pmatrix} \tag{Eq. 64}$$

However, more commonly used is the scalar product of the end-to-end distance, because it refers directly to the square value of its length:

$$\vec{Q} \cdot \vec{Q} = \left(x_1^2 + x_2^2 + x_3^2 \right) = \left| \vec{Q} \right|^2 \tag{Eq. 65}$$

One comes to the following expression for the mean square value of the end-to-end distance (see [69] and [66] for details) as already described in Eq. 60:

$$\left\langle Q_{eq}^2 \right\rangle = \left\langle \left| Q_{eq}^2 \right| \right\rangle = N_K l_K^2 \tag{Eq. 66}$$

The mean value over all polymer coils of the dyadic product $\left\langle \vec{Q}\vec{Q} \right\rangle$ describes the conformation distribution of the polymer coils in solution.

To transform this tensor to its non dimensional shape **A**, that only reflects the general state of deformation and orientation of the polymer coil, it has to be divided with the third of $\left\langle \vec{Q}_{eq}^2 \right\rangle$:

$$\frac{\left\langle \vec{Q}\vec{Q} \right\rangle}{\dfrac{\left\langle \vec{Q}_{eq}^2 \right\rangle}{3}} = \mathbf{A} \tag{Eq. 67}$$

To describe the temporal evolution of the conformation **A** during the CaBER experiment, the evolution equation for the ith mode of the appropriate spectrum (see chapter 4.1.3) has to be solved:

$$\overset{\nabla}{\mathbf{A}}_i = -\frac{1}{\tau_i} \left(f_i \mathbf{A}_i - \mathbf{I} \right) \tag{Eq. 68}$$

Here $\overset{\nabla}{\mathbf{A}}_i$ is the upper convected derivative of $\mathbf{A}_i$:

$$\begin{aligned}
\overset{\nabla}{\mathbf{A}} &= \dot{\mathbf{A}} - \left(\nabla \vec{v} \right)^T \cdot \mathbf{A} - \mathbf{A} \cdot \left(\nabla \vec{v} \right) \\
&= \frac{\partial}{\partial t} \mathbf{A} + \vec{v} \cdot \nabla \mathbf{A} - \left(\nabla \vec{v} \right)^T \cdot \mathbf{A} - \mathbf{A} \cdot \left(\nabla \vec{v} \right)
\end{aligned} \tag{Eq. 69}$$

with $\dot{\mathbf{A}}$ being the substantial temporal derivative. The product of Nabla operator ∇ with the conformation tensor **A** equals the *gradient* of **A** [67]:

$$\nabla \mathbf{A} = grad\mathbf{A} = \begin{pmatrix} \dfrac{\partial \mathbf{A}}{\partial x_1} \\[2mm] \dfrac{\partial \mathbf{A}}{\partial x_2} \\[2mm] \dfrac{\partial \mathbf{A}}{\partial x_3} \end{pmatrix} \qquad \text{(Eq. 70)}$$

Another gradient needed is the velocity gradient:

$$\nabla \vec{v} = \mathbf{L}^T \qquad \text{(Eq. 71)}$$

Combining the information on the conformation one comes to following expression for the upper convected derivative:

$$\overset{\triangledown}{\mathbf{A}} = \begin{bmatrix} \dot{A}_{11} - 2A_{11}\dot{\varepsilon}_{11} & 0 & 0 \\ 0 & \dot{A}_{22} + A_{11}\dot{\varepsilon}_{11} & 0 \\ 0 & 0 & \dot{A}_{33} + A_{11}\dot{\varepsilon}_{11} \end{bmatrix} \qquad \text{(Eq. 72)}$$

Inserting this expression into Eq. 68 results in the conformations of the polymer coil in longitudinal direction (z- or 1-direction) and axial direction (r- or 2-direction, conformation in 2- and 3-direction is the same for uniaxial elongation, therefore only direction 2 is used in the following) for uniaxial deformation:

$$\dot{A}_{zz,i} - 2\dot{\varepsilon}A_{zz,i} = -\frac{1}{\tau_i}\left(f_{zz,i}A_{zz,i} - 1\right) \qquad \text{(Eq. 73)}$$

$$\dot{A}_{rr,i} + \dot{\varepsilon}A_{rr,i} = -\frac{1}{\tau_i}\left(f_{rr,i}A_{rr,i} - 1\right) \qquad \text{(Eq. 74)}$$

However, the z-direction (or 1-direction) is enough to describe the conformation of the polymer coil, because it is the direction in which the filament grows during the experiment and therefore $A_{rr,i} \ll A_{zz,i}$. The differential equation for $A_{zz,i}$ can be solved via a few assumptions:

A_{zz} is greater than 1 during the filament evolution ($A_{zz} = 1$ only at equilibrium state!):

$$A_{zz,i} \gg 1 \qquad \text{(Eq. 75)}$$

finite extensibility is not yet reached (see chapter 4.3.2):

$$A_{zz,i} \ll L_i^2 \qquad \text{(Eq. 76)}$$

and correspondingly is:

$$f_i \cong 1 \qquad \text{(Eq. 77)}$$

Insertion of Eq. 73 in Eq. 43 and integration gives:

$$\frac{A_{zz,i}}{A_{zz,0,i}} = \left(\frac{D_0}{D}\right)^4 \cdot e^{\frac{-t}{\tau_i}} \qquad \text{(Eq. 78)}$$

This expression again can be inserted into Eq. 56 so that for the polymer stress results:

$$\Delta\sigma_p = \sigma_{p,zz} = \sum_{i=1}^{N_{\text{modes}}} g_i \cdot \left(\frac{D_0}{D}\right)^4 \cdot e^{\frac{-t}{\tau_i}} \qquad (\text{Eq. 79})$$

Inserting this expression again in Eq. 55 and resolving for the temporal dependency of the filament diameter D gives:

$$D = \left(\frac{D_0 \cdot \sum\limits_{i=1}^{N_{\text{modes}}} g_i \cdot e^{\frac{-t}{\tau_i}}}{2 \cdot \gamma}\right)^{\frac{1}{3}} D_0 \qquad (\text{Eq. 80})$$

With the assumption that only the longest mode of relaxation is of relevance in the elastic flow regime $\sum\limits_{i=1}^{N_{\text{modes}}} g_i e^{\frac{-t}{\tau_i}} \cong G \cdot e^{\frac{-t}{\tau_0}}$ and that all this does not only apply to Zimm fluids but also for every other polymer fluid with the longest relaxation time τ_0, one comes to the following fairly simple expression for the time dependence of the filament diameter:

$$D = \left(\frac{G_0 \cdot D_0}{2 \cdot \gamma}\right)^{\frac{1}{3}} D_0 \cdot e^{\frac{-t}{3 \cdot \tau_0}} \qquad (\text{Eq. 81})$$

Only the longest mode of relaxation is excited, as the CaBER experiment as a surface tension driven flow "naturally" uses a Weissenberg number *We* of 2/3 [26]. This confirms the validity of the above asssumtion leading to Eq. 81. The longest relaxation time of uniaxial deformation of a polymer can therefore be determined via a linear fit of lnD as a function of t.

3.3.3.5   Elongational viscosity

Determination of the elongational viscosity is like in shear flow or SAOS experiments possible via the ratio of stress and deformation rate:

$$\eta_E = \frac{\sigma}{\dot{\varepsilon}} \qquad (\text{Eq. 82})$$

The driving force in the fluid filament is, like mentioned before, given by the surface tension (see Eq. 48), the deformation rate was derived in Eq. 43. Inserting these expressions into Eq 82 gives:

$$\eta_E = -\frac{\gamma}{\dfrac{dD}{dt}} \qquad (\text{Eq. 83})$$

However, one has to keep in mind, that the elongational viscosity provided from CaBER experiments is not constant for most of the investigated polymer fluids. The provided viscosity is a transient one, because the deformation of the polymer coil is increasing with time and is not measured at equilibrium conditions, however determination is achieved at a constant deformation rate $\dot{\varepsilon}$. Despite this "drawback" compared with other elongational devices, the CaBER gives very interesting data, because most of the arising elongational flow fields in technical application are of a transient nature.

4 Molecular and Kinetic Theories

4.1 Molecular models

4.1.1   Random walk theory

Eq. 67 showed that for the evaluation of the conformation **A** it is of utmost importance to know the mean value of the end-to-end distance at equilibrium conditions $\left\langle Q_{eq}^2 \right\rangle$. Via the *random walk theory*, it is possible to describe the dimensions even of dynamic polymer coils in solution with the radius of gyration R_G and the average end-to-end distance $\langle Q^2 \rangle^{1/2}$ of the chain [105]. They can be calculated for a polymer coil in its unperturbed dimensions from the bond angles and lengths and the steric factors of the monomer units as shown in the following chapter.

The end-to-end distance $\vec{Q}_0$ of a freely jointed chain directly describes the absolute distance of the chain ends as shown in Fig. 22.
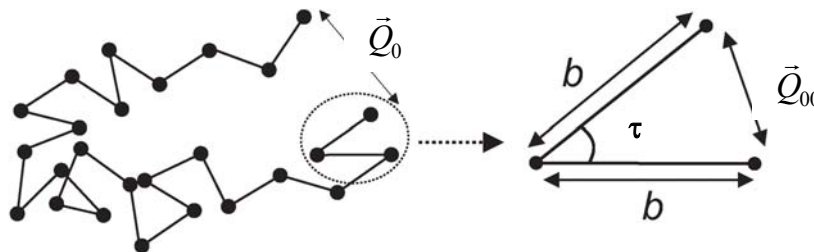

Figure 22: Definition of end-to-end distances $\vec{Q}_0$ and $\vec{Q}_{00}$.

For a close-up of a polymer chain with two bond lengths b, the distance Q_{00} of the ends can simply be calculated from the bond angle τ between the two bonds:

$$\vec{Q}_{00}^2 = 2b^2 - 2b^2 \cos \tau \tag{Eq. 84}$$

For N bonds in the polymer coil and a random angle τ, the second term equals zero. The average end-to-end distance (denoted by the brackets ‹ ›) for all possible conformations, $\langle Q^2 \rangle_{00}$, is therefore:

$$\vec{Q}_{00}^2 = Nb^2 \tag{Eq. 85}$$

In a real polymer coil, not all angles τ are possible. As one can see in Fig. 23, in a real polymer chain, the bond angle τ is fixed and the rotation of the chain is restricted and reduced to the most probable torsion angle θ. Additional short-range interactions of the polymer chain

segments can be captured with an additional factor ζ. In consideration of all these short-range interactions, the end-to-end distance of a polymer coil in its unperturbed dimensions, $\langle Q^2 \rangle_0$, can be described with the following expression:

$$\langle Q^2 \rangle_0 = Nb^2 \left(\frac{1-\cos\tau}{1+\cos\tau} \right) \left(\frac{1-\cos\theta}{1+\cos\theta} \right) \zeta \qquad \text{(Eq. 86)}$$
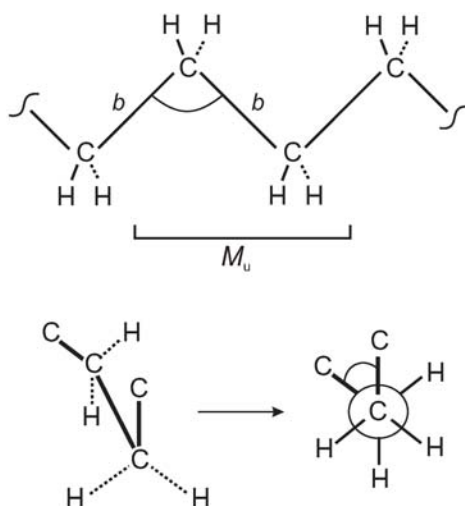

Figure 23: Schematic depiction of a hydrocarbon polymer.

Fortunately, most of the variables in Eq. 86 are fixed for a polymer-solvent system and can be combined into a constant, the so-called characteristic ratio C_∞:

$$\langle Q^2 \rangle_0 = C_\infty Nb^2 \qquad \text{(Eq. 87)}$$

The characteristic ratio C_∞ contains all steric hindrance factors that reduce a freely jointed chain to a polymer chain in its unperturbed dimensions. The characteristic ratio is listed for a lot of polymers in the "Polymer Handbook" [106]. The number of bond lengths N can be calculated from the degree of polymerization P or the molar mass M (and the molar mass of a monomer unit in the chain M_u):

$$N = 2P \qquad \text{(Eq. 88)}$$

$$N = \frac{2M}{M_u} \qquad \text{(Eq. 89)}$$

With the bond length b (0.154 nm for a simple polyethylene backbone) the average end-to-end distance $\langle Q^2 \rangle_0$ of a polymer coils in its unperturbed dimensions (so-called theta-conditions) can be calculated directly from Eq. 87.

For polymers with a more complicated backbone structure and different bond lengths along the backbone (for example polysaccharides), it is not possible to assume a simple bond length b. In this case, the average end-to-end distance is not described via the characteristic ratio, but the steric hindrance parameter σ.

$$\left\langle Q^2 \right\rangle_0 = \sigma^2 \cdot \left(\frac{K}{\sqrt{M_u}} \right)^2 \cdot M \qquad \text{(Eq. 90)}$$

The characteristic ratio as well as the hindrance parameter is a measure for the rigidity of the polymer chain. However, both values are not suitable to compare the rigidity of different chain types, since Eq. 87 and 90 both need an additional measure of the bond length that differs for different chain types. Therefore, the bond length b and the characteristic ratio C_∞ are combined to obtain a general measure for the rigidity of the chain. The so-called persistence length L_p is defined as:

$$L_p = \frac{C_\infty \cdot b}{2} \qquad \text{(Eq. 91)}$$

The persistence length can be seen as half of the shortest chain length that is needed to form a circle without obstruction from the chain rigidity. The smaller the persistence length (or C_∞), the more flexible a chain is and the more coiled it is in its unperturbed dimensions. The persistence length is independent of the chain type and can be used to compare the rigidity and coil expansion of different polymers without knowledge of the bond length.

The average end-to-end distance is not experimentally observable. Directly measurable (for example via light scattering, see chapter 3.2.1) is the radius of gyration R_G. The radius of gyration R_G is correlated to the end-to-end distance [107]:

$$\left\langle Q^2 \right\rangle_0 = 6R_G^2 \qquad \text{(Eq. 92)}$$

In the following chapters, the dimensions of a polymer coil are expressed in form of the radius rather than the end-to-end distance. The radius of gyration is the average distance of all mass points in a polymer coil from the center of gravity. Other than in a homogeneous hard sphere, the polymer segment density in a real coil is highest in the center of gravity and decreases with the distance from the midpoint as shown in.Fig. 24.
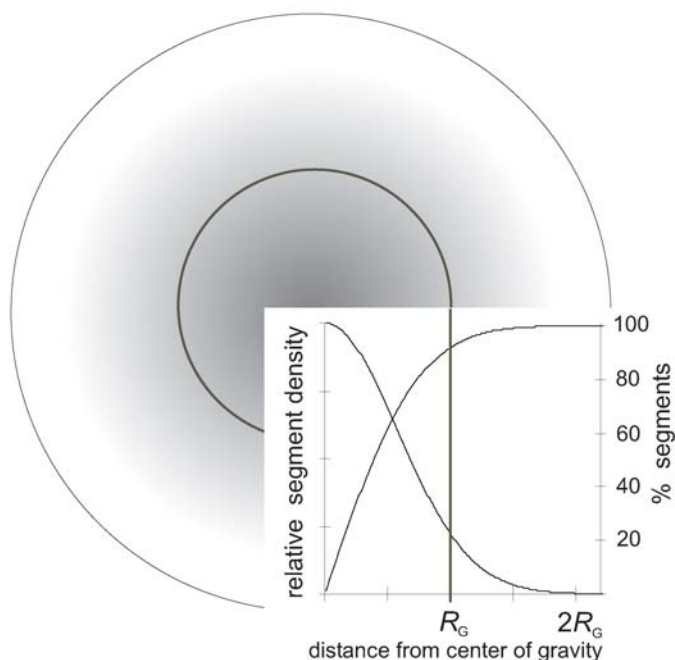
Figure 24: Definition of the radius of gyration R_G.

According to Fig. 24 only 92% of the polymer segments are inside a sphere with the radius R_G, 8% of the segments are outside of this sphere.

4.1.2   Elastic dumbbell

As Eq. 68 showed, the upper convected devirative of the conformation tensor **A** is of utmost importance for analysis of elongational data. First of, an explanation on the basis of a simple molecular model, the elastic dumbbell or bead and spring model, is to be found. In Fig. 25, the polymer is modeled as a series of beads equally spaced along the polymer backbone and connected to each other by springs.
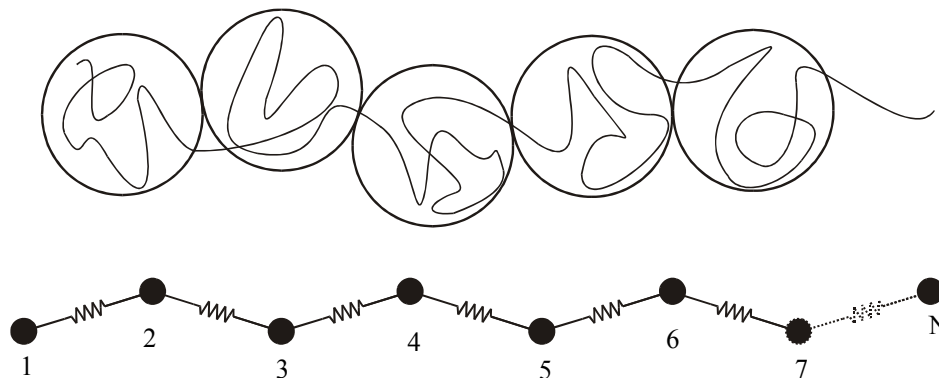

Figure 25: Schematic depiction of a polymeric chain modelled by beads and springs.

The beads in Fig. 25 account for the viscous forces of a polymer, the springs account for the elastic forces in the molecule. The portion of the chain represented by a single spring

is called a submolecule. The bead-spring model is appropriate if the internal motions of each submolecule are rapid enough that they remain nearly at equilibrium under flow. Long-range changes in conformation controlled by cooperative and therefore slow relaxation processes are well represented by the bead and spring model. Surprisingly, for dilute polymer solutions in the linear visco-elastic regime, even the much faster relaxation processes (even of the single submolecule) are well described by the bead and spring model [108].

The longest mode of relaxation, which is that of the entire molecule, can be captured via the *elastic dumbbell model*. The elastic dumbbell has just one spring with a bead at each end of it, like described by Kuhn [104]. For an elastic dumbbell in a solvent there are three different forces to be considered, the viscous drag, the elastic spring force and a random Brownian force (the inertia of the beads can be neglected). The configuration of the dumbbell is described simply by the end-to-end vector $\vec{Q}$. The balance of the three forces described above is given by:

$$\frac{1}{2}\zeta\left(\dot{\vec{Q}} - \vec{Q}\cdot\nabla\mathbf{v}\right) + k_B T\left(\frac{3}{\langle Q_{eq}^2\rangle}\right)\vec{Q} + k_B T\frac{\partial\ln\psi}{\partial\vec{Q}} = 0 \qquad \text{(Eq. 93)}$$

The first term in Eq. 93, $\mathbf{F}^d = \frac{1}{2}\zeta\left(\dot{\vec{Q}} - \vec{Q}\cdot\nabla\mathbf{v}\right)$, is the drag force, which is directly proportional to the difference between the rate of stretching of the spring $\dot{\vec{Q}}$ and the continuum fluid element containing the spring $\vec{Q}\cdot\nabla\mathbf{v}$.

The second term of Eq. 93 is the elastic spring force $\mathbf{F}^s$. The shape assumed, $\mathbf{F}^s = k_B T\left(\frac{3}{\langle Q_{eq}^2\rangle}\right)\vec{Q}$, is that of a linear or Hookean spring. It is an appropriate expression, if the molecule is stretched to no more than about a third of its maximum extension.

The third term of Eq. 93 is the Brownian force $\mathbf{F}^b = k_B T\frac{\partial\ln\psi}{\partial\vec{Q}}$. It represents the average force exerted by bead 2 as a result of random bombardments by the surrounding solvent molecules.

If Eq. 93 is solved for $\dot{\vec{Q}}$ and inserted into a probability balance function:

$$\frac{\partial}{\partial t}\psi + \frac{\partial}{\partial\vec{Q}}\cdot\left(\dot{\vec{Q}}\psi\right) = 0 \qquad \text{(Eq. 94)}$$

with ψ being the probability balance function for $\vec{Q}$ the result is the *Smoluchowski equation* (see [69] p. 125 for details):

$$\frac{\partial\psi}{\partial t} + \frac{\partial}{\partial\vec{Q}}\cdot\left[(\vec{Q}\cdot\nabla\mathbf{v})\psi - \frac{2k_B T}{\zeta}\frac{\partial\psi}{\partial\vec{Q}} - \frac{6k_B T}{\zeta\langle Q_{eq}^2\rangle}\vec{Q}\psi\right] = 0 \qquad \text{(Eq. 95)}$$

To solve this equation it is multiplied with $\langle\vec{Q}\vec{Q}\rangle$ and the summands are integrated partially:

$$\frac{d\langle \vec{Q}\vec{Q}\rangle}{dt} = -\left(-\nabla \mathbf{v}^T \cdot \langle \vec{Q}\vec{Q}\rangle - \langle \vec{Q}\vec{Q}\rangle \cdot \nabla \mathbf{v}\right) - \frac{4k_B T}{\zeta}\mathbf{I} - \frac{12k_B T}{\zeta\langle Q_{eq}^2\rangle}\langle \vec{Q}\vec{Q}\rangle \qquad \text{(Eq. 96)}$$

With the upper convected derivative and transforming $\langle \vec{Q}\vec{Q}\rangle$ to its dimensionless form **A** via division with $\langle Q_{eq}^2\rangle / 3$ we come to following expression:

$$\overset{\triangledown}{\mathbf{A}} = -\frac{12k_B T}{\zeta\langle Q_{eq}^2\rangle}(\mathbf{A}-\mathbf{I}) \qquad \text{(Eq. 97)}$$

The prefactor has the unit of a reciprocal time, its reciprocal value equals the longest relaxation time of the spring:

$$\tau = \frac{\zeta\langle Q_{eq}^2\rangle}{12k_B T} \qquad \text{(Eq. 98)}$$

With this result we finally come to the most simple evolution equation of the conformation tensor **A**, as already shown in Eq. 68, derived from the bead and spring model:

$$\overset{\triangledown}{\mathbf{A}} = -\frac{1}{\tau}(\mathbf{A}-\mathbf{I}) \qquad \text{(Eq. 99)}$$

4.1.3   Rouse/ Zimm Theory

To describe the relaxation behaviour of a polymer coil completely, the longest mode of relaxation is not sufficient. Incorporating different modes of relaxation the *Rouse model* is the earliest and simplest molecular model predicting a nontrivial distribution of polymer relaxation times.

The derivation of the constitutiv equation for the dumbbell model Eq. 93 can also be extended to allow multiple beads and springs. From the force balance for such a model one obtains [69, 109]:

$$\zeta_b\left(\dot{\vec{Q}}_i - \vec{Q}_i \cdot \nabla \mathbf{v}\right) + k_B T \sum_{j=1}^{N_s} C_{ij}\left(\left(\frac{3}{\langle Q_{eq}^{\ 2}\rangle}\right)\vec{Q}_j \frac{\partial \ln\psi}{\partial \vec{Q}_j}\right) = 0 \qquad \text{(Eq. 100)}$$

where

$$C_{ij} = \begin{cases} 2 \ \textit{if } i=j \\ -1 \ \textit{if } i=j \ +1 \text{ or } i=j-1 \\ 0 \ \textit{otherwise} \end{cases} \qquad \text{(Eq. 101)}$$

$\vec{Q}_j$ is the end-to-end vector of the jth spring in the chain and N_s is the number of springs. The constant ζ_b is the drag coefficient for a single bead, and $\left(\frac{3}{\langle Q_{eq,j}^{\ 2}\rangle}\right)$ is calculated for a single spring. With $N_{K,s}$ the number of Kuhn steps corresponding to the portion of the

polymer comprising a single spring, is $N_{K,s} = N_K / N_s$. It is very important to note, that Eq. 100 for spring i is coupled to the corresponding equations for the neighbouring springs, $i-1$ and $i+1$, because beads attached to spring i feel forces from the neighbouring springs. This implies that Eq. 100 is a matrix equation with off-diagonal matrix elements.

Rouse transformed this matrix equation into a set of *uncoupled equations* [110]:

$$\zeta_b \left(\dot{\tilde{Q}}_i - \tilde{Q}_i \cdot \nabla \mathbf{v} \right) + 4 k_B T \sin^2 \left(\frac{i\pi}{2(N_s+1)} \right) \left[\left(\frac{3}{\langle Q_{eq}{}^2 \rangle} \right) \tilde{Q}_i + \frac{\partial \ln \psi}{\partial \tilde{Q}_i} \right] = 0 \qquad \text{(Eq. 102)}$$

where $\tilde{Q}_i$ is a transformed end-to-end vector. The first normal mode. i=1, corresponds to cooperative relaxation of the entire chain, whereas the other normal modes, i=2,3,...,n, correspond to successively higher harmonics, which involve increasingly more localized motion.

The normal-mode decomposition allows for a break-up of for example the complete conformation of a polymer coil into the sum of the single contributions (compare Eq. 56):

$$\mathbf{A} = \sum_{i=1}^{N_s} \mathbf{A}_i \qquad \text{(Eq. 103)}$$

Each $\mathbf{A}_i$ obeys an *upper convected Maxwell equation* (see chapter 4.3.1), as already derived in Eq. 68:

$$\overset{\triangledown}{\mathbf{A}}_i = \frac{1}{\tau_i} \cdot (\mathbf{A}_i - \mathbf{I}) \qquad \text{(Eq. 104)}$$

where:

$$\tau_i = \frac{\zeta_b}{16 k_B T \beta_s^2 \sin^2(i\pi / 2(N_s+1))} \qquad \text{(Eq. 105)}$$

The stress contribution, arising from one of the modes can be described via conformation and modulus:

$$\boldsymbol{\sigma}_i = \left(\mathbf{A}_i - \mathbf{I} \right) \cdot G_i \qquad \text{(Eq. 106)}$$

where:

$$G_i = G = n k_B T \qquad \text{(Eq. 107)}$$

As the relaxation time τ is responsible for the conformation $\mathbf{A}$ and the conformation itself effects the stress $\boldsymbol{\sigma}$ we have confirmation of the distribution in Eq. 56 and 68 here.

Since the total friction drag acting on the molecule must be divided among $N_s + 1$ beads, the drag coefficient ζ_b that one must assign to each bead should be inversely proportional to the number of beads $N_s + 1$ used to describe the chain. Hence $\zeta_b = N \zeta_0 / (N_s + 1)$ where N is the number of monomers in the whole chain, and ζ_0 is the drag coefficient per monomer. Thus, Eq. 105 can be rearranged to a form that is independent of N_s [69, 111]

$$\tau_i \approx \frac{\zeta_0 N^2 b^2}{6\pi^2 i^2 k_B T} = \frac{6(\eta - \eta_s)}{\pi^2 i^2 \nu k_B T} \qquad \text{(Eq. 108)}$$

Here b is statistical segment lenght. The polymer contribution to the shear viscosity is $\eta - \eta_s$. The second equality in Eq. 108 derives from following relationship

$$\eta - \eta_s = v k_B T \sum_{i=1}^{N_s} \tau_i \qquad \text{(Eq. 109)}$$

However, in most polymer fluids, the relaxation modes observed do not correspond very well to the mode distribution predicted by the Rouse theory. For dilute polymer solutions, there are *hydrodynamic interactions* that affect the visco-elastic properties of the solution and that are unaccounted for in the Rouse theory. These hydrodynamic interactions between the single polymer coils referred to as *entanglements* are discussed in chapter 4.4.1 and 4.4.2.

The failure to predict the correct frequency dependence of the modulus G and the failure to predict the correct molecular weight dependence of the intrinsic viscosity *[η]* (see chapter 3.1) can be corrected by accounting for hydrodynamic interactions [69, 112, 113].Suppose a force $\mathbf{F}_c$ is exerted by a bead on the Newtonian solvent at the origin. This force sets the surrounding solvent in motion; away from the origin at a point $\mathbf{r}$ the solvent velocity (calculated according to the Stokes equation) reaches the steady state value

$$\mathbf{v}' = \mathbf{\Omega} \cdot \mathbf{F}_c \qquad \text{(Eq. 110)}$$

where $\mathbf{\Omega}$ is the *Oseen tensor* [114]

$$\mathbf{\Omega}(\mathbf{r}) = \frac{1}{8\pi\eta_s r} \left[\mathbf{I} + \frac{\mathbf{rr}}{r^2} \right] \qquad \text{(Eq. 111)}$$

and $\mathbf{I}$ is the unit tensor. The influence of a force applied by a bead in asolvent therefore decays as 1/r as the distance r from the bead increases. If the number of beads N_s+1 is large, then the longer relaxation times depend on a single dimensionless parameter

$$h \equiv h^* \sqrt{N_s} \qquad \text{(Eq. 112)}$$

where

$$h^* \equiv \frac{\zeta_b}{\sqrt{12\pi^3} R_s \eta_s} \qquad \text{(Eq. 113)}$$

where ζ_b is the friction parameter for each bead and R_s is the root mean square lenght of a spring at equilibrium [115]. At high molecular weights $h \to \infty$, this defines the *nondraining limit*. In the nondraining limit, Zimm found a set of approximate normal modes [112]. From these the relaxation times are obtained. It turns out that their spacing is changed from $\tau_i \sim i^{-2}$ (*Rouse theory*) to $\tau_i \sim i^{-3/2}$ from *Zimm theory*. Therefore, the Rouse time τ_i in Eq. 105 is to be replaced by the Zimm spectrum.

4.2 Kinetic models of linear viscoelasticity

4.2.1 Maxwell Model

During the latter half of the nineteenth century, scientist began to note that a number of materials showed time dependence in their elastic response. When materials like gum rubber were loaded in shear or extension, an instantenous deformation, as expected for a Hookean solid, was followed by a continous deformation or "creeping" behaviour. When the load was removed, part of the deformation recovered instantly, more recovered with time, and in some materials there was a permanent set [66].

Today one calls this time-dependent response visco-elasticity. It is typical for all polymeric materials. A common way to measure this phenomenon is by stress relaxation.
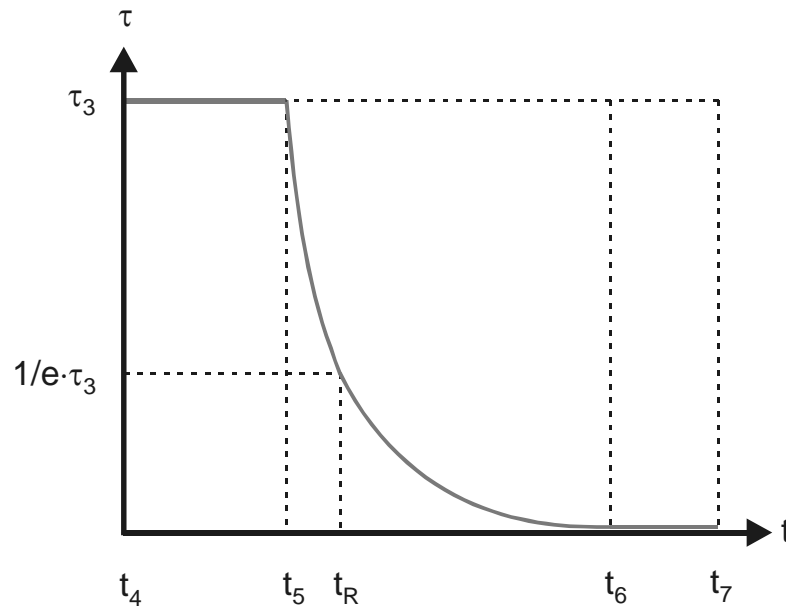

Figure 26: Stress response versus time for a polymer fluid. The longest relaxation time can be evaluated according to $\tau_0 = t_R - t_5$.

As illustrated in Fig. 26, when a polymeric liquid is subject to a step increase in strain, the stress relaxes in an exponential fashion. If a purely viscous liquid is subjected to the same deformation, the stress relaxes instantly to zero. If we convert stress relaxation data to a relaxation modulus

$$G(t) = \frac{\sigma(t)}{\gamma}$$

(Eq. 114)

all the data for small strains fall on the same curve. This linear dependence of stress relaxation on strain shown in Eq. 114 is called *linear visco-elasticity*.

In an early attempt to model the experiments on visco-elastic solids, Boltzmann [116] suggested that small changes in stress equal small changes in the modulus times the strain

$$d\sigma = \gamma dG \qquad\qquad\text{(Eq. 115)}$$

In terms of the relaxation modulus one comes to

$$d\sigma = Gd\gamma = G\frac{d\gamma}{dt}dt = G\dot{\gamma}dt \qquad\qquad\text{(Eq. 116)}$$

Integrating this expression gives

$$\sigma = \int_{-\infty}^{t} G(t-t')\dot{\gamma}(t')dt' \qquad\qquad\text{(Eq. 117)}$$

With $G(t) = G_0 e^{-t/\tau}$ one comes to the single relaxation or simple Maxwell model [117]

$$\sigma = \int_{-\infty}^{t} G_0 e^{-(t-t')/\tau}(t-t')\dot{\gamma}(t')dt' \qquad\qquad\text{(Eq. 118)}$$

The concept of linear visco-elasticity can also be written in a differential form [111]

$$\sigma + \tau\frac{d\sigma}{dt} = \eta\dot{\gamma} \qquad\qquad\text{(Eq. 119)}$$

This Maxwell model can be represented as a series combination of springs, elastic elements, and viscous dashpots as illustrated in Fig. 27.
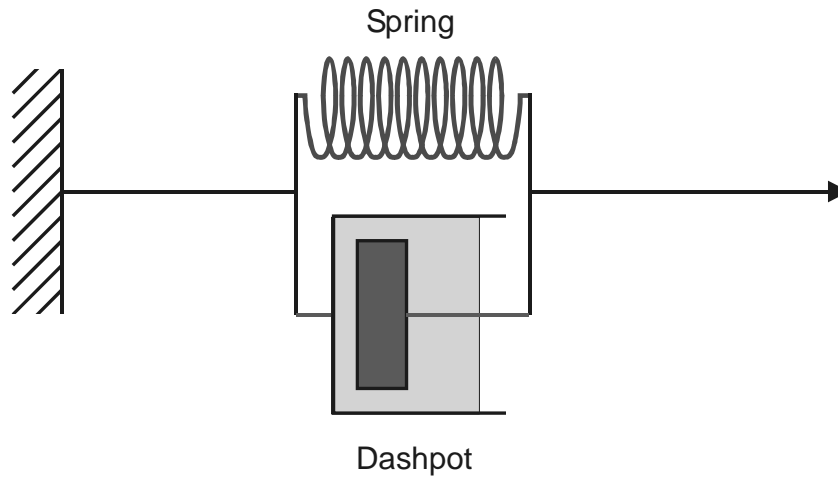

Figure 27: Spring and Dashpot representation of the Maxwell model.

Fig. 27 and Eq. 119 show, that for slow motions the dashpot or Newtonian behaviour dominates, whereas for rapidly changing stresses the elastic (derivative term) behaviour dominates. However, for large strains another type of derivative is needed, because the linearity between stress and strain is left.

4.3 Kinetic models of non-linear viscoelasticity

4.3.1   Upper convected Maxwell (UCM) – Lodge/UCM – Olderoyd-B

During World War II, Karl Weissenberg made shear flow experiments to improve predictions of the pressure drop through spray nozzles [118]. He found that "in addition to the shear stress there is a pull along the lines of flow". This "pull" is caused by so-called *normal stresses*, that are reffered to as non-linear material functions, as are shear thinning behaviour in the non-Newtonian flow regime and elongational thickening. The simple Maxwell model (Eq. 119), describing linear visco-elasticity, discussed in chapter 4.2.1 is not able to predict these non-linear phenomena.

Perhaps the simplest way to combine time dependent phenomena and rheological nonlinearity is to incorporate nonlinearity into the simple Maxwell equation (Eq. 119). This can be done via replacing the substantial time derivative in a tensor version of Eq. 119 with the upper-convected time derivative of $\boldsymbol{\sigma}$ [109]:

$$\boldsymbol{\sigma} + \tau \overset{\triangledown}{\boldsymbol{\sigma}} = 2\eta_0 \mathbf{D} \qquad\qquad (\text{Eq. 120})$$

This equation, called the *upper-convected Maxwell (UCM)*, is non-linear because $\overset{\triangledown}{\boldsymbol{\sigma}}$ contains products of the velocity gradient $\nabla \mathbf{v}$ and the stress tensor $\boldsymbol{\sigma}$. For small strain amplitudes, the non-linear terms disappear and the upper convected time derivative reduces to the substantial time derivative and Eq. 120 becomes the simple Maxwell model again.

The same result is obtained via the approach already introduced in chapter 4.1.3 via Eq. 104:

$$\overset{\triangledown}{\mathbf{A}_i} = \frac{1}{\tau_i} \cdot (\mathbf{A}_i - \mathbf{I})$$

When the conformation from Eq. 106 is written in the form $\dfrac{\boldsymbol{\sigma}}{G} + \mathbf{I} = \mathbf{A}$ and inserted in Eq. 104 one comes to:

$$\overset{\triangledown}{\boldsymbol{\sigma}} + G\overset{\triangledown}{\mathbf{I}} = -\frac{1}{\tau}\boldsymbol{\sigma} \qquad\qquad (\text{Eq. 121})$$

As the upper convected derivative of $\mathbf{I}$ equals 2$\mathbf{D}$, Eq. 121 becomes Eq. 120, meaning that molecular and kinetic theory both result in the same conclusion concerning the stress evolution described in Eq. 120.

However, the question remains if the *UCM* predicts the elastic components of shear and extension. First Eq. 120 can be written in expanded form as follows:

$$\boldsymbol{\sigma} + \tau \frac{\partial}{\partial t}\boldsymbol{\sigma} + \tau \mathbf{v} \cdot \nabla \boldsymbol{\sigma} - \tau (\nabla \mathbf{v})^T \cdot \boldsymbol{\sigma} - \tau \boldsymbol{\sigma} \cdot \nabla \mathbf{v} = 2\eta_0 \mathbf{D} \qquad\qquad (\text{Eq. 122})$$

The term $\nabla \boldsymbol{\sigma}$ is zero, because we consider a homogenous flow field. The symmetry of the shearing flow leads to a stress tensor (see Eq. 25) containing only the components $\sigma_{12}, \sigma_{21}, \sigma_{11}, \sigma_{22}$ and σ_{33}. Using

$$v_1 = \dot{\gamma} x_2 = \frac{dv_1}{dx_2} x_2 \text{ and } v_2 = v_3 = 0 \tag{Eq. 123}$$

for the velocity gradient, one comes to the following expression

$$(\nabla \mathbf{v})^T \cdot \boldsymbol{\sigma} = \begin{pmatrix} \dot{\gamma}\sigma_{12} & \dot{\gamma}\sigma_{22} & 0 \\ 0 & 0 & 0 \\ 0 & 0 & 0 \end{pmatrix} : \nabla \mathbf{v} \cdot \boldsymbol{\sigma} = \begin{pmatrix} \dot{\gamma}\sigma_{12} & 0 & 0 \\ \dot{\gamma}\sigma_{22} & 0 & 0 \\ 0 & 0 & 0 \end{pmatrix}.$$

Thus Eq. 122 becomes

$$\begin{pmatrix} \sigma_{11} & \sigma_{12} & 0 \\ \sigma_{21} & \sigma_{22} & 0 \\ 0 & 0 & \sigma_{33} \end{pmatrix} + \tau \frac{\partial}{\partial t} \begin{pmatrix} \sigma_{11} & \sigma_{12} & 0 \\ \sigma_{21} & \sigma_{22} & 0 \\ 0 & 0 & \sigma_{33} \end{pmatrix} - \tau \begin{pmatrix} 2\dot{\gamma}\sigma_{11} & \dot{\gamma}\sigma_{22} & 0 \\ \dot{\gamma}\sigma_{22} & 0 & 0 \\ 0 & 0 & 0 \end{pmatrix}$$
$$= \eta_0 \begin{pmatrix} 0 & \dot{\gamma} & 0 \\ \dot{\gamma} & 0 & 0 \\ 0 & 0 & 0 \end{pmatrix} \tag{Eq. 124}$$

To obtain the steady state results the time derivative is set to zero. It immediatly becomes obvious that $\sigma_{22} = \sigma_{33} = 0$. With this result for σ_{22}, it follows that $\sigma_{12} = \eta_0 \dot{\gamma}$, from which it can be obtained that $\sigma_{11} = 2\eta_0 \tau \dot{\gamma}^2$. This result implies that the shear viscosity is a constant η_0, the first normal stress coefficient also is a constant $2\eta_0 \tau$ and the second normal stress coefficient is zero. The non-linear upper convected Maxwell equation can also be written in an integral form

$$\sigma = \int_{-\infty}^{t} \frac{\eta_0}{\tau^2} e^{-(t-t')/\tau} (\mathbf{B}(t,t') - \mathbf{I}) dt' \tag{Eq. 125}$$

with **I** being the unit tensor and **B** being the finger tensor ([66], p. 29). This equation is usually referred to as the *Lodge/UCM* equation. Thus, although Eq. 125 has some of the qualitive behaviour of real polymeric fluids, it is still far from being a quantitative constitutive equation for most polymeric fluids.

However, for dilute solutions of polymers, the *UCM* equation, or a simple variation of it like the *Lodge/UCM* equation, seems to be satisfactory. For these solutions, polymer molecules do not entangle very much with each other, and the visco-elastic properties of the polymer solutions are particularly simple. In most dilute solutions the longest relaxation times τ is so small that visco-elasticity is shown at very high strain rates.

On the other hand, if the solvent viscosity is very high, the longest relaxation time becomes very big, even for dilute solutions at low shear rates [64] (see chapter 6.1.1). Such solutions are referres to as Boger fluids. Although the *UCM* equation gives the polymer contribution to the stress in such a dilute solution, the solvent contribution to the stress cannot be neglected, and so the total stress tensor $\boldsymbol{\sigma}$ in these solutions is the sum of the polymeric and solvent contributions

$$\boldsymbol{\sigma} = \boldsymbol{\sigma}_p + \boldsymbol{\sigma}_s \qquad \text{(Eq. 126)}$$

Here $\boldsymbol{\sigma}_p$ is given by the *UCM* equaion and $\boldsymbol{\sigma}_s$ is usually just a Newtonian term $2\eta_s \mathbf{D}$, where η_s is the solvent viscosity. The combination of these two terms is the *Olderoyd-B constitutive equation*

$$\boldsymbol{\sigma} + \tau_1 \overset{\triangledown}{\boldsymbol{\sigma}} = 2\eta \left\{ \mathbf{D} + \tau_2 \overset{\triangledown}{\mathbf{D}} \right\} \qquad \text{(Eq. 127)}$$

4.3.2   FENE-P/ FENE-PM

The rheological data for dilute solutions indicate that the main limitation of the elastic dumbbell (see chapter 4.1.2) and the *Olderoyd-B constitutive equation* is that it assumes that the polymer molecules are infintly extensible, which is objectionable for larger polymer extensions [69]. This defect can be corrected simlpy by making the relation between the sring force $\mathbf{F}^s$ and the molecular extension $\vec{Q}$ nonlinear, such that the stress becomes very large as the molecular extension approaches the fully extended length L of the molecule.

For the freely jointed chain model (random walk theory see chapter 4.1.1 also [105] for detail) the force-extension relationship can be assumed to be a *Warner Spring Law* [119] also known as the finite extensibility (FENE) spring:

$$\mathbf{F}_{FENE}{}^s = \frac{3k_B T}{Q_{eq}^2} f \cdot \vec{Q} \ \text{ with } \ f = \frac{1}{1 - \left(\dfrac{\vec{Q}}{L} \right)^2} \qquad \text{(Eq. 128)}$$

As $\vec{Q}$ is an element of f, the Smoluchowski equation (see Eq. 95) can not be solved and no analytic expression for the stress tensor is obtained unless an approximation is made. This is done via the *preaveraged quantity* [120] $\langle \vec{Q}^2 \rangle$. When the average value of $\vec{Q}^2$ is used the Smoluchowski equation can be solved to give rise to an expression for the stress as already derived in Eq.106:

$$\boldsymbol{\sigma} = f \cdot (\mathbf{A} - \mathbf{I}) \cdot G \qquad \text{(Eq. 129)}$$

$$\text{with } G = nk_B T \ \text{ and } \ f = \frac{1}{1 - \dfrac{tr\mathbf{A}}{L^2}} \qquad \text{(Eq. 130)}$$

Since the non-linearity in the spring law shows up mostly at high molecular extension, the predictions of the preaveraged FENE dumbbell model (FENE-P) are changed from those of an elastic dumbbell at high shear rates in shearing flows, and in elongational flows when the extension rate $\dot{\varepsilon}$ exceeds the critical value for a coil-stretch transition.

If one assumes that the polymer coil has not just one, but different modes of relaxation, so that one longest relaxation time is not enough for a complete description one has to use a multi-mode version of the FENE dumbbell model (FENE-PM).

4.4 Characterization of the concentrated polymer solution

4.4.1   Entanglement concept

In nondilute polymer solutions and melts, the polymer coils interpenetrate each other enough that the molecular motions of one chain are greatly slowed by the interfering effects of other chains. These interferences are usually referred to as intermolecular entanglements.

However, to understand the entanglement behaviour of the polymer chain and therefore the flow behaviour of complex polymeric fluids, it is important to know about the solution conformation of the polymer. Fig. 28 gives an overview of the different conformations of polymers in solution, that are due to different chain flexibilities and thermodynamical interactions of the polymer chain with the solvent.
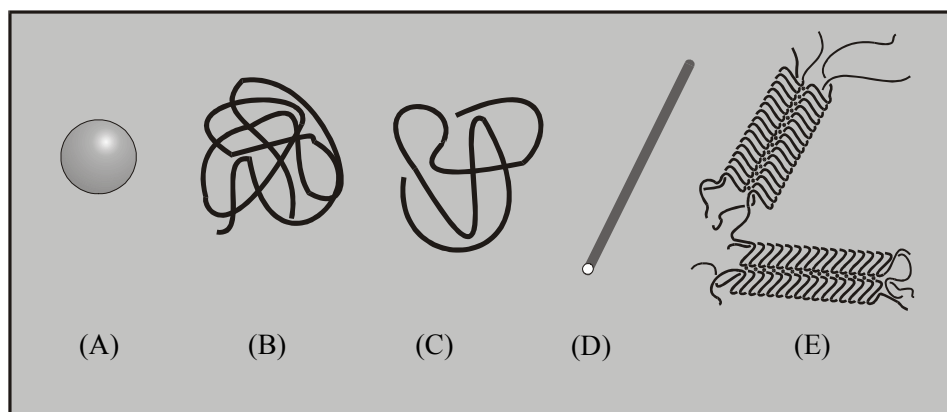
Figure 28: Examples of the structure of polymers in solution: sphere (A), random coil (B), expanded coil (C), rod-like structure (D) and aggregated structure (E).

Another very important factor that influences the flow behaviour of polymer fluids is the molar mass. Bueche [121] postulated a direct proportinonality between the zero-shear viscosity in the Newtonian flow regime and the molar mass. Above a critical value for the molar mass M_c, entanglements between the single polymer coils result. Via a so-called slip factor that was introduced and that refers to the velocity that a moving polymer molecule drags with on an entangled neighbouring molecule, a relationship between molar mass and zero-shear viscosity derives

$$\eta_0 \propto M^{1,0} \text{ for } M \leq M_c \tag{Eq. 131}$$

and

$$\eta_0 \propto M^{3,4} \text{ for } M \geq M_c \tag{Eq. 132}$$

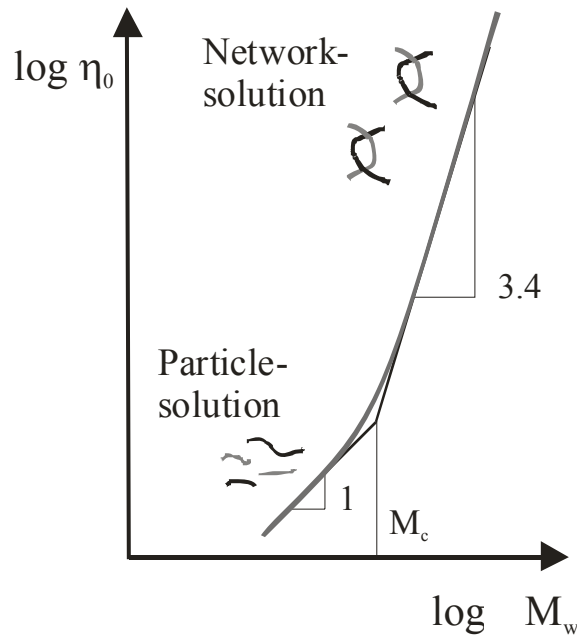This molar mass dependence is shown schematically in Fig. 29 for polymers in different states of solution.

Figure 29: Schematic Depiction of the molar mass dependece of the zero-shear viscosity for different states of solution.

Graessley [122] extended this theory by Bueche, because it was not plausible to him that the molecule can rotate freely in a concentrated solution, whereas relative motion is imposed on the system as molecules, which had been close enough to each other to entangle, separate. The number of entanglements for a particular polymer, therefore, must depend on its rate of entanglement formation with approaching molecules.

If the entanglement process is modeled as a first-order kinetic process [123], the elastic character of entanglements is well described, but a shear rate independent flow behaviour is obtained. However, the process of entanglement is a *cooperative process,* diffusion of the chain segments and the build-up of entanglement loops by random motion happens simultaneously for multiple polymer chains. In steady shear flow, the entanglement density between any two passing molecules will depend on the characteristic time necessary for entanglement compared to the contact time between the molecules. As the molecules pass, disentanglement occurs.

For an entanglement to exist, two molecules first must be within a certain distance of each other. Second, the molecules must stay in this "sphere" for a finite time. Hence, the entanglement density is reduced by high shear rates, because fewer molecules will remain in the "entanglement sphere", with increasing shear rate disentanglement is favoured in comparison to entanglement, the shear viscosity decreases [45, 124].

The approach of the *entanglement concept* was difficult to extend to visco-elastic effects quantitatively and has been abandoned in favor of the *reptation model* described in the following chapter.

4.4.2   Reptation concept

In 1971 DeGennes proposed a new model for molecular motion in concentrated polymer solution [125]. He described the relaxation of polymers by sliding along its own contour like a snake. DeGennes called this motion *reptation*. The mesh of constraints confines the molecule laterally to a tube like region [126] as shown in Fig. 30.
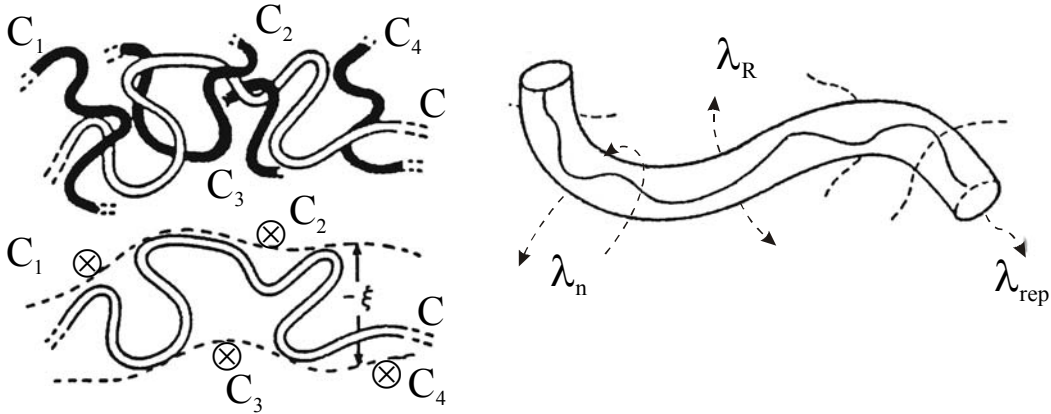

Figure 30: Schematic depiction of the reptation concept. The polymer chain slides along its own contour (build by entanglements of other chains) and has three different modes of relaxation.

The chain changes its conformation by sliding back and forth along the tube. Because it is a diffusive process, the time required for the chain to vacate the original tube is proportional to the square of the *countour lenght* L_t of the tube divided by the diffusion coefficient of the snaking motion. The diffusion coefficient of the snaking motion is proportional to M^1, while the square of the tubes contour lenght is proportional to M^2. Thus the reptation time, the time τ_d (corresponds with τ_{rep} in Fig. 30) for disengagement from the tube is proportional to $M^2/M^{-1} = M^3$ [127]. Hence the longest relaxation time, $\tau_1 = \tau_d$ is predicted to be proportional to M^3, not too different from the measured scaling law $\tau_1 \sim M^{3.4 \pm 0.1}$.

The diameter, a, of the tube corresponds to the entanglement spacing, M_e, that is a strand of polymer that spans a random walk end-to-end distance a

$$a^2 = \frac{4}{5} \frac{\rho N_A k_B T \left\langle R^2 \right\rangle_0}{M G_N^0} \tag{Eq. 133}$$

The tube itself is a random walk, each step of it has a lenght a. This random walk of the tube is called the *primitive path* of the chain [128]. The lenght of this primitive path (or the contour lenght) is therefore $L_t = aM/M_e$.

The repatation theory has been controversial, because experimental data and numerical simulations usually show some derivations from the behaviour expected for pure reptation. A prime example is the observed 3.4 power law for the viscosity by Kröger et al. [129] which differs from the predicted 3.0 power law [127]. These deviations are due to relaxation processes other than reptation. The most important of these are *primitive-path fluctuations* and *constraint release*, that correspond with the other two relaxation times in Fig.30 [130].

Doi and Edwards developed a constitutive equation for entangled polymeric fluids [128, 130] that combine the linear visco-elastic response predicted by DeGennes [125] for a reptating chain with a non-linear response to large deformations. Analysis ot the reptation process [125] shows that after a time *t,* only a fraction *P(t)* of the original tube remains unvacated

$$P(t) = \sum_{iodd} \frac{8}{\pi^2 i^2} \exp\left[\frac{-i^2 t}{\tau_d}\right] \qquad \text{(Eq. 134)}$$

The linear relaxation modulus is *P(t)* times G_N^0

$$G(t) = \sum_{iodd} G_i \exp\left[-t / \tau_i\right], \qquad G_i = 8 G_N^0 / \pi^2 i^2, \qquad \tau_i = \tau_d / i^2 \qquad \text{(Eq. 135)}$$

The storage and loss moduli, *G'* and *G''*, are obtained from the relaxation spectrum in the usual way (see chapter 4.1.3). That is, using

$$G' = \sum G_i \left[\omega^2 \tau_i^2 / (1 + \omega^2 \tau_i^2)\right], \qquad G'' = \sum G_i \left[\omega \tau_i / (1 + \omega^2 \tau_i^2)\right] \qquad \text{(Eq. 136)}$$

The longest relaxation mode of the relaxation modulus in Eq. 135 is the dominant one, it accounts for 96 % of the zero-shear viscosity. Thus, the reptation model predicts that for a nearly monodisperse melt, the relaxation spectrum is dominated by a single relaxation time $\tau_1 = \tau_d$. This is in reasonable accord with experimental data at low and moderate frequencies. However, at higher frequencies there is a deviation from the Doi-Edwards model, apparantly because reptation is the only relaxation process considered, *primitive-path fluctuations* and *constraint release* are neglected.

4.4.3   Molecular modelling of viscosity - States of solution

To describe the viscous properties of a polymer fluid exactly, the models described above in chapter 4.2 - 4.4 have to be assigned to the different states of solution, a polymeric fluid can adopt.

The standardization of the zero-shear viscosity η_0 via the product of $\rho \cdot M$ found by Bueche for polymer melts [121], can be transferred to concentrated polymer solutions via a plot according to $c \cdot M$. The transfer of this model to the ideally diluted polymer solution does not give satisfactory results. This is due to the fact that the idea of a free interpenetration of the polymer coils in a homogenous network solution is not given by every polymer-solvent system. Daoud et al. [131] showed via the determination ot the radius ot gyration by light scattering methods, that there can be a coil contraction with increasing concentration. This indicated that there ought to be more states of solution than the ideally diluted- and the concentrated solution.

A first approach to describe the region between the two limits was introduced by Simha, who described the state of solution via a so-called *overlap parameter*, that is the product of intrinsic viscosity *[η]* and concentration *c* [132]. Onogi extended this model via expressing this relation by a virial equation that introduced the specific viscosity η_{sp}, that is independent of the solvent [133]

$$\eta_{sp} = \sum_{k=1}^{n} B_k \cdot (c \cdot [\eta])^k \qquad\qquad\qquad\qquad\text{(Eq. 137)}$$

This approach was then extended by Bouldin via including the thermodynamical quality of the solvent, resulting in five different states of solution for a polymer in a thermodynamically good solvent [46] as shown in Fig. 31.
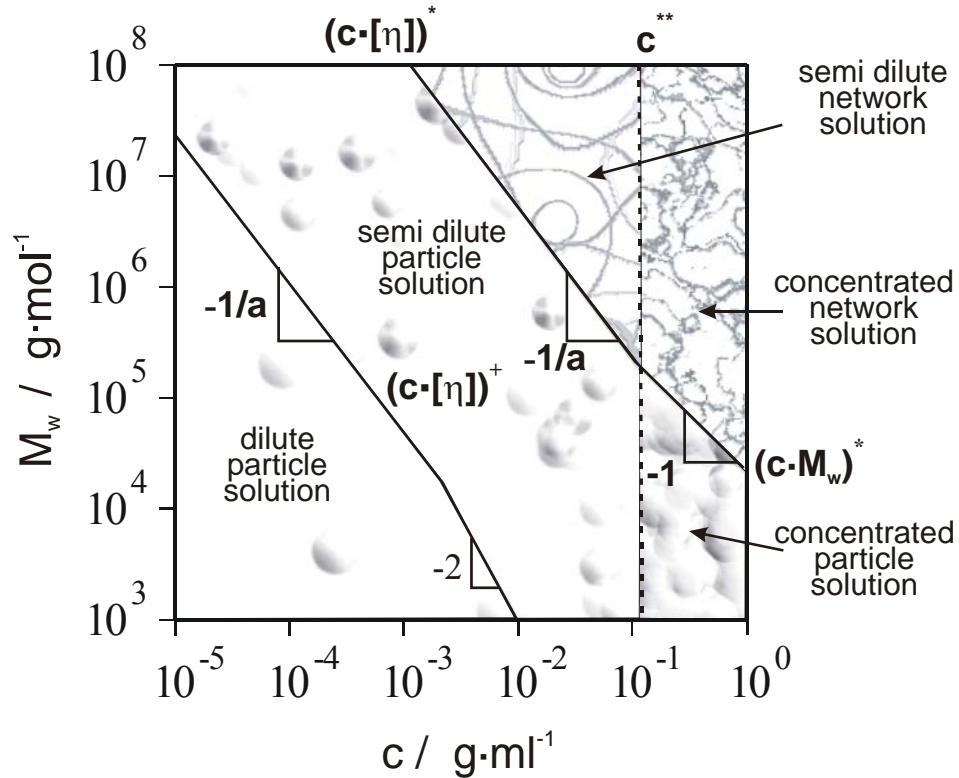

Figure 31: The five states of solution for polystyrene in toluene in dependence of molar mass and consentration.

In the following these five states of solution are to be explained in detail.

1. Ideally diluted particle solution $\left((c \cdot [\eta]) < (c \cdot [\eta])^+ \right)$

In an ideally diluted particle solution, the single polymer coils are isolated from each other, because of the ample disctance between the molecules. There is no interpenetration occuring between the chain segments, so that the viscosity is dominated only by the hydrodynamical volume of the polymer coils. The transition concentration c^+ was empirical determined to be $\sim \dfrac{c^*}{100}$.

Above a critical molar mass, the slope of the transition line to the next state of solution can be evaluated via the reciprocal value of a, the exponent of the $[\eta]$-M-relationship (see chapter 3.1). Below this critical molar mass, the $[\eta]$-M-relationship becomes independent of solvent influences and the slope becomes -2, which is the apparent solvent quality of the theta state (see chapter 3.1). In this state of solution the Zimm theory (see chapter 4.1.3 for details) applies. The polystyrene Boger fluids investigated in this work do reflect this state of solution.

2. Semi dilute particle solution $\left(c < c^{**}; (c \cdot [\eta])^+ < (c \cdot [\eta]) < (c \cdot [\eta])^*\right)$

In the region of the semi dilute particle solution (in the literature this state of solution is oftgen referred to as "dilute"), the rheological material functions are dominated by polymer-solvent interactions. Although the single polymer coils start to interact with each other, the coils are not able at this concentration to build-up enduring entanglements. To minimize polymer-polymer interactions, coil contraction may be the result.

3. Semi dilute network solution $\left(c < c^{**}; (c \cdot [\eta]) > (c \cdot [\eta])^*\right)$

When the critical product of concentration and intrinsic viscosity $(c \cdot [\eta])^*$ is exceeded, the polymer coils are able to form enduring entanglements and reptation begins to dominate the polymer movements. The degree of entanglement dominates the viscosity of the polymer fluid in the respective solvent.

In thermodynamically good solvents, the onset of an inhomogenous network results, because the free interpenetration of the polymer coils is hindered by the solvation of the chain. Under pseudo-ideal theta conditions, the coil is not expanded by solvation, because the polymer-solvent interactions fit the polymer-polymer interactions. Free interpenetration of the polymer coils is therefore possible and a homogenous network results. Under theta conditions, the semi dilute network solution does therefore not exist.

4. Concentrated particle solution $\left(c > c^{**}; (c \cdot M) < (c \cdot M)^*\right)$

The state of the concentrated solution is reached, when the coils are shrinked to theta dimensions. The rheological material functions like the viscosity are then dominated by polymer-polymer interactions, polymer-solvent interactions can be neglected. However, the so-called Bueche parameter $c \cdot M_w$ is not surpassed yet, so that the polymer coils do not form enduring entanglements, the viscosity is directly proportional to the product of concentration and molar mass. Interestingly the Rouse theory (see chapter 4.1.3 for details) applies here.

5. Concentrated network solution $\left(c > c^{**}; (c \cdot M) > (c \cdot M)^*\right)$

In the regime of the concentrated network solution, the Bueche parameter is surpassed. That means that the polymer chains are long enough, under theta conditions, to form enduring entanglements to build up a homogenous enduring network. The resulting viscosity scales with $M^{3.4}$ as described in chapter 4.4.2. The behaviour of the polymer coils in this state of solution (reflected by the higher concentrated MHEC solutions investigated in this work) is described via the reptation concept (see chapter 4.4.2).

5 Structural Analysis of investigated polymers

5.1 Molecular structural parameters of investigated polystyrenes

The polystyrenes investigated in this work came from Polysciences Inc. (2.8 Mg/mol), Polymer Standard Sevices (16.8 Mg/mol and 23.6 Mg/mol) and Polymer Laboratories (all remaining samples). To correlate the rheological properties of a polymer with its molecular composition, several structural parameters have to be determined. First of all, the investigated polystyrene standards were fully characterized in regards of their intrinsic viscosities in the miscellenous solvents used in this work via viscosimetry (see chapter 3.1). Determination of the structure-property relationship of the polymer in the respective solvent is necessary for obtaining information on the thermodynamical solvent quality and therefore the coil structure of the polymer in the investigated solutions.

The Huggins plots for the different polystyrene standards in toluene as a solvent are shown in Fig. 32.
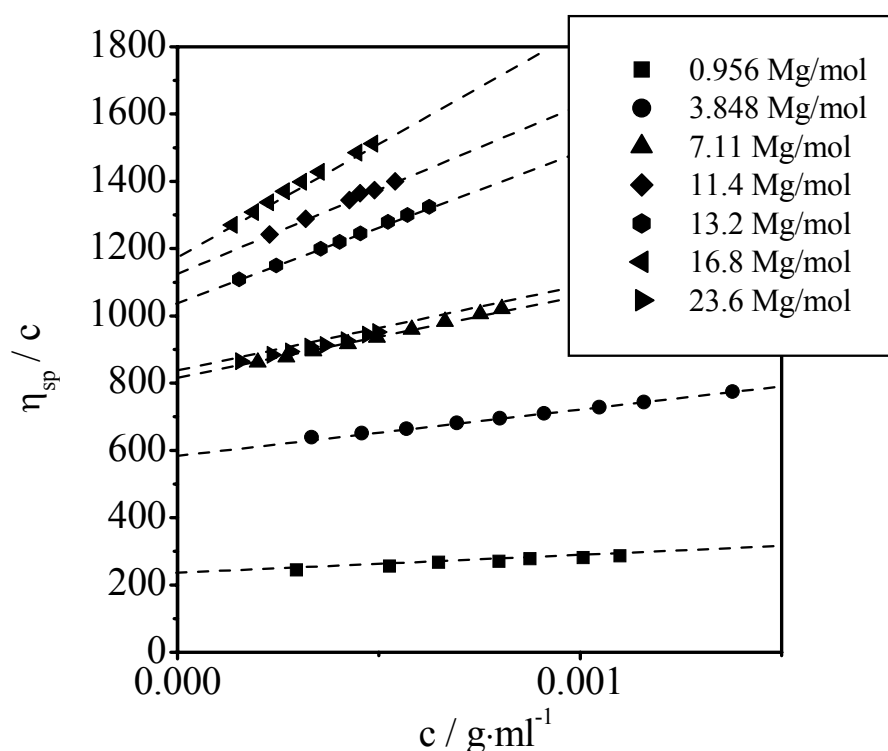
Figure 32: Huggins plots for the investigated polystyrenes in toluene, given molar masses are specifications provided by the manufacturers (for experimental conditions see chapter 8.2).

Via the intrinsic viscosities of the polystyrenes in toluene one can evaluate the molar masses very accuratly, because polystyrene in toluene belongs to the best characterized polymer-solvent-systems at all. However, the [η]-M-relationship used was originally determined by Kulicke et al. [43] and is back-uped by dynamic light-scattering results [44]:

$$[\eta] = 8.62 \cdot 10^{-3} \cdot M_w^{0.736} \tag{Eq. 138}$$

The intrinsic viscosities of the investigated polystyrenes are listed in Table 1 together with the evaluated weight-average molar masses, the molar masses provided by the manufacturers and the polydispersity index.

As one can see there is a vast difference between the provided molar masses and the actual molar masses determined via viscosimetric measurements. This deviation reaches its maximum of about 400 % for the sample with a provided molar mass of 23.6 Mg/mol. However, all viscosimetric measurements were repeated at least twice, so that the data is to be reliable. In the following chapters this *"true"* molar mass will be used for calculations referring to the molar mass of the polystyrenes.

Another solvent used for the polystyrenes in the following chapters is diethylphthalate (DEP). This solvent was used, because the coil expansion is supposed to be closer to theta conditions, as it is in the familiar solvent dioctylphthalate (DOP) [134], as in toluene. As for the polystyrenes in toluene the intrinsic viscosities of the polystyrene standards were determined to establish a new [η]-M-relationship. Fig. 33 shows the Huggins plots for the viscosimetric measurements of the polystyrenes in DEP.
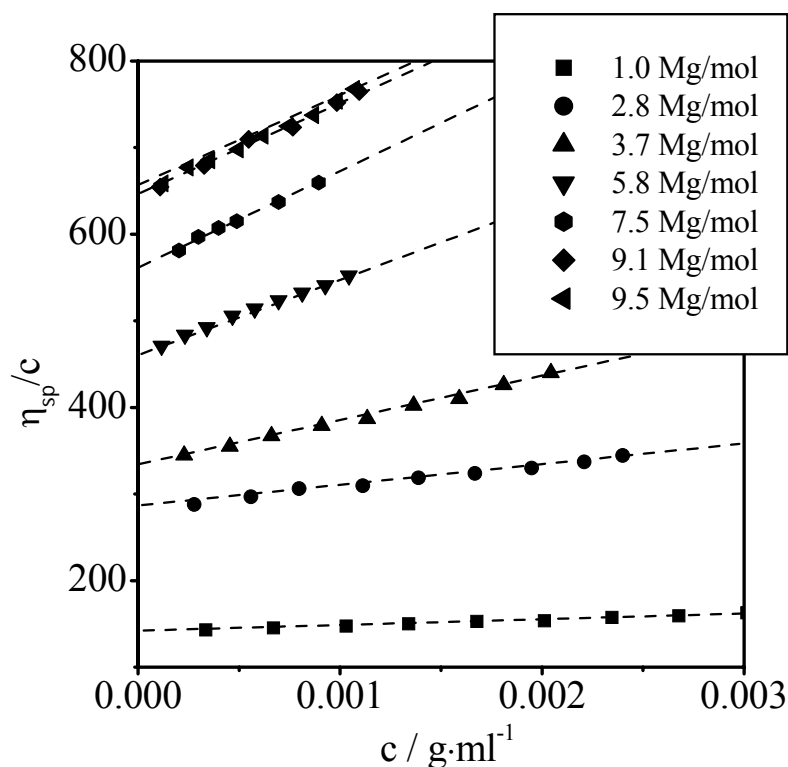
Figure 33: Huggins plots for the investigated polystyrenes in diethylphthalate, given molar masses are evaluated according to Eq. 138 (for experimental conditions see chapter 8.2).

The intrinsic viscosities determined are listed in Table 6.

Table 6: Intrinsic viscosities [η] of investigated polystyrene standards in diethylphthalate (DEP) with corrected M_w.

M_w / Mg/mol	1.0	2.8	3.7	5.8	7.5	9.1	9.5
[η] / cm³/g	140	283	339	464	559	644	669

For the viscosimetric measurements in DEP, the same trend as for the previous measurements in toluene is observed regarding the molar mass dependence of the intrinsic viscosity. The trend does not follow the expected intrinsic viscosities for the provided molar masses. The results obtained for the measurements in toluene are therefore confirmed.

Combining the measured intrinsic viscosities in DEP and the evaluated molar masses from the measurements in toluene gives a new [η]-M-relationship for polystyrene in diethylphthalate, as shown in Fig. 34.
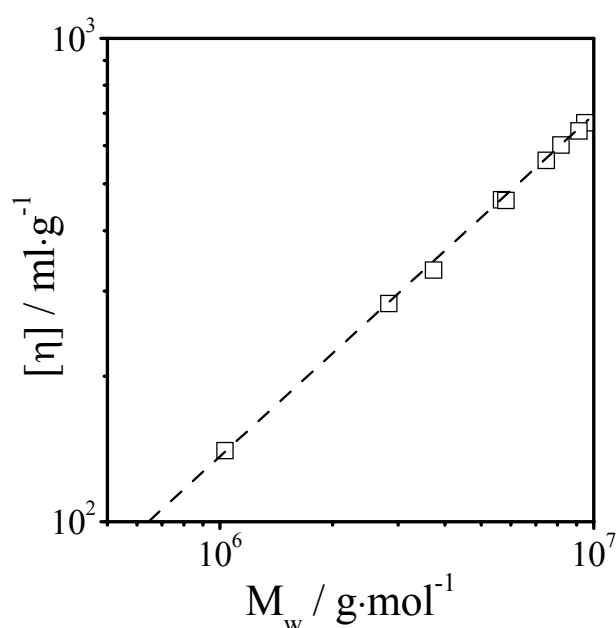
Figure 34: [η] versus M_w for the investigated polystyrene standards in diethylphthalate.

Linear regression of the data in Fig. 34 results in the [η]-M-relationship for polystyrene in DEP:

$$[\eta] = 8.23 \cdot 10^{-3} \cdot M_w^{0.702}$$

(Eq. 139)

As the factor *a* of 0.702 shows, DEP is a thermodynamically inferior solvent compared to toluene, the polymer coils therefore exist more compact in solution. However, theta conditions are not even remotely reached, because *a* does not show a value close to 0.5 (see chapter 3.1 for details). The influence of diethylphthalate as a solvent on the flow properties of polystyrene is to be discussed in chapter 6.1.

In addition to these two *"regular"* solvents, polystyrene oligomers are utilized as a solvent for the polystyrene standards in the upcoming chapters. The main effect these so-called *Boger fluids* [64, 135, 136] show is that the coils are almost in theta conditions and that the relaxation processes are slowed down to a high degree because of the pronounced zero-shear viscosity. This pronounced viscosity and the resulting increasing relaxation times for polystyrene fluids at a very low concentration lead to an enhanced detectability of relaxation processes as will be shown in chapter 6.1.3.1.

As the shear viscosity of polystyrene oligomers, and therefore also for the prepared Boger fluids themselves is very ample (about 50 Pas, see chapter 6.1.1 for details), viscosimetry is an analytical method that cannot be used to determine the coil dimensions of the polymer. However, one assumes that the polymer coil exists close to theta conditions, because the environment is very similar to a polymer melt [102], because the polymer coil does "see" only styrene in its neighbourhood. Solomon et al. [134] showed via viscosimetric measurements with polystyrene in a solvent mixture of styrene oligomers and dioctylphthalate (DOP) that the excluded volume factor ν lies beneath the ideal theta value of 0.5 (see chapter 3.2.3), as shown in Fig. 35.
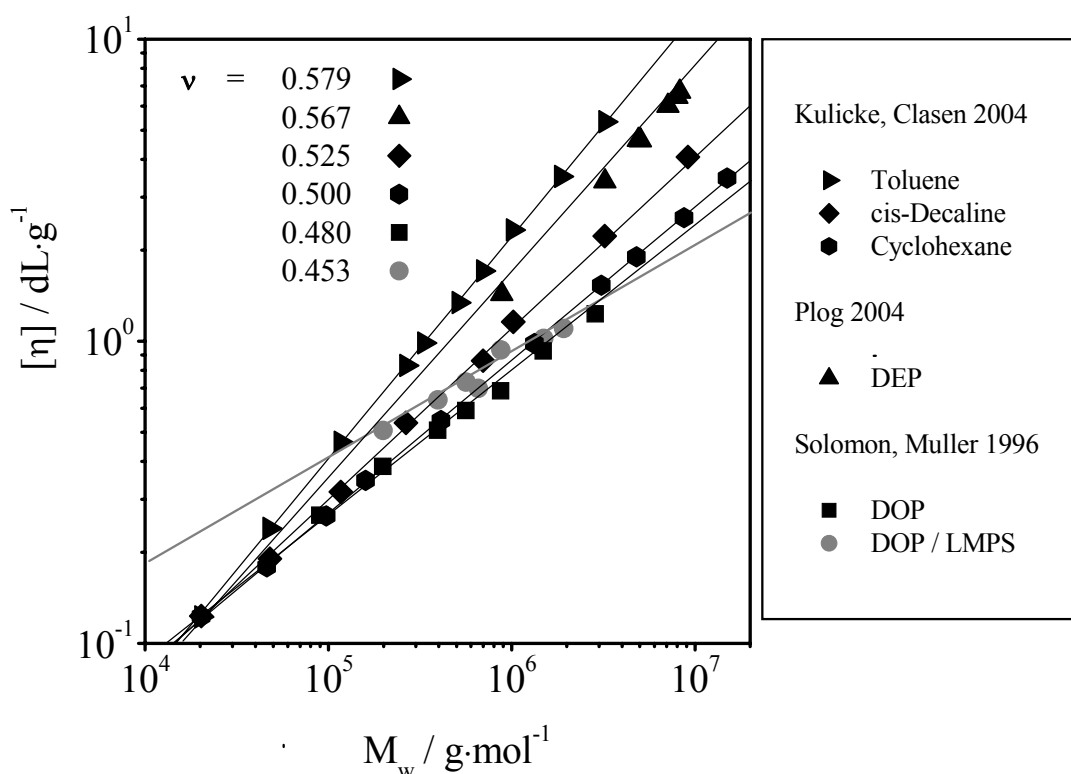
Figure 35: Intrinsic viscosity [η] versus weight-average molar mass M_w for polystyrene standards of varying molar masses in different solvents.

Fig. 35 shows that the [η]-M-relationships for polystyrene in the different solvents start from the same origin in molar mass of about 2×10^4 g/mol that is the critical molar mass the dissolved polystyrenechains start to form coils in solution. From this origin, the different [η]-M-relationships show a slope that is dependent of the thermodynamical quality of the solvent (see chapter 3.1). The [η]-M-relationship for polystyrene in a solvent mixture of DOP and low molar mass polystyrene (LMPS, styrene oligomer) yields an excluded volume factor

of 0.453 that corresponds to a factor *a* of 0.359. This means that the polymer coils in this solvent are shrinked below theta conditions. This can be explained by a preferential attraction of the better of the two solvents (styrene oligomere) in the solvent mixture to the polystyrene coil. The coil therefore contracts to reduce the amount of preferential concentration of the better solvent [137].

5.2 Molecular structural parameters of investigated MHECs

The investigated MHECs were provided by Wolff Cellulosics GmbH (for details on the polymer see chapter 2.2), and were blended from different native cellulosic pulp samples to provide different molar mass distributions (MMD, see chapter 3.2.3 for details) for the different application areas. However blending of cellulosic derivatives is also a standard method to minimize the effect of single native pulps on the shear viscosity and other flow properties of the finished product [47, 48].

The exact blending composition of the different MHEC samples is summarized in Table 2, together with the degree of substitution (DS) and molar degree of substitution (MS) for the complete blended samples.

As can be seen in Table 2, the different pulps used for blending of the samples differ in their molar mass or intrinsic viscosity, which results in different MMDs for the blended MHEC samples. In addition to this the investigated MHECs were split into two batches of 5 samples each, that were synthezised under different slurry conditions resulting in varying DS and MS for the batches, as can be seen in Table 2. According to the blending composition (provided by the manufacturer) in the first batch sample MHEC 5 should show the broadest distribution, followed by sample MHEC 1, MHEC 2, MHEC 3 and finally MHEC 4 with the most narrow distribution. For the second batch the same order is observed, starting with sample MHEC 10 and ending with sample MHEC 9, with decreasing width of the MMD.

As for the polystyrenes discussed in the previous chapter, the same structural parameters have to be determined for the investigated methyhydroxyethyl celluloses to correlate the molecular structure to the rheological behaviour discussed in the following chapters. Again the investigated MHECs were fully characterized in regards of their intrinsic viscosities in water as the solvent via viscosimetry (see chapter 3.1). The results are shown in Fig. 36 in form of the Huggins plots.
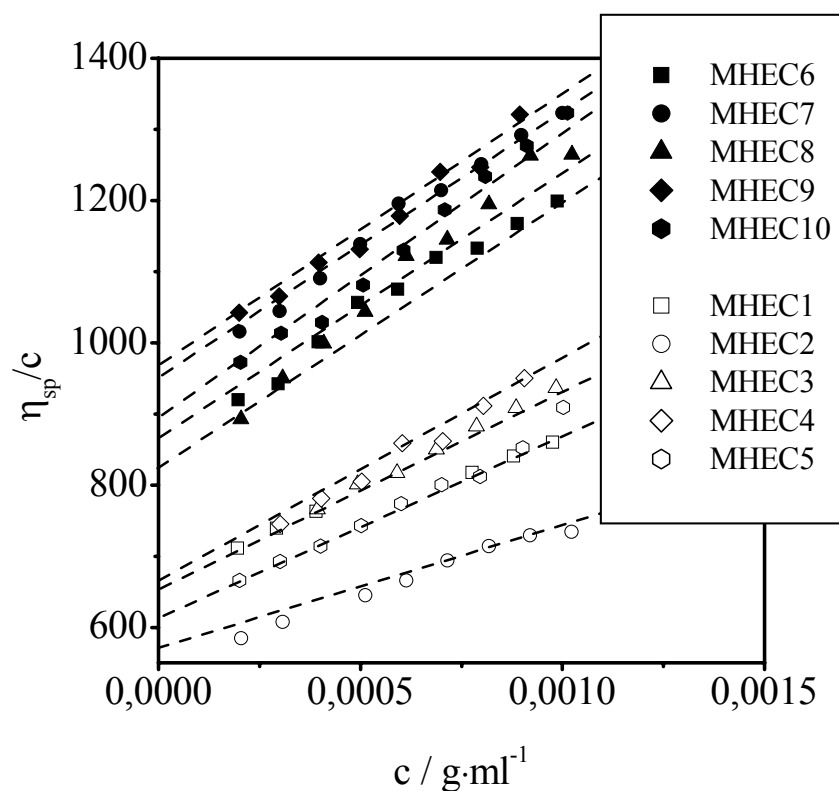
Figure 36: Huggins plots for the investigated MHECs in water (for experimental conditions see chapter 8.2).

As Fig. 36 shows, are the slopes $k_H \cdot [\eta]^2$ for all investigated MHECs about the same. The Huggins-coefficient k_H is in the order of (O)1, so that one can assume that the thermodynamical interactions of the coils with the solvent and therefore the solution structure is the same for all samples.

For more precise information on the solution structure or the quality of the solvent, the molar masses of the MHECs had to be determined. However, there is no [η]-M-relationship for MHEC in water that allows for direct evaluation of the molar masses, determination was achieved via combined means of SEC/MALLS/DRI (see chapter 3.2.3). The results for the two different batches are shown in Figs. 37 to 38 in form of the differential molar mass distributions and particle size distributions.
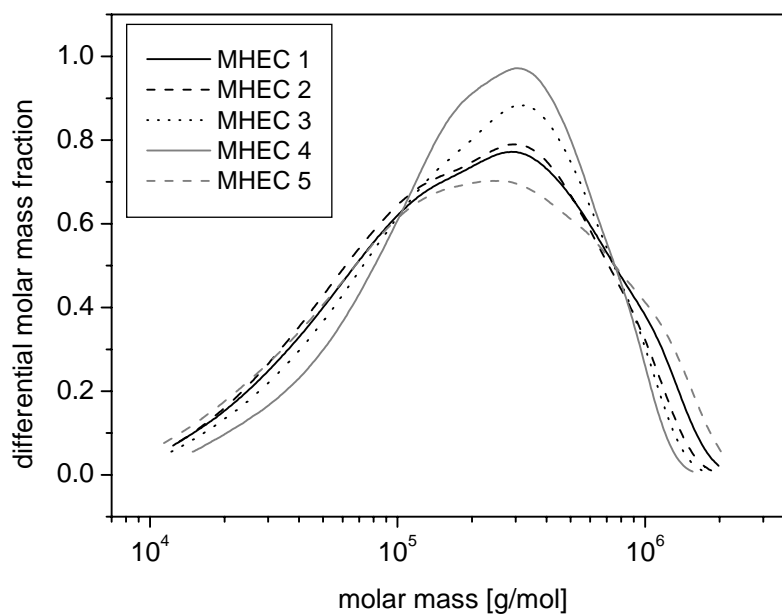
Figure 37: Differential molar mass distributions achieved via combined means of SEC/MALLS/DRI for the first batch of MHECs (MHEC 1-5, for experimental conditions see chapter 8.2).
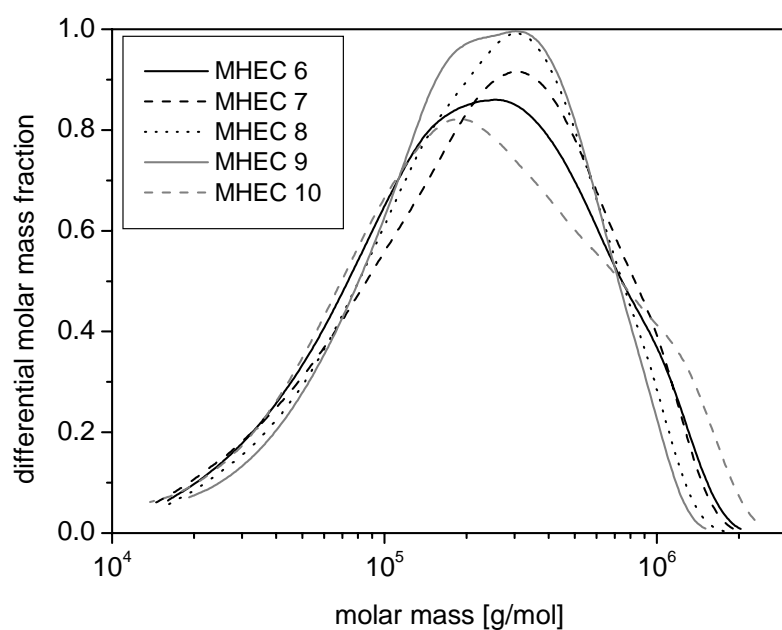
Figure 38: Differential molar mass distributions achieved via combined means of SEC/MALLS/DRI for the second batch of MHECs (MHEC 6-10, for experimental conditions see chapter 8.2).
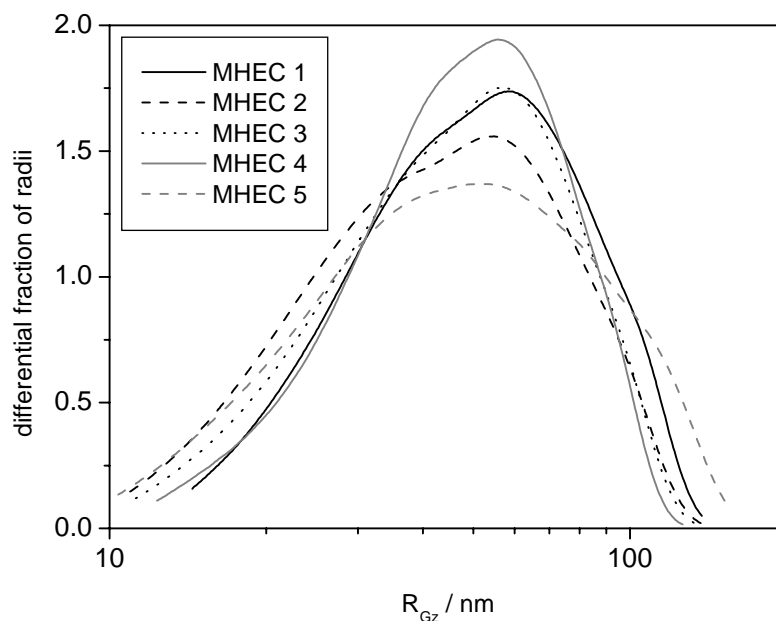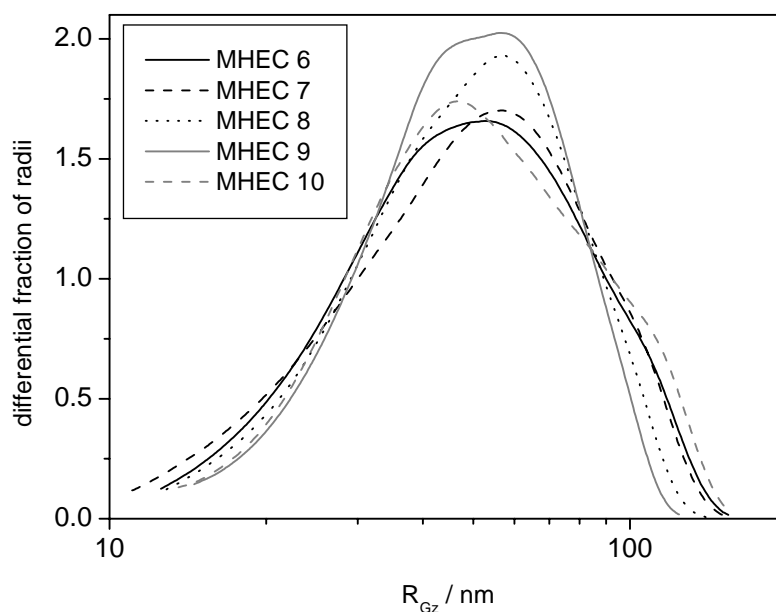
Figure 39: Differential particle size distributions achieved via combined means of SEC/MALLS/DRI for the first batch of MHECs (MHEC 1-5, for experimental conditions see chapter 8.2).

Figure 40: Differential particle size distributions achieved via combined means of SEC/MALLS/DRI for the second batch of MHECs (MHEC 6-10, for experimental conditions see chapter 8.2).

As can be seen in Fig. 37 and 38, the trend of width in the MMD correlates very well for both batches of samples with the expected order in blending composition (see Table 2 for details), the same accounts for the particle size distributions shown in Fig. 39 and 40. The

molecular structural parameters determined so far for the investigated MHECs are summarized in Table 3.

As one can see in Table. 3 the weight average molar masses M_w of the MHECs are very close together, varying from only 294 Kg/mol for the sample MHEC 2 to 360 Kg/mol for the sample MHEC 10. However, one has to keep in mind that the determined molar mass only accounts for the molecular dispersed fraction of the investigated polymer solution. As one can see in chapter 3.2.3 (Fig. 12) there is a series of filters and a precolumn in the light scattering device. Unsolvable parts of the solution are separated there to protect the SEC-columns from contamination. The molecular dispersed fraction of a sample is characterized by the recovery rate, ranging from 72-99 wt%.

The polydispersity M_w/M_n shows at least for the samples 2, 3, 4 and 5 (1st batch, varying from 2.3-3.5) and for the samples 7, 8, 9 and 10 (2nd batch, varying from 2.1-2.9) the expected order in regards of the blending composition (see Table 2). Another important characteristic of a polymer is its particle-, or better coil size, characterized via the radius of gyration R_G. It varies from 71 nm for the sample MHEC 2 to 91 nm for the sample MHEC 10; the samples show the same order as in regards of the molar mass.

Combining the information on the molecular structure achieved via light scattering leads to the R_G-M-relationship shown in Fig. 41.
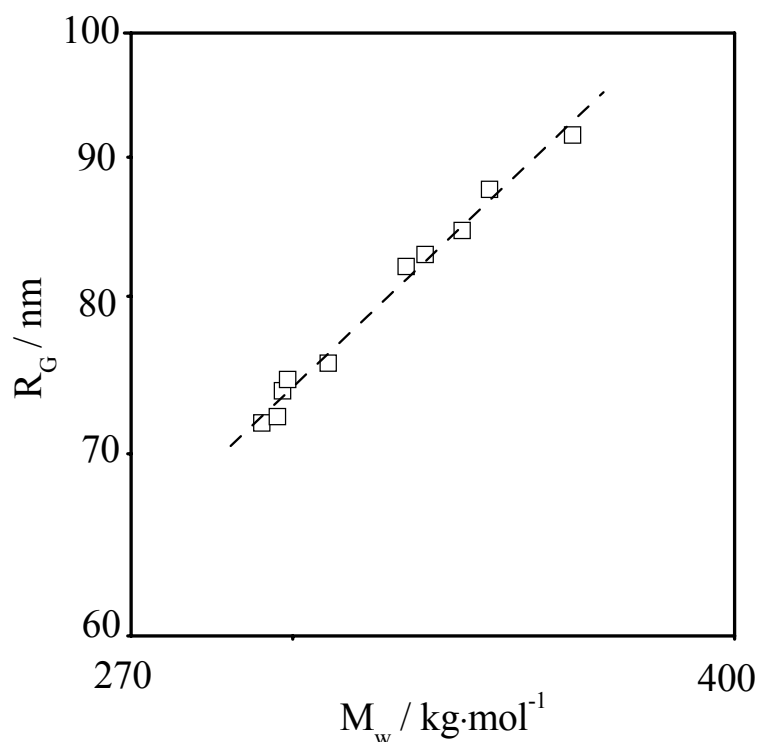

Figure 41: R_G as a function of M_w for the investigated MHECs 1-10.

Linear regression of the data in Fig. 41 results in the R_G-M-relationship for methylhydroxyethyl cellulose in water:

$$R_G = 2.33 \cdot 10^{-2} \cdot M_w^{0.58} \hspace{4cm} \text{(Eq. 140)}$$

With $a = 3\nu - 1$ one comes to a value of 0.74 for a, which means that water is a fairly good solvent for MHEC.

5.3 Molecular structural parameters of investigated hmHECs

The hmHECs investigated in this work were provided by our project partner Beiersdorf AG (see chapter 8.2 for details). The manufacturer gave just a few specifications on the polymers. These specifications are summarized in Table 7.

Table 7: Molecular structural parameters of the investigated hmHECs provided by manufacturer.

Sample	Lenght of hydrophobic modification[+]	Molar mass / Dalton[+]
hmHEC 1	*16*	*700.000*
hmHEC 2	*16*	*600.000*

[+] Data provided by the manufacturer

As this information on the molecular structure is a little "*insufficient*", the two investigated hydrophobically modified hydroxyethyl celluloses were characterized in the same manner as the polystyrenes and the MHECs, to get in the position to correlate the molecular structure to the rheological behaviour discussed in the chapters following.

First off the hmHECs were characterized in regards of their intrinsic viscosities in water as the solvent via viscosimetry. The results are shown in Fig. 42 in form of the Huggins plots.

When reducing the slope $k_H \cdot [\eta]^2$ with the intrinsic viscosity one comes to almost the same Huggins-coefficient k_H in the order of (O)1 for both samples, meaning that the thermodynamical interaction of the coils with the solvent water is comparable.
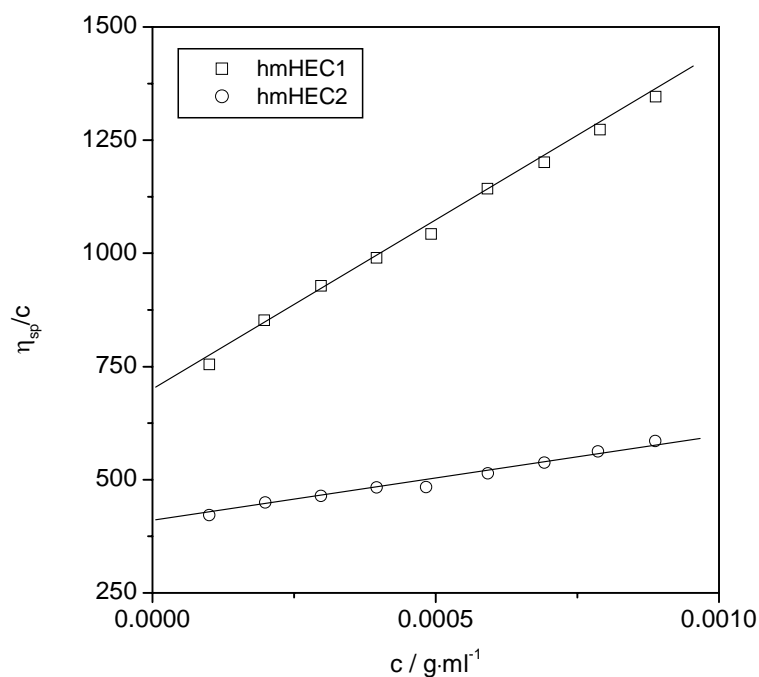
Figure 42: Huggins plots for the investigated hmHECs in water (for experimental conditions see chapter 8.2).

For determination of the molar mass and its distribution as for the particle size and its distribution of the two hmHECs, light scattering experiments have been accomplished. The results are shown in Fig. 43 and 44.
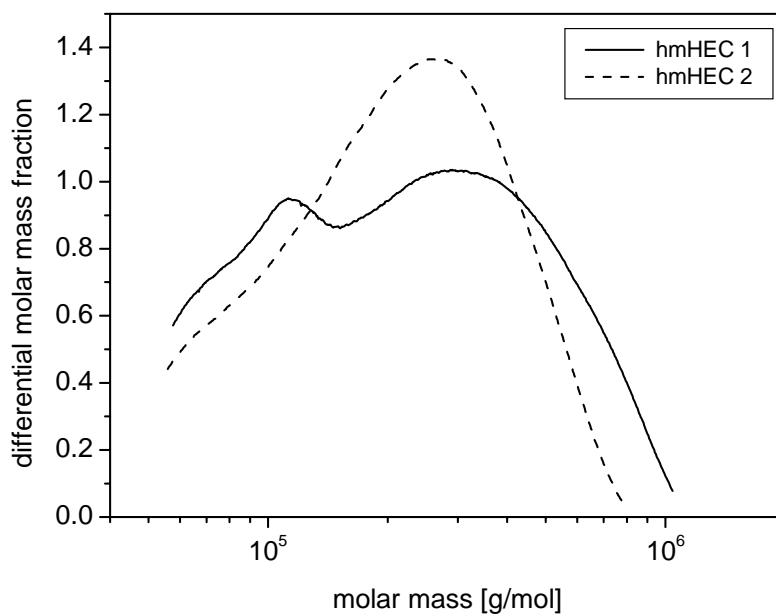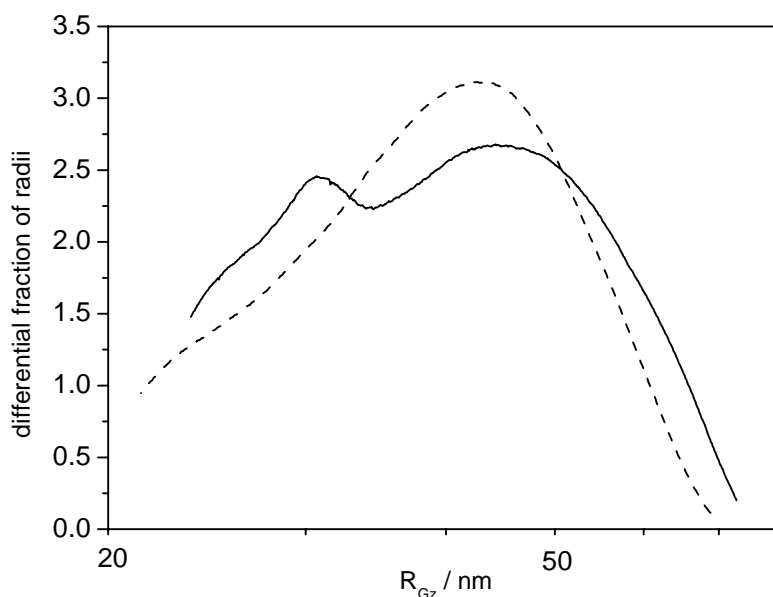

Figure 43: Differential molar mass distributions achieved via combined means of SEC/MALLS/DRI for the investigated hmHECs (experimental conditions see chapter 8.2).

Figure 44: Differential particle size distributions achieved via combined means of SEC/MALLS/DRI for the investigated hmHECs (experimental conditions see chapter 8.2).

The determined molecular structural parameters of the hmHECs are summarized in Table 4.

Figs. 43 and 44 and Table 4 show that the two investigated hmHECs exhibit almost the same weight average molar mass M_w, but a very different shape of its distribution. As the sample hmHEC 1 shows almost a bimodal distribution, the MMD of sample hmHEC 2 is more narrow, which reflects in the different polydispersities.

However, one has to keep in mind, as earlier described (compare Table 3 in chapter 2.2), that the determined structural molecular parameters only account for the molecular dispersed fraction of the investigated solution. The recovery rates of the light scattering measurements here are very low at about 50 wt.% for the hmHECs. This is due to the fact that these hydrophobically modified cellulosic derivatives tend to pronounced structure build-up via hydrogen-bonding and hydropgobic interactions. These gel structures are again separated from the investigated solution via filters and the pre-column in the light scattering device (see Fig. 12 in chapter 3.2.3).

6 Results and Discussion

6.1 Rheological characterisation of investigated polystyrenes

6.1.1 Steady shear flow

The polystyrene standards investigated in this work were fully characterized in regards of their viscous properties via shear flow experiments. The influencing parameters on the shear behaviour examined in this chapter include the concentration, the molar mass (and its distribution) and the solvent.

In former works accomplished in this working group the concentration and molar mass dependence of the viscous behaviour could already be shown for the system polystyrenes in toluene [44]; The molar mass dependence of the zero-shear viscosity is shown in Fig. 45, the concentration dependence of the zero-shear viscosity is shown in Fig. 46.
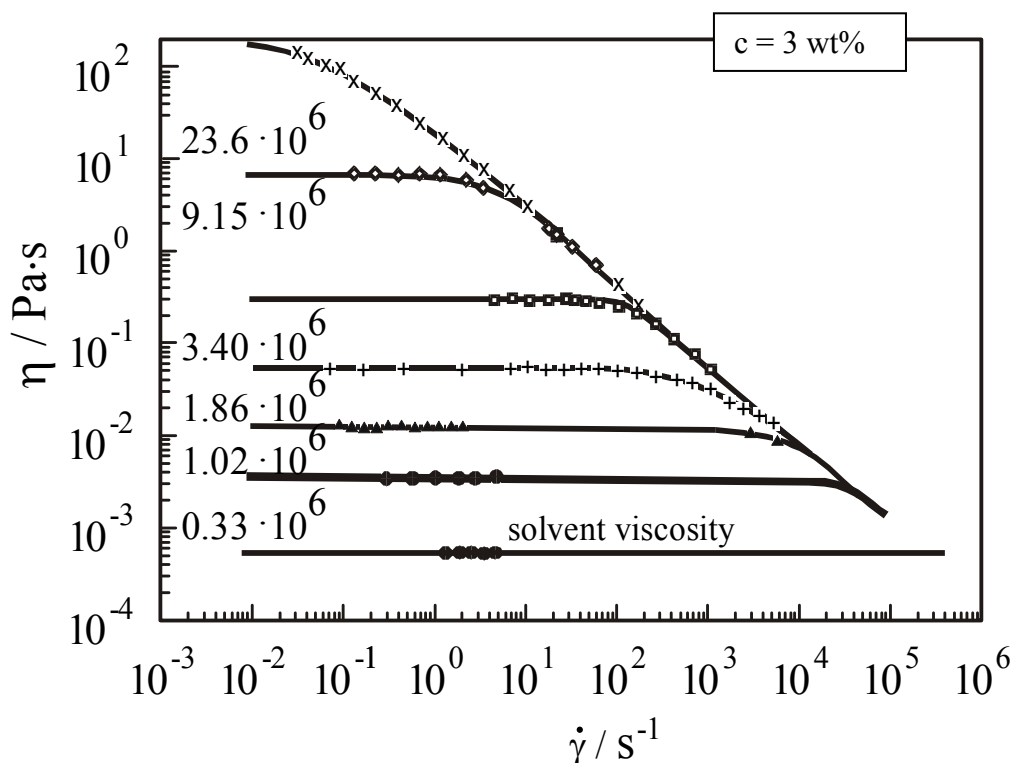

Figure 45: Molar mass dependence of the zero-shear viscosity for polystyrene solutions in toluene (3 wt%) for different molar masses (shown in g/mol in the figure) at 25°C (data taken from [44]).
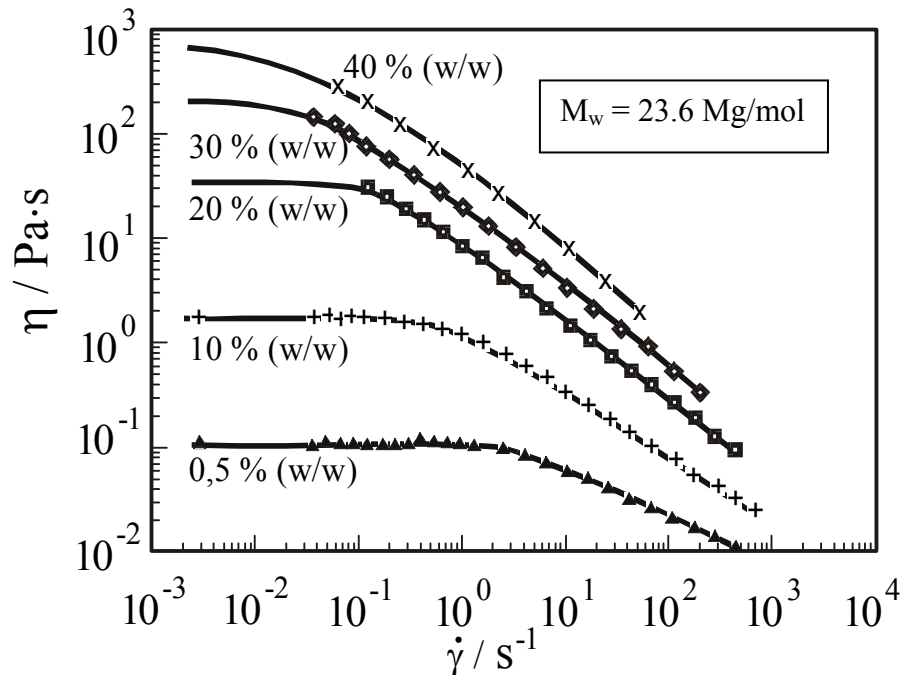
Figure 46: Concentration dependence of the zero-shear viscosity for polystyrene solutions in toluene (23.6 Mg/mol) for different concentrations at 25°C (data taken from [44]).

As Fig. 45 and Fig. 46 show, the influence of the concentration on the zero-shear viscosity is more pronounced than the influence of the molar mass, the viscosity scales with a higher power for an increasing concentration, than for an increasing molar mass.

For semi dilute network solutions the dependence of the shear viscosity from the shear rate observed in Fig 45 and 46 was described by Graessley [122] via the Entanglement concept (see chapter 4.4.1). At small shear rates, the entanglements between the single polymer coils are unravel. However, they entangle again at the same time scale, so that the total number of entanglements keeps constant and therefore also the viscosity, which depends mainly on tghe entanglement density. At a critical shear rate $\dot{\gamma}_{crit.}$, that corresponds to the reciprocal value of the longest relaxation time τ_0 of the polymer solution, the shear viscosity decreases, because more entanglements are unraveled than build up. The flow curves in Fig. 45 show all the same slope of -0.818, that was derived theoretically as the highest slope achievable by Graessley for polymer melts and concentrated polymer solutions, even though the molar masses of the polystyrenes investigated are different from each other. However the concentration is constant for the solutions, so that after complete disentanglement of the coils, the viscosity is only influenced by the segment density. As this segment density is constant for a constant concentration, the slope of the flow curves has to be the same. In Fig. 46 the investigated solutions do not have the same segment density because of different concentrations, so that the resulting slopes in the non-Newtonian flow regime differ from each other.

The polystyrene standards investigated in this work were additionally characterized in regards of their visco-elastic flow behaviour in other solvents than toluene. Fig. 47 shows the flow curves for the investigated polystyrene standards in diethylphthalate (DEP) at a constant concentration of 1.0 wt% at a temperature of 25°C.

Diethylphthalate was chosen as a solvent, because its solvent quality was suposed to be closer to θ-conditions (see chapter 3.1) than for toluene. As the elastic components of the investigated solutions were of high interest (see upcoming chapters) a thermodynamical worse solvent than toluene was chosen, because of the resulting elasticity enhancement via coil shrinkage. As could be seen in chapter 5.1 that is only partly true as altogether DEP is thermodynamically very similar to toluene. Nevertheless, DEP is a good solvent to use, because its vaporating- and boiling points are much higher than for toluene, so that the solutions prepared are much longer stable in DEP than for toluene.
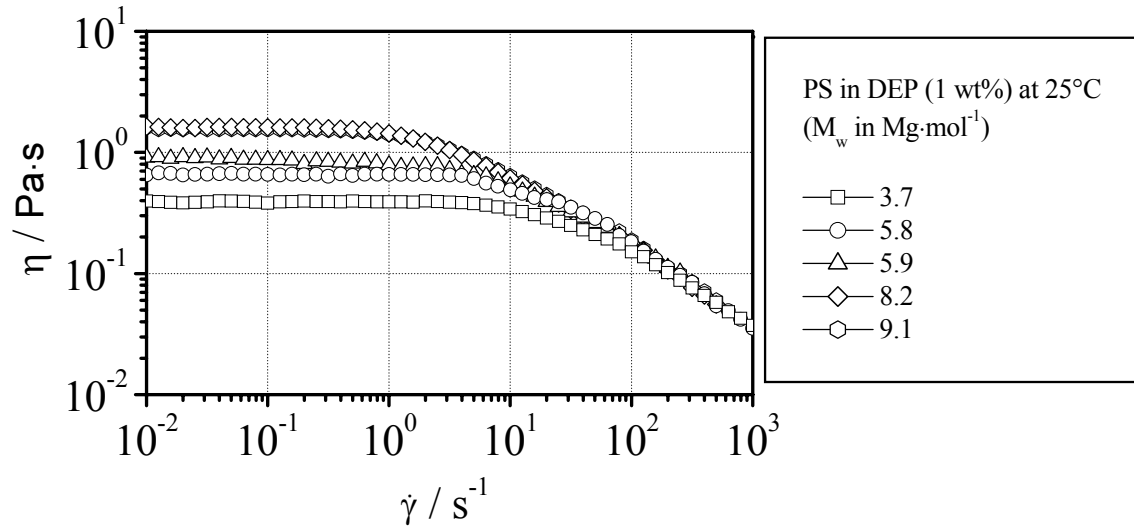

Figure 47: Shear viscosity η versus shear rate $\dot{\gamma}$ for polystyrene standards with different molar masses (see Table 1 for details) in diethylphthalate (1.0 wt%) at 25°C.

As Fig. 47 shows, the zero-shear shear viscosity can be detected for all molar masses at a concentration of 1.0 wt%, giving the highest value of 1.6 Pas for the 9.1 Mg/mol polystyrene and the lowest value of 0.4 Pas for the 3.7 Mg/mol polystyrene. The critical shear rate shifts to smaller values for an increaing molar mass, because the longest relaxation times resulting via the reciprocal value increase with molar mass.

To quantify the viscous and elastic components of shear flow the shear stress σ and the first normal stress difference N_1 are the right means. Fig. 48 shows these material functions for the poylstyrene standards already investigated in Fig 47.
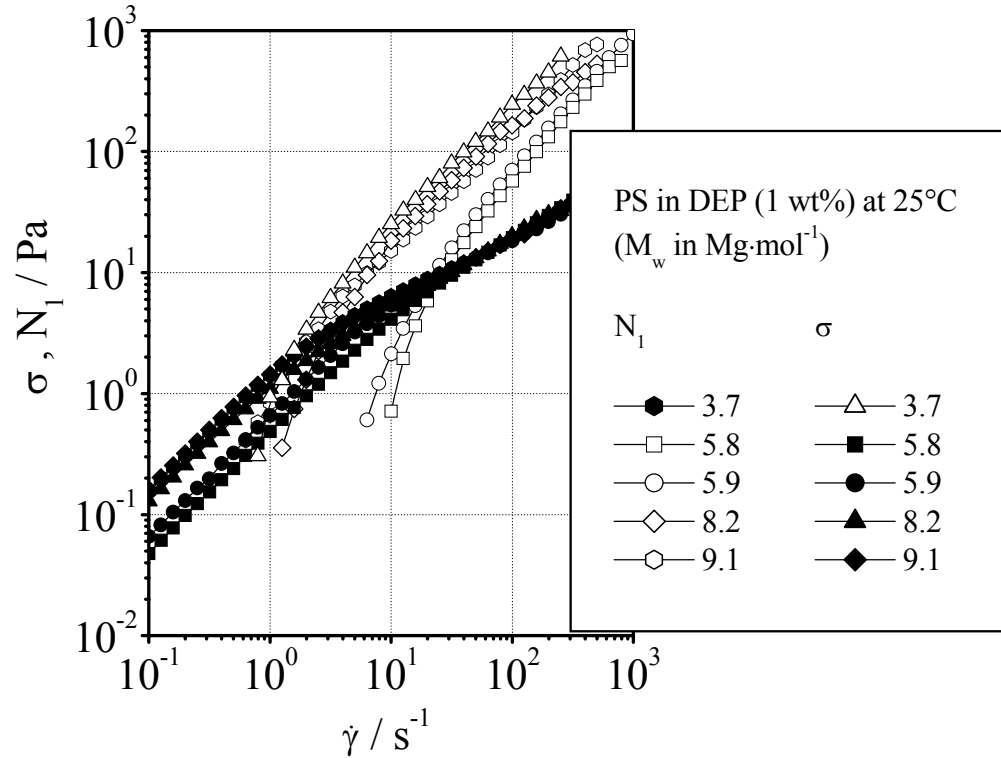
Figure 48: Shear stress σ and 1ˢᵗ normal stress difference N₁ versus shear rate γ̇ for polystyrene standards with different molar masses (see Table 1 for details) in diethylphthalate (1.0 wt%) at 25°C.

The shear stresses, representing the viscous part of the shear flow behaviour, for the investigated polystyrenes shown in Fig. 48 all follow, as expected, almost the same trend. However, the first normal stress differences, representing the elastic part of the shear flow behaviour, show a slightly more distinctive trend for the different molar masses, above all in regards of the shear rate where N_1 occurs. As expected the first normal stress difference occurs at lower shear rates with increasing molar mass. However, the differences between the three samples with the higher molar masses (5.9-9.1 Mg/mol) and the two samples with the lower molar masses (3.7-5.8 Mg/mol) are not very pronounced.

To investigate the influence of the solvent quality on the elastic behaviour of polystyrene, two additional solvents were used for determination of the material functions of shear flow. In Fig. 49 the shear viscosity η and the first normal stress difference N_1 is compared for the sample with a molar mass of 8.2 Mg/mol at 2.0 wt% in the solvents toluene, DEP and trans decalin.
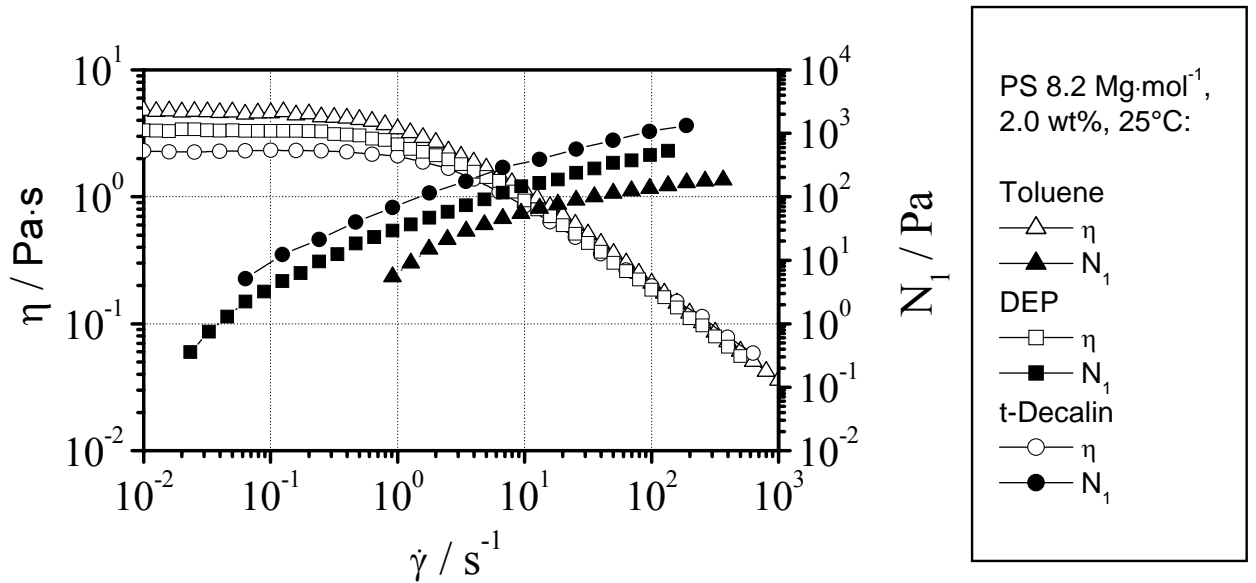
Figure 49: Shear viscosity η and first normal stress difference N_1 versus shear rate $\dot{\gamma}$ for a polystyrene standard with M_w = 8.2 Mg/mol at 2.0 wt% in different solvents at 25°C.

As one can see in Fig. 49, the zero-shear viscosity is dependent on the coil expansion. With increasing thermodynamical quality of the solvent, the zero-shear viscosity increases, for the elastic component of shear flow, the first normal stress difference N_1, the opposite trend can be observed. With decreasing coil expansion, that is with decreasing thermodynamical quality of the solvent the onset and the maximum value of N_1 shifts to lower shear rates.

To emphasise the influence of the concentration on the shear flow behaviour, Fig. 50 comprisingly shows the results for steady shear flow for the polystyrene standard with a molar mass of 5.8 Mg/mol in DEP for various concentrations ranging from 0.0001 – 5.0 wt%. The zero-shear viscosities in this concentration range vary from approx. 0.002 – 350 Pas, over almost five orders of viscosity. The slope of the flow curves in the non-Newtonian flow regime reach almost the maximum value of 0.818 for the solution with a concentration of 5.0 wt%, because at this concentration the state of the concentrated network solution is reached (see chapter 4.4.3 for details). From a concentration of 0.1 wt% on, no shear thinning behaviour can be observed anymore, the shear viscosity remains constant, means that the solutions show just Newtonian behaviour.
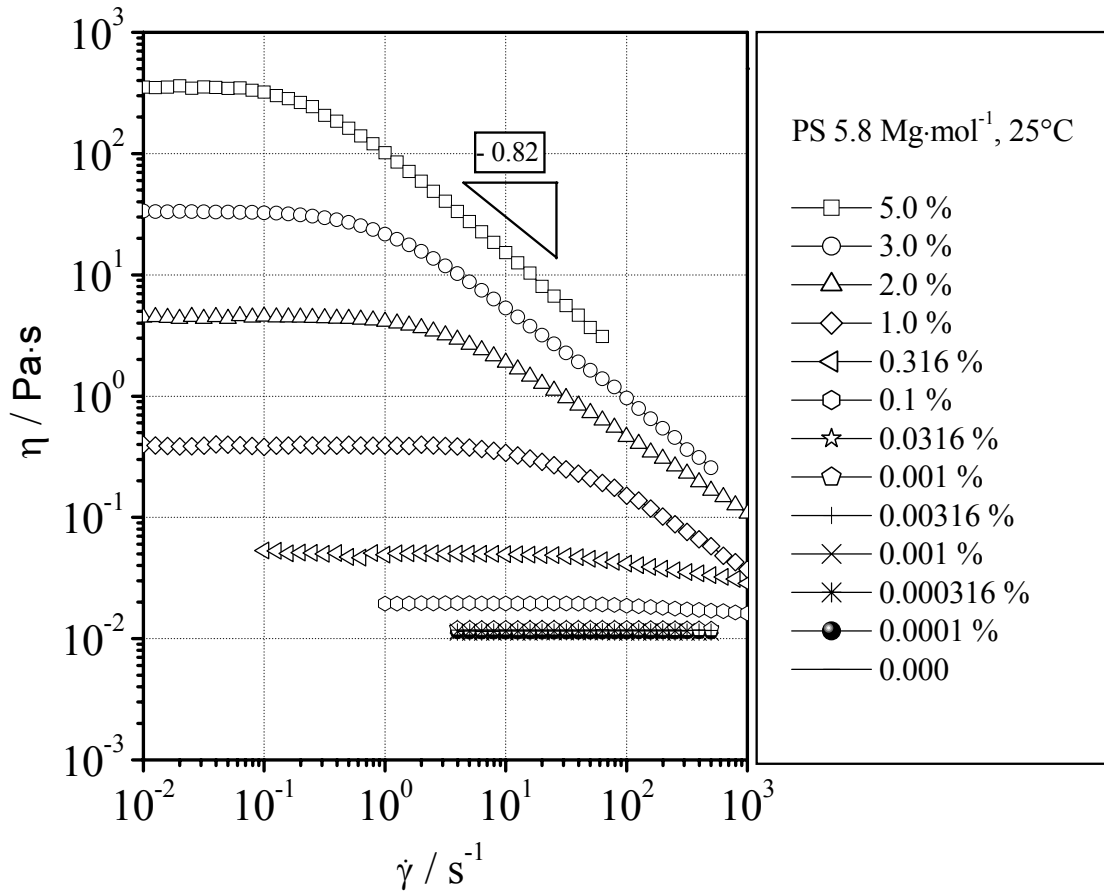
Figure 50: Shear viscosity η versus shear rate $\dot{\gamma}$ for a polystyrene standard with M_w = 5.8 Mg/mol at different concentrations in diethylphthalate at 25°C.

6.1.1.1 Structure-property-relationships of shear flow

For the regime of the semi dilute solutions (see chapter 4.4.3 for details) one can summarize the flow properties in form of the shear viscosity η quantitativly via a series of so-called structure-property relationships. As varying parameter the so-caled opverlap parameter, the product of concentration c and intrinsic viscosity $[\eta]$, is used instead of the molar mass M_w, because it incorporates the solvent influence on the coil size [132]. However, it can always be transferred to the molar mass via the Mark-Houwink-Sakurada-relationship (see chapter 3.1 Eq. 12).

The zero-shear viscosity (or specific viscosity) η_0 or η_{sp} can then be plotted as a function of the overlap parameter $c[\eta]$ as shown in Fig. 51 for the investigated polystyrenes in diethylphthalate. A mathematical discription of this correlation is given via an extended Huggins virial equation (see Eq. 9) [44]:

$$\eta_{sp} = c \cdot [\eta] + k_H \left(c \cdot [\eta] \right)^2 + B_n \left(c \cdot [\eta] \right)^n \qquad \text{(Eq. 141)}$$

Whereas the Huggins-Equation (see Eq. 9) breaks of after the second term, which is perfect for particle solutions, complete description including network solutions is achieved via the higher order terms, combined in one with a power of n.

The dependence of the zero-shear viscosity from the overlap parameter can then be described via following relationship:

$$\eta_0 = \eta_S \left(c \cdot [\eta] + k_H \left(c \cdot [\eta] \right)^2 + B_n \left(c \cdot [\eta] \right)^n + 1 \right) \qquad \text{(Eq. 142)}$$
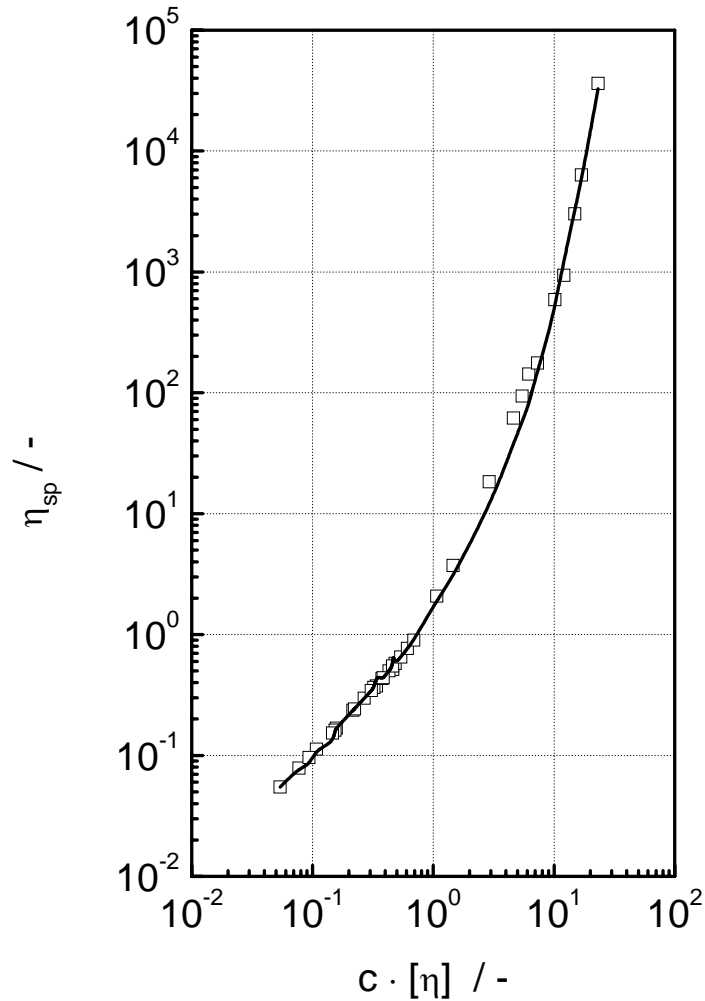

Figure 51: Specific viscosity η_{sp} versus overlap parameter $c[\eta]$ for polystyrene in diethylphthalate. The solid line corresponds to the linear regression according to Eq 141.

In addition to the Huggins constant K_H and the intrinsic viscosity $[\eta]$, determined via viscosimetric measurements (see chapter 3.1) the constants B_n and n are essential; They can be achieved via linear regression of the curve at high overlap parameters $c[\eta]$. This leads to the $\eta_0 - [\eta] - c$-relationship for polystyrene in diethylphthalate:

$$\eta_0 / Pa \cdot s = 1.10 \cdot 10^{-2} \left(c \cdot [\eta] + 0.368 \cdot c \cdot [\eta]^2 + 8.46 \cdot 10^{-3} \cdot c \cdot [\eta]^{4.82} + 1 \right) \qquad \text{(Eq. 143)}$$

The exponent n is theoretically correlated to the exponent a of the Mark-Houwink-Sakurada-relationship and therefore incorporates the solvent quality.

$$n = \frac{3.4}{a}$$

(Eq. 144)

Because of its easy handling these $\eta_0 - [\eta] - c$- or $\eta_0 - M - c$-relationships were provided for various polymer-solvent systems in the past [1]

The dependence of the longest relaxation time on different molecular parameters for dilute solutions was already described by Rouse and Ferry [110, 138] (see chapter 4.1.3 for details). Here the interest lies on the longest relaxation time τ_0 because it is the reciprocal value of the critical shear rate $\dot{\gamma}_{crit.}$, the shear rate where the shear viscosity leaves the Newtonian flow regime. The longest relaxation time of dilute solutions as well as concentrated soltions here is directly correlated with the molar mass [139, 140]. The influence of the solvent can be accounted for with a modification of the Rousse model via the intrinsic viscosity [45, 46]:

$$\tau_0 = K_\tau \cdot c^{-(1+1/a)} \cdot \left(\left(c \cdot [\eta] \right)^2 + K_H \cdot \left(c \cdot [\eta] \right)^3 + B_n \cdot n \left(c \cdot [\eta] \right)^{n+1} \right)$$

(Eq. 145)

Plotting of $\tau_0 \cdot c^{1+1/a}$ versus the overlap parameter $c[\eta]$ gives a mastercurve that takes into account only the third term of Eq. 145, because the non-Newtonian flow regime is usually not to be detected in dilute solutions. Fig. 52 shows this plot for the investigated polystyrenes in diethylphthalate.
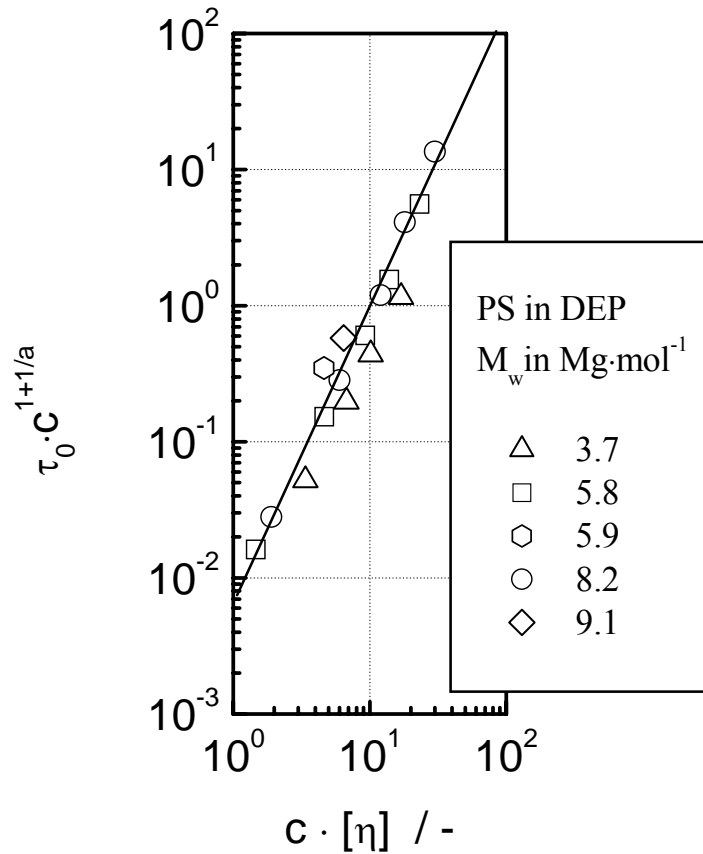
Figure 52: Longest relaxation time of shear flow τ_0 versus overlap parameter $c[\eta]$ for polystyrene in diethylphthalate. The solid line corresponds to the linear regression of the third term of Eq 145.

This leads to the $\tau_0 - [\eta] - c - relationship$ for polystyrene in diethylphthalate:

$$\tau_0 / s = 1.29 \cdot 10^{-10} \cdot c^{-2.423} \cdot \left(\left(c \cdot [\eta] \right)^2 + 0.368 \cdot \left(c \cdot [\eta] \right)^3 + 8.46 \cdot 10^{-3} \cdot \left(c \cdot [\eta] \right)^{5.82} \right) \qquad \text{(Eq. 146)}$$

Another crucial parameter to describe a flow curve is the slope n in the non-Newtonian flow regime. Whereas for polymer melts and concentrated polymer solutions a constant slope of about -0.818 is observed, which was theoretically derived via the entanglement concept by Graessley [122, 139], the slopes of the flow curves of polymer solutions in the semi dilute state of solution are often not as steep. Fig. 53 shows the slopes n of the flow curves for polystyrene in DEP as a function of the overlap parameter $c[\eta]$.
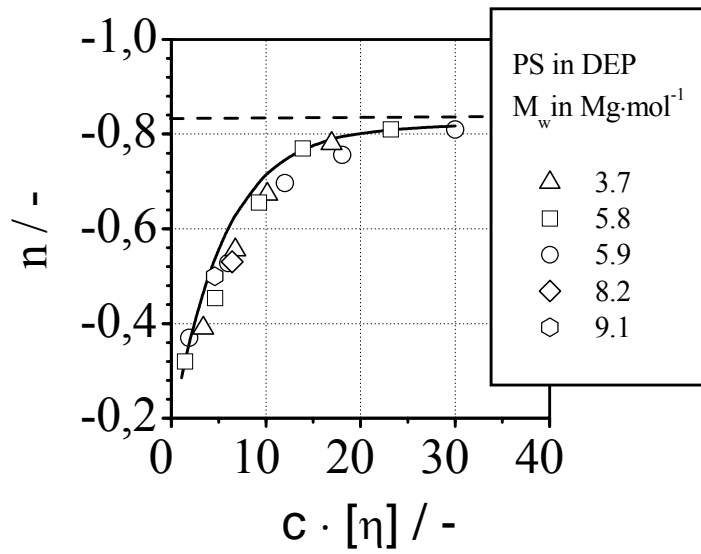
Figure 53: Slope of the flow curve n in the non-Newtonian flow regime versus overlap parameter $c[\eta]$ for polystyrene in diethylphthalate. The solid line corresponds to the $n - [\eta] - c$ -relationship (Eq.147).

The slope of the flow curve n can also be described via a virial equation of the overlap parameter [45]:

$$n = -0.82 + k_{n1} \cdot 10^{k_{n2} \cdot c[\eta]}$$ (Eq. 147)

The constants k_{n1} and k_{n2} can be determined via linear regression according to Eq. 148, as can be seen in Fig. 54:

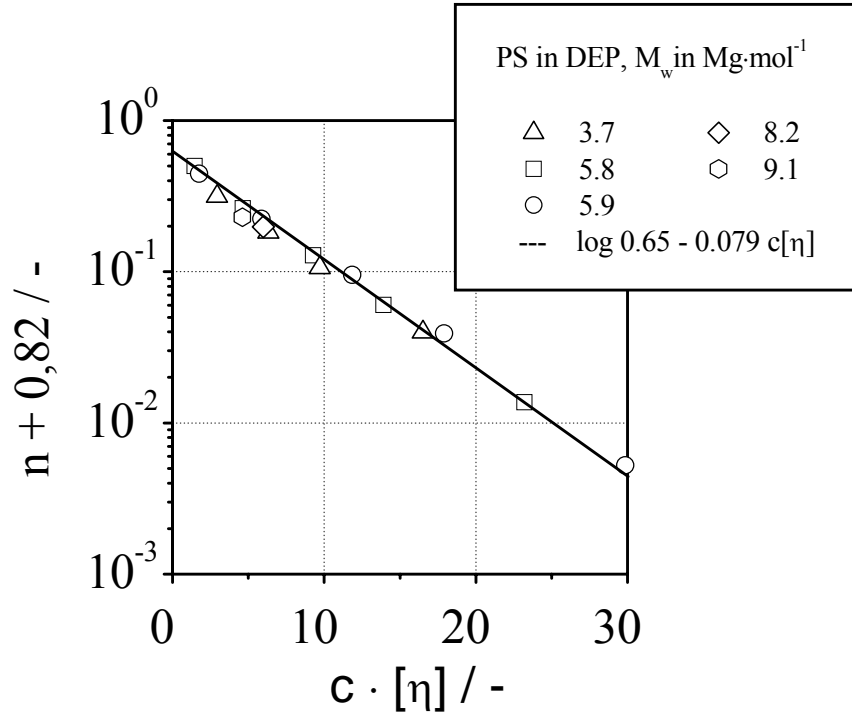$$\log(n + 0.82) = \log k_{n1} + k_{n2} \cdot c[\eta]$$ (Eq. 148)

Figure 54: Slope of the flow curve n in the non-Newtonian flow regime versus overlap parameter $c[\eta]$ for polystyrene in diethylphthalate according to Eq. 148. The solid line corresponds to the linear regression of the presented data.

The description of the shear flow behaviour of a polymer fluid over the whole regime of shear rates is possible via its critical parameters. As can be seen in Fig. 55 a normalization of the flow curves for polystyrene in DEP is possible via reduced variables like η / η_0 and $\dot{\gamma} \cdot \tau_0$ with normalization of the slopes. Whereas this normalization is very accurate for the purely Newtonian or non-Newtonian flow regime, minor derivations can be observed in between these two regimes close to a reduced shear rate of $\dot{\gamma} \cdot \tau_0 = 1$, which is due to different widths of the transition area. A closer investigation of this transition area can be achieved via the modified Carreau model [141, 142]:

$$\eta = \eta_0 \cdot \left[1 + \left(\dot{\gamma} \cdot \tau_0 \right)^b \right]^{\frac{n}{b}} \hspace{3cm} \text{(Eq. 149)}$$

Besides the parameters zero-shear viscosity η_0, longest relaxation time τ_0 and slope of the flow curve *n*, the modified Carreau model uses the so-called transition parameter *b* to fit the shear viscosity.

However, the transition parameter is independent of molar mass and concentration, it only depends on the width of the molar mass distribution of the investigated polymer [65]. Further discussion on this specific topic will follow in chapter 6.1.3.2.
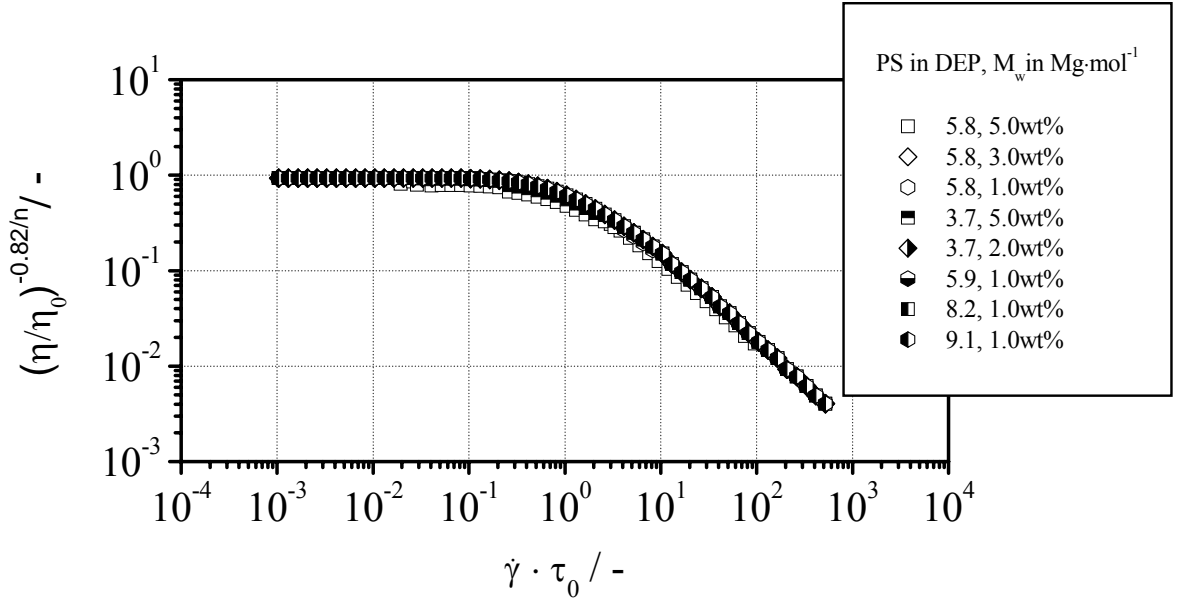
Figure 55: Reduced viscosity $\eta / \eta_0^{-0.82/n}$ versus reduced shear rate $\dot{\gamma} \cdot \tau_0$ for polystyrene in diethylphthalate at different molar masses and concentrations.

With the modified Carreau model, it is now possible to evaluate the shear viscosity of the investigated polymer fluid over the whole range of shear rates. The crucial parameters needed for the evaluation are obtained via the different structure-property-relationships discussed in this chapter. Table 8 gives an overview on these structure property-relationships obtained for the system polystyrene in diethylphthalate.

Table 8: Structure-property-relationships of shear flow for the investigated polystyrenes in diethylphthalate.

$\eta_0 - [\eta] - c$	$\eta_0 / Pa \cdot s = 1.10 \cdot 10^{-2} \left(c \cdot [\eta] + 0.368 \cdot c \cdot [\eta]^2 + 8.46 \cdot 10^{-3} \cdot c \cdot [\eta]^{4.82} + 1 \right)$
$\tau_0 - [\eta] - c$	$\tau_0 / s = 1.29 \cdot 10^{-10} \cdot c^{-2.423} \cdot \left(\left(c \cdot [\eta] \right)^2 + 0.368 \cdot \left(c \cdot [\eta] \right)^3 + 8.46 \cdot 10^{-3} \cdot \left(c \cdot [\eta] \right)^{5.82} \right)$
$n - [\eta] - c$	$n = -0.82 + 0.65 \cdot 10^{0.079 \cdot c[\eta]}$

6.1.2   Small amplitude oscillatory shear (SAOS)

To quantify the visco-elastic flow behaviour of polymer solutions, oscillatory experiments have to be accomplished according to the *Rheological Circle* [65] (see Fig. 13). The elastic components of a polymer solution can then directly be correlated with the storage modulus *G'*, whereas the viscous components are represented by the loss modulus *G''* (see chapter 3.3.2 for a detailed discussion).
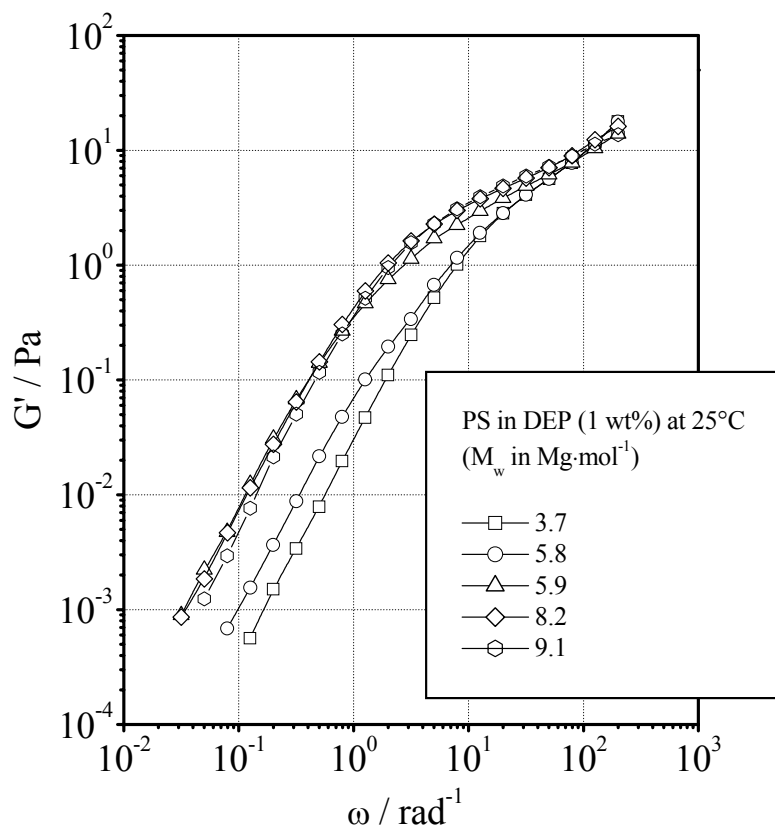

Figure 56: Storage modulus G' versus angular frequency ω for polystyrene standards with different molar masses (see Table 1 for details) in diethylphthalate (1.0 wt%) at 25°C.

For investigation of the molar mass dependence of the moduli of SAOS measurements, Figs. 56 and 57 show exemplarily the storage- and the loss moduli for the investigated polystyrene standards at 1.0 wt% in diethylphthalate for the different molar masses at 25°C.

As one can see in Figs. 56 and 57, the evolution of the moduli *G'* and *G''* with increasing angular frequency *ω* is very much the same for the whole range of molar masses from 3.7 – 9.1 Mg/mol. The slopes at low frequencies very much reflect the theoretical values of 2 for the elastic component *G'* and 1 for the viscous component *G''*. For this concentration of 1.0 wt% the plateau value of the storage modulus is not reached in the investigated regime of angular frequencies. The network parameters of the temporary networks, that are build-up via the polymer coils that can not slide along each at high frequencies, can thus not be determined.
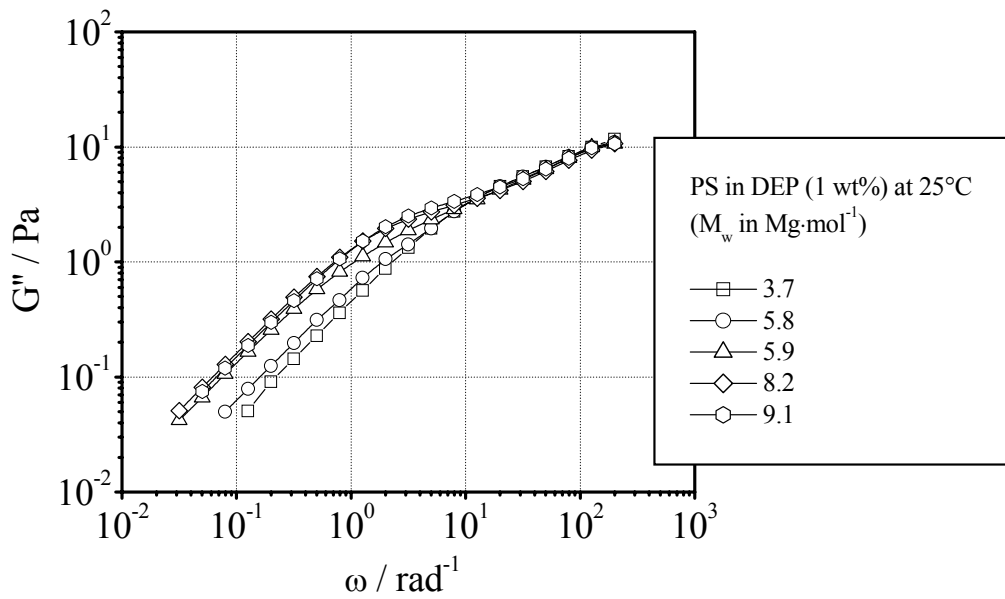
Figure 57: Loss modulus G'' versus angular frequency ω for polystyrene standards with different molar masses (see Table 1 for details) in diethylphthalate (1.0 wt%) at 25°C.

For investigation of the concentration dependence of the moduli, Figs. 58 and 59 show the storage- and the loss moduli G' and G'' for the investigated polystyrene standard with a molar mass of M_w = 5.8 Mg/mol for a concentration range from 0.00316 – 5.0 wt% in diethylphthalate at 25°C.

As Figs. 58 and 59 demonstrate has the concentration, as expected, a far more pronounced influence on the visco-elastic properties of the investigated polystyrene than the molar mass. In the investigated range of concentrations the slopes at low frequencies equal the theoretical values of 2 for the elastic component G' and 1 for the viscous component G'' like expected for a standard system.

However, the plateau modulus G'_p here is only reached for the higher concentrated solutions with 5.0- and 3.0 wt%. As can be seen in Fig. 58 the 5.0 wt% solution has a value of approx. 300 Pa for the plateau modulus, for the 3.0 wt% solution the plateau modulus has a value of approx. 100 Pa. For the lower concentrations from 0.00316 – 2.0 wt% the angular frequency is still not high enough to prevent the entangled polymer coils from relaxation, plateaus in G' are thus not reached yet.
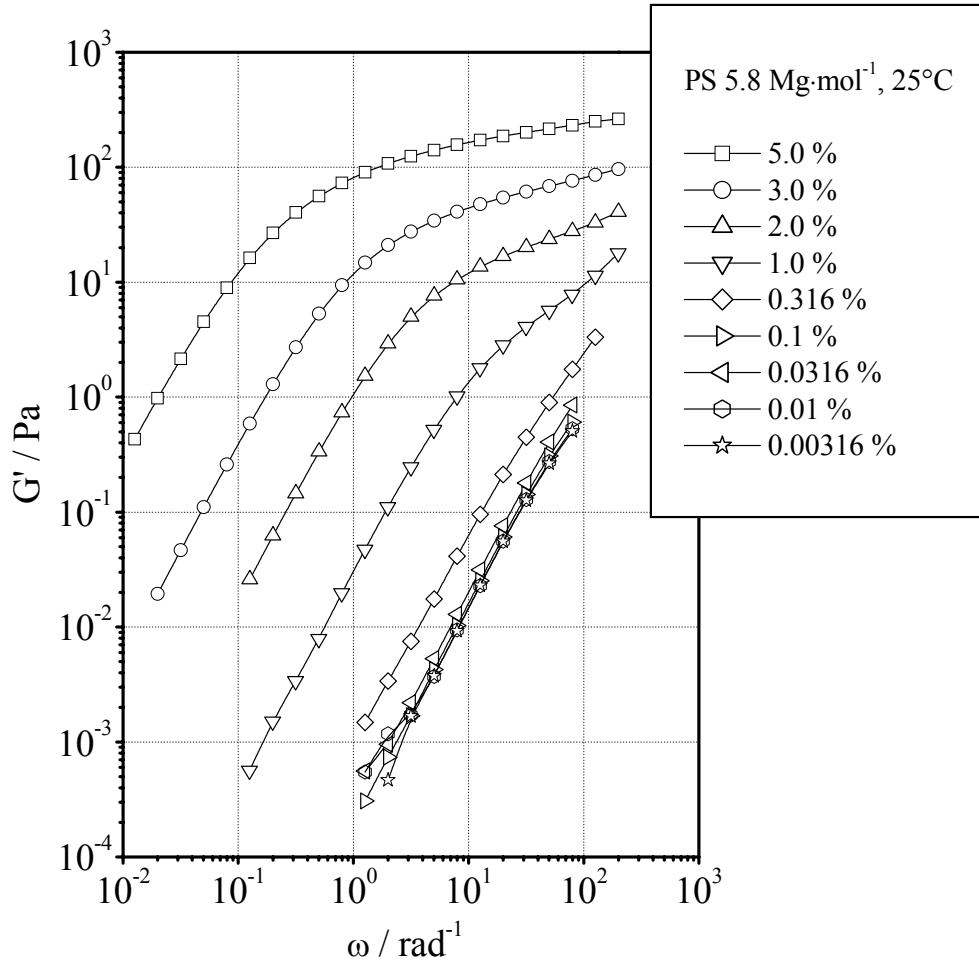
Figure 58: Storage modulus G' versus angular frequency ω for a polystyrene standard with M_w = 5.8 Mg/mol for different concentrations in diethylphthalate at 25°C.

As one can see in Fig. 59 very nicely, the trend for the loss moduli *G''* for the higher concentrated solutions (5.0- and 3.0 wt%) do follow the theoretical trend shown in Fig. 17. For these concetrations the angular frequency is already high enough to enter the third region considered for ocillatory strains, the transition area between plateau- and glassy region. At these high oscillatory strains the polymer solution starts to behave like a glassy solid, visco-elastic responses can not be observed anymore.

As polystyrene standards are very well characterized polymer systems in a variety of different solvents (see [143] for example) that do not build aggregated structures in solution, a correlation of the complex viscosity $|\eta|^*$ and the shear viscosity η, according to the Cox-Merz rule [144] to qualitatively discuss energetic interactions between the polymer coils, is set aside.
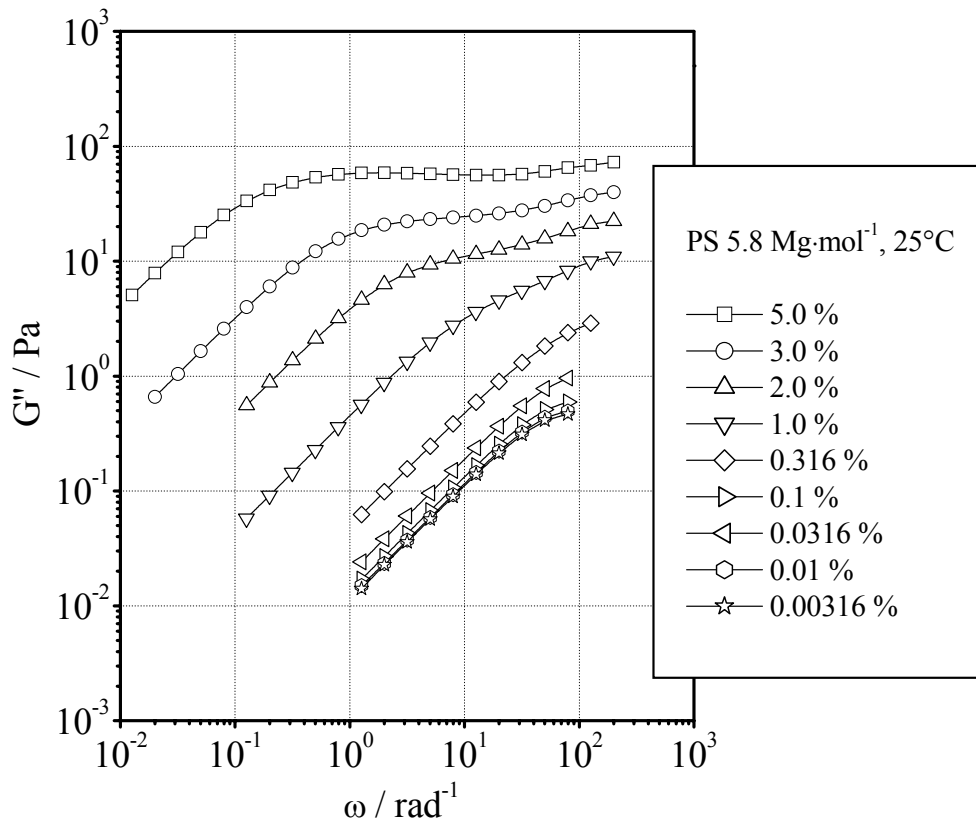
Figure 59: Loss modulus G'' versus angular frequency ω for a polystyrene standard with M_w = 5.8 Mg/mol for different concentrations in diethylphthalate at 25°C.

6.1.3 Uniaxial Deformation

6.1.3.1 Influence of concentration/ numerical simulations

To complete the quantification of the visco-elastic flow behaviour of polystyrene in solution, elongational experiments have to be accomplished according to the *Rheological Circle* [65] (see Fig. 13).

An advantage of elongational characterization of a polymer fluid is its pronounced sensitivity to visco-elastic effects. The determination of a longest relaxation time as a characteristic viscoelastic parameter via a capillary break-up experiment has recently gained much attention mainly because of the simplicity of this approach. Following the derivation of Entov and Hinch [26], the elastic thinning of a polymer solution filament in a CaBER like experiment can be described by an exponential decrease in time as described by Eq. 81. The longest relaxation time τ_0 of the polymers undergoing a molecular unravelling in the uniaxial flow can be easily determined from this relationship. The validity of this approach and its consistency with other determination methods have been shown in several publications for a range of different polymers, molar masses and concentrations in dilute to semi dilute solutions [27-33]. In these cases, the exponential decay of the filament could be observed over sufficiently long times.

However, the more dilute a solution becomes, the harder is the detection of a distinct regime of purely exponential thinning regime, since the initial Newtonian flow and the finite extensibility cannot be neglected during the short exponential thinning. Nevertheless, linear fits of experimental data in a semi log plot to Eq. 81 are often performed even for very dilute solutions to extract a relaxation time. The critical overlap concentration $c*$ of a polymer solution is one of its most important characteristic values. It does not only define the borderline between two distinct viscoelastic property regimes, but also the theoretical approach of a dilute solution by Rouse/Zimm theory or an entangled solution by the enhanced reptation concept.

The general definition of a dilute polymer solution refers to the critical concentration $c*$. It is generally accepted that for concentrations $c/c* < O(1)$ the steric and frictional interactions of neighbouring polymer coils are negligible and the rheological response of the fluid is solely governed by the hydrodynamic interactions of the isolated polymer coil and the solvent. However, this definition of diluteness is only applicable in the equilibrium state of polymer coils (for example for SAOS flow). Especially in elongationally-dominated flow fields, the coil-stretch transition of a polymer coil leads to an increased interaction volume and a domain overlap of the extended coils as reported by [83] and therefore to polymer-polymer interactions even for concentrations of $c/c* < O(1)$. The term "ultradilute" solution has been introduced recently to describe systems that remain truly dilute even when the polymer chains are in a highly stretched and deformed non-equilibrium state [145].

The capillary break-up experiment provides a convenient means for probing chain-chain interactions as a function of polymer concentration through measurements of the characteristic time-scale of the fluid in a strong elongational flow and several investigations of the transient elongational behaviour of a range of different polymers and molar masses [28, 30-33] in semi dilute to dilute solutions have been reported.

Recently Bazilevskii et al. [27], Stelter et al. [29] and Tirtaatmadja et al. [146] focussed on polymer in dilute to very ultradilute solution, finding that the characteristic relaxation time in capillary break-up experiments depends on the concentration in contrast to the Rouse/Zimm theory. In addition to this Bazilevskii et al. and Tirtaatmadja et al. observed a power law dependency of the relaxation time on the concentration. Whereas these authors generally reported on higher then expected relaxation times in capillary break-up, Bazilevskii et al. [27] also found for very dilute solutions relaxation times even below the lowest predicted Zimm relaxation time.

This chapter focuses on the detailed investigation of the capillary break-up dynamics and relaxation times of dilute to ultradilute polymer solutions. However, in order to analyze the dynamics of the capillary break-up process in very dilute solutions quantitatively it is necessary to answer the question of how much stress is carried by the polymer and how much by the solvent? In other words, under what physical conditions does a coil-stretch transition on the molecular scale occur and affect the resulting macroscopic fluid dynamics. This provides an effective distinction between a dilute and an ultradilute polymer solution. Viscoelastocapillary thinning and breakup of a fluid filament captures the naturally occurring transient elongational flow fields associated with jet break-up, drop formation and other free-surface deformations of complex fluids. Since the deformation rate is not constant in these surface tension driven flows, a satisfactory description of the occurrence of coil-stretch

transition in this evolving flow field requires more than a simple definition of a critical concentration.

Therefore, in this chapter experimental investigations on a surface-tension-driven flow (CaBER) of narrowly distributed polystyrenes in dilute and ultradilute solutions in high and low viscous solvents are presented together with numerical calculations of the stress evolution. For these calculations a FENE-PM (see chapter 4.3.2 for details) chain algorithm is utilized to determine the contribution of the polymer chains in different states of coil-stretch transition to the overall stress balance as a function of concentration and molar mass.

Fig. 60 to Fig. 70 show the experimentally determined temporal mid-diameter evolution of the investigated polystyrene boger fluids and solutions in diethylphthalate for different molar masses and concentrations.
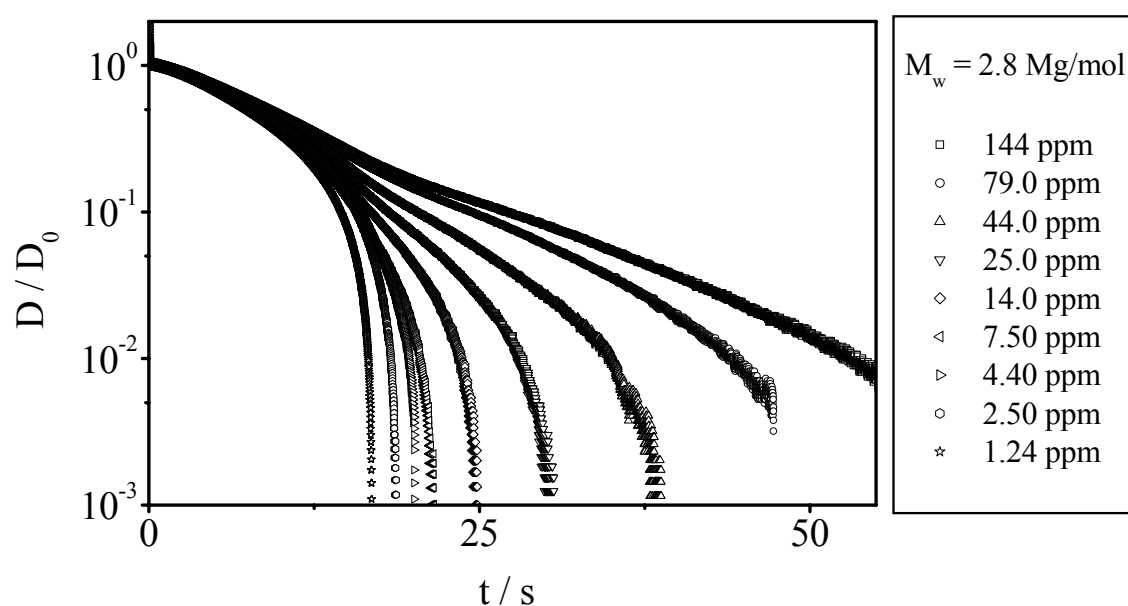

Figure 60: Normalized filament diameter D/D_0 versus time for investigated polystyrene boger fluids , M_w=2.8 Mg/mol at various concentrations and 25°C.

Figure 61: Normalized filament diameter D/D_0 versus time for investigated polystyrene boger fluids , M_w=5.7 Mg/mol at various concentrations and 25°C.

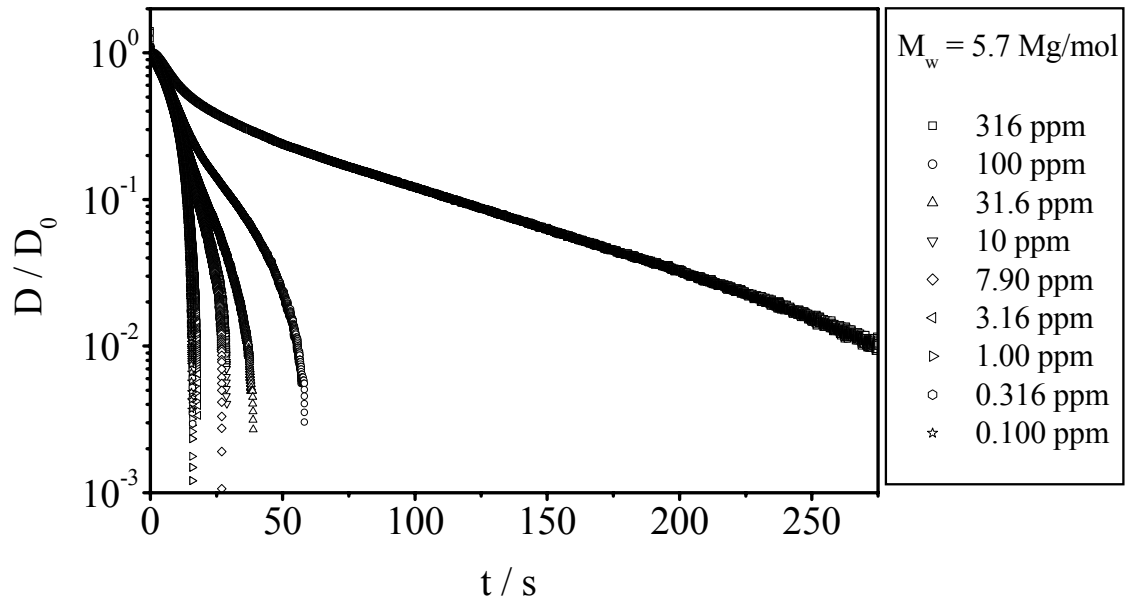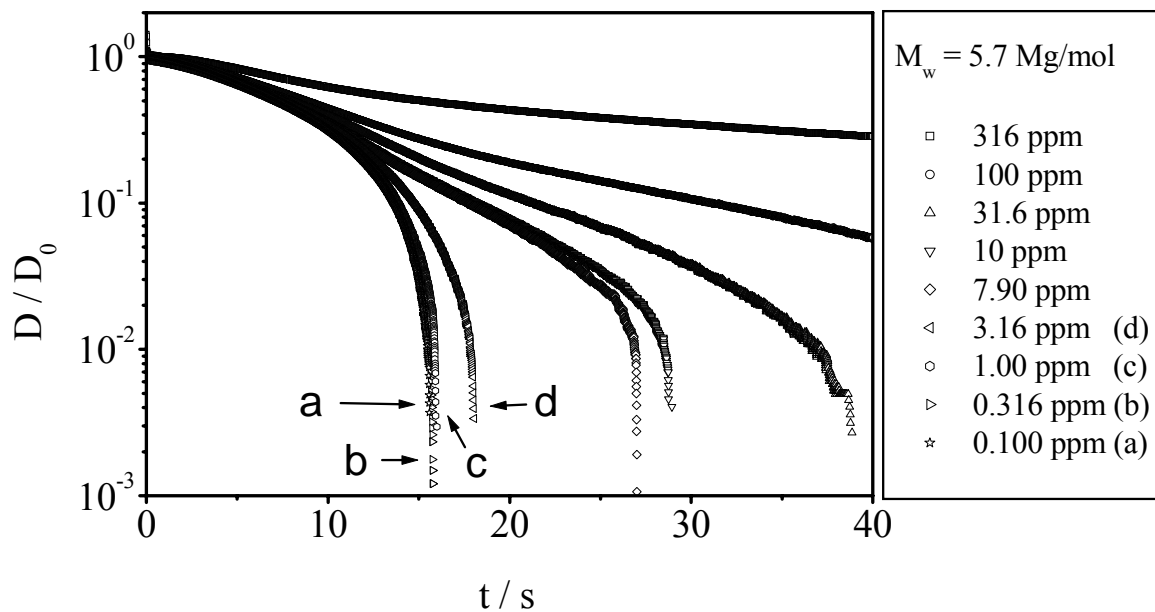*Figure 62: Normalized filament diameter D/D_0 versus time for investigated polystyrene boger fluids , M_w=5.7 Mg/mol at various concentrations and 25°C.*

Figure 63: Normalized filament diameter D/D₀ versus time for investigated polystyrene boger fluids , M_w=8.2 Mg/mol at various concentrations and 25°C.

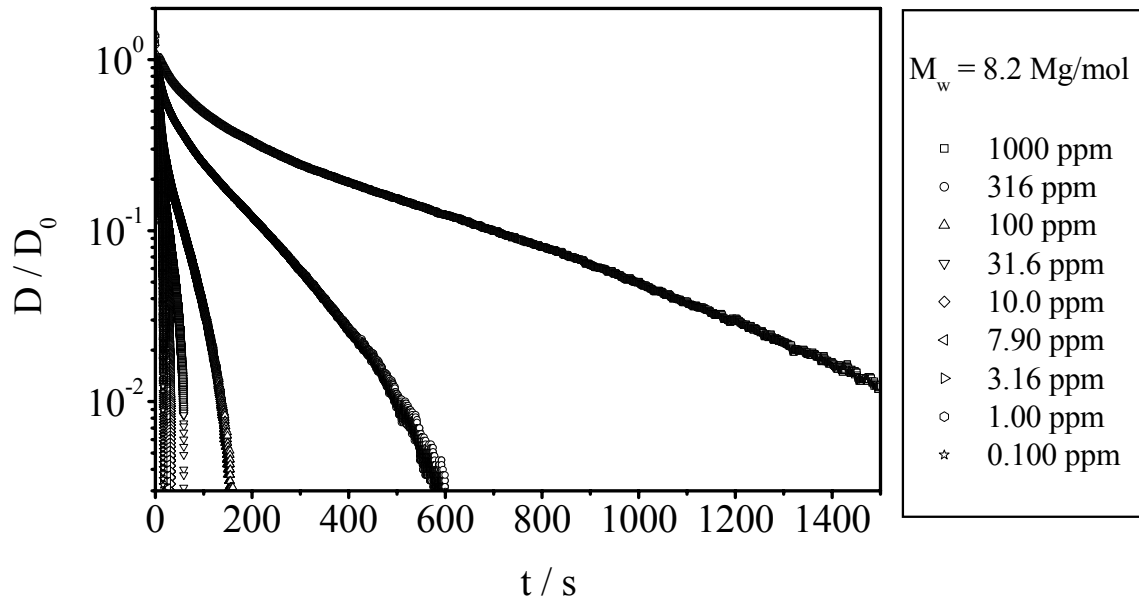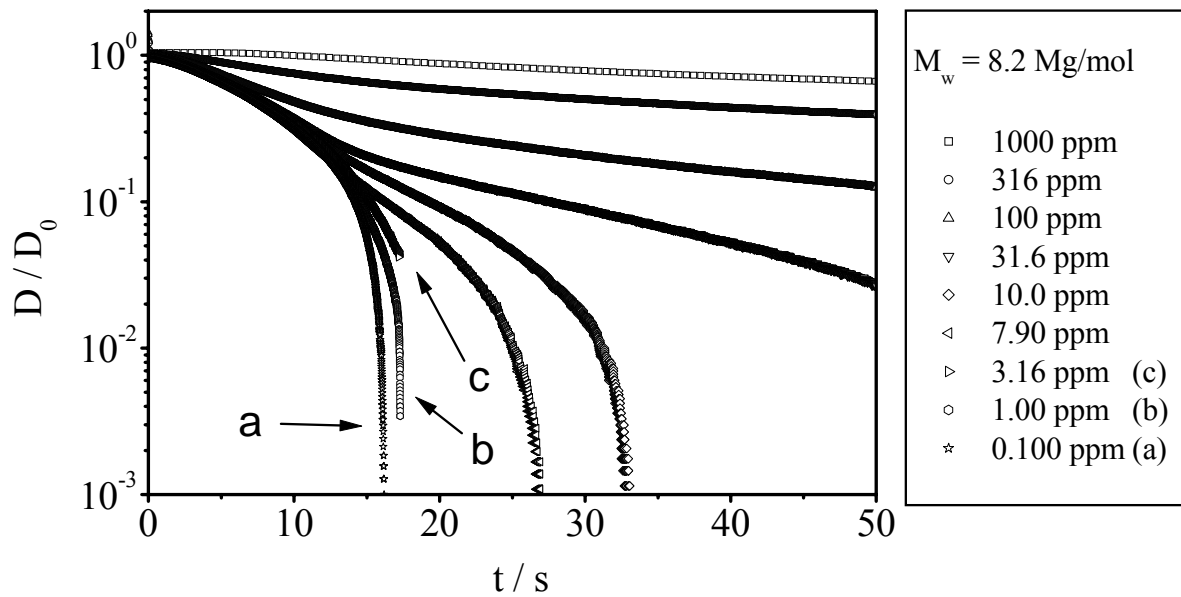*Figure 64: Normalized filament diameter D/D₀ versus time for investigated polystyrene boger fluids , M_w=8.2 Mg/mol at various concentrations and 25°C.*

Figure 65: Normalized filament diameter D/D₀ versus time for investigated polystyrene standrd M_w=2.8 Mg/mol in diethylphthalate at various concentrations and 25°C.

Figure 66: Normalized filament diameter D/D₀ versus time for investigated polystyrene standrd M_w=2.8 Mg/mol in diethylphthalate at various concentrations and 25°C.
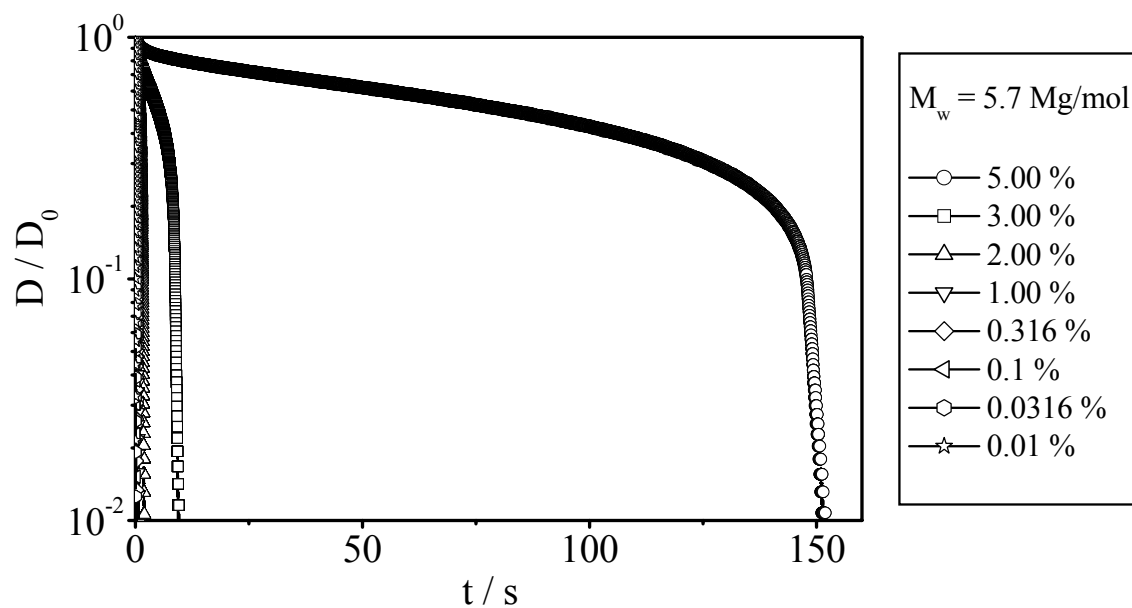
Figure 67: Normalized filament diameter D/D$_0$ versus time for investigated polystyrene standrd M$_w$=5.7 Mg/mol in diethylphthalate at various concentrations and 25°C.
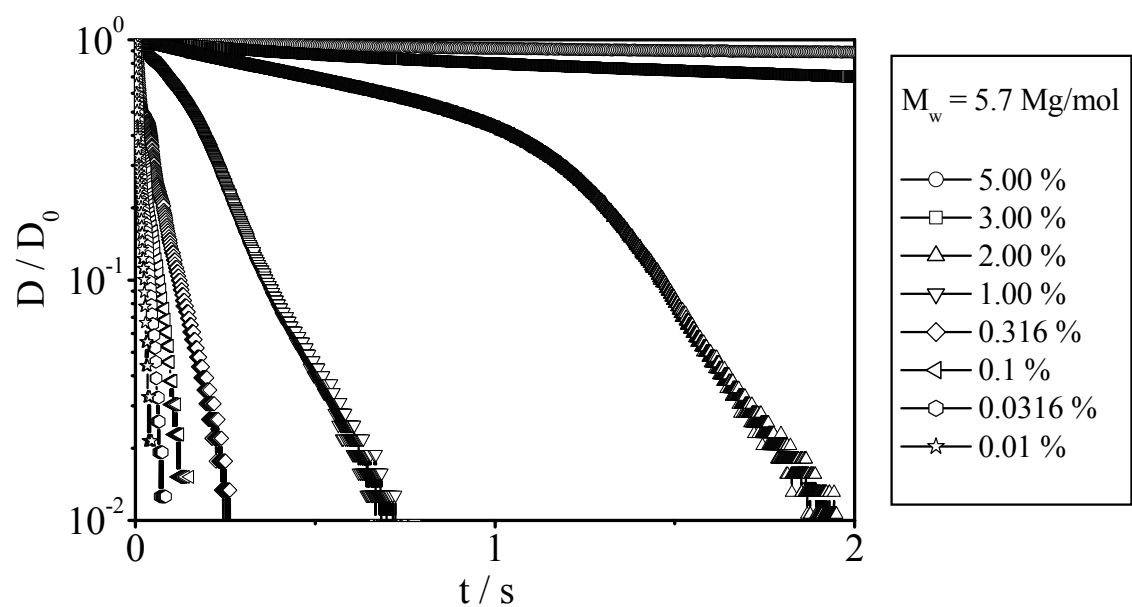
Figure 68: Normalized filament diameter D/D$_0$ versus time for investigated polystyrene standrd M$_w$=5.7 Mg/mol in diethylphthalate at various concentrations and 25°C.
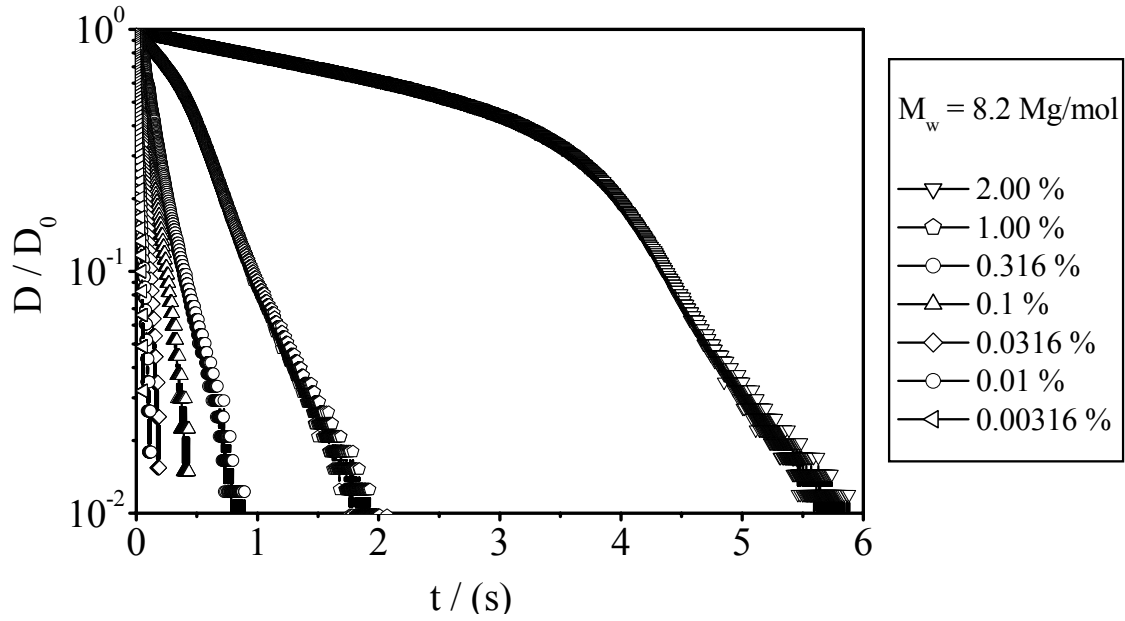
Figure 69: Normalized filament diameter D/D_0 versus time for investigated polystyrene standrd M_w=8.2 Mg/mol in diethylphthalate at various concentrations and 25°C.

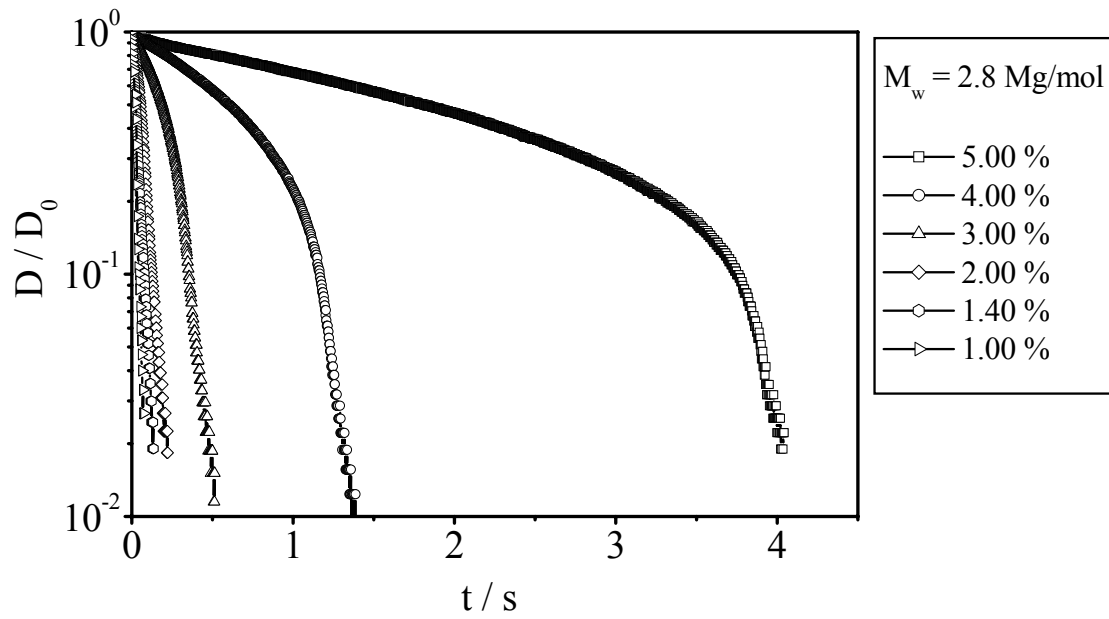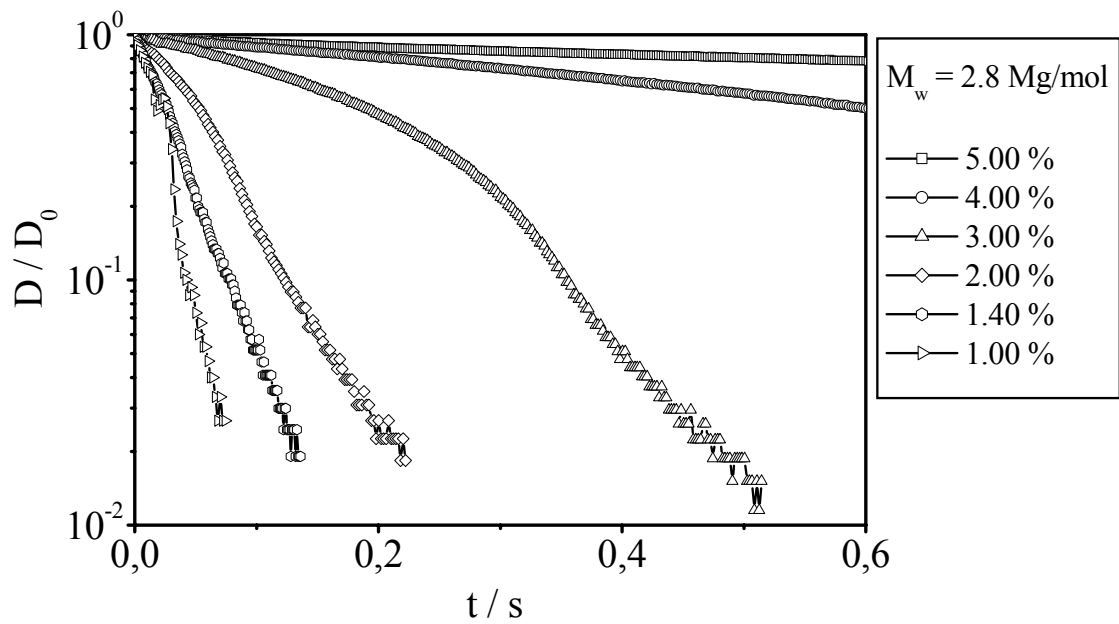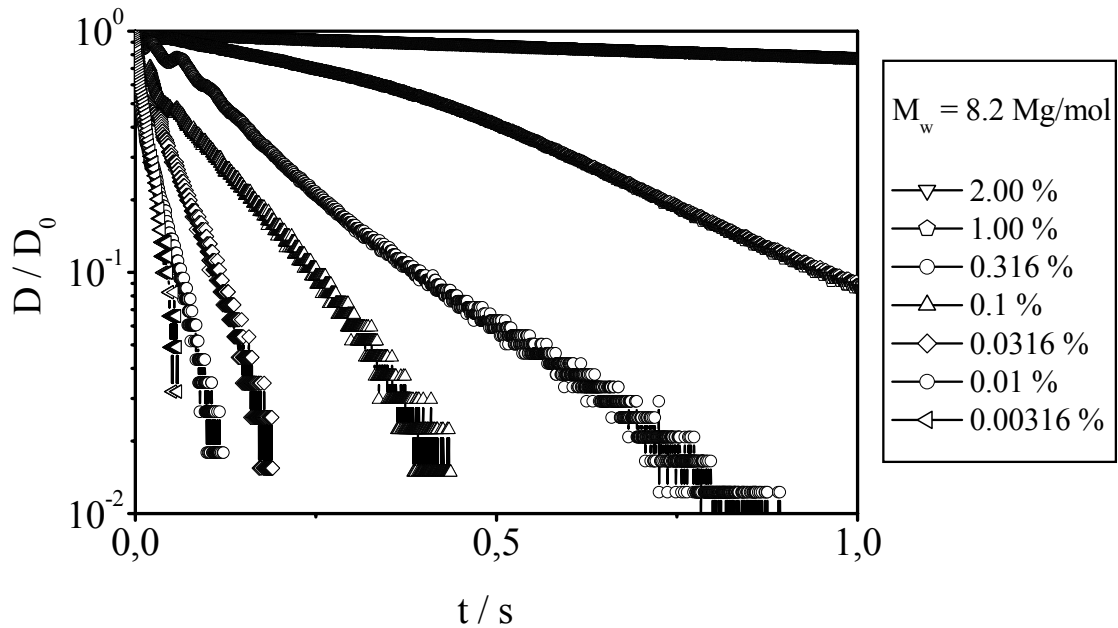*Figure 70: Normalized filament diameter D/D_0 versus time for investigated polystyrene standrd M_w=8.2 Mg/mol in diethylphthalate at various concentrations and 25°C.*

It can clearly be seen in Figs. 60 to 64, that at early times all solutions follow the thinning behaviour of the Newtonian solvent, controlled by an initial balance of the viscous term $3\eta_s\dot{\varepsilon}$ in the force balance of Eq. 81 and the capillary pressure. The polymeric stress of the initial conformation $A^0_{zz,i}$ (Eq. 73), caused by the step strain, is rapidly decaying in this primary phase since the extension rate is not sufficiently high enough to keep at least the

longest mode excited. However, with an increasing extension rate, the system crosses over to the second phase of the exponential thinning according to Eq. 81. The crossover shifts to earlier times and higher ratios $D(t)/D_0$ with rising concentrations. At late times the finite extensibility limit of the polymer is approached and the factor f_i (chapter 4.3.2) cannot longer be neglected. In this third phase the extension rate increases again and reaches a quasi-Newtonian state of thinning of the fully extended polymer coils that leads into the ultimate filament break-up. This third phase is not observed for the dithyphthalate solutions in Figs. 65 to 70, as the filament diameter drops below the resolution limit of the experiment before the finite extensibility shows effect. The first phase of Newtonian thinning in Figs. 65 to 70 shows a concentration dependence at higher concentrations since the Newtonian viscosity is determined by the solution rather then by the pure solvent as shown in Figs. 60 to 64 for the boger fluids.

The relaxation times τ_0 determined from fitting of the second phase in Figs. 60 to 70 to Eq. 81 from capillary break-up experiments are shown in Fig. 71.
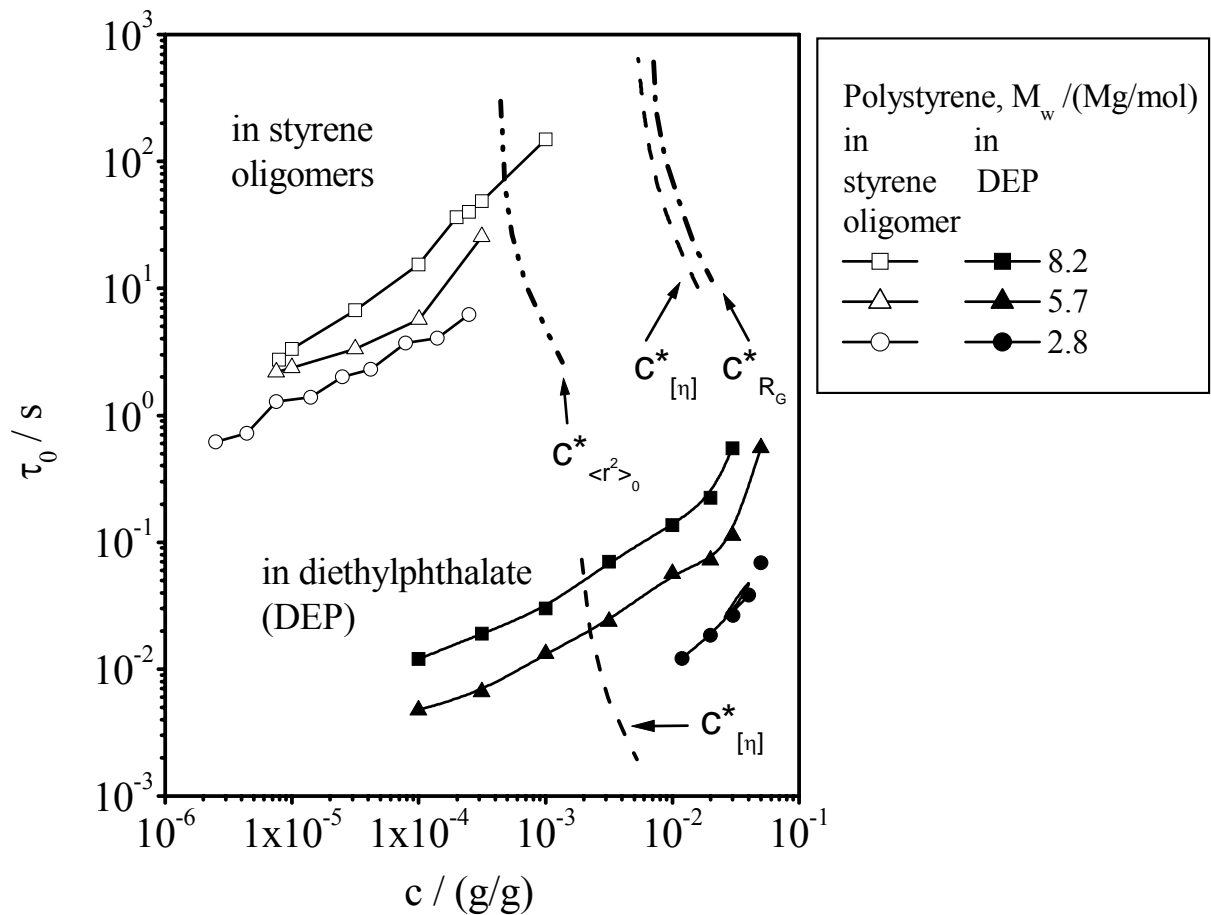
Figure 71: Relaxation times τ_0 versus concentration c, determined by fitting of the experiments in Figs. 60 to 70 to Eq. 81. Critical concentrations c* were determined by extrapolating the experimental data to the critical values determined via Eqs. 150 to 153.

The relaxation times show a strong dependence on the concentration and are decreasing with a decreasing concentration.

In addition to the obtained relaxation times Fig. 71 also depicts a rough estimation of the critical concentration calculated from the intrinsic viscosity

$$c^*_{[\eta]} = \frac{1}{[\eta]}$$

(Eq. 150)

which is obtained by extrapolating the observed trends of relaxation times to these respective concentrations.

However, a direct determination of the intrinsic viscosity of the boger fluids via a Huggins extrapolation of directly determined steady shear viscosities is hardly possible because of the high solvent viscosity and therefore the required resolution for a differentiation of the zero-shear viscosities of a dilution series. In contrast to an earlier publication [32], polystyrene in styrene oligomers as a solvent might actually lead to slightly less then theta

conditions of the solution (see chapter 5.1 for details). So far there are no reported reliable direct measurements of the intrinsic viscosity for a pure polystyrene boger fluid. Solomon and Muller [134] reported on intrinsic viscosity measurements of polystyrene dissolved in the theta solvent mixture dioctylphthalte/styrene oligomer that showed an excluded volume exponent ν of slightly less then 0.5 as can be seen in Fig. 35 in comparison to several Mark-Houwink relationships of polystyrene in solvents of different quality.

This observation may also be explained by a preferential attraction of the better of the two solvents in the solvent mixture towards the high polymer, and the contraction of the coil to reduce the amount of preferential concentration of the better solvent. In the following the constant K_η of the Mark-Houwink relation derived from Solomon and Muller is to be used for the investigated boger fluids to determine intrinsic viscosities from the molar mass for the calculations of the critical concentration from Eq. 11 and the Zimm relaxation time in the following section. However, the nature of boger fluids is still not fully understood, and it should be considered for the calculated Zimm times in the following that there might be slight deviations due to this uncertainty of the intrinsic viscosities.

The Mark-Houwink relation for the system polystyrene in DEP, shown in Figure 35, was determined for this report from capillary viscometric measurements of the intrinsic viscosity to $[\eta] = 8.1 \cdot 10^{-3} cm^3 g^{-1} M_w^{0.704}$ (see chapter 5.1 for details) with M_w in the units of g/mol.

To avoid the controversial discussion of the definition of the critical concentration, geometrical calculations are incorporated in Fig. 71, outgoing from a finite radius of the polymer coil [25]:

$$c_R^* = \frac{M}{\frac{4}{3}\pi R^3 N_A} \qquad \text{(Eq. 151)}$$

The definition of the radius as the radius of gyration R_G, assuming near theta conditions for boger fluids, leads to the critical concentration:

$$R \equiv R_G = \sqrt{\frac{b^2 C_\infty M}{3 M_u}} \qquad \text{(Eq. 152)}$$

The much more conservative radius definition via the mean square end to end distance gives:

$$R \equiv \sqrt{\langle r^2 \rangle_0} = \sqrt{6 R_g^2} \qquad \text{(Eq. 153)}$$

The critical concentrations of the investigated solutions of polystyrene/styrene oligomers and polystyrene/DEP are listed in Table 9 and 10.

Table 9: Critical concentrations of the investigated polystyrene boger fluids.

M_w / (Mg/mol)	$c^*_{[\eta]}$ / (g/cm^3)	c^*_{RG} / (g/cm^3)	$c^*_{<r^2>0}$ / (g/cm^3)	$c^\S$ / (g/cm^3)
8.2	$5.6 \cdot 10^{-3}$	$7.0 \cdot 10^{-2}$	$4.8 \cdot 10^{-4}$	$5.3 \cdot 10^{-7}$
5.7	$6.4 \cdot 10^{-3}$	$8.4 \cdot 10^{-3}$	$5.7 \cdot 10^{-4}$	$8.7 \cdot 10^{-7}$
2.8	$7.0 \cdot 10^{-3}$	$1.2 \cdot 10^{-2}$	$8.1 \cdot 10^{-4}$	$2.1 \cdot 10^{-6}$

Table 10: Critical concentrations of the investigated polystyrene solutions in diethylphthalate.

M_w / (Mg/mol)	$c^*_{[\eta]}$ / (g/cm^3)	c^*_{RG} / (g/cm^3)	$c^*_{<r^2>0}$ / (g/cm^3)
8.2	$1.6 \cdot 10^{-3}$	$6.6 \cdot 10^{-2}$	$4.4 \cdot 10^{-4}$
5.7	$2.1 \cdot 10^{-3}$	$7.9 \cdot 10^{-3}$	$5.4 \cdot 10^{-4}$
2.8	$3.5 \cdot 10^{-3}$	$1.1 \cdot 10^{-2}$	$7.6 \cdot 10^{-4}$

The observed relaxation times of the DEP solutions span the range from already close to or above the critical concentration in the semi dilute regime, whereas the relaxation times of the boger fluids lie below even the most conservative definition of c^*.

In these dilute solutions the relaxation times of isolated coils should be independent of the concentration according to Eq. 151. In contrast to this, the relaxation times show even below the most conservative definition of the critical concentration a strong decrease with a decreasing concentration. Similar observations of concentration dependent relaxation times below c^* have recently been reported by Bazilevskii et al. [27] and Stelter et al. [29] for polyacrylamide in water/glycerol mixtures and by Tirtaatmadja et al. [146] for polyethylene oxide in water/glycerol mixtures.

To evaluate these relaxation times obtained from uniaxial extension, one can compare them to relaxation times obtained from different flow fields. Lindner et al. [147] calculated relaxation times for dilute aqueous solutions down to 250 ppm from normal stress data fitted to an appropriate constitutive equation, in good agreement with the Zimm relaxation times. However, for the boger fluids investigated in this report the elastic response can be observed to even lower concentrations with from small amplitude oscillatory shear (SAOS) [32]. The Zimm relaxation times for the investigated boger fluids for the have been obtained from fitting the moduli *G'* and *G''* (Eq. 154 and 155 already incorporating the oligomeric nature of the solvent):

$$G' = \frac{\eta_s \tau_s \omega}{1 + (\tau_s \omega)^2} + \frac{cRT}{M_w} \sum_{i=1}^{N_{modes}} \left[\frac{(\tau_0 \omega)^2}{i^{4+2\tilde{\sigma}} + (\tau_0 \omega)^2} \right] \qquad \text{(Eq. 154)}$$

$$G'' = \frac{\eta_s \omega}{1+(\tau_s \omega)^2} + \frac{cRT}{M_w} \sum_{i=1}^{N_{modes}} \left[\frac{(\tau_0 \omega) i^{2+\tilde{\sigma}}}{i^{4+2\tilde{\sigma}} + (\tau_0 \omega)^2} \right] \qquad \text{(Eq. 155)}$$

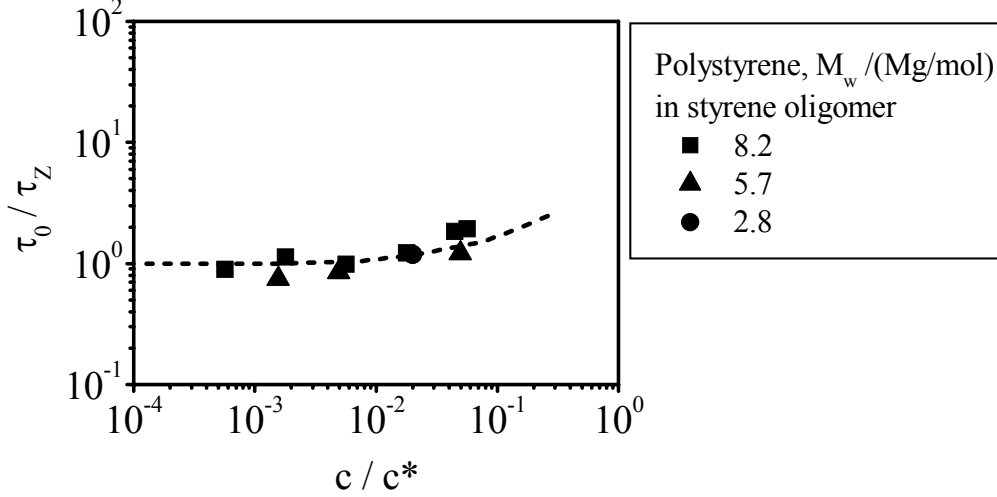The obtained longest relaxation times are given in Fig. 72.

Figure 72: Reduced relaxation times τ_0/τ_z versus reduced concentration c/c*, determined from SAOS experiments and fits to Eqs. 154 and 155.

Shown are the dimensionless values τ_0/τ_Z as a function of c/c^* (with c^* as the critical concentration from Eq. 150. To obtain the Zimm relaxation time τ_z (assuming a Zimm spectrum for the isolated polymer coil in solution), the universal ratio can be calculated to:

$$U_{\eta\tau} = \frac{\sum_i \tau_i}{\tau_0} \cong \zeta(3\nu) \qquad \text{(Eq. 156)}$$

with ζ as the Riemann zeta function and ν as the excluded volume exponent, giving a Zimm relaxation time τ_Z of:

$$\tau_Z = \frac{1}{\zeta(3\nu)} \frac{[\eta]\eta_s M_w}{RT} \qquad \text{(Eq. 157)}$$

Obviously at low concentrations in Fig. 72 the Zimm relaxation time is adhered to in SAOS experiments. Approaching the critical concentration, the relaxation time increases due to arising intermolecular interactions with an increasing concentration. The approach in Fig. 72 to obtain a master curve by reducing the concentration by c^* is backed up by the consideration that the polymer viscosity η_p can be expanded as a Taylor series in the concentration (see Eq. 142). This gives in combination with Eqs. 154, 157 and 9 a dependence on the reduced concentration c/c^*:

$$\tau_0 = \frac{1}{\zeta(3\nu)} \frac{[\eta]\eta_s M_w}{RT} \left(1 + K_H \left(\frac{c}{c^*}\right) + B_n \left(\frac{c}{c^*}\right)^{n-1} \right) = \tau_z \left(1 + K_H \left(\frac{c}{c^*}\right) + B_n \left(\frac{c}{c^*}\right)^{n-1} \right) \qquad \text{(Eq. 158)}$$

Using this approach one can also plot the longest relaxation times of the capillary break-up experiments in their reduced form τ_0 / τ_Z as a function of c/c^* as shown in Fig. 73.
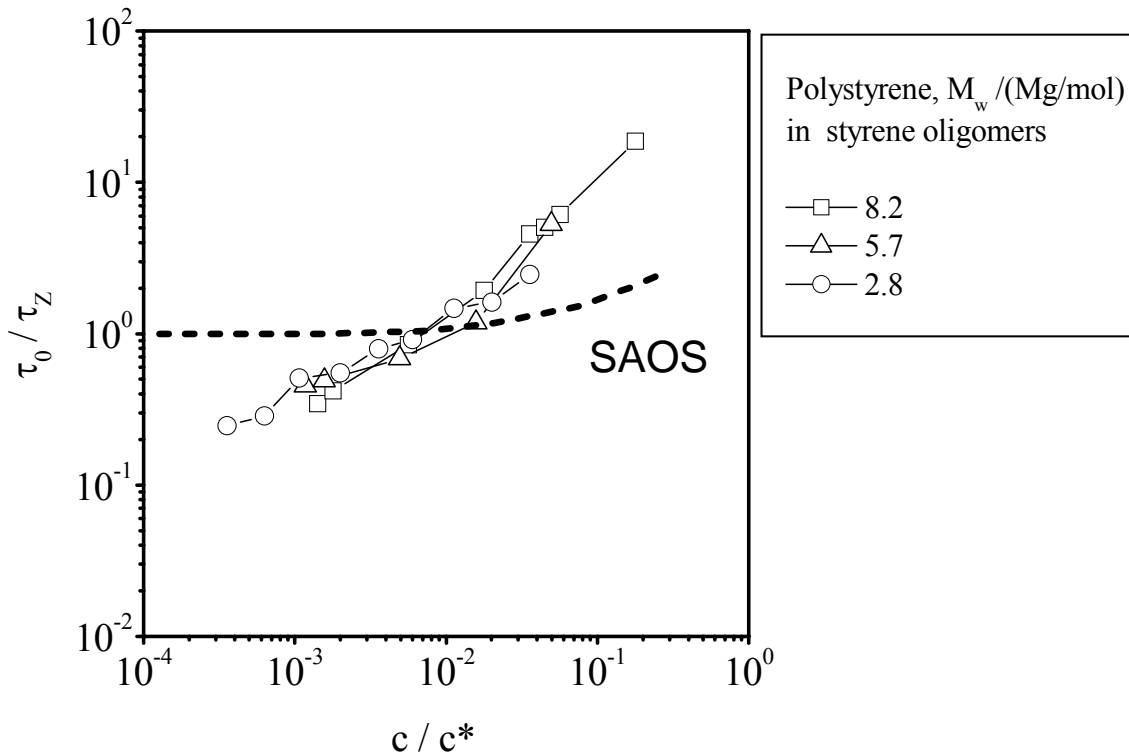

Figure 73: Reduced relaxation times τ_0 / τ_z versus reduced concentration c/c*, determined from CaBER experiments and fits to Eq. 81 in comparison to the theoretical Zimm relaxation times.

It can clearly be seen from the obtained mastercurve that the expected scaling of the longest relaxation time τ_0 with the molar mass M to the power 3ν (obtained from the definition of the Zimm relaxation time in Eq. 157, incorporating the molar mass dependence of the intrinsic viscosity $[\eta]$ according to Eq. 12 is adhered to when using an excluded volume exponent ν of 0.453 comparable the ν reported by Solomon and Muller [134]. Comparing this mastercurve to the trend of the relaxation times from the SAOS experiments as also shown in Fig. 73, it can clearly be seen that the relaxation times in uniaxial extension show already at much lower concentrations a deviation to higher values from the Zimm time in comparison to the oscillatory shear experiment.

In addition to this, Fig. 73 seems to indicate that at very low concentrations the relaxation time in uniaxial extension falls below the Zimm relaxation time and this is in accordance with a similar observation of Bazilevskii et al. [27] for very dilute polyacrylamide/water/glycerol solutions. For an explanation of this peculiar phenomenon, one has to go deeper into the details of the break-up dynamics at very low concentrations.

Generally lowering the concentration of a polymer in solution and approaching its Zimm relaxation time leads to the question whether the flow is still dominated by the timescale of the viscous solvent or of the polymer. One dimensionless number that captures these timescales is the Deborah number De:

$$De_0 = \frac{\tau}{\sqrt{\rho R_0^3 / \gamma}}$$

(Eq. 159)

In Eq. 159 the Deborah number is defined for the capillary break-up experiment as the polymer relaxation time relative to the Rayleigh time for the initial filament radius R_0 that determines the flow time scale for the necking process of a liquid filament. This Deborah number is thus an intrinsic quantity that cannot be selected but is rather set by the surface tension [148] and this in contrast to the governing, selectable Weissenberg number $We = \tau \dot{\varepsilon}$ of the filament stretching experiment.

The other dimensionless number is the Ohnesorge number Oh

$$Oh = \frac{\mu}{\sqrt{\rho R_0 \gamma}}$$

(Eq. 160)

that incorporates the viscosity controlled capillary time $\mu R_0 / \gamma$ relative to the Rayleigh time.

The ratio of the Deborah to the Ohnesorge number therefore defines the polymer to the viscous timescale:

$$\frac{De}{Oh} = \frac{\tau \gamma}{\mu R_0}$$

(Eq. 161)

For ratios below 1, the elastic forces of the polymeric contribution to the observed flow are negligible compared to the viscous forces and a capillary break-up experiment will not allow the extraction of a polymeric relaxation time. The polymeric influence on the ratio De/Oh is solely by its relaxation time, we therefore expect for the Zimm relaxation times a lower limit of the molar mass for a given experimental setup of surface tension γ, solvent viscosity μ and initial Radius.

However, even for $De/Oh > 1$ the observation of a thinning process mainly dominated by the elastic forces and an exponential decrease of the filament diameter according to Eq. 81 is not possible if the concentration is not high enough. In this case the temporal evolution of the stress distribution in the filament has to be taken into account. The transition from the initial balance of capillary and viscous force to the balance of capillary and elastic forces is shifted to later times, since the elastic contribution $\Delta \sigma_p$ in the force balance (Eq. 81) depends on the modulus G and hence on the concentration c:

$$G = nkT = \frac{c N_A kT}{M_w}$$

(Eq. 162)

Figs. 74 to 76 show the temporal stress distribution for three different concentrations of the same polymer obtained from numerical integration of the following set of ordinary differential equations already derived in the previous chapters. For the polymer conformation in the different room directions Eqs. 73 and 74 are consulted:

$$\dot{A}_{zz,i} - 2\dot{\varepsilon} A_{zz,i} = -\frac{1}{\tau_i}\left(f_{zz,i} A_{zz,i} - 1\right) \qquad \dot{A}_{rr,i} + \dot{\varepsilon} A_{rr,i} = -\frac{1}{\tau_i}\left(f_{rr,i} A_{rr,i} - 1\right)$$

(Eq. 163)

With known conformations the elatic contribution to the stress can be evaluated according to Eq. 56:

$$\Delta\sigma_p = \sigma_{p,zz} - \sigma_{p,rr} = \sum_{i=1}^{N_{modes}} g_i \cdot f_i \cdot \left(A_{11,i} - A_{22,i}\right)$$
(Eq. 164)

The visous stress $3\eta_s\dot{\varepsilon}$ and the capillary pressure $\dfrac{\gamma}{\left(\dfrac{D}{2}\right)}$ can then be evaluated via the

force balance already shown in Eq. 55:

$$\frac{\gamma}{\left(\dfrac{D}{2}\right)} = 3\eta_s\dot{\varepsilon} + \left(\sigma_{p,11} - \sigma_{p,22}\right) \text{ with } D = \left(\frac{G_0 \cdot D_0}{2\cdot\gamma}\right)^{\frac{1}{3}} D_0 \cdot e^{\frac{-t}{3\cdot\tau_0}} \text{ and } \dot{\varepsilon} = \frac{-2}{D}\frac{dD}{dt} \text{ (Eq. 165)}$$

Solving these equations demands known initial diameter D_0 (from experimental data), modulus $G = nk_BT$, surface tension γ of the investigated fluid, relaxation time τ (from experimental data or via fitting in the elastic thinning regime) and that $A_{zz} \neq 0$.
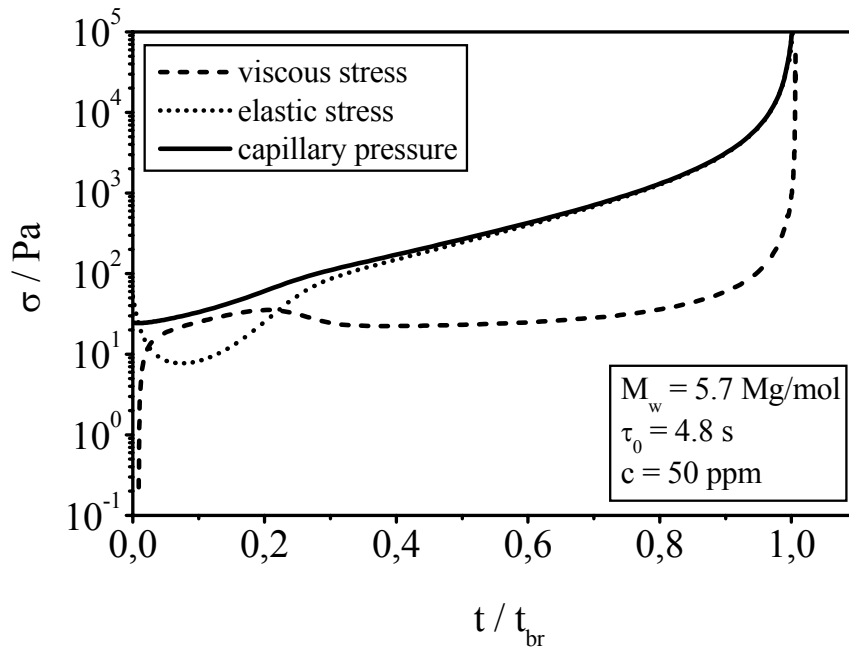
Figure 74: Numerical Simulation of the stress distribution in capillary break-up experiments. Shown are the driving capillary pressure and the stress distribution between the solvent and the polymer for a 50 ppm polystyrene boger fluid (M_w = 5.7 Mg/mol).
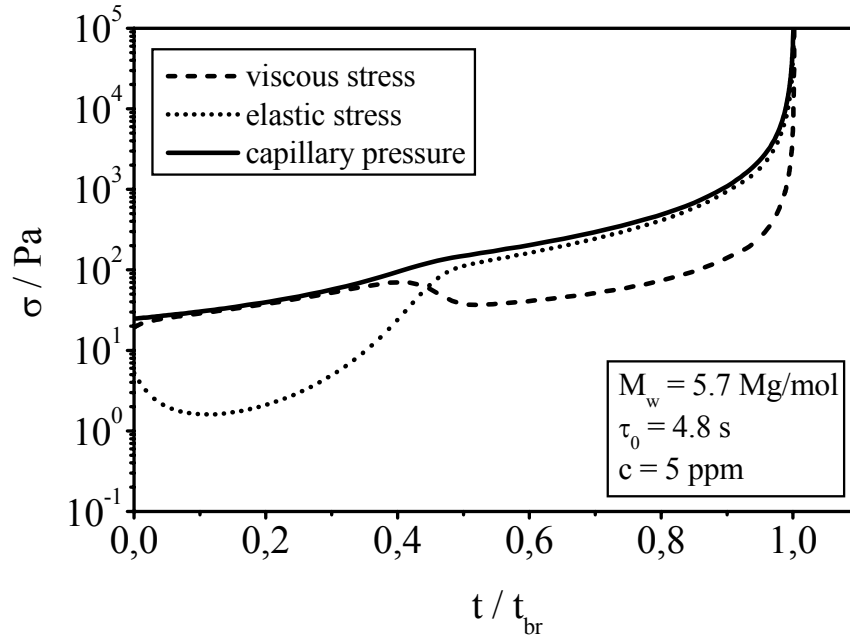
Figure 75: Numerical Simulation of the stress distribution in capillary break-up experiments. Shown are the driving capillary pressure and the stress distribution between the solvent and the polymer for a 5 ppm polystyrene boger fluid (M_w = 5.7 Mg/mol).
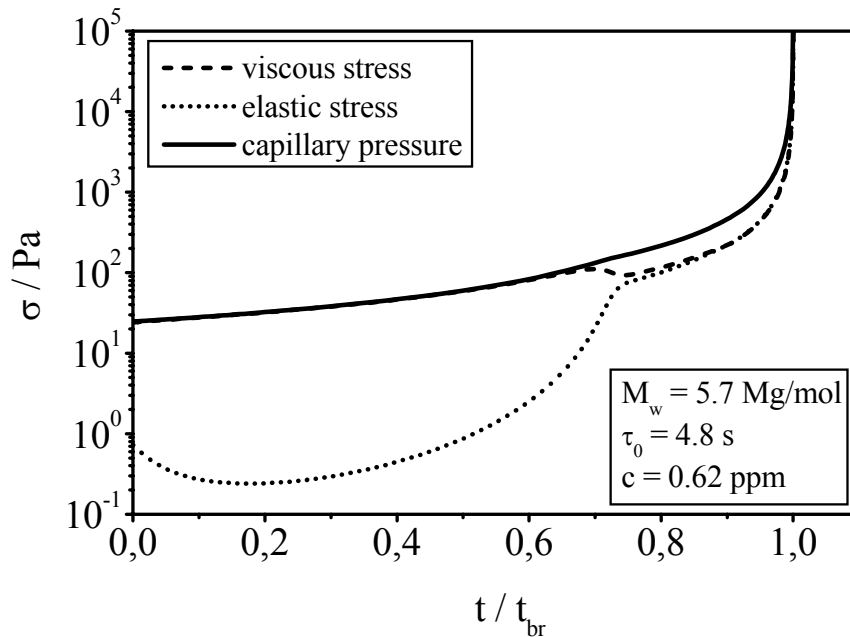
Figure 76: Numerical Simulation of the stress distribution in capillary break-up experiments. Shown are the driving capillary pressure and the stress distribution between the solvent and the polymer for a 0.62 ppm polystyrene boger fluid (M_w = 5.7 Mg/mol).

It can clearly be seen, that for lower concentrations the transition from a solvent dominated to an elasticity dominated flow shifts to later times during the thinning process. While this shifts the desired observation range of the elastic thinning regimes to smaller radii and therefore to the lower resolution limit of the experimental setup, it also means a faster approach of the finite extensibility limit of the polymer. Once also the higher modes of the

configuration **A** reach their finite extensibility limit that is incorporated in the evolution equations via the factor f_i and therefore in our numeric calculation in Figs. 74 to 76, the flow pattern again crosses over to a Newtonian flow of the expanded coils and the respective increasing filament thinning resulting in the final break-up. An extraction of a relaxation time by the simple exponential fit to Eq. 81 is therefore not possible once the finite extensibility starts to dominate the flow. At low concentrations, these two limiting effects are closing in on each other on the time axis and may alter the observed slope of the time dependent filament thinning in the semi log plot. This is demonstrated in Fig. 77 for numerical calculations of a dilution series of a polystyrene boger fluid.
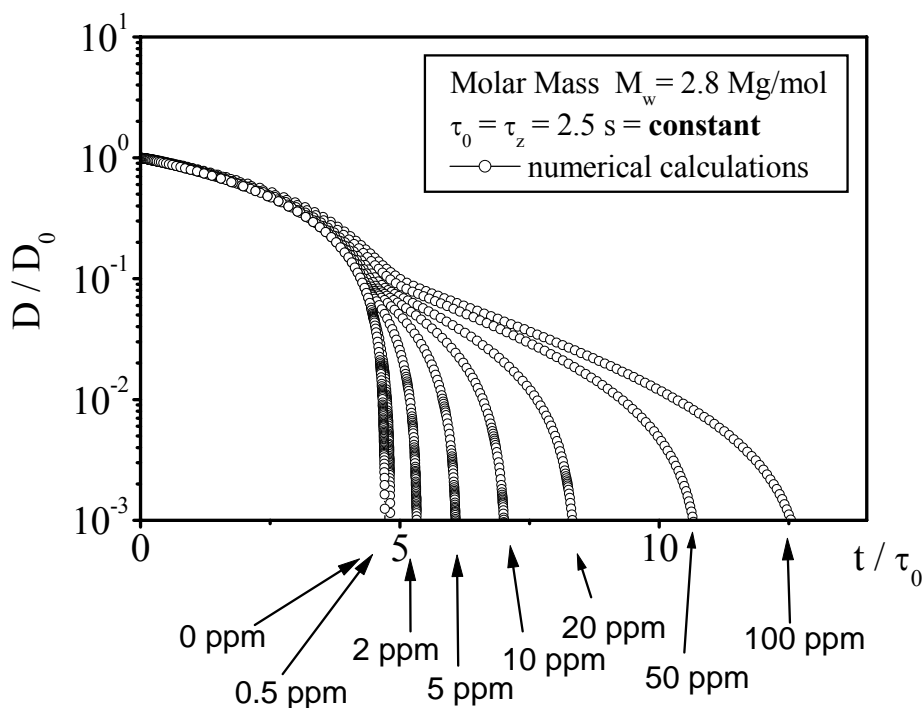
Figure 77: Numerical Simulation of the normalized diameter D/D_0 as a function of the reduced time t/τ_0 for a dilution series of a polystyrene boger fluid (M_w = 2.8 Mg/mol) with constant longest relaxation time τ_0.

The longest relaxation time τ_0 for these calculations is chosen to be constant for all dilutions and the value is assumed to agree with the Zimm time τ_z. As one can see, the break-up times are decreasing with a decreasing concentration, however, at the same time the slope of the curves in the intermediate thinning regime in the semi log plot of Fig. 77 seems to become steeper and suggests relaxation times below the Zimm time used for these calculations. This effect is also enhanced by a "smearing out" of the transition from the initial Newtonian thinning to the elastic regime.

The ultimate limit of the capillary break-up experiment for the observation of the polymeric contribution can be seen in Fig. 76. Even though all modes of the polymer configuration have reached their finite extensibility limit at late times, the contribution of the viscous forces of the solvent dominates the flow behaviour. The minimum concentration at which even the sum of all modes of elastic forces of the fully expanded coils just balance the viscous forces of the solvent can be obtained from the force balance in Eq. 55.

Following Entov and Hinch [26], close to the finite extensibility limit with $A_{zz} \gg A_{rr}$ and a negligible temporal change of A_{zz} the relevant evolution equation (Eq. 73) reduces to

$$2\dot{\varepsilon} A_{zz,i} = \frac{1}{\tau_i} f_i A_{zz,i} \qquad \text{(Eq. 166)}$$

This gives for f_i:

$$f_i = 2\dot{\varepsilon}\tau_i \qquad \text{(Eq. 167)}$$

and with $\text{tr}\mathbf{A} = A_{zz}$ a solution for A_{zz} at the finite extensibility limit:

$$A_{zz,i} = L_i^2 \left(1 - \frac{1}{2\dot{\varepsilon}\tau_i} \right) \qquad \text{(Eq. 168)}$$

Combining Eqs. 167 and 168 in the polymer contribution $\Delta\sigma_p$ (Eq. 56) with $A_{zz} \gg A_{rr}$ we obtain for the finite extensibility limit:

$$\Delta\sigma_p = \sum_i^{N_m} 2G\dot{\varepsilon}\tau_i L_i^2 \left(1 - \frac{1}{2\dot{\varepsilon}\tau_i} \right) \qquad \text{(Eq. 169)}$$

or:

$$\Delta\sigma_p \approx \frac{2}{\zeta(5\nu)} G\dot{\varepsilon}\tau_z L^2 \qquad \text{(Eq. 170)}$$

From this we get the maximum, constant polymer viscosity $\eta_p \approx 2G\tau_z L^2 / 3\zeta(5\nu)$ for the finite extension limit in the thinning filament. Now assuming that the viscous stress carried by the solvent starts to dominate even at late times if the viscous stress in Eq. 55 becomes larger than the polymer stress in Eq. 170, the polymer contribution is only observable in capillary break-up experiments for:

$$\frac{2}{3\zeta(3\nu)} \frac{G\tau_z L^2}{\eta_S} > 1 \qquad \text{(Eq. 171)}$$

Replacing the modulus according to Eq. 162, we derive a lowest possible polymer concentration $c^\S$ for an observable polymer contribution to a capillary break-up experiment:

$$c^\S > \frac{3}{2} \frac{1}{[\eta]\cdot L^2} \zeta(3\nu) \qquad \text{(Eq. 172)}$$

At the concentration $c^\S$ the extended polymer is still contributing to the overall stress at late times, however, this concentration marks the point below which even a fully extended polymer will carry less stress than the solvent.

The concentrations $c^\S$ of the investigated polymers are shown in Table 9. $c^\S$ was also chosen for the numerical calculation in Fig. 76 where it can clearly be seen that viscous and polymeric stresses have the same contribution to the overall stress at late times.

With regard to these limitations of a direct extraction of the relaxation time from an assumed elastic thinning regime, we have also used a different approach to obtain the relaxation times close to the critical concentration limit $c^\S$ of Eq. 172. Therefore the numerical integration of Eqs. 163 to 165 for the calculation of the filament thinning with the longest relaxation time τ_0 as the only adjustable parameter has been used to obtain the best

concordance of several single numerical calculations with the experimentally obtained filament thinning profiles in Figs. 60 to 70. The derived best fits to the experimental data are shown exemplarily for several decades of concentration and one molar mass in Fig. 78. In addition to this, the calculated stress distributions for each of the concentrations are shown in Figs. 79 to 83.
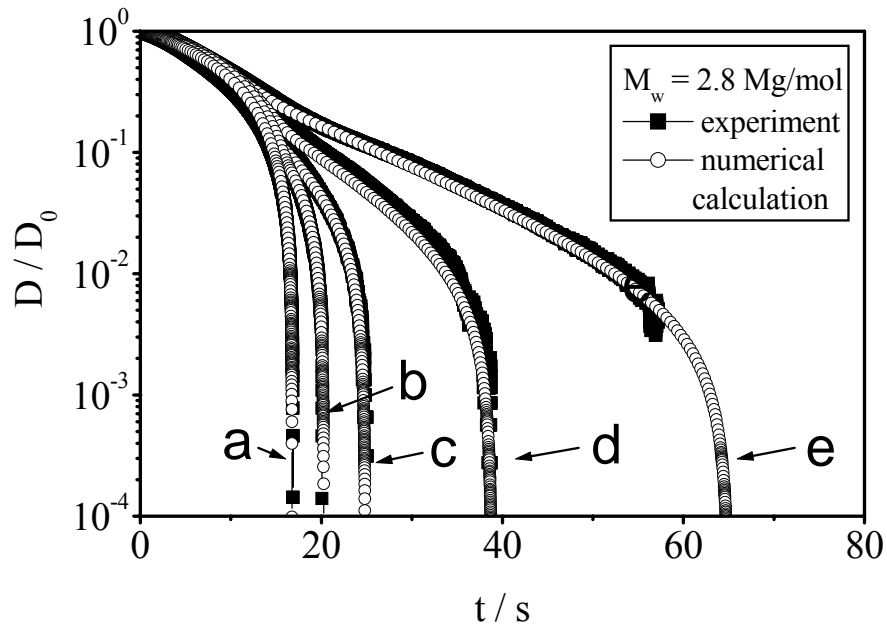
Figure 78: Comparison of numerical calculated filament evolution with experimental data for a dilution series of a polystyrene boger fluid (M_w = 2.8 Mg/mol.)
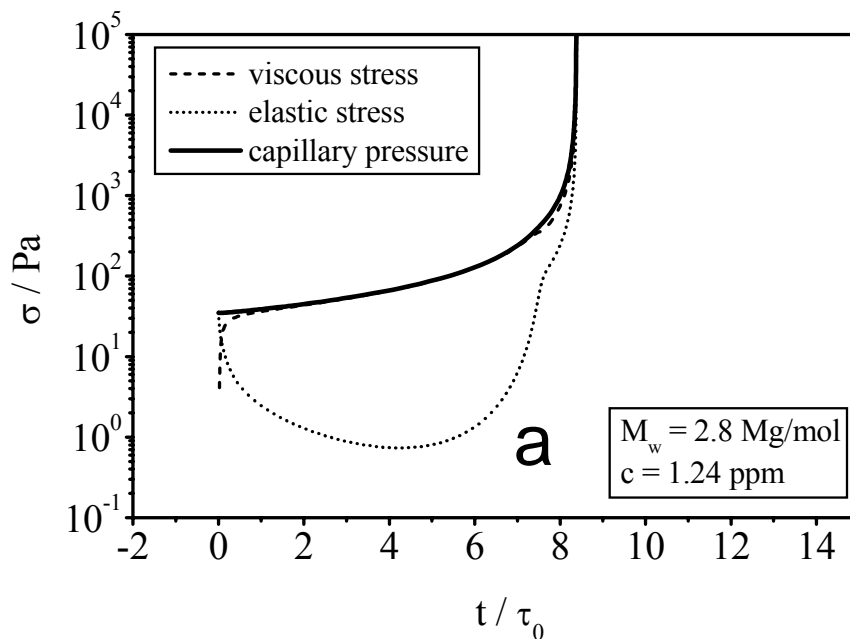
Figure 79: Numerical Simulation of the stress distribution in capillary break-up experiments. Shown are the driving capillary pressure and the stress distribution between the solvent and the polymer for a 1.24 ppm polystyrene boger fluid (M_w = 2.8 Mg/mol).
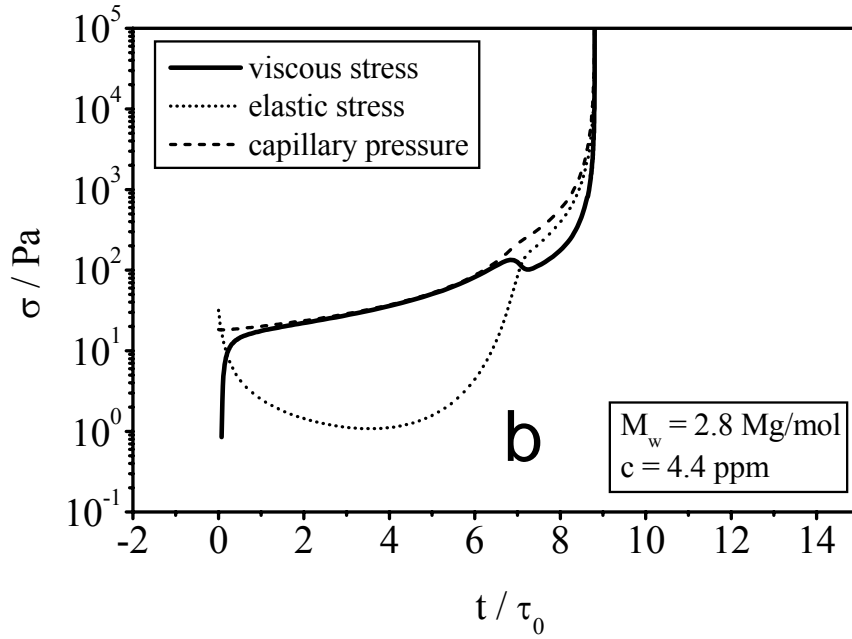
Figure 80: Numerical Simulation of the stress distribution in capillary break-up experiments. Shown are the driving capillary pressure and the stress distribution between the solvent and the polymer for a 4.4 ppm polystyrene boger fluid (M_w = 2.8 Mg/mol).
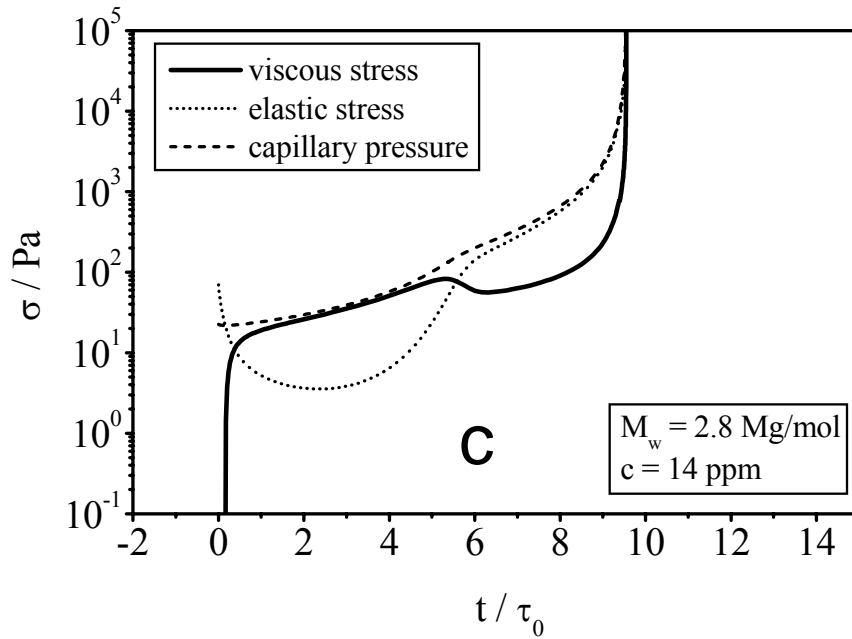
Figure 81: Numerical Simulation of the stress distribution in capillary break-up experiments. Shown are the driving capillary pressure and the stress distribution between the solvent and the polymer for a 14 ppm polystyrene boger fluid (M_w = 2.8 Mg/mol).
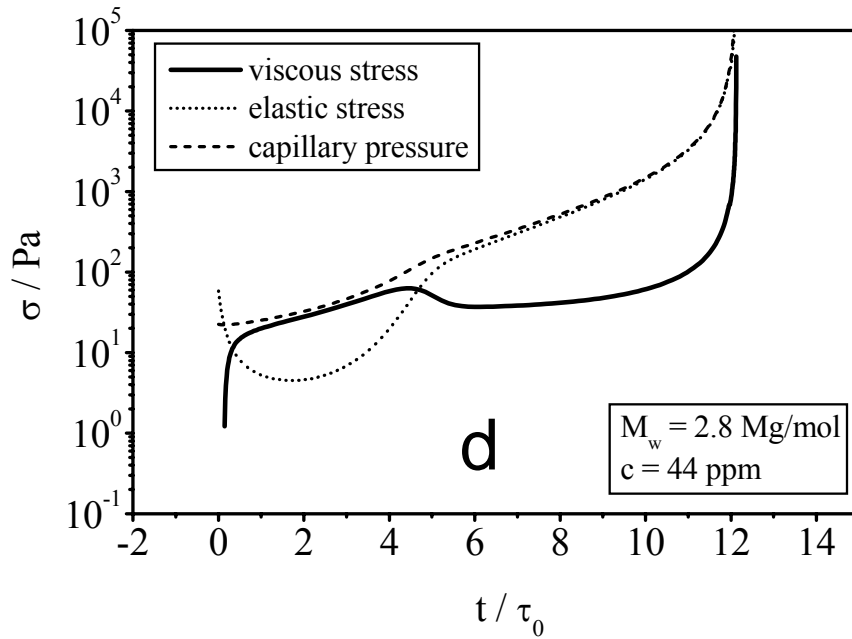
Figure 82: Numerical Simulation of the stress distribution in capillary break-up experiments. Shown are the driving capillary pressure and the stress distribution between the solvent and the polymer for a 44 ppm polystyrene boger fluid (M_w = 2.8 Mg/mol).
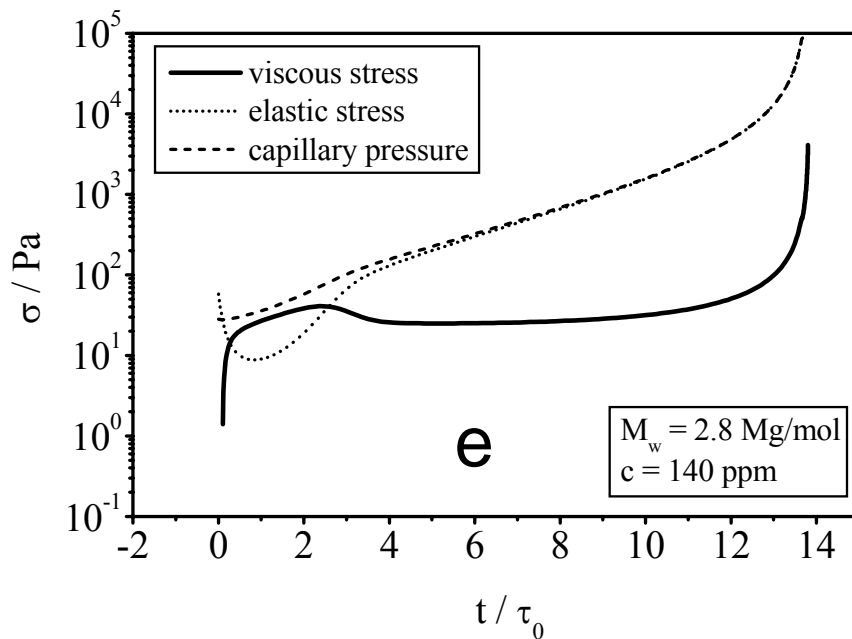
Figure 83: Numerical Simulation of the stress distribution in capillary break-up experiments. Shown are the driving capillary pressure and the stress distribution between the solvent and the polymer for a 140 ppm polystyrene boger fluid (M_w = 2.8 Mg/mol).

The relaxation times derived from the numerical calculations were then used to replot the reduced relaxation times of Fig. 73. As it can be seen in Fig. 84, the actual relaxation times in uniaxial extension reach a constant value at low concentrations in accordance with the constant relaxation times obtained from the SAOS experiments at low concentrations. However, one has to note that the constant value of reduced relaxation times obtained for the

molecular unravelling in uniaxial extension from the numerical calculations is slightly lower than 1, the average molecular unravelling time from Fig. 84 at low concentrations is a factor of ~ 1.38 lower than the Zimm times.
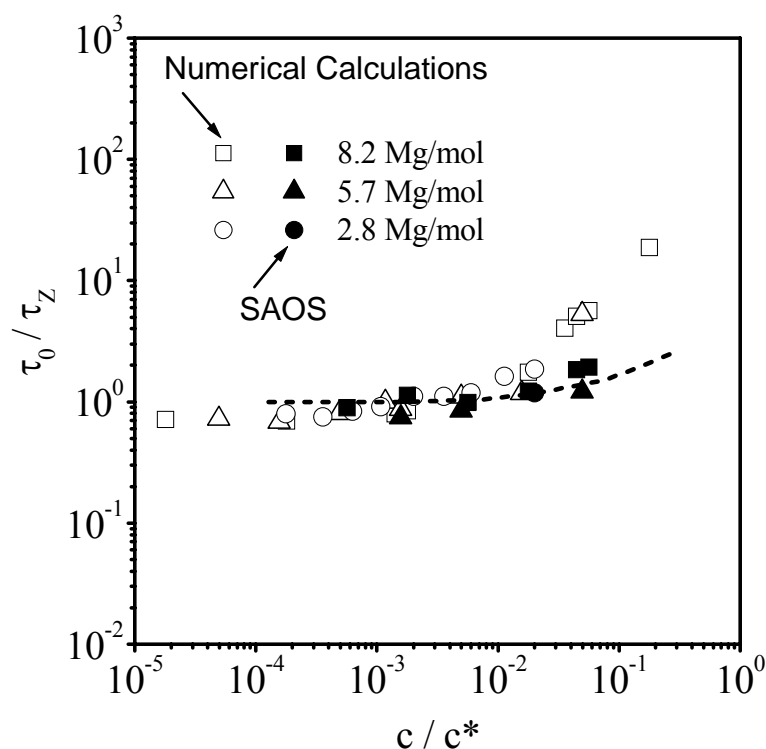
Figure 84: Reduced relaxation times τ_0 / τ_z versus reduced concentration c/c*, obtained from best fits of numerically calculated filament evolution. For comparison also the relaxation times from SAOS experiments (see Fig. 73) are given.

Relaxation times obtained from the numerical calculations of the uniaxial flow at higher concentrations are as expected in very good agreement with the directly extracted relaxation times from the fit of Eq. 81 to the experimental data. Still, these values are higher than the relaxation times obtained from the oscillatory shear flow experiments. This can also be seen in Fig. 85 for polystyrene in the good solvent diethylphthalate.
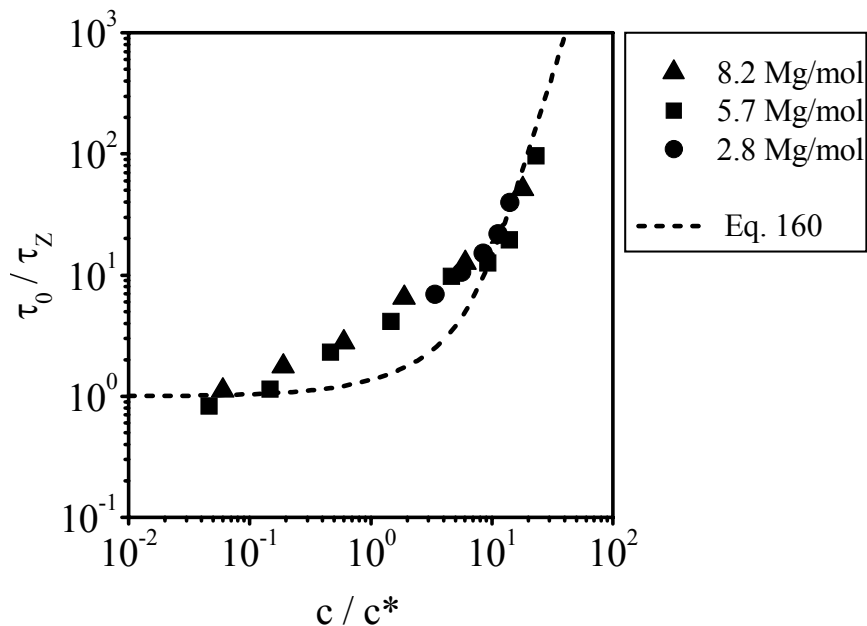
Figure 85: Reduced relaxation times τ_0 / τ_z versus reduced concentration c/c* for dilution series of polystyrene in diethylphthalate at different molar masses. In addition the theoretical concentration dependence according to Eq. 158 is shown.

Since these solutions have a much smaller viscosity than the observed boger fluids, the observable range of relaxation times is shifted to higher concentrations determined by the low viscosity limit of the Ohnesorge number Oh in Eq. 160 and it is therefore not possible to obtain relaxation times close to the Zimm limit neither via capillary break-up, nor via SAOS experiments. However, for this system one is able to experimentally determine the required constants K_H and B_n and n of the structure property relationship in Eq. 141 from capillary viscometric measurements at lower, and cone and plate shear rheometry at higher concentrations for several different molar masses as shown in Fig. 51, to fully obtain Eq. 141 over the observable range of concentrations Eq. 141 is also shown in Fig. 51. In this case the intrinsic viscosities could directly be determined for the required calculation of c^*. Again, it can be seen that the relaxation times start to rise from their lowest possible value at much smaller concentrations than expected from the approach of Eq. 141.

The onset of the rising relaxation times gives a rough estimation of a concentration of ultradilution. Below this concentration (and above $c^\S$) one is still able to observe the presence of the polymer in a delayed break-up time and a deviation from the Newtonian behaviour of the solvent, although the onset of this deviation shifts with decreasing concentration to later times and smaller diameters of the filament and might be lost in the observation resolution of the experiment. The relaxation time, or better, the molecular unravelling time is in this case constant and that of the single polymer coil.

Above the concentration of ultradilution the concentration of the polymer coils is high enough, that the long range interactions of the increasing hydrodynamic radius of unravelling polymer coils lead to an increase of relaxation time of the solution. The scaling of the relaxation time in this regime with the reduced concentration seems to obey the following relation as proposed by Tirtaatmadja et al. [146]:

$$\frac{\tau_0}{\tau_Z} \sim \left(\frac{c}{c^*}\right)^m \qquad\qquad\qquad\qquad\qquad \text{(Eq. 173)}$$

We determined a gradient of m = 0.58 in Fig. 51 for the system polystyrene in the relative good solvent DEP in comparison to m= 0.65 observed by Tirtaatmadja et al. [146] for PEO in glycerol/water mixtures. In contrast to this, for the investigated polystyrene dissolved in the near theta solvent of styrene oligomers a gradient of m = 0.89 is obtained from Fig. 85.

However, a correlation of the gradient m or the concentration of an ultradilution with the solvent quality of the investigated system is not possible yet. Whereas the concentration of ultradilution of the system polystyrene in the good solvent DEP is roughly ~1.2 decades below c* in the definition of Eq. 150, the concentration of ultradilution is roughly ~2.5 decades below c*. After disussion of the influence of the concentration on the elongational behaviour of polystyrene in solution a more detailed look on the molar mass or the molar mass distribution follows in the next chapter.

6.1.3.2   Influence of molar mass/ molar mass distribution

To investigate the influence of the molecular weight distribution on the flow behaviour of polymer solutions defined blends were prepared, using the standard system polystyrene in diethylphthalate already discussed in the previous chapters in terms of their rheological behaviour in steady shear flow or SAOS experiments.

The polystyrene standard solutions investigated in this chapter were blended from different narrowly distributed polystyrene standards with varying molar masses to achieve an approx. constant molar mass M_w of 5.8 Mg/mol with different molecular weight distributions varying in M_w/M_n from approx. 1.0 to 1.84 (first of the manufacturers specifications were used for primary evaluation of molar mass distribution). The true molar masses of the polystyrene standards were acquired via viscosimetry in toluene and the Mark-Houwink-Sakurada equation [25] (see Table 1 in chapter 2.1 for details).

In Tab. 11 the absolute composition of the investigated polystyrene blends are listed together with the width of the MMD.

Table 11: Absolute blending composition of investigated polystyrene blends 1.0 - 3.0 (for details on the used polystyrenes see Table 1).

Blend	Blend Composition / wt%						M_w / M_n (Q)
	PS 1	PS 2	PS 3	PS 4	PS 5	PS 6	
1.0	-	-	100	-	-	-	1.00 - 1.05
1.1	-	22.2	66.0	9.8	2.0	-	1.06
1.2	0.3	34.0	46.6	13.5	5.3	0.3	1.11
1.5	7.7	37.3	32.2	13.7	7.8	1.3	1.36
2.0	18.9	33.7	25.0	12.3	7.7	2.4	1.66
3.0	27.6	30.3	20.6	10.6	7.5	3.5	1.84

The flow curves shown in Fig 86 for these blends (1.0 wt% in diethylphthalate) show approx. the same flow characteristics. The zero-shear viscosities η_0 for the investigated polystyrene blends balance between values of 0.3-0.5 Pas. The transition area between the Newtonian- and non-Newtonian flow regime does not allow for qualitative or quantitative evidence on the shape of the molar mass distribution. The flow curves were then fitted via the modified Carreau model [141]:

$$\eta = \eta_0 \cdot \left[1 + (\dot{\gamma} \cdot \tau_0)^b \right]^{n/b}$$
(Eq. 174)

with *n* as the slope of the flow curve and *b* being the transition parameter. The obtained values for the longest relaxation times of steady shear flow are summarized in Table 12. In favor of clarity only the Carreau fit for the flow curve of blend 1.5 is shown in Fig. 86.
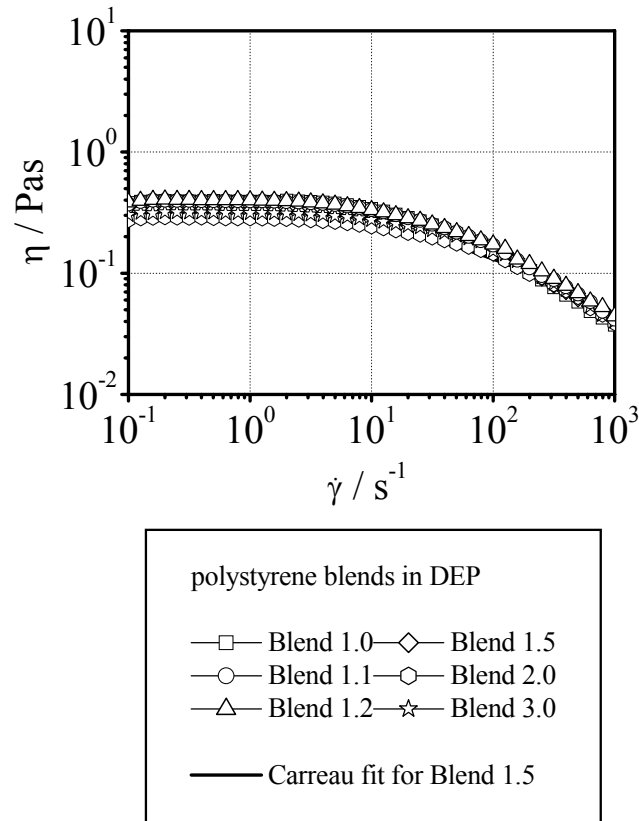
Figure 86: Shear viscosity η versus shear rate $\dot{\gamma}$ for investigated polystyrene blends 1.0 – 3.0 in diethylphthalate (1.0 wt%) at 25°C.

In contrast to this the results of uniaxial elongation in a CaBER experiment are shown in Fig. 87 for the same polystyrene blends.

Fig. 87 shows, that in contrast to steady shear flow experiments one can determine pronounced differences in the capillary thinning behaviour for the investigated polystyrene blends. In the linear regime of this semi-logarithmic plot one can evaluate longest relaxation times according to Eq. 81.
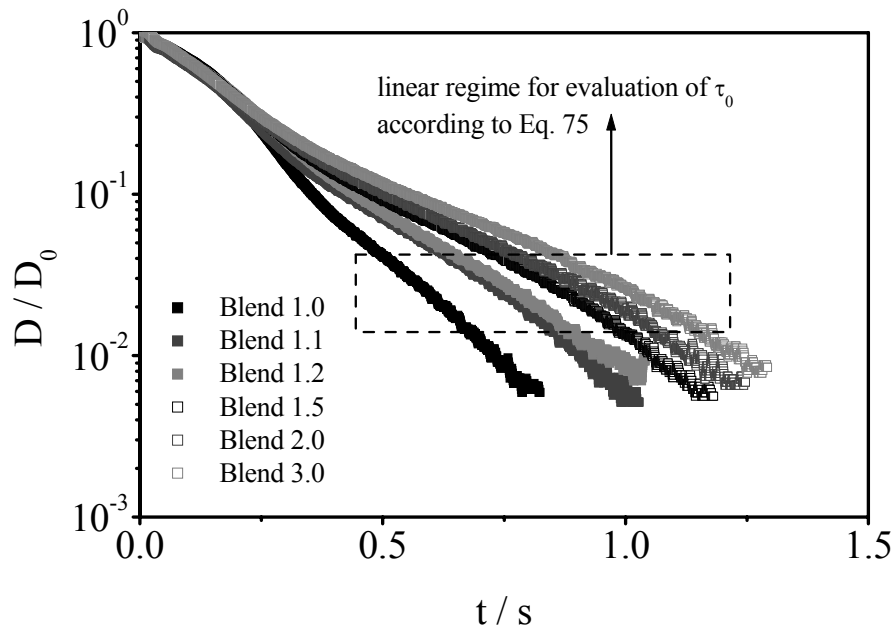
Figure 87: Normalized filament diameter D/D_0 versus time for the investigated polystyrene blends 1.0-3.0 in diethylphthalate at 1.0 wt% and 25°C.

The longest relaxation times obtained via the CaBER experiments are summarized in Table 12 together with the longest relaxation times of shear flow for the six investigated blends.

Table 12: Longest relaxation times τ_0 determined via CaBER experiments for polystyrene blends 1.0 - 3.0 (for details on the used polystyrenes see Table 1).

Blend	τ_0 shear flow	τ_0 CaBER
1.0	0.018	0.062
1.1	0.019	0.076
1.2	0.019	0.083
1.5	0.021	0.098
2.0	0.025	0.104
3.0	0.025	0.120

As one can see from Table 12, the longest relaxation time in uniaxial elongation increases with a factor 2 from blend 1.0 to blend 3.0, whereas the longest relaxation times of steady shear flow stay at a constant value of about 0.02 s.

For a correlation of linear viscoelastic terms like η_0 and J_0 with the MMD of a polymer, different approaches have been made in literature [149-151] with the general form

$$\hat{a} = \hat{a}_M \cdot P \qquad\qquad\qquad\text{(Eq. 175)}$$

with P being a correction term that depends on different modes of the MMD and $\hat{a}$ and $\hat{a}_M$ being a viscoelastic characteristic value of the distributed and the mondisperse sample. To correlate the relaxation behaviour of the polystyrene blends with the MMD, a model equation was searched for, that directly relates the ratio of relaxation times of monodisperse (blend 1.0) and polydisperse samples with the MMD. The factor P in the majority of approaches is of the form

$$P = \left(\frac{M_X}{M_W^y} \right)^c \qquad\qquad\qquad\text{(Eq. 176)}$$

with M_x being the x-mean molar mass $M_X = \dfrac{\sum n_i \cdot M_i^x}{\sum n_i \cdot M_i^{x-1}}$ and y and c being empirical or theoretical predicted parameters. Least square fits of the experimentally obtained values of τ_0 and $\tau_{0,M}$ as our characteristic viscoelastic properties as a function of P (see Eq. 176) for several different x-mean distributions and c and y as fitting parameters were accomplished to determine the best suited M_X. As shown in Fig. 88, the best correlation could be obtained for M_X as the z+2 average molar mass.
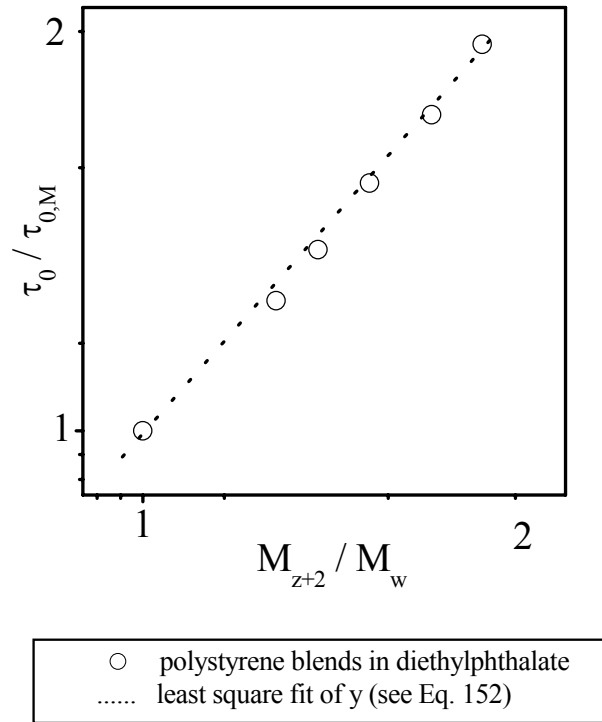

Figure 88: Least square fit of the parameters c and y (see Eq. 176) to M_{z+2}/M_w for investigated polystyrene blends in diethylphthalate.

The least square fit of the data in Fig. 88 gave the following equation to describe the dependency of the relaxation times from the width of the MMD:

$$\frac{\tau_0}{\tau_{0,M}} = \left(\frac{M_{z+2}}{M_w^1}\right)^{1.22}$$

(Eq. 177)

with $\quad M_{z+2} = \dfrac{\sum n_i \cdot M_i^5}{\sum n_i \cdot M_i^4}$

The integraly determined longest relaxation time of uniaxial elongation in CaBER like experiments of a distributed sample is hence mainly influenced by the M_{z+2} mean molar mass of the MMD. As expected has the high molar mass tail of the molecular weight distribution the most pronounced influence on the elongational behaviour. However, one has to keep in mind, that the quantitative correlation in Eq. 177 of the M_{z+2} mean molar mass and the values of c and y are so far purely empirical.

Another important material function of elongational rheology is the elongational viscosity η_e. According to the Trouton ratio for uniaxial flow fields [89], this elongational viscosity should show thrice the value of the zero-shear viscosity in the Newtonian flow regime, as can be seen by comparison of the values of the respective viscosities in Fig. 89 with and Fig. 86.
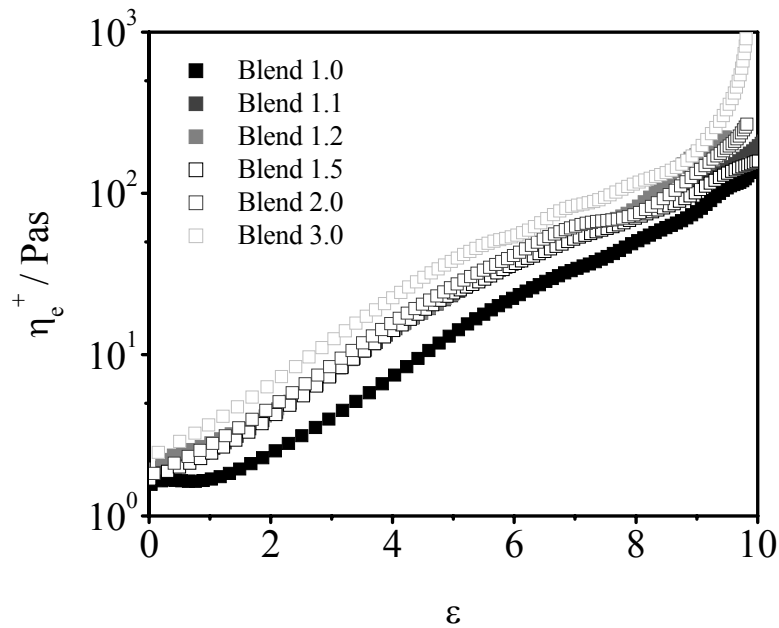
Figure 89: Apparent elongational viscosity η_e^+ versus Hencky strain ε for the investigated polystyrene blends 1.0 - 3.0 in diethylphthalate at 1.0 wt% and 25°C.

Fig. 89 also shows that for the investigated polystyrene solutions the steady state extensinal viscosity η_e is not reached in the regime of available strains. The first thing getting obvious is that, in contrast to steady shear, one can observe differences in the elongational viscosity of the investigted blends; The absolute values are increasing with increasing broadness of the MMD from blend 1.0 to blend 3.0. However one has to keep in mind that the viscosity observed here is the transient elongational viscosity η_e^+, which is, compared to the steady state value η_e, the more interesting material function regarding to application, because

elongational flow fields in polymer processing usually are instationary ones. The value of the transient elongational viscosity η_e^+ for the investigated polystyrene solutions is increasing over the whole regime of extension, reaching values around 300-400 Pas. These considerably high values, compared to the moderate zero-shear viscosities of about 0.3-0.5 Pas, are a result of pronounced strain hardening processes of the polymer coil in uniaxial elongation [100, 152].

To point out the influence of the high-molar mass fraction on the elongational behaviour in capillary breakup, two polystyrene standards of different weight-average molar masses M_w (PS 1b and PS 5, see Table 1 for details) were blended at a constant concentration of 250 ppm in styrene oligomer (low molecular weight polystyrene, LMPS) as the solvent. The absolute blending composition of the investigated binary blends is summarized in Table 13 together with the resulting weight average molar masses and the polydispersities.

Table 13: Absolute blending composition of investigated binary polystyrene blends (for details on the used polystyrenes see Table 1).

Blend	Blend Composition / wt%		M_w Mg/mol	M_w / M_n (Q)
	PS 1b	PS 5		
90	9.9	90.1	7.65	1.15
50	49.8	50.2	5.49	1.31
10	90.2	9.8	3.32	1.10
3.1	96.9	3.1	3.00	1.04
1.0	99.0	1.0	2.88	1.01
0.31	99.7	0.3	2.85	1.00
0.1	99.9	0.1	2.84	1.00

The resulting zero shear viscosity of these Boger fluids [153] is very high compared to a solution in DEP, so that relaxation actions of the polymer coils are slowed down to a high degree which therefore leads to an improved detectability even at concentrations below c[*] (critical overlap concentration). The results of steady shear flow measurements for these Boger fluids are shown in Fig. 90.
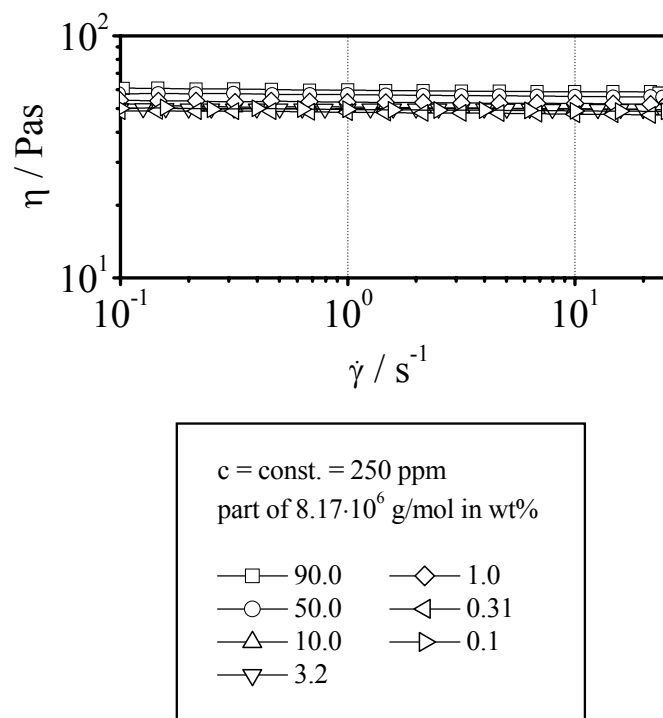
Figure 90: Shear viscosity η versus shear rate $\dot{\gamma}$ for investigated binary polystyrene blends in styrene oligomer (for absolute composition see Table 13), 250 ppm at 25°C.

Fig. 90 shows that almost no differences in zero shear viscosity can be detected for the set of investigated binary Boger blends, the values balance around 50 Pas, which is a fairly high value for a polymer solution. In comparison to this one has to keep in mind that honey for example has a zero-shear viscosity of about 1-5 Pas! However, the missing differences in the flow curves were expected for a mainly solvent dominated shear flow in a dilute solution. In contrast to this, the results of uniaxial elongation for this set of Boger blends are shown in Fig. 91.
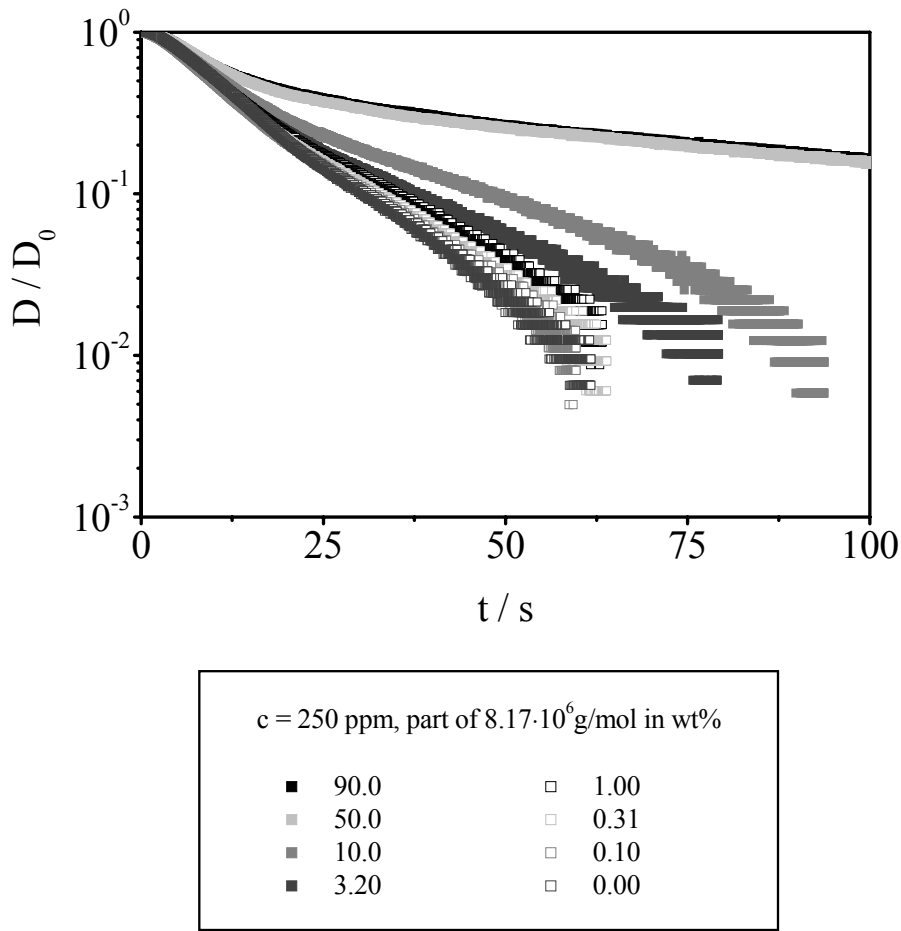
Figure 91: Normalized filament diameter D/D_0 versus time for the investigated binary polystyrene blends in styrene oligomer (for absolute composition see Table 13), 250 ppm at 25°C.

As shown in Fig. 91, a fraction of 0.31 wt% of the high-molecular species already results in measureable longer breakup times. Since the CaBER experiment reacts very sensitive to the longest relaxation time of the high-moleclar edge of the MMD according to Eq. 81, tiny amounts of high-molecular species already lead to a pronounced influence on the elongational behaviour.

However, one has to keep in mind, that in contrast to the blends in Fig. 87, these binary blends do not have a constant weight average molar mass M_w, but rather an increasing M_w (see Table 13 for details) with an increasing part of the high molecular weight species. Therefore, one would naturally expect the relaxation time to rise with increasing part of high molecular weight species.

A better way to observe the influence of the distribution is again to plot a reduced $\tau_0 / \tau_{0,M}$. The required $\tau_{0,M}$ can be obtained from the pure low and high molar mass solutions, since the relaxation time dependence scales with $M_w^{3\nu}$ for narrow distributions [32, 33], with ν being the excluded volume coefficient:

$$\tau_{0,M} = (2.3 \pm 1.7) \cdot 10^{-10} M_w^{(1.62 \pm 0.05)} \qquad \text{(Eq. 178)}$$

We obtain $\tau_{0,M} = (1.6) \cdot 10^{-10} M_w^{(1.62)}$ in good agreement with Anna and McKinley [32] and can therefore plot $\dfrac{\tau_0}{\tau_{0,M}} = f\left(\dfrac{M_{z+2}}{M_w}\right)$. The results are shown in Fig 8.
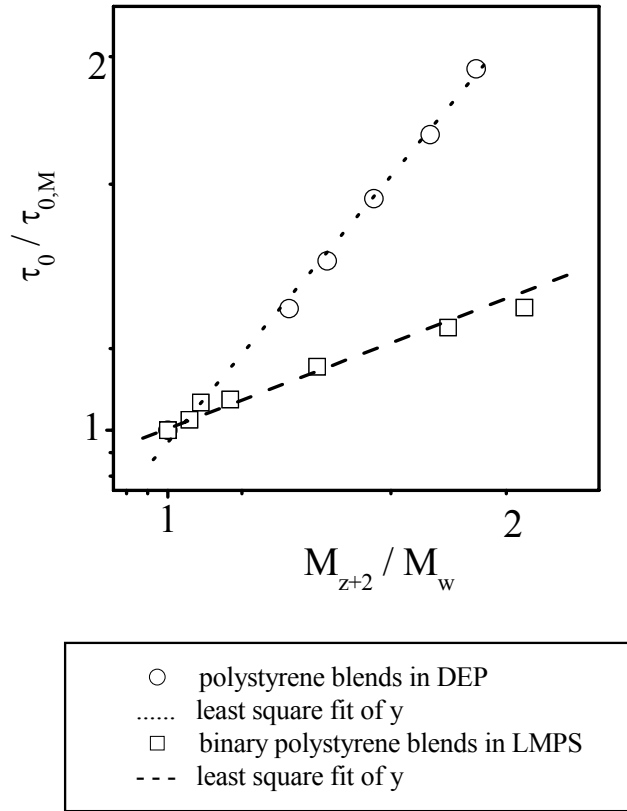
Figure 92: Least square fit of the parameters c and y (see Eq. 176) to M_{z+2}/M_w for investigated polystyrene blends in diethylphthalate and binary blends in LMPS.

From Fig. 92 one can see that the relaxation times of the binary blends do not scale with the same exponent c as the polystyrene blends in DEP (see Eq. 178). Still, linear fitting of the data works out quiet well, as shown in Fig. 92. However, one has to keep in mind, that we are dealing not with a flory distribution in this case, but a bimodal distribution of the molar mass. In addition to this the styrene oligomers are a worse solvent than diethylphthalate and close to theta conditions [134]. We therefore refrain from comparing c for diethylphthalate and Boger fluid.

As for the polystyrene blends in DEP, Fig. 93 shows the transient elongational viscosity η_e^+ for the investigated binary polystyrene blends.
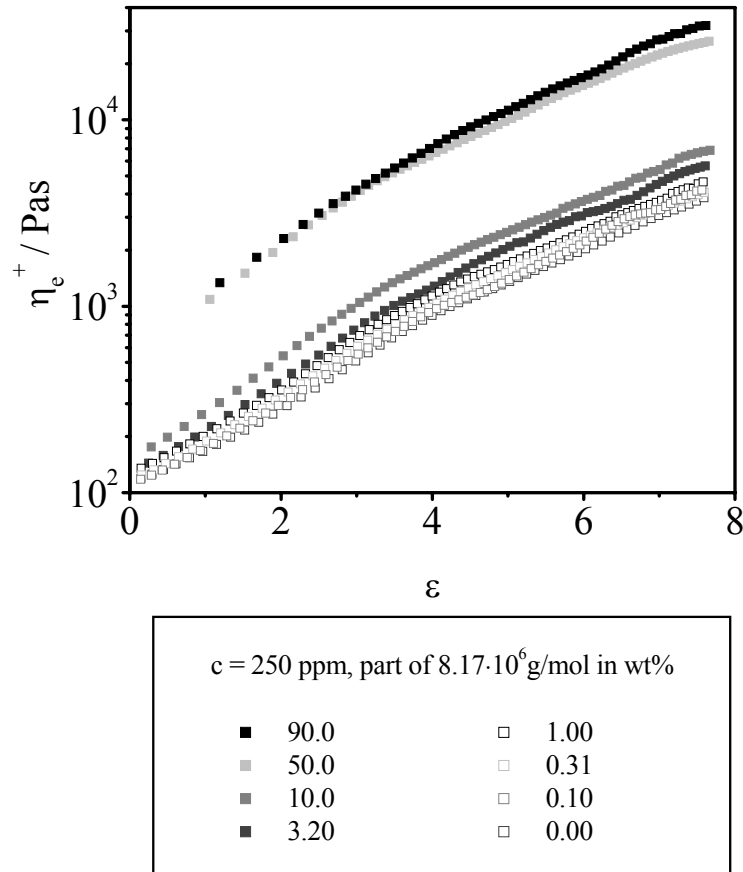
Figure 93: Apparent elongational viscosity η_e^+ versus Hencky strain ε for the investigated binary polystyrene blends in styrene oligomer (for absolute composition see Table 13), 250 ppm at 25°C.

As one can see in Fig. 93, even for these very dilute solutions of 250 ppm the steady state value of the elongational viscosity is not reached in the regime of available strains. Again the Trouton ratio of three is met in the regime of Newtonian flow as one can see via comparing the elongational values of about 140-150 Pas with the zero-shear viscosity of about 45-50 Pas deriving from Fig. 90.

However, for the two blends with the highest amount of high molecular weight fraction, blend 50 and blend 90, the transient elongational viscosity does not start from the equilibrium value, but it seems to start of with a higher value. This may be the result of an initial deformation in the test fluid, resulting in pre-stretched polymer coils resulting in a higher viscosity yield. As for the blends in DEP one can observe again, that, in contrast to the results from steady shear flow, the evolution of the transient elongational viscosity is clearly distinguishable for the binary blends.

6.2 Rheological characterisation of investigated MHECs and hmHECs

6.2.1 Steady shear flow

As shown for the polystyrene standards in chapter 6.1.1, the methylhydroxyethyl celluloses investigated in this work were also fully characterized in regards of their viscous properties via shear flow experiments.

The influencing parameters examined here include the concentration and the solvent (for the influence of the molar mass or its distribution see chapter 6.2.3.2 for a detailed discussion).

Figure 94: Shear viscosity η versus shear rate $\dot{\gamma}$ for methylhydroxyethyl celluloses 1-10 with different molar masses (see Table 3 for details) in water (1.0 wt%) at 20°C.

The MHEC samples investigated in this work were blended from different cellulose samples (see chapter 5.2 for details), before synthesis was achieved via Williamson etherification (see chapter 2.2). As the resulting MHECs were, according to the manufacturer, very similar in terms of their rheological behaviour , the primary task was to work out specific differences in their flow comportment.

Fig. 94 shows the flow curves for the full set of investigated MHECs in water at 1.0 wt% and 20°C (this temperature was used instead of RT for the MHECs, because it is the standard temperature the manufacturer and project partner uses). As one can see in Fig. 94, the flow curves partially exhibit very pronounced yielding points. For a better resolution of this effect, one can also plot the shear viscosity η versus the shear stress σ instead of the shear rate $\dot{\gamma}$, as can be seen in Fig. 95.

This plot has the advantage that if a polymer solution exhibits a real yielding point, one finds a sudden drop in shear viscosity in contrast to a linear decrease with the slope of exactly -1.0 (according to Newtons law of viscosity, see Eq. 22) for the plot shown in Fig. 94. As Fig. 95 shows, the samples MHEC 4, 5, 9 and 10 show real yielding points of about 10 Pas, whereas the other samples do not exhibit a sudden viscosity drop. However, this yielding point is a result of an unwanted structure build-up in solution via H-bonding between the single MHEC coils.

Figure 95: Shear viscosity η versus shear stress σ for methylhydroxyethyl celluloses 1-10 with different molar masses (see Table 3 for details) in water (1.0 wt%) at 20°C.

Fig. 96 shows the flow curves of the same set of MHECs investigated at 2.0 wt% in water as the solvent. The first thing that attracts attention here is that the yielding points seem to have vanished for the higher concentrated solutions.

A possible reason for this unexpected behaviour is that the zero-shear viscosity η_0 of about 30 Pas of the respective solutions more than compensates the value of the yielding point itself ($\sim$ 10 Pas).
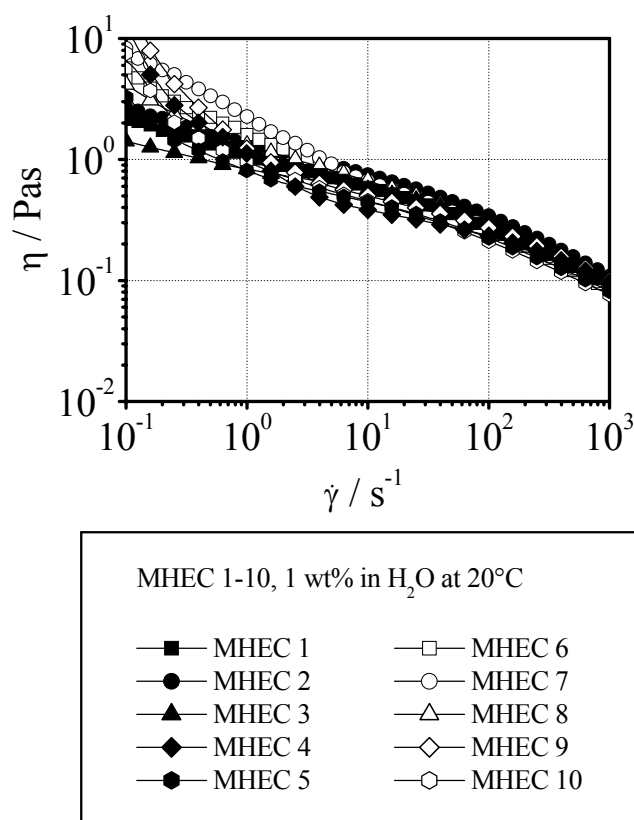
Figure 96: Shear viscosity η versus shear rate $\dot{\gamma}$ for methylhydroxyethyl celluloses 1-10 with different molar masses (see Table 3 for details) in water (2.0 wt%) at 20°C.

As yielding points prevent the direct determination of – and the comparability of the flow curves in terms of their zero-shear viscosities η_0, a solvent had to be used that suppresses the structure build-up via breaking of the H-bonds between the hydroxyethylgroups of a MHEC coil with the protons of another MHEC coil. The first choice fell on NaOH in water (2.0 wt%) because of its very pronounced alkalinity.

The same flow curves shown in Fig. 94 and Fig. 96 for the investigated MHECs in water at concentrations of 1.0 or 2.0 wt% are shown again in Figs. 97 and 98 for the same concentrations in aqueous NaOH (2.0 wt%).
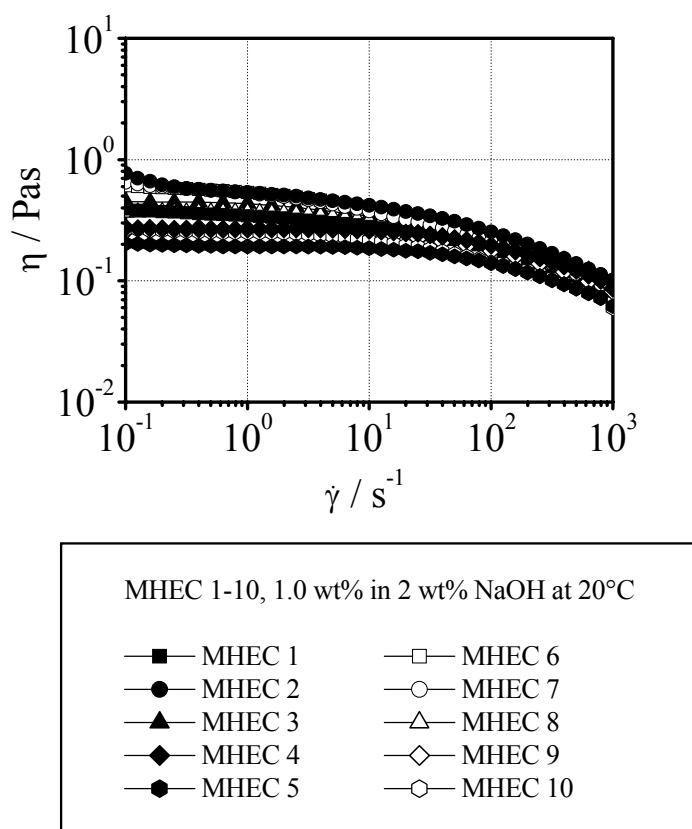
Figure 97: Shear viscosity η versus shear rate $\dot{\gamma}$ for methylhydroxyethyl celluloses 1-10 with different molar masses (see Table 3 for details) in 2 wt% NaOH (1.0 wt%) at 20°C.

As one can see in Fig. 97, the yielding points observed for the respective MHEC solutions in water disappear for the use of NaOH as solvent. The MHEC solutions are better molecularly dispersed without the strong structure build-up, so that the zero-shear viscosities can be determined for both concentrations. For the 1.0 wt% solutions the zero-shear viscosities range from approx. 0.2 – 0.7 Pas (see Fig. 97), whereas for the 2.0 wt% solutions (see Fig. 98) the zero-shear viscosity ranges from 2 – 16 Pas for the investigated set of 10 MHECs. However both figures show that the flow curves are very much alike each other inside each one of the two different sets of MHECs (see chapter 5.2 for details).

In contrast to the flow curves for the polystyrene standards (see chapter 6.1.1) one can see that the transition area from the Newtonian- to the non-Newtonian flow regime is much broader. This is directly correlated to the width of the molar mass distribution (MMD) shown in Fig. 37 and 38 in chapter 5.2. As the investigated MHECs are far from being ideal standard systems like the investigated polystyrenes, the transition is naturally far more broad (a more detailed discussion on this topic will follow in chapter 6.2.3.2).

The third material function yielded via shear flow experiments is the slope of the flow curve *n* in the non-Newtonian flow regime. Figs. 97 and 98 show that the slopes are very much the same for the ten samples and each respective concentration. For the 1.0 wt% solutions this characteristic has a value of 0.43, whereas the slopes of the flow curves for the 2.0 wt% solutions balance around 0.64.
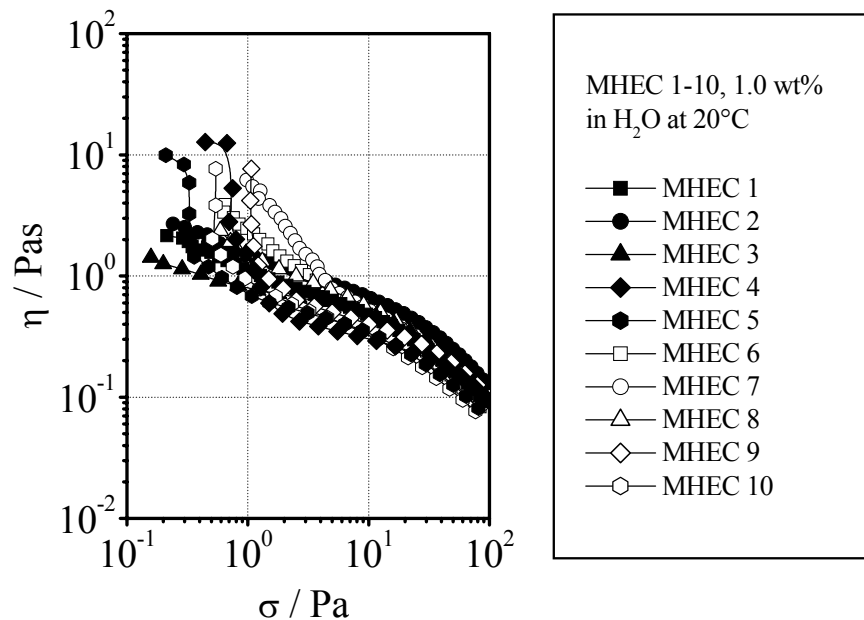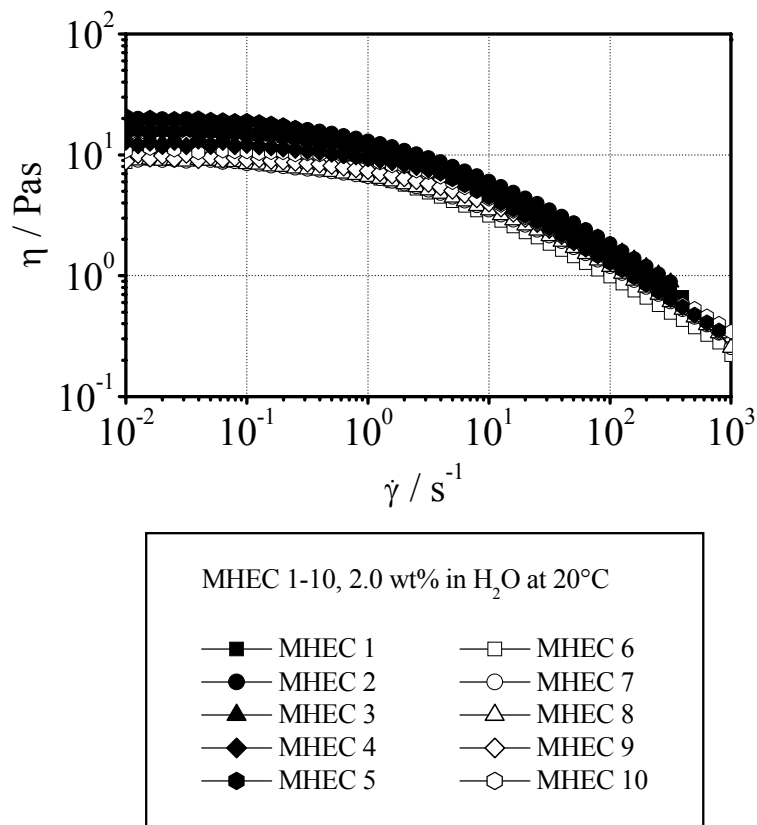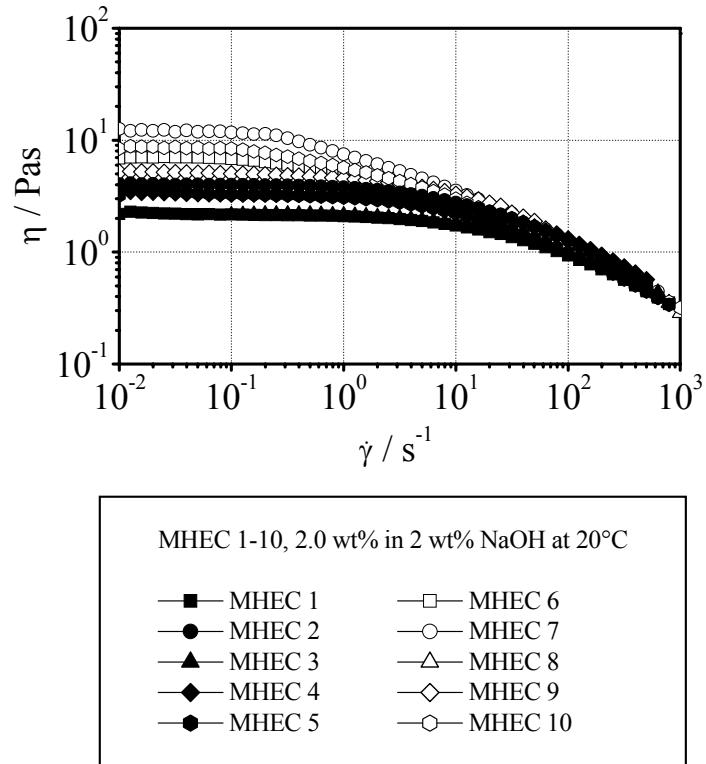
Figure 98: Shear viscosity η versus shear rate $\dot{\gamma}$ for methylhydroxyethyl celluloses 1-10 with different molar masses (see Table 3 for details) in 2 wt% NaOH (2.0 wt%) at 20°C.
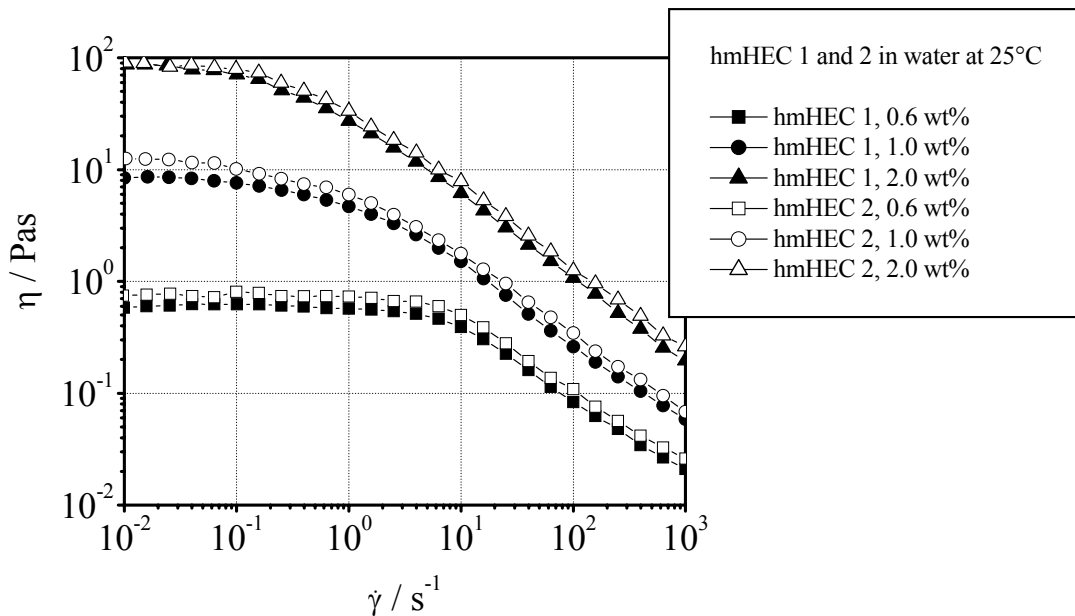
Figure 99: Shear viscosity η versus shear rate $\dot{\gamma}$ for both investigated hmHECs at different concentrations in water at 25°C.

The two hmHECs investigated in this work are supposed to see application as stabilizing agents in cosmetic emulsions. The stabilizing effect results from their amphiphilic

like nature, that makes it possible for these polymers to be solved in hydrophobic and hydrophibic solvents.

As for the MHECs, the question was again if the two samples could be distinguished from each other with rheological means. As it could be seen in chapter 5.3, the molecular weight distributions of the two investigated samples show very ample differences from each other (see Fig. 43 for details). While sample hmHEC 1 shows a bimodal distribution with a very pronounced shoulder in the regime of small molar masses, sample hmHEC 2 exhibits an almost normal distribution resulting in a much smaller polydispersity index. As can be seen in Fig. 99 these ample differences in terms of their MMD do not reflect in the results of steady shear flow. For all three investigated concentrations, the flow curves very much look alike.

However, in terms of their zero-shear viscosity that was an expected result, as the weight-average molar masses M_w are very similar to each other, the differences in terms of the broadness of their distributions Q does not affect the transition area between Newtonian and non-Newtonian flow regime. Steady shear flow therefore does not yield any qualitative or quantitative information on distinguishing the two samples in regards of their molar mass distribution.

6.2.2   Small amplitude oscillatory shear (SAOS)

As for the polystyrenes in chapter 6.1.2, the visco-elasticity of the investigated MHECs and hmHECs was analyzed further via SAOS experiments. The elastic components of the visco-elastic behaviour of these cellulosic derivatives can again be correlated with the storage modulus G', whereas the viscous components are represented by the loss modulus G'' (see chapter 3.3.2 for a detailed discussion).

For the methylhydroxyethyl and the hydrophobically modified hydroxyethyl celulloses a comparison of the shear viscosity η and the from SAOS measurements obtained complex viscosity η^* according to the empirical rule of Cox and Merz [144] is also very usefull. As there may be energetic interactions via ionic groups in the backbone of the MHEC or the hydrophobic modifications of the HECs and the fact that both polymers tend to structure build-up via Van der Waals- and London interactions, particularly H-bonding, this comparison may yield quatitative information on the level of energetic interactions.

Figure 100: Storage moduli G' versus angular frequency ω for methylhydroxyethyl celluloses 1-10 in 2 wt% NaOH (1.0 wt%) at 20°C.

As shown in Fig. 100 and Fig. 101 for the 1.0- or 2.0 wt% solutions of the investigated MHECs 1-10 in 2 wt% NaOH, there is no distinctive information gained from the frequency dependence of the storage moduli G'. For the 1.0- and 2.0 wt% solutions, the high frequency limit of about 200 rad/s (maximum frequency achievable by used ARES II rheometer, for detailed specifications refer to chapter 8.2.2) is not large enough to enter the plateau regime of the storage modulus, means that the network parameters are not accessible for both

concentrations without extrapolation. The moduli for the 2 wt% solutions at least show a slight snap off at a frequence of about 10 rad/s.

As for the evolution of the storage moduli G' one can observe very analogue trends within one of the two investigated concentrations shown here. The slopes of the curves lie somewhere in between the theoretically predicted value of 2 and a slope of 1 for both concentrations. Only the sample MHEC 3 at 2.0 wt% gives the theoretical value of 2 at low frequencies. The only differences between the two concentrations is that, on the one hand, the values of the moduli for the higher concentration outrank the values for the lower concentration with about one order of magnitude as expected. On the other hand, the yielding points discussed in chapter 6.2.1 for the 1.0 wt% solutions are observed here also in the minimum behaviour observed in Fig. 100. At low frequencies the aggregated structures in solution behave like a "real" gel, resulting in a fake first plateau modulus for very small deformations.
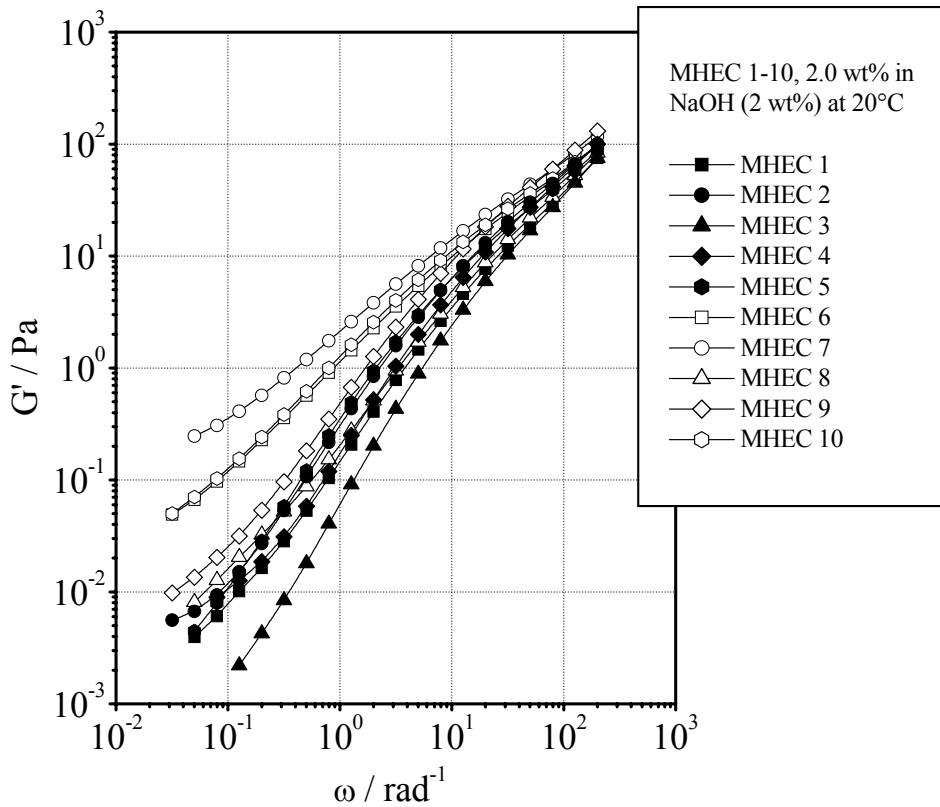
Figure 101: Storage moduli G' versus angular frequency ω for methylhydroxyethyl celluloses 1-10 in 2 wt% NaOH (2.0 wt%) at 20°C.
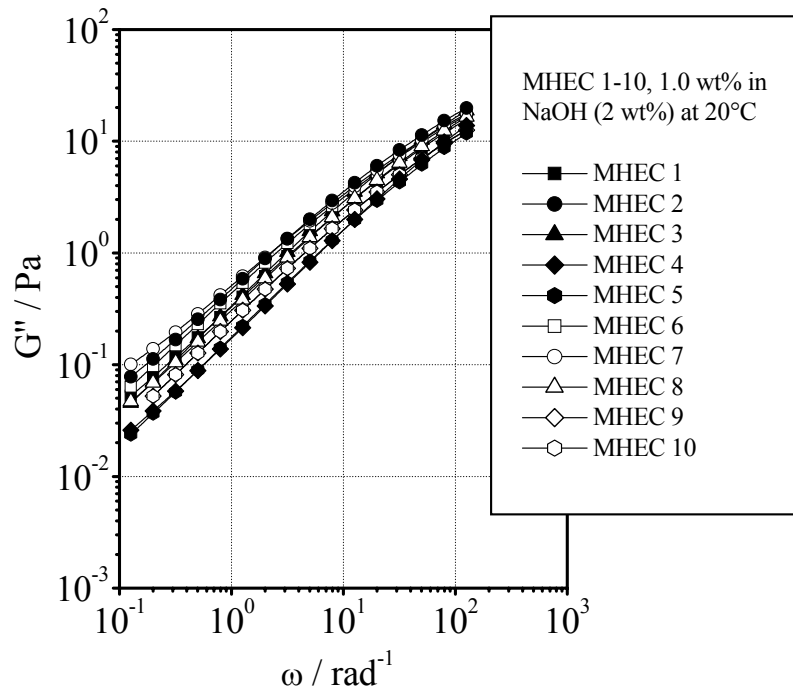
Figure 102: Loss moduli G'' versus angular frequency ω for methylhydroxyethyl celluloses 1-10 in 2 wt% NaOH (1.0 wt%) at 20°C.

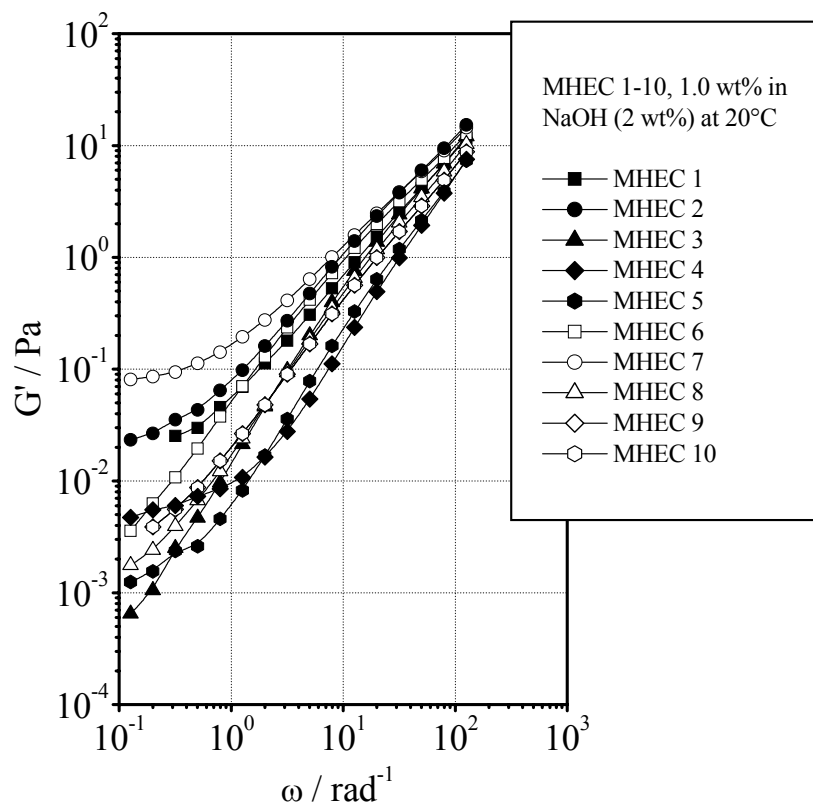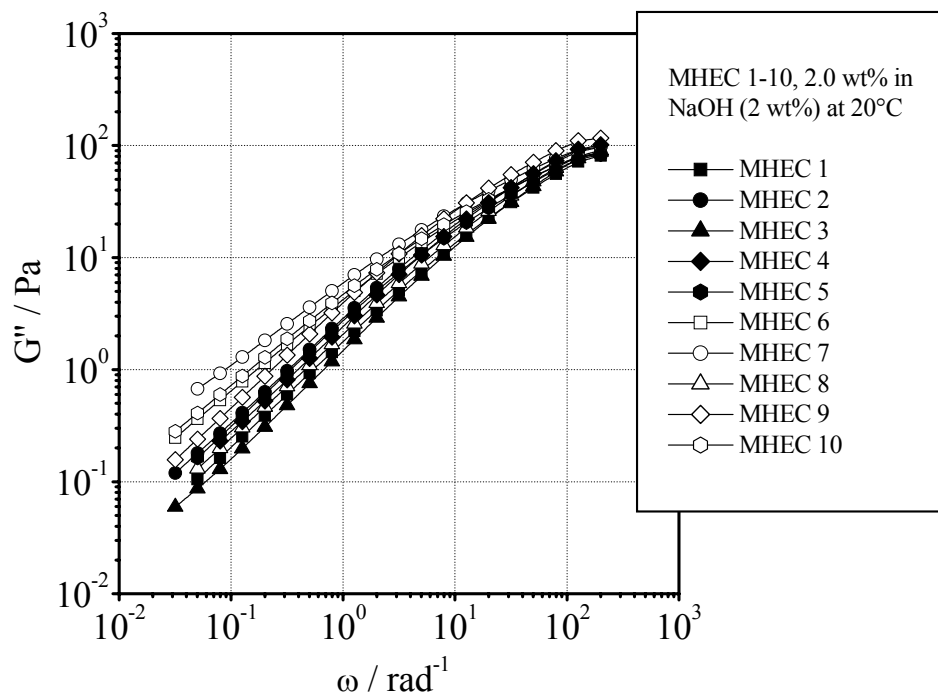*Figure 103: Loss moduli G'' versus angular frequency ω for methylhydroxyethyl celluloses 1-10 in 2 wt% NaOH (2.0 wt%) at 20°C.*

The same trends discussed before for the storage moduli G' for both concentrations of the investigated MHECs also applies for the loss moduli G''. The slope for both concentrations fits very well to the theoretically predicted value of 1 (see chapter 3.3.2 for

details). Again the absolute values for the loss moduli of the higher concnetrated soltions outrank the ones for the lower concentrations with about (O)1. This is due to the fact that not only the elastic properties of the resulting gels in form of G' increase with concentration (because more inserted energy can be stored elastically in a network wich consists of more and denser meshs), but also the flexibility in form of G'' of the network.

A qulitative discussion of energetic interactions between the single polymer coils can happen in form of the Cox-Merz plot shown in Fig. 104. As one can see in form of the comparisson of the shear viscosities η and complex viscosities η^* for a set of selected MHECs (not all material functions for the whole set of investigated MHECs were plotted, to keep a certain degree of clarity in the figure), are the different viscosities in good agreement with each other. This result reflects the fact that the Cox-Merz rule applies just for the non-Newtonian flow regime [144] where the increasing deformation already degraded the aggregated structures responsible for the yielding points. As the number of ionic groups in the sidechain is very small for MHEC the energetic interactions are not ample enough to result in a derivation of the complex viscosity from the shear viscosity.
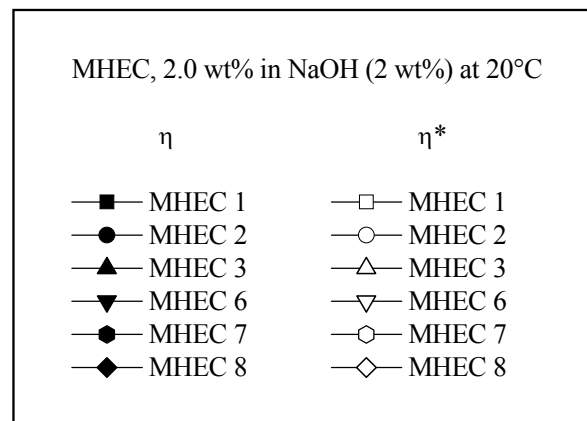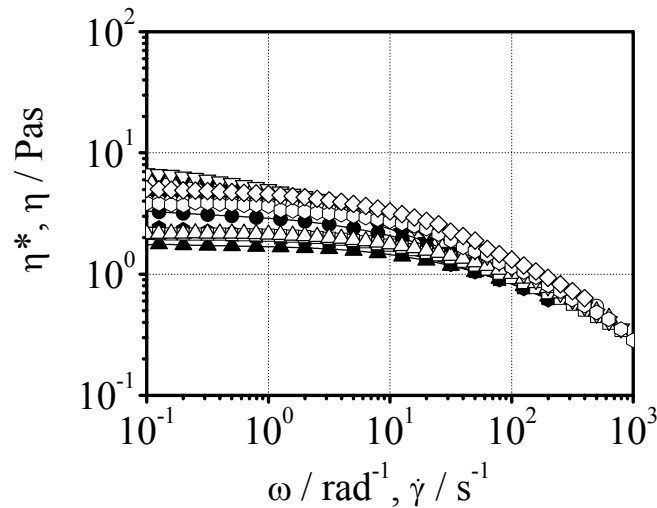
Figure 104: Comparison of shear viscosity η and complex viscosity η^* for methylhydroxyethyl celluloses 1-3 and 6-8 in 2 wt% NaOH (2.0 wt%) at 20°C.
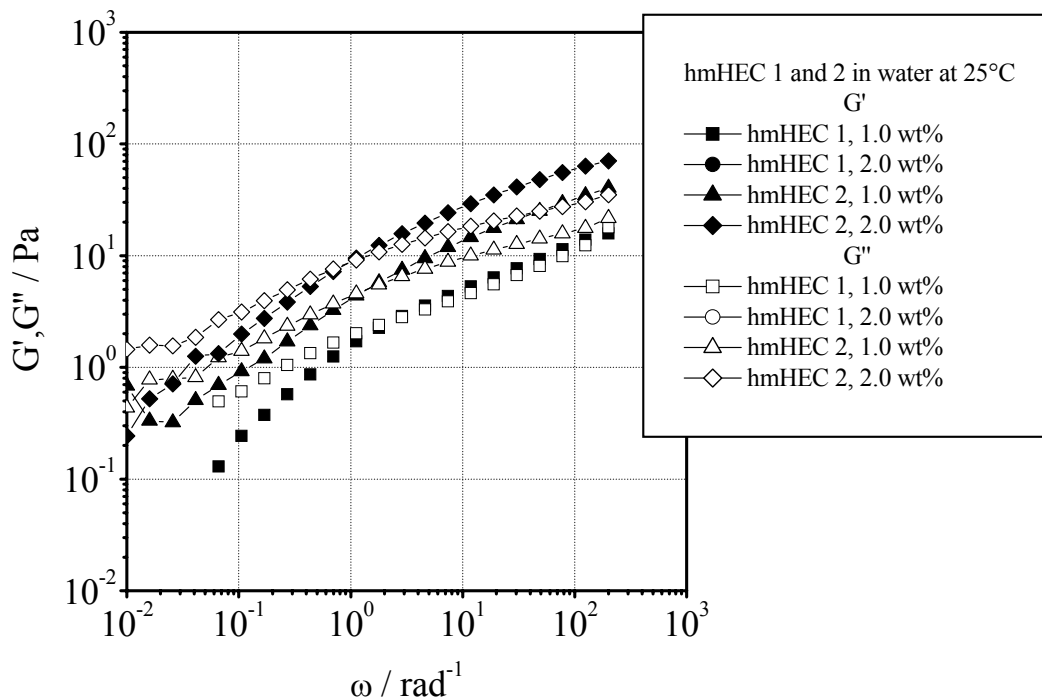
Figure 105: Storage moduli G' and loss moduli G'' versus angular frequency ω for both investigated hmHECs at different concentrations in water at 25°C.

As shown in Fig. 105 for the 1.0- or 2.0 wt% solutions of the investigated hmHECs 1 and 2 in water, there is no distinctive information gained from the frequency dependence of the storage moduli *G'* and loss moduli *G''*. For the 1.0- and 2.0 wt% solutions, the high frequency limit of about 200 rad/s (maximum frequency achievable by used ARES II rheometer, for detailed specifications refer to chapter 8.2.2) again, is not large enough to enter the plateau regime of the storage modulus, means that the network parameters are not accessible for both concentrations without extrapolation.

As shown in Fig. 106, comparison of the shear viscosity η and the complex viscosity η^* via the Cox-Merz plot yields higher values for the shear viscosity of the sample hmHEC 2. This is due to the fact, that the structure build-up resulting in higher values of the viscosity via hydrophobic interactions is a shear induced phenomenon. The SAOS experiment does not "see" this effect of shear thickening, thus the complex viscosity shows lower values.
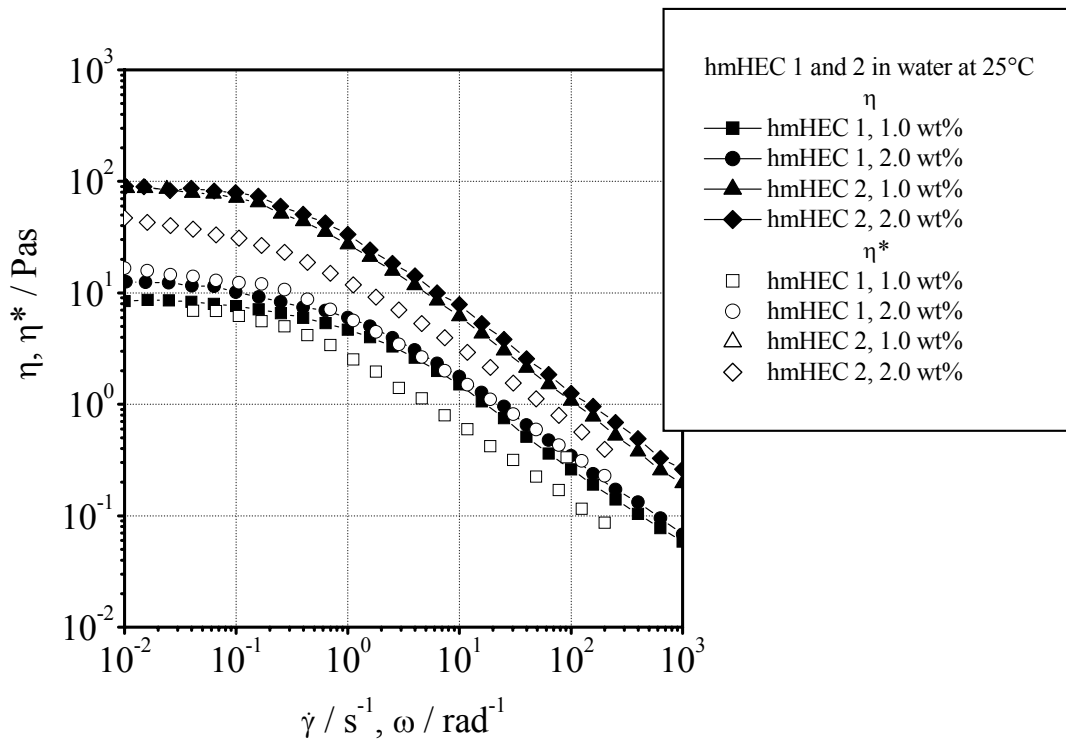
Figure 106: Comparison of shear viscosity η and complex viscosity η^* for both investigated hmHECs at different concentrations in water at 25°C.

6.2.3   Uniaxial Deformation

6.2.3.1   Influence of concentration

To point out the influence of the concentration on the break-up behaviour of the investigated methylhydroxyethyl celluloses, the results for uniaxial elongation are shown in Fig. 107 for the 1.0 wt% solutions and in Fig. 108 for the 2.0 wt% solutions in 2.0 wt% NaOH. The results of the elongational experiments of the purly aqueous solutions are not presented here, because the influence of aggregated structures on the break-up behaviour is far more explicit than on the steady shear - or oscillatory shear characteristics.

The aggregated structures in the non-molecularly dispersed MHEC solutions lead to yielding points that are too strong to be "cracked" by the surface trension driven flow, meaning that if the surface tension of the investigated fluid is not big enough, the filament remains at a defined constant diameter.
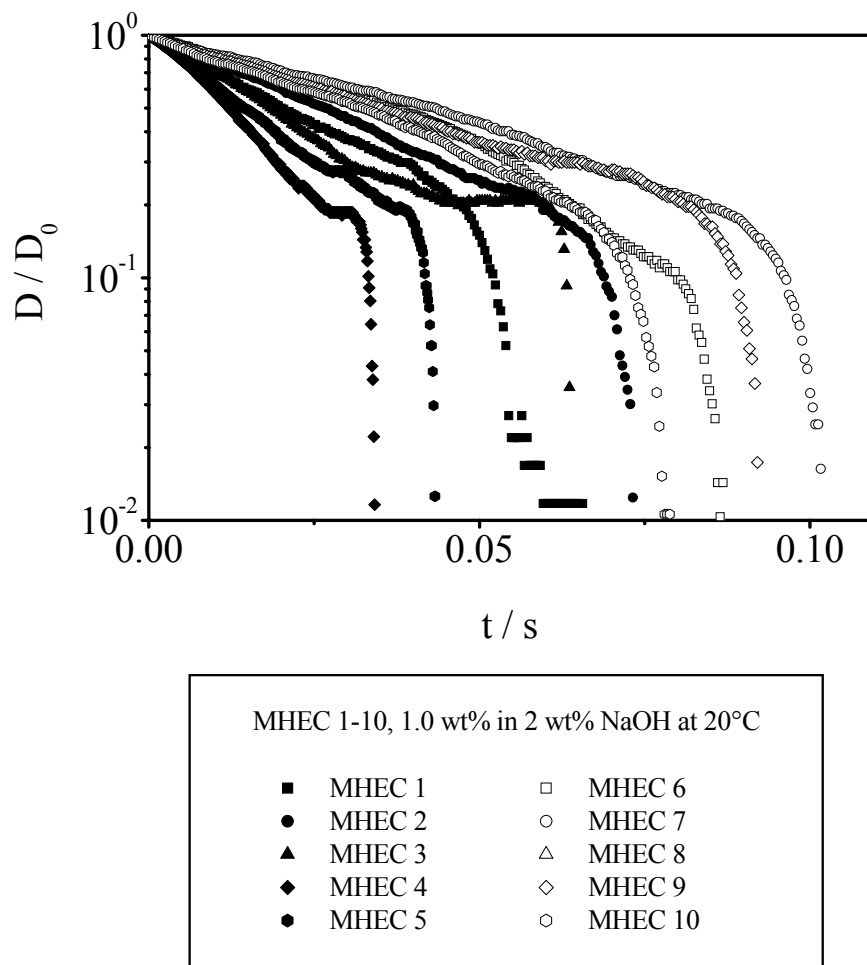
Figure 107: Normalized filament diameter D/D₀ versus time for the investigated methylhydroxyethyl celluloses 1-10 in 2 wt% NaOH (1.0 wt%) at 20°C.

As one can see in Fig. 107, the same trend as for the steady shear flow experiments for the same MHEC solutions (compare 6.2.1 for details) is observed in capillary break-up. Whereas the yielding points led to an increase in shear viscosity η for shear flow experiments, the same yielding points result in stationary filament diameters for the same solutions in elongational flow. After this plateau region, the filament collapses because of the growing stress in the axial direction of the filament and the diameter decreases instantly. However, in addition to the yielding stresses one observes no "smooth" evolutions of the filament diameters with time for the 1.0 wt% solutions. This may be due to the very short time scales of the experiments, the longest break-up time for the sample MHEC 10 is about 10^{-1} s. For this time scale, surface effects like the migrating behaviour of the polymer coils to the surface of the filament to repeatingly refresh the surface are not neglectible. Another influencing parameter is that MHEC is a surface active substance via the hydrophobic methylgroups. This leads to inhomogenieties on a molecular scale, again leading to everything but a perfect behaviour in capillary break-up.
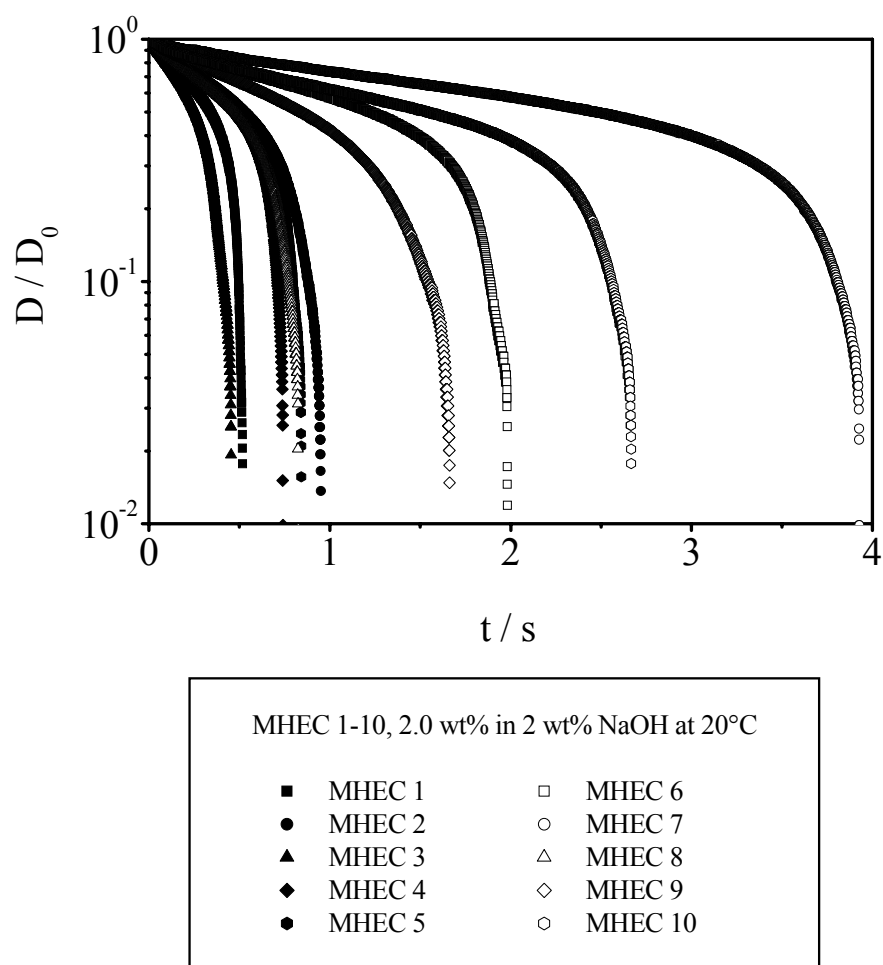
Figure 108: Normalized filament diameter D/D$_0$ versus time for the investigated methylhydroxyethyl celluloses 1-10 in 2 wt% NaOH (2.0 wt%) at 20°C.

Compared to Fig. 107, the results for the 2.0 wt% solutions of the same MHECs in 2.0 wt% NaOH shown in Fig. 108 do exhibit a far nicer behaviour in capillary break-up. The concentration is ample enough to over compensate the effects induced by the yielding points already discussed in chapter 6.2.1. In addition to this, the absolute break-up times of the experiment increase pronouncly compared to the break-up times observed in Fig. 107, the longest break-up time is in the order of 4 s for the sample MHEC 10, surface build-up does not disturb the experiment anymore, because its time scale is of no relevance for the filament evolution.

As the data for both concentrations implicate, the broadness of the molar mass distributions shown in chapter 5.2 seem to have an influence on the bereak-up behaviour in uniaxial elongation. A detailed look at this importnant issue is given in the next chapter.

6.2.3.2   Influence of molar mass/ molar mass distribution

Since the influence of the width of the MMD on the elongational behaviour of polymer fluids was already discussed on polystyrene standards in chapter 6.1.3.2 the same should apply for the investigated MHECs.

To point out the influence of the molar mass or the molar mass distribution on the break-up behaviour of the investigated methyhydroxyethyl celluloses three samples with long break-up times and pronounced differences in the molar mass distribution were chosen for deeper analysis. The absolute molar masses and their distributions were determined for the investigated commercial MHECs 6, 7 and 10 to correlate the results with the elongational behaviour. Determination of the absolute molar masses and the molar mass distributions was achieved via coupled methods of size exclusion chromatography (SEC), multi angle laser light scattering (MALLS) and differential refractometer (DRI) [154] (see chapter 3.2.3 for details). The results of the light scattering experiments for the three different MHECs are shown in Fig. 109 in terms of the differential molar mass distributions.
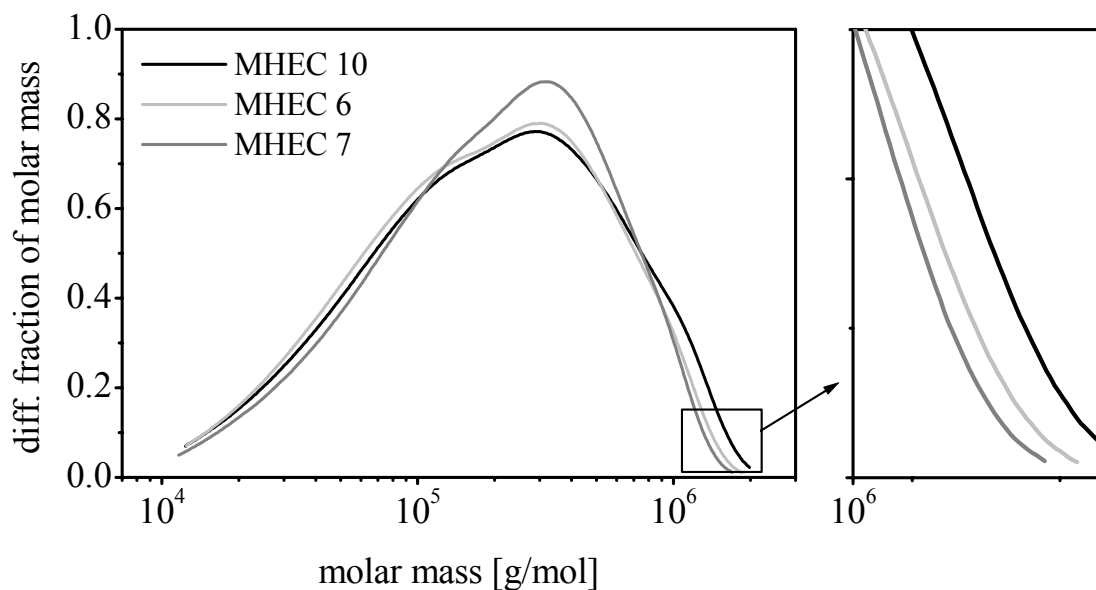
Figure 109: Differential molar mass distributions achieved via combined means of SEC/MALLS/DRI for selected MHECs 6, 7 and 10 (for experimental conditions see chapter 8.2).

As shown in Fig. 109 the sample MHEC 10 exhibits the broadest distribution of the molar mass that also is close to being bimodular. The other two samples MHEC 6 and MHEC 7 follow up with MHEC 6 having a broader distribution than MHEC 7; all three samples have very similar weight average molar masses. The determined mean values of the molar mass distribution and the polydispersity indices for the investigated MHECs were already listed in Table 3 (see chapter 5.2 for details). For a better overview, the very same mean values are listed together with the recovery rates of the SEC for the three here investigated MHEC samples in Table 14. The recovery rate is the fraction of polymer that reaches the differential refractometer based on the amount of polymer that was originally injected.

Table 14: Mean molar masses and recovery rates for the investigated MHECs 6, 7 and 10.

Sample	M_w Kg/mol	M_w/M_n	M_z Kg/mol	Recovery Rate wt%
6	*323*	*2,9*	*655*	*79*
7	*294*	*2,5*	*577*	*70*
10	*341*	*3,5*	*738*	*74*

As one can see from Table 14 the weight-average molar masses M_w are very close together for the three samples, it varies around 300 kg/mol, whereas the polydispersity index M_w/M_n varies from 2.5 for the sample MHEC 7 to 3.5 for the sample MHEC 10. Another very important measure for the broadness of the molar mass distribution is the z-average molar mass M_z. This mean value represents the standard mean value used that describes the high molar mass tail of the distribution best. As one can see, this parameter increases in the same manner as the polydispersity indices do for the three samples from 577 kg/mol for the narrowest distributed sample MHEC 7 to 738 kg/mol for the broadest distributed of the three samples, MHEC 10.

The results of steady shear flow experiments for these three investigated MHECs at 2.0 wt% in 2 wt % NaOH are shown in Fig. 110 together with the Carreau fits of the flow curves according to the modified Carreau model [102] (see Eq. 149 for details). The obtained relaxation times are listed together with the other Carreau parameters in Table 15.

Table 15: Carreau parameters for the investigated MHECs 6, 7 and 10.

Sample	η_0 / Pas	τ_0 Carreau / s	b	n
6	*12.8*	*0.18*	*0.53*	*-0.70*
7	*7.9*	*0.17*	*0.53*	*-0.61*
10	*9.3*	*0.17*	*0.53*	*-0.65*

As one can see in Fig. 110 and Table 15, the differences in the molar mass distribution of the methylhydroxyethyl celluloses do not reflect in the results for steady shear flow. The zero-shear viscosities η_0 show very mucthe same values, they balance from 7.9 -12.8 Pas. However, most significant for the fit parameters is the constant value for the longest relaxation time of shear flow τ_0 at 0.17 s and for the transition parameter b of 0.53.
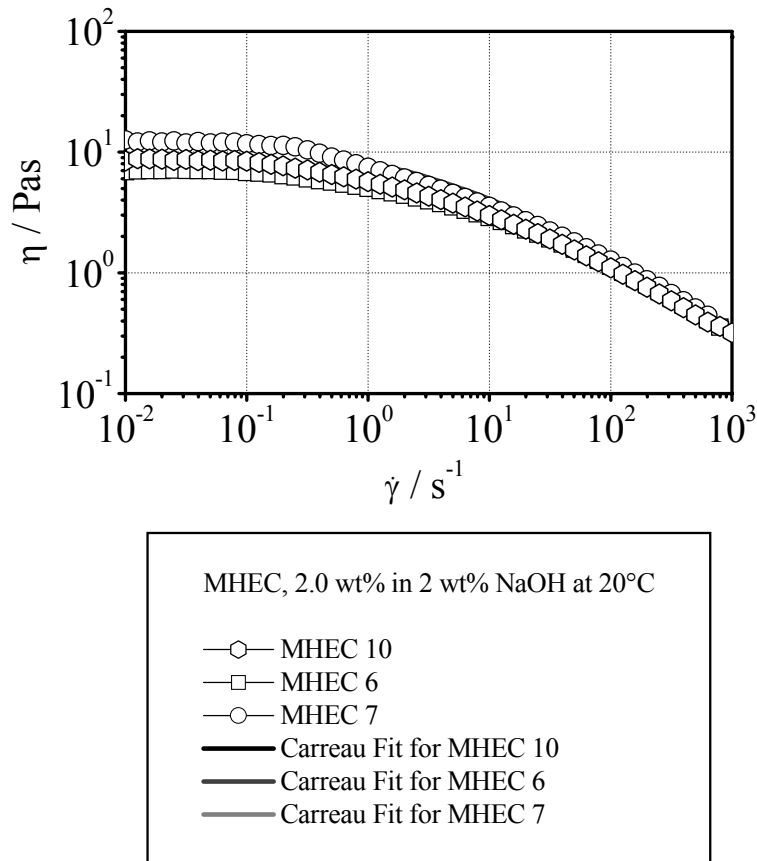
Figure 110: Shear viscosity η versus shear rate γ̇ for selected methylhydroxyethyl celluloses 6, 7 and 10 in 2 wt% NaOH (2.0 wt%) at 20°C.

This transition parameter *b* is a direct measure for the width of the molar mass distribution of a polymer, but here it fails to confirm the results of the light scattering experiments shown in Fig. 109. This is due to the fact that in the past *b* was discussed to be just a insufficient measure for the broadness of the distribution [141], another reason for the failure to predict a trend in the broadnes of the distribution is that the distributions are still quiet alike each other, only differing in the high molar mass tail. The transition parameter *b* therefore is no sensitive measure for the MMD, another method than steady shear has to be consulted to get quantitative information instead.

As one could already see in chapter 6.2.3.1, uniaxial elongation is an appropriate means to determine differences in flow behaviour between the investigated MHEC samples. To point out the influence of the MMD on the elongational behaviour of the MHECs, Fig. 111 shows the results of the CaBER experiments for the samples MHEC 6, 7 and 10 at 2.0 wt% in 2 wt% NaOH instead of the full set of samples as shown in Fig. 108.
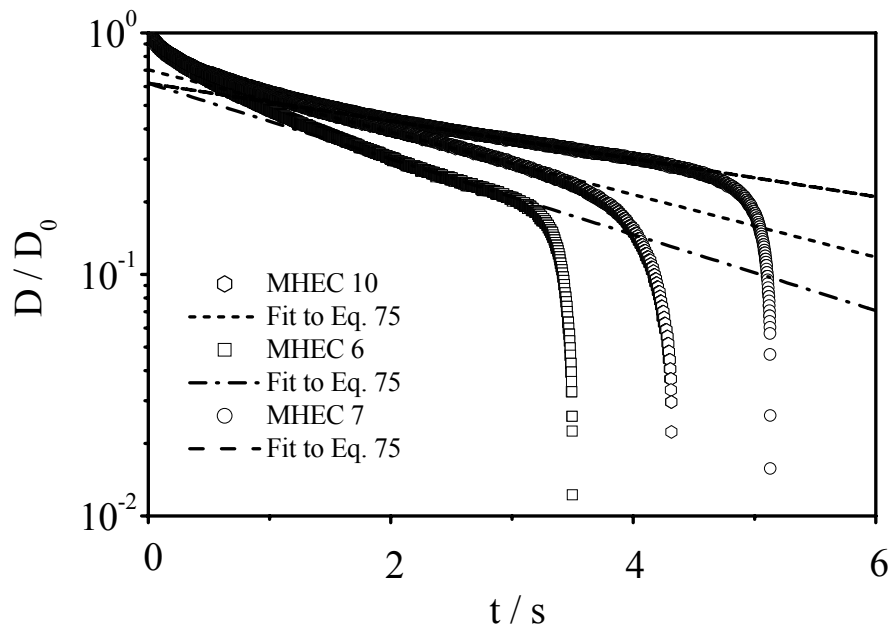
Figure 111: Normalized filament diameter D/D_0 versus time for selected methylhydroxyethyl celluloses 6, 7 and 10 in 2 wt% NaOH (2.0 wt%) at 20°C. The three lines represent the respective fits according to Eq. 81 for the three MHECs.

However the determined MMDs shown in Fig. 109 do not correlate with the results for uniaxial elongation for the MHECs shown in Fig. 111, because sample MHEC 10 with the broadest distribution and hence the highest ratio of high molecular weight polymer does not show the longest breakup time. Instead, as shown in Fig. 111 the sample MHEC 7 with the narrowest distribution shows the longest breakup time.

As shown in Table 14, the ratios of recovery for the light scattering experiments indicate a rather large amount of not molecularly dispersed sample that is seperated from the solution by filtration and the following pre- columns, especially for the sample MHEC 7 with about 30 wt%. To adjust the sample preparation for the CaBER experiments to the sample preparation for the light scattering measurements the MHEC solutions were centrifuged and again examined via CaBER measurements. The results are shown in Fig. 112.
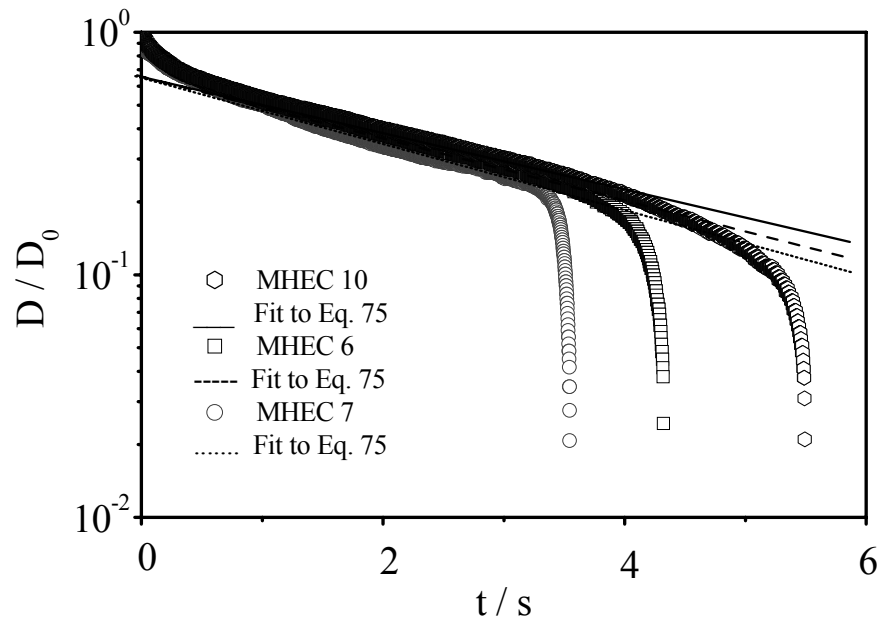
Figure 112: Normalized filament diameter D/D$_0$ versus time for selected methylhydroxyethyl celluloses 6, 7 and 10 in 2 wt% NaOH (2.0 wt%) after centrifugation at 20°C. The three lines represent the respective fits according to Eq. 81 fot the three MHECs.

In contrast to Fig. 111 the centrifuged samples show the order in breakup times expected from the distributions determined with light scattering. Sample MHEC 10 with the broadest MMD shows the longest breakup time sample MHEC 7 with the narrowest MMD the shortest breakup time. The results of the CaBER experiments and the results of light scattering can thus be correlated with the same sample preparation, because in both cases only the *molecularly dispersed fraction* of the sample is characterized. The relaxation times evaluated from Figs. 111 and 112 via Eq. 81 are listed together with the relaxation times of the non-centrifuged samples in Table 16.

Table 16: Longest relaxation times τ_0 of uniaxial elongation for MHECs 6, 7 and 10.

Sample	τ_0 CaBER / s centrifuged	τ_0 CaBER / s Non centrifuged
10	*1.14*	*1.12*
6	*1.08*	*0.92*
7	*0.98*	*1.85*

As one can see from Fig. 111 and Fig. 112 as well as from Table 16 the relaxation times show pronounced differences for the three here investigated MHEC samples, as it was expected in regards of their MMDs.

Comparing the breakup behaviour of the molecularly dispersed samples of MHEC to the polystyrene blends (see chapter 6.1.3 for detail) one can observe differences in the shape of the curves. Whereas the polystyrene blends show a steady thinning in the semi-log plot of Fig. 89 in accordance with Eq. 81, for late times the MHECs show a sudden increase in the thinning rate and a fast breakup. Stelter et al. [29] showed that the elongational behaviour of polymer solutions differs for ionic or non-ionic polymers. The main reason for this is that ionic polymers form more rigid and therefore more expanded polymer coils than non-ionic polymers of the same molar mass. This results in shorter breakup-times because the coils are closer to their finite extensibility. This effect results qualitativly in different shapes of the curves shown in Fig. 111 and Fig. 112 for the rigid MHECs and in Fig. 89 for the more flexible polystyrenes. Stelter et al. also showed that this effect quantitativly results in two distinct $\eta_{E,t}/\tau_0$ dependencies for flexible or rigid like behaviour where $\eta_{E,t}$ refers to the terminal elongational viscosity that is obtained once the polymer chains have reached their finite extensibility limit [29]. In Fig. 114 the steady state terminal elongational viscosity is ploted versus the relaxation times for the investigated polymers. The terminal elongational viscosity $\eta_{E,t}$ has been determined from the general transient elongational viscosity

$$\eta_E = \frac{-\sigma}{dD_{mid}/dt}$$
(Eq. 179)

that has been extrapolated at late times to its time independent limit. As can be seen in Fig. 113 the transient elongational viscosity η_E^+ does not reach its equilibrium state in the regime of Henckey strains that yield reasonable results.
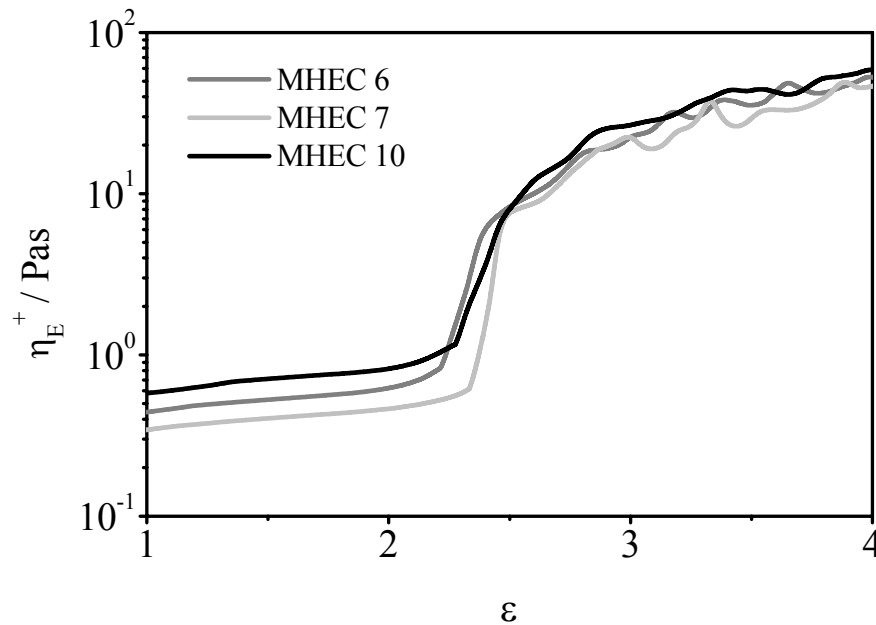
Figure 113: Apparent elongational viscosity η_E^+ versus Hencky strain ε for the investigated MHECs 6, 7 and 10 at 2.0 wt% in 2 wt% NaOH at 25°C.

As Fig. 113 also shows, do the three MHEC solutions behave like a Newtonian fluid until a Henckey strain of about 2.2. The elongational viscosity observed at these early times is independent of the strain and shows values aroung 0.7 Pas, less than the zero-shear viscosities

shown in Fig. 110. This is due to the fact that gthe centrifuged samples are examined here in the CaBER experiment, whereas the aggregated structures count for the zero-shear viscosity. After a Hencky strain of four, the transient elongatinal viscosities decrease again (not shown in Fig. 113), because the time dependent derivation of the filament diameter (see Eq. 179 for the definition of the elongational viscosity) does not yield reasonable results.
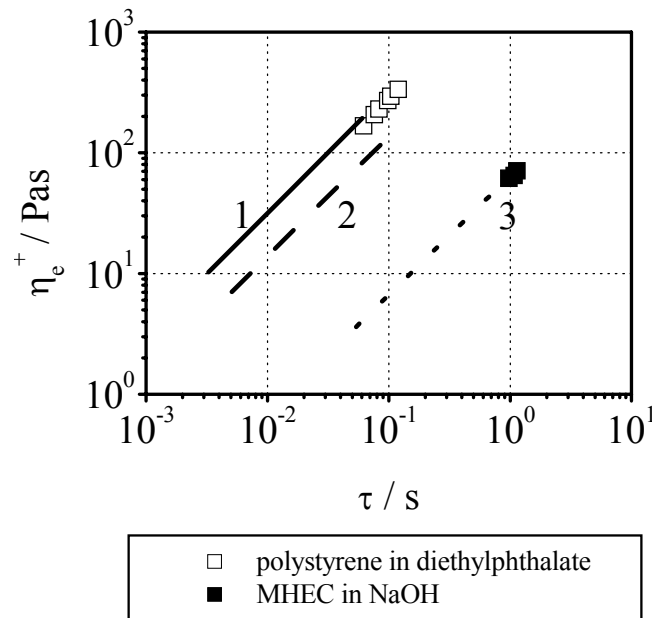
Figure 114: Comparison of two distinct η_E^+/τ_0 dependencies for flexible (1) or rigid like behaviour (2) according to Stelter et al. [29] to experimental data.

Fig. 114 shows that the polystyrene blends in diethylphthalate correspond well to the behaviour of flexible polymers in elongational flows observed by Stelter et al. (line 1). In comparison to this the MHECs in NaOH show the expected lower values for $\eta_{E,t}/\tau_0$ since they are much more rigid. However, these values do not fit the trend for rigid like behaviour found by Stelter et al. which is diagrammed by line 2 in Fig. 114, but even lower values. Nevertheless, a linear trend can be observed for the relaxation times of the MHEC solutions (line 3 in Fig. 114). The shift of the linear trend to higher relaxation times is probably due to higher concentrations used in this work and an even greater expansion due to the ionization by the NaOH. As the concentrations used for the MHEC solutions are relativly high (2.0 wt%) a structure buildup via hydrogen bonding may be an issue even though NaOH is used as asolvent. These aggregates may have great influence on the elongational behaviour of the MHEC solutions even in the centrifuged state and superpose the results obtained for the single polymer coil.

However, the absolute measured MMDs of the MHECs can be consulted to evaluate the ratio $\dfrac{\tau_0}{\tau_{0,M}}$ qualitatively according to Eq. 176. With the CaBER relaxation times (see Table 16) uniform values for $\tau_{0,M}$ should be the result if Eq. 176 is also valid for the MHECs. The evaluated values for $\tau_{0,M}$ are listed in Table 17 for the MHECs 6, 7 and 10.

Table 17: Longest relaxation times τ_0 of uniaxial elongation for MHECs 6, 7 and 10.

Sample	$\tau_{0,M}$ theor. / s
10	*0.140*
6	*0.136*
7	*0.134*

As table 17 shows, the theoretical predicted longest relaxation times for a hypothetical monodisperse MHEC sample are in good agreement with each other. In addition to this the calculated longest relaxation time $\tau_{0,M}$ is in fairly good agreement with the longest relaxation times for shear flow predicted by the modified Carreau model as shown in Fig. 110 and Tab. 15.

To verify the results obtained for the MHECs in regards to the molar mass distribution, the investigated hmHECs were also characterized via CaBER experiments as can be seeen in Figs. 115 and 116.

Figure 115: Normalized filament diameter D/D_0 versus time for selected hydrophobically modified hydroxyethyl celluloses (hmHEC) 1 and 4 in water (2.0 wt%) as raw solutions and after centrifugation at 20°C.

As can be seen in chapter 5.3, the molar mass distributions of the two samples are considerably different from each other. Whereas both samples show approx. the same weight-average molar mass M_w of about 270 kg/mol, sample hmHEC 1 is the much broader distributed polymer ($M_w / M_n = 2.6$ in comparison to 1.3 for the sample hmHEC 2), showing an almost bimodal distribution. This result suggests that this sample was blended from two

different cellulose pulps, whereas the sample hmHEC 2 was synthezised from one homogenous cellulose sample. The high molar mass tail of the molar mass (see Fig. 43 for details) has an even more distinctive influence on the break-up behaviour as for the MHECs. As one can see in Figs. 115 and 116, the broader distributed sample hmHEC 1 shows a break-up time of about 80 s in the uncentrifuged state, that is about 20 times higher as the break-up time of the same sample after centrifugation. The aggregated structures in solution again slow down the break-up process very much. However, the high molar mass fraction of the sample hmHEC 1 seems to have great influence on the gelation behaviour, because for the sample hmHEC 2 the difference between non-centrifuged and centrifuged solution is not as pronounced.
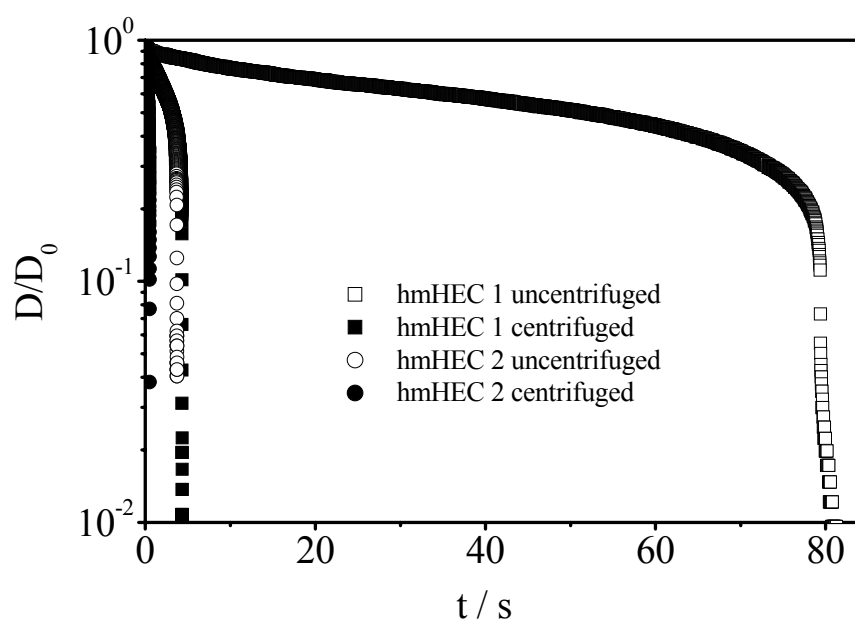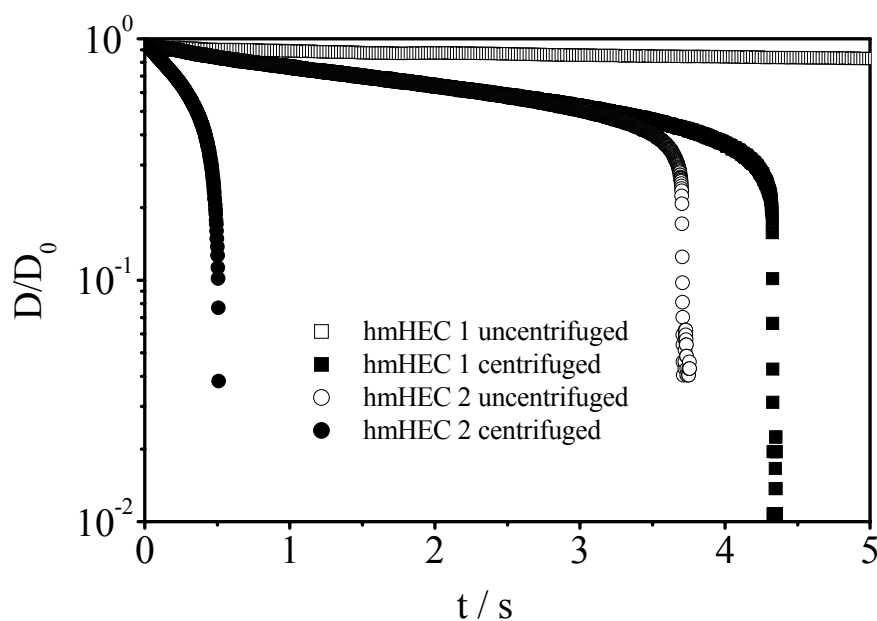

Figure 116: Normalized filament diameter D/D_0 versus time for selected hydrophobically modified hydroxyethyl celluloses (hmHEC) 1 and 4 in water (2.0 wt%) as raw solutions and after centrifugation at 20°C.

7 Outlook

In recent years rheology made a big leap forward by introduction of rheometers that worked, although presenting a new level of robustness, with increasing sensitivity and accuracy. To take advantage of rheology as an analytical method that allows for the detection of an overall picture of the visco-elasticity of a polymer fluid, all three different types of strain available, steady shear flow, small amplitude oscillatory shear and elongation, have to be utilized. However, for elongational rheology one major problem existed for the last decades, since only polymer melts could be characterized satisfactorily.

As it could be shown in this work the new method of uniaxial elongation in capillary break-up is the right means to easily monitor elastic phenomena in the non-Newtonian flow regime of polymer solutions. This applies since capillary break-up establishes, in contrast to previously introduced methods of elongational rheology, a surface tension controlled flow field. For this special case the Weissenberg number *We* naturally chooses a value of 2/3 [69] independently of the investigated polymer fluid, ensuring that the critical Weissenberg number of 1/2 for the onset of non-Newtonian flow behaviour [86] is exceeded. This effect can be utilized in the future to monitor the relevant elongational material functions for a whole range of polymer containing formulations in technical applications, where elongational flow fields play a major role. Especially in application fields for cosmetic, pharmaceutical and medical industry, where complex fluids are utilized for body care- and health care products e.g. uniaxial elongation in capillary break-up should be the proper method to obtain the information needed to prevent unwanted flow anomalies like filament build-up, squirting and spattering.

In regards of the concentration dependence of the longest relaxation times of ultradilute polymer solutions in uniaxial elongation, a correlation of the gradient *m* for the relation $\frac{\tau_0}{\tau_z} \sim \left(\frac{c}{c^*}\right)^m$ to the solvent quality of the investigated system is an issue that is still to be clarified. Whereas *m* for polystyrene in DEP was found to be 0.58, the value of *m* increased for the near theta solvent styrene oligomer to a value of 0.89. The future discussion of this issue should also take into account the possibility of increasing long range interactions due to the polymeric nature of the solvent in the boger fluids.

In terms of the influence of the molar mass distribution on the elongational behaviour of polymer solutions there also is still questions to be clarified in the future. The scaling law determined for the investigated polystyrene blends and blended MHECs is to be dicusssed via other polymer-solvent systems, especially water soluble biopolymers.

8 Appendix

8.1 Abbreviations

8.1.1   Latin letters

a	exponent of the [η]-M-relationship
A	area, Eyring coefficient
A_2	2. virial coefficient
A_3	3. virial coefficient
b	bond length
B_1, B_2, B_n	constants of the virial equation
Bo	Bond number
c	concentration
C_∞	characteristic ratio
c^*	critical concentration of polymer coil overlap
$c^*_{[\eta]}$	critical concentration of viscosimetry
c^*_{LS}	critical concentration of light scattering
$c \cdot [\eta]$	overlap parameter
d	diameter of a polymer coil
D	capillary diameter, filament diameter
D_0	initial filament diameter
De	Deborah number
DIN	German industrial standards
DRI	differential rhefractometer
Eq.	equation
f	function
F	force, sphere factor of the visco-balance
Fig.	figure
g	gravity constant
h	height, cylinder height
Δh	correction factor of cylinder height
hmHEC	hydrophobically modified hydroxyethyl cellulose
ISO	International Organization for Standardization

IUPAC	International Union of Pure and Applied Chemistry
K	constant, constant of the capillary viscosimeter
K_b	known capillary constant
K_{FS}	Fuoss constant
$K_{[\eta]}$	constant of the Kuhn-Mark-Houwink-Sakurada equation ($[\eta]$-M-equation)
K_H	Huggins constant
K_n	constant of the $[\eta]$-M-equation determined with number average molar masses
K_{SB}	Schulz-Blaschke constant
K_w	constant of the $[\eta]$-M-equation determined with mass average molar masses
KMHS	Kuhn-Mark-Houwink-Sakurada equation
l	length, capillary length
L_p	persistence length
m	correction factor of the Hagenbach correction
m_{coil}	mass of a single polymer coil
m_i	mass of fraction i
$m_{polymer}$	mass of the polymer
M	molar mass,
M_n	number average molar mass
M_u	molar mass of a monomer unit
M_w	weight average molar mass
M_z	centrifuge average molar mass
M_η	viscosity average molar mass
M_1, M_2	start and end marks at capillary and falling sphere viscosimeters, molar mass of different solvent components
Mg	mega (10^6) gramms
MALLS	multi angle laser light scattering
MHEC	methylhydroxyethyl cellulose
MMD	molar mass distribution (new for MMD)
MWD	molecular weight distribution (obsolete term for MMD)
n	number, rotational frequency
N	number of bonds in a polymer chain

N_A	Avogadro number
NaN_3	sodium azide
$NaOH$	sodium hydroxide
$NaNO_3$	sodium nitrate
Oh	Ohnesorge number
p	pressure
Δp	pressure difference
pH	reciprocal hydrogen ion concentration
P	degree of polymerization
PEO	polyethyleneoxide
PS	polystyrene
q	polydispersity correction factor
q_n	polydispersity correction factor for number average molar masses
q_w	polydispersity correction factor for mass average molar masses
Q	polydispersity
r	radius of a sphere
$\langle r^2 \rangle^{1/2}$	average end-to-end distance
r_o	end-to-end distance of a polymer coil with unperturbed dimensions
r_{oo}	end-to-end distance of a freely jointed chain
R	radius, gas constant
R_G	radius of gyration
$R_{G,\theta}$	radius of gyration at theta-condition
$R_{H,\theta}$	hydrodynamic radius at theta-conditions
R_s	radius of the shaft
R_{sph}	equivalent radius of a hard sphere
R_1, R_2, R_3, R_4	Radii of the double gap fixture
Re	Reynolds number
SEC	size exclusion chromatography
t	time
t_b	flow time in a capillary visc. with a known capillary constant
$t_{solution}$	characteristic measurement time of a polymer solution
$t_{solvent}$	characteristic measurement time of the solvent

t_{min}	minimum flow time
T	temperature, torque
υ	velocity
$\Delta\upsilon$	velocity difference
V	volume
V_{coil}	equivalent volume of a single polymer coil in solution
$V_{polymer}$	volume of polymer in solution (equivalent fraction)
$V_{solvent}$	volume of free solvent
w(M)	fraction of molar mass
x_i	molar fraction
x, y, z	direction in space
w_i	mass fraction
y_1, y_2	fraction (w_1, x_i or ϕ_i)

8.1.2 Greek symbols

α	cone angle
α_{RG}	expansion factor for the radius of gyration
$\alpha^3_{[\eta]}$	expansion factor for the intrinsic viscosity
ε	correction factor of the Flory constant for non-theta-conditions, Henckey strain
ϕ, ϕ_i	volume fraction
Φ	Flory constant
Φ_θ	Flory constant at theta-condition
$\dot{\gamma}$	shear rate
$\dot{\gamma}_{crit}$	critical shear rate of the onset of non-Newtonian flow behavior
$\dot{\gamma}_{max}$	maximum shear rate
ϑ	Hagenbach correction
η	dynamic viscosity
$[\eta]$	intrinsic viscosity, limiting viscosity number
η_0	zero shear viscosity
η_1, η_2	viscosity of different solvent components
η_i	relative viscosity increment

η_p	polymer viscosity
η_s	solvent viscosity
η_t	time dependent viscosity
η_{sp}	specific viscosity
η_r	relative viscosity
ν	kinematic viscosity, Flory exponent (exponent of the R_G-M-relationship)
θ	theta-condition, torsion angle
ρ	density
ρ_1, ρ_2	density of different solvent components
ρ_{equ}	equivalent density (density of the polymer coil in the solution conformation without the solvent)
$\rho_{solution}$	solution density
$\rho_{solvent}$	solvent density
σ	shear stress, hindrance parameter
τ	bond angle, relaxation time
ω	angular frequency
ξ	radius conversion factor
ζ	correction factor for short range rotational interactions

8.2 Experimental Section

8.2.1   Sample preparation

The methylhydroxyethylcelluloses (MHEC) used were made available from Wolff Cellulosics GmbH (Walsrode, Germany). The investigated hmHECs were provided by Beiersdorf AG (Hamburg, Germany). The polystyrenes (1.8 Mio. g/mol with PDI = 1.02 and 6.0 Mio. g/mol with PDI=1.22) came from Polysciences Inc. and the molecular weights and PDIs were verified by SEC with a multi-angle light scattering detector. The other polystyrene standards used for this work where acquired from polymer laboratories (PL) and Polymer Standard Sevices (PSS). The given molar masses were also stated to be crosschecked via SEC/MALLS/DRI

Preparation of the polystyrene solutions was done by solving the respective amount of polymer in the accordant solvent. Homogenization was achieved by permanent agitation over a period of time not shorter than, at least 7 days (polystyrene in diethylphthalate, toluene or t-decalin) with alternating temperature or at least 60 days for Boger fluids (polystyrene in styrene oligomere). The solutions were prepared by adding the polymer to the oligomer (degased Picolastic A-5, Fxsupply, USA) at room temperature (1.8 M - 0.166wt% and 6.0 M - 0.107wt %). The samples were placed in an oven at 100°C, without stirring, until the polymer dissolved (1-2 weeks). The experimental concentrations were achieved by diluting the above samples with Picolastic A-5.

Preparation of the MHEC solutions was achieved by solving the respective amount of polymer in the accordant solvent (2.0 wt% NaOH). Homogenization was achieved by permanent agitation over a period of time not shorter than 3 days.

All concentrations stated are in wt%.

8.2.2   Mechanical rheometry

Intrinsic viscosities [η] where determined with an Ubbelohde micro capillary Ic (polystyrene) or IIc (MHEC, hmHEC) in a watertub temperated at 25.0 ± 0.05 °C.

Steady shear flow and SAOS measurements where achieved on a rate controlled rheometer of the type Ares II (torque: $4 \cdot 10^{-7}$ bis 0.01 N·m, TA Instruments) with cone and plate geometries (50 mm diameter, 4° cone angle). Elongational characterization was carried out on a CaBER (capillary breakup elongational rheometer) device (ThermoHaake, Germany). All measurements were carried out at 25°C (298 K, RT).

8.2.3   SEC/MALLS/DRI

The solvent for elution was prepared by water that was filtered with ionic exchange columns (Adsorber, Universal and Research, Novodirect, Kehl/Rh.) and addition of 200 ppm NaN$_3$ (sodium azide) as bacericide and 0.1 mol/l NaNO$_3$ (sodium nitrate) as low molecular

electrolyte. Filtrating of this solvent was achieved with a cellulosic filter of a pore size of 0.1 μm (Sartorius GmbH, Germany).

The solvent was advanced with a HPLC-pump (Gynkotek, Germany) with a flow rate of 0.513 ml/min.

Degasing was done on-line with a Degasser ERC 3315a (ERC, Germany).

Determination of the molar mass and its distribution of the MHECs was achieved using a combined method of size exclusion chromatography (SEC, 4 columns TSK PWXL: G3000, G4000, G5000 & G6000, ToSoHass), multi-angle laser light scattering (MALLS, DAWN-F light scattering photometer, Wyatt Technology) and differential refractometer (DRI, Showa Denko).

9 Literature

1. Grigorescu, G. and W.M. Kulicke, *Prediction of viscoelastic properties and shear stability of polymers in solution.* Advances in Polymer Science, 2000. **152**: p. 1-40.
2. Heinze, T.L., T., Progr. Polym. Sci., 2001: p. 1689-1762.
3. Eggersdorfer, M., S. Warwel, and G. Wulff, *Nachwachsende Rohstoffe - Perspektiven für die Chemie.* 1993, Ludwigshafen, Aachen: VCH.
4. Fecht, U.-H., Chem. Ing. Tech., 1997. **69**: p. 546.
5. Kettembeil, S., Chem. Rundschau, 1995. **48**: p. 4.
6. Greenway, T.M., *Cellulosic polymers.* 1994: Carl Hanser Verlag, München.
7. Belitz, H.-D., Grosch, W., *Lehrbuch der Lebensmittelchemie.* 1992, Berlin.
8. Pomeranz, Y., *Functional Properties of Food Components.* 2 ed. 1991, San Diego: Academic Press.
9. Domsch, A., *Die kosmetischen Präparate.* 1992, Augsburg: Verlag für chem. Industrie.
10. Seidel, C., Kulicke, W.-M., Hess, C., Hartmann, B., Lechner, M. D. & Lazik, W., *Influence of the cross-linking agent on the gel structure of starch derivatives.* Starch-Stärke, 2001. **53**: p. 305-310.
11. Bieleman, J., *Lackadditive.* 1998, Weinheim: Wiley-VCH Verlag. 395.
12. Clasen, C. and W.M. Kulicke, *Determination of viscoelastic and rheo-optical material functions of water-soluble cellulose derivatives.* Progress in Polymer Science, 2001. **26**(9): p. 1839-1919.
13. Kulicke, W.M., et al., *Characterization of aqueous carboxymethylcellulose solutions in terms of their molecular structure and its influence on rheological behaviour.* Polymer, 1996. **37**(13): p. 2723-2731.
14. Laschet, M., et al., *Examination of the flow behaviour of HEC and hmHEC solutions using structure-property relationships and rheo-optical methods.* Colloid and Polymer Science, 2004. **282**(4): p. 373-380.
15. Clasen, C. and W.M. Kulicke, *Rheo-optical studies of barley (1 -> 3)(1 -> 4)-beta-glucan solution: Detection of the flow behavior of aggregates in the sol state.* Journal of Rheology, 2003. **47**(2): p. 321-335.
16. Clasen, C. and W.M. Kulicke, *A convenient way of interpreting steady shear rheo-optical data of semi-dilute polymer solutions.* Rheologica Acta, 2001. **40**(1): p. 74-85.
17. Plog, J.P., Kulicke, W.-M.; Clasen, C., *Influence of the molar mass distribution on the elongational behaviour of polymer solutions in capillary breakup.* Applied Rheology, 2005. **15**(1): p. 28-37.
18. Schittenhelm, N. and W.M. Kulicke, *Producing homologous series of molar masses for establishing structure-property relationships with the aid of ultrasonic degradation.* Macromolecular Chemistry and Physics, 2000. **201**(15): p. 1976-1984.
19. Heins, D., et al., *Characterization of acetyl starch by means of NMR spectroscopy and SEC/MALLS in comparison with hydroxyethyl starch.* Starch-Starke, 1998. **50**(10): p. 431-437.
20. Kauper, P., et al., *Development and evaluation of methods for determining title pattern of functionalization in sodium carboxymethylcelluloses.* Angewandte Makromolekulare Chemie, 1998. **260**: p. 53-63.
21. Pfefferkorn, P., et al., *Determination of the Molar Mass and the Radius of Gyration, Together with their Distributions for Methyl Hydroxyethyl Celluloses.* Cellulose (Dordrecht, Netherlands), 2003. **10**(1): p. 27-36.
22. Kulicke, W.M., S. Lange, and D. Heins, *Advantages of determining the molar mass distributions of water-soluble polymers and polyelectrolytes with FFFF-MALLS and*

SEC-MALLS. ACS Symposium Series, 1999. **731**(Chromatography of Polymers): p. 114-140.

23. Thielking, H. and W.M. Kulicke, *Determination of the structural parameters of aqueous polymer solutions in the molecular, partially aggregated, and particulate states by means of FFFF/MALLS.* Journal of Microcolumn Separations, 1998. **10**(1): p. 51-56.

24. Thielking, H. and W.M. Kulicke, *On-line coupling of flow field-flow fractionation and multiangle laser light scattering for the characterization of macromolecules in aqueous solution as illustrated by sulfonated polystyrene samples.* Analytical Chemistry, 1996. **68**(7): p. 1169-1173.

25. Kulicke, W.-M. and C. Clasen, *Viscosimetry of Polymers and Polyelectrolytes.* 2004, Heidelberg: Springer.

26. Entov, V.M. and E.J. Hinch, *Effect of a spectrum of relaxation times on the capillary thinning of a filament of elastic liquid.* Journal of Non-Newtonian Fluid Mechanics, 1997. **72**(1): p. 31-53.

27. Bazilevskii, A.V., V.M. Entov, and A.N. Rozhkov, *Breakup of an Oldroyd liquid bridge as a method for testing the rheological properties of polymer solutions.* Polymer Science Series A, 2001. **43**(7): p. 716-726.

28. Stelter, M. and G. Brenn, *Validation and application of a novel elongational device for polymer solutions.* Journal of Rheology, 2000. **44**(3): p. 595-616.

29. Stelter, M., et al., *Investigation of the elongational behavior of polymer solutions by means of an elongational rheometer.* Journal of Rheology, 2002. **46**(2): p. 507-527.

30. Liang, R.F. and M.R. Mackley, *Rheological Characterization of the Time and Strain Dependence for Polyisobutylene Solutions.* Journal of Non-Newtonian Fluid Mechanics, 1994. **52**(3): p. 387-405.

31. Bazilevskii, A.V., et al., *Degradation of polymer solution filaments.* Vysokomolekulyarnye Soedineniya Seriya a & Seriya B, 1997. **39**(3): p. 474-482.

32. Anna, S.L., et al., *An interlaboratory comparison of measurements from filament-stretching rheometers using common test fluids.* Journal of Rheology, 2001. **45**(1): p. 83-114.

33. Anna, S.L. and G.H. McKinley, *Elasto-capillary thinning and breakup of model elastic liquids.* Journal of Rheology, 2001. **45**(1): p. 115-138.

34. Kulicke, W.M., et al., *Use of Polyelectrolytes in Mechanical Solid-Liquid Separation.* Chemie Ingenieur Technik, 1993. **65**(5): p. 541-552.

35. von Homeyer, A., et al., *Optimization of the polyelectrolyte dosage for dewatering sewage sludge suspensions by means of a new centrifugation analyser with an optoelectronic sensor.* Colloid and Polymer Science, 1999. **277**(7): p. 637-645.

36. Parker, S., et al., *Flocculation and dewatering of sewage sluge using polyelectrolytes.* Angewandte Makromolekulare Chemie, 1997. **250**: p. 15-30.

37. Kulicke, W.M., M. Kotter, and H. Grager, *Drag Reduction Phenomenon with Special Emphasis on Homogeneous Polymer-Solutions.* Advances in Polymer Science, 1989. **89**: p. 1-69.

38. Kulicke, W.M., N. Böse, and M. Bouldin, eds. *The role of polymers in enhanced oil recovery.* Water-Soluble Polymers for Petroleum Recovery, ed. D.N. Schulz and G.A. Stahl. 1988, Plenum Press: New York. 1-18.

39. Zeidler, H., et al., *Rheologie pathologischer Gelenkflüssigkeiten. 1. Weitere Ergebnisse zur Viskoelastizität.* Rheologica Acta, 1979. **18**: p. 151-167.

40. Altmann, S., et al., *Rheology of Pathological Synovial-Fluids .2. Structural Rheology of Hyaluronic-Acid.* Rheologica Acta, 1980. **19**(5): p. 642-659.

41. Ver Strate, G. and M.J. Struglinski, *Polymers as Lubricating-Oil Viscosity Modifiers*, in *ACS Symposium Series 462 - Polymers as Rheology Modifiers*, D.N. Schulz and J.E. Glass, Editors. 1991, American Chemical Society: Washington, DC. p. 256-272.

42. Kulicke, W.M., D. Roessner, and W. Kull, *Characterization of Hydroxyethyl Starch by Polymer Analysis for Use as a Plasma-Volume Expander.* Starch-Starke, 1993. **45**(12): p. 445-450.

43. Kniewske, R. and W.M. Kulicke, *Study on the Molecular-Weight Dependence of Dilute-Solution Properties of Narrowly Distributed Polystyrene in Toluene and in the Unperturbed State.* Makromolekulare Chemie-Macromolecular Chemistry and Physics, 1983. **184**(10): p. 2173-2186.

44. Kulicke, W.M. and R. Kniewske, *The Shear Viscosity Dependence on Concentration, Molecular- Weight, and Shear Rate of Polystyrene Solutions.* Rheologica Acta, 1984. **23**(1): p. 75-83.

45. Kulicke, W.M., et al., *Shear and Degradation of Polymer-Solutions.* Angewandte Makromolekulare Chemie, 1986. **142**: p. 29-49.

46. Bouldin, M., W.M. Kulicke, and H. Kehler, *Prediction of the Non-Newtonian Viscosity and Shear Stability of Polymer-Solutions.* Colloid and Polymer Science, 1988. **266**(9): p. 793-805.

47. Klemm, D., et al., *Comprehensive Cellulose Chemistry - Functionalization of Cellulose.* Vol. 2. 1998, Weinheim: Wiley-VCH.

48. Klemm, D., et al., *Comprehensive Cellulose Chemistry.* Vol. 1. 1998, Weinheim: Wiley-VCH.

49. Krässig, H., et al., *Cellulose*, in *Ullmann's Encyclopedia of Industrial Chemistry*, W. Gerhartz, Editor. 1992, Wiley VCH: Weinheim. p. 375-418.

50. Glass, J.E., ed. *Polymers in aqueous media - Performance through association.* Advances in Chemistry Series, ed. M.J. Comstock. 1989, American Chemical Society: Washington, DC. 575.

51. Glass, J.E., *Water-Soluble Polymers - Beauty with Performance.* 1986, North Dakota: ACS.

52. Landoll, L.M., *Hydrophobically modified polymers.* 1985: United States.

53. Flory, P.J., *Die Konformation linearer Makromoleküle.* Angewandte Chemie, 1977. **22**: p. 787.

54. Vollmert, B., *Grundriss der Makromolekularen Chemie.* Vol. 3. 1980, Karlsruhe: E. Vollmert - Verlag.

55. Elias, H.G., *Makromoleküle: Physikalische Strukturen und Eigenschaften.* 6 ed. 2001, Weinheim: Wiley-VCH.

56. Rayleigh, J.S., J. W., *On James Bernoulli's theorem in probabilities.* Philosophical Magazine, 1899. **47**(5): p. 246-251.

57. Debye, P., *Angular dissymmetry of the critical opalescence in liquid mixtures.* Journal of Chemical Physics, 1959. **31**: p. 680-687.

58. Mie, G., *Beiträge zur Optik trüber Medien spezieller kolloidaler Metalllösungen.* Annalen der Physik, 1908. **25**: p. 377-445.

59. Kulicke, W.-M. and N. Böse, *Bestimmung der Molmassenverteilung sowie der Stabilitätsgrenze von Polyacrylamiden unter Benutzung einer kombinierten Ausschlußchromatographie-Kleinwinkel-Laser-Streulichtphotometer-Anlage.* Coll.&Polym. Sci., 1984. **262**: p. 197-207.

60. Barth, H.G., *A practical approach to steric exclusion chromatography of water-soluble polymers.* Journal of Chromatographic Science, 1980. **18**(9): p. 409-29.

61. Gosch, C.I., *Polymeranalytische Charakterisierung mittels Größenausschlußchromatographie, Fluß Feld-Fluß Fraktionierung und Lichtstreuung von Polysaccharid-Derivaten.* Disseration, 2002.

62.   Graessley, W.W., *Entangled linear, branched and network polymer systems. Molecular theories.* Adv. Polym. Sci., 1982. **47**: p. 67-117.

63.   Freeman, S.M.W., K., *Some new rheological phenomena and their significance for the constitution of materials.* Nature, 1948. **162**: p. 320-323.

64.   Boger, D.V. and K. Walters, *Rheological phenomena in focus.* Rheology series, 4. 1993, Amsterdam, London, New York: Elsevier.

65.   Kulicke, W.-M., *Fließverhalten von Stoffen und Stoffgemischen.* 1986, Basel, Heidelberg, New York: Hüthig und Wepf.

66.   Macosko, C., *Rheology: Principles, Measurements, and Applications.* 1994, New York: VCH Publishers.

67.   Zachmann, H.G., *Mathematik für Chemiker.* Vol. 5. Auflage. 1994: VCH, Weinheim.

68.   Barnes, H.A., J.F. Hutton, and K. Walters, *An Introduction to rheology.* 1989, Amsterdam: Elsevier.

69.   Larson, R.G., *The structure and rheology of complex fluids.* 1999, New York: Oxford University Press.

70.   Astarita, G. and L. Nicodemo, *Extensional flow behavior of polymer solutions.* The Chemical Engineering Jounal, 1970. **1**: p. 57-66.

71.   Oliver, D.R. and R. Bragg, *The triple jet:a new method for measurement of extensional viscosity.* Rheologica Acta, 1974. **13**: p. 830-835.

72.   Binding, D.M. and K. Walters, *On the Use of Flow through a Contraction in Estimating the Extensional Viscosity of Mobile Polymer-Solutions.* Journal of Non-Newtonian Fluid Mechanics, 1988. **30**(2-3): p. 233-250.

73.   Fuller, G.G., et al., *Extensional Viscosity Measurements for Low-Viscosity Fluids.* Journal of Rheology, 1987. **31**(3): p. 235-249.

74.   Ng, S.L., et al., *Extensional viscosity measurements of dilute solutions of various polymers.* Journal of Non-Newtonian Fluid Mechanics, 1996. **65**(2-3): p. 291-298.

75.   Hermansky, C.G. and D.V. Boger, *Opposing-Jet Viscometry of Fluids with Viscosity Approaching That of Water.* Journal of Non-Newtonian Fluid Mechanics, 1995. **56**(1): p. 1-14.

76.   Gupta, R.K. and T. Sridhar, in *Rheological Measurement*, A.A. Collyer and D.W. Clegg, Editors. 1998, Elsevier Applied Science: London. p. 211-245.

77.   Sridhar, T., *An Overview of the Project-M1.* Journal of Non-Newtonian Fluid Mechanics, 1990. **35**(2-3): p. 85-92.

78.   Dontula, P., et al., *Can extensional viscosity be measured with opposed nozzle devices?* Rheologica Acta, 1997. **36**(4): p. 429-448.

79.   Li, J.M. and W.R. Burghardt, *Flow Birefringence in Axisymmetrical Geometries.* Journal of Rheology, 1995. **39**(4): p. 743-766.

80.   Burghardt, W.R., et al., *Uniaxial extensional characterization of a shear thinning fluid using axisymmetric flow birefringence.* Journal of Rheology, 1999. **43**(1): p. 147-165.

81.   Harrison, G.M., J. Remmelgas, and L.G. Leal, *Comparison of dumbell-based theory and experiment for a dilute polymer solution in a corotating two-roll mill.* Journal of Rheology, 1999. **43**(1): p. 197-218.

82.   Arendt, O., *Rheo-optical study of polyurethane solutions in extensional flows.* Applied Rheology, 1997. **7**(6): p. 259-265.

83.   Dunlap, P.N. and L.G. Leal, *Dilute Polystyrene Solutions in Extensional Flows - Birefringence and Flow Modification.* Journal of Non-Newtonian Fluid Mechanics, 1987. **23**: p. 5-48.

84.   Ng, R.C.Y. and L.G. Leal, *Concentration Effects on Birefringence and Flow Modification of Semidilute Polymer-Solutions in Extensional Flows.* Journal of Rheology, 1993. **37**(3): p. 443-468.

85. Fuller, G.G., *Optical Rheometry of Complex Fluids*. 1995, London: Oxford University Press.

86. Haas, R. and W.M. Kulicke, *Flow Behavior of Dilute Polyacrylamide Solutions through Porous-Media .2. Indirect Determination of Extremely High Molecular-Weights and Some Aspects of Viscosity Decrease over Long-Time Intervals*. Industrial & Engineering Chemistry Fundamentals, 1984. **23**(3): p. 316-319.

87. Kullicke, W.M. and R. Haas, *Flow Behavior of Dilute Polyacrylamide Solutions through Porous-Media .1. Influence of Chain-Length, Concentration, and Thermodynamic Quality of the Solvent*. Industrial & Engineering Chemistry Fundamentals, 1984. **23**(3): p. 308-315.

88. Matta, J.E. and R.P. Tytus, *Liquid Stretching Using a Falling Cylinder*. Journal of Non-Newtonian Fluid Mechanics, 1990. **35**(2-3): p. 215-229.

89. Sridhar, T., et al., *Measurement of Extensional Viscosity of Polymer-Solutions*. Journal of Non-Newtonian Fluid Mechanics, 1991. **40**(3): p. 271-280.

90. McKinley, G.H. and T. Sridhar, *Filament-stretching rheometry of complex fluids*. Annual Review of Fluid Mechanics, 2002. **34**: p. 375-415.

91. Christanti, Y. and L.M. Walker, *Surface tension driven jet break up of strain-hardening polymer solutions*. Journal of Non-Newtonian Fluid Mechanics, 2001. **100**(1-3): p. 9-26.

92. Cooper-White, J.J., et al., *Drop formation dynamics of constant low-viscosity, elastic fluids*. Journal of Non-Newtonian Fluid Mechanics, 2002. **106**(1): p. 29-59.

93. Amarouchene, Y., et al., *Inhibition of the finite-time singularity during droplet fission of a polymeric fluid*. Physical Review Letters, 2001. **86**(16): p. 3558-3561.

94. Bazilevskii, A.V., V.M. Entov, and A.N. Rozhkov. *Liquid filament microrheometer and some of its applications*. in *Third European Rheology Conference*. 1990: ElsevieApplied Science.

95. Entov, V.M., V.I. Kordonskil, and I.V. Prokhorov, *Rapid stretching of polymer solutions*. Soviet Physics, Doklady, 1988. **33**(8): p. 628-630.

96. Doyle, P.S., et al., *Relaxation of dilute polymer solutions following extensional flow*. Journal of Non-Newtonian Fluid Mechanics, 1998. **76**(1-3): p. 79-110.

97. Kolte, M.I. and P. Szabo, *Capillary thinning of polymeric filaments*. Journal of Rheology, 1999. **43**(3): p. 609-625.

98. McKinley, G.H. and A. Tripathi, *How to extract the Newtonian viscosity from capillary breakup measurements in a filament rheometer*. Journal of Rheology, 2000. **44**(3): p. 653-670.

99. Spiegelberg, S.H. and G.H. McKinley, *Stress relaxation and elastic decohesion of viscoelastic polymer solutions in extensional flow*. Journal of Non-Newtonian Fluid Mechanics, 1996. **67**: p. 49-76.

100. Gupta, R.K., D.A. Nguyen, and T. Sridhar, *Extensional viscosity of dilute polystyrene solutions: Effect of concentration and molecular weight*. Physics of Fluids, 2000. **12**(6): p. 1296-1318.

101. Spiegelberg, S.H., D.C. Ables, and G.H. McKinley, *The role of end-effects on measurements of extensional viscosity in filament stretching rheometers*. Journal of Non-Newtonian Fluid Mechanics, 1996. **64**(2-3): p. 229-267.

102. Bird, R.B., R.C. Armstrong, and O. Hassager, *Dynamics of polymeric liquids - Fluid mechanics*. Vol. 1. 1977, New York: John Wiley & Sons.

103. Papageorgiou, D.T., *On the Breakup of Viscous-Liquid Threads*. Physics of Fluids, 1995. **7**(7): p. 1529-1544.

104. Kuhn, W., Kolloid-Z, 1934. **68**: p. 2.

105. Flory, P.J., *Statistical Mechanics of Chain Molecules*. 1969, New York: Hanser.

106.   Brandrup, J. and E.H. Immergut, *Polymer Handbook*. 4 ed. 1999, New York: John Wiley & Sons.

107.   Lechner, M.D., K. Gehrke, and E.H. Nordmeier, *Makromolekulare Chemie: Ein Lehrbuch für Chemiker, Materialwissenschaftler und Verfahrenstechniker*. 1993, Basel: Birkhäuser Verlag.

108.   Lodge, T.P.M., J. W.; Schrag, J. L., J Polym Sci, 1982. **20**: p. 1409.

109.   Bird, R.B., et al., *Dynamics of polymeric liquids - Kinetic theory*. Vol. 2. 1987, New York: John Wiley & Sons.

110.   Rouse, P.E., *A theory of the linear viscoelastic properties of dilute solutions of coiling polymers*. Journal of Chemical Physics, 1953. **21**: p. 1272-1280.

111.   Ferry, J.D., *Viscoelastic Properties of Polymers*. 1 ed. 1980, New York: John Wiley & Sons. 641.

112.   Zimm, B.H., J. Chem. Phys., 1956. **24**: p. 249.

113.   Bird, R.B., R.C. Armstrong, and O. Hassager, *Dynamics of polymeric liquids - Fluid mechanics*. Vol. 1. 1987, New York: John Wiley & Sons.

114.   Oseen, C.W., Arf. Mat. Astr. Fys., 1910. **6**(29): p. 1.

115.   Amelar, S., et al., *How Good Is the Bead-Spring Model*. Journal of Non-Crystalline Solids, 1991. **131**: p. 551-555.

116.   Boltzmann, L., Ann. Phys. Chem., 1876. **7**: p. 624.

117.   Maxwell, J.C., Phil. Trans., 1867. **157**(49).

118.   Weissenberg, K., Nature, 1947. **159**: p. 310.

119.   Warner, H.R., I&EC Fundam, 1972. **11:379**.

120.   Peterlin, A., Macromol. Chem., 1961. **44**: p. 338.

121.   Bueche, F., *Viscoity of polymers in concentrated solutions*. Journal of Chemical Physics, 1956. **25**: p. 599-600.

122.   Graessley, W.W., *Entanglement concept in polymer rheology*. Advances in Polymer Science, 1974. **16**: p. 179-226.

123.   Lodge, A.S., Trans. Farraday Soc., 1956. **52**: p. 120.

124.   Kehler, H.K., W. M., *Determination of numbers of entanglement in stationary and flowing polymer-solutions*. Chemie Ingenieur Technik, 1986. **58**: p. 802-804.

125.   De Gennes, P.-G., J Chem Phys, 1971. **55**: p. 572.

126.   Edwards, S.F., Proc Phys Soc, 1967. **92**: p. 9.

127.   Doi, M., *Explanation for the 3.4-power law for viscosity of polymeric liquids on the basis of the tube model*. Journal of Polymer Science, Polymer Physics Edition, 1983. **21**: p. 667-684.

128.   Doi, M.E., S. F., *Dynamics of concentrated polymer systems. Part 2. Molecular motion under flow*. Journal of the Chemical Society, Faraday Transactions 2: Molecular and Chemical Physics, 1978. **74**: p. 1802-1817.

129.   Kröger, M.L., W.; Hess, S., J Rheol, 1993. **37**: p. 1057.

130.   Doi, M.E., S. F., *Dynamics of concentrated polymer systems. Part 4. Rheological properties*. Journal of the Chemical Society, Faraday Transactions 2: Molecular and Chemical Physics, 1979. **75**: p. 38-54.

131.   Daoud, M., Cotton, J. P., Farnoux, B., Jannik, G., Sarma, G., Benoit, M., Dupressix, R., Picot, C. & De Gennes, P.-G., *Solutions of flexible polymers. Neutron experiments and interpreretation*. Macromolecules, 1975. **6**: p. 804-818.

132.   Simha, R. and J.L. Zakin, *Solution viscosities of linear flexible high polymers*. J. Coll. Sci., 1962. **58**: p. 270-287.

133.   Onogi, S., Masuda, T., Miyanaga, N. & Kimura, Y., *Dependence of viscosity of concentrated polymer solutions upon molecular weight and concentration*. Journal of Polymer Science, Polymer Physics Edition, 1967. **5**: p. 899-913.

134. Solomon, M.J. and S.J. Muller, *Study of mixed solvent quality in a polystyrene dioctyl phthalate polystyrene system.* Journal of Polymer Science Part B-Polymer Physics, 1996. **34**(1): p. 181-192.

135. Mackay, M.E.B., D. V., J Non-Newt Fluid Mech, 1987. **22**: p. 235.

136. Boger, D.V., Binnington R., Trans. Soc. Rheol., 1977. **221**: p. 515.

137. Solomon, M.J. and S.J. Muller, *The transient extensional behavior of polystyrene-based Boger fluids of varying solvent quality and molecular weight.* Journal of Rheology, 1996. **40**(5): p. 837-856.

138. Ferry, J.D., Pure Appl. Chem, 1978. **50**: p. 299.

139. Graessley, W.W., Hazelton, R., Lindemann, R., Trans. Soc. Rheol., 1967. **11**: p. 26.

140. Ferry, J.D., Landel, R. L., Williams, M. L., J. Appl. Phys, 1955. **26**: p. 359.

141. Yasuda, K., R.C. Armstrong, and R.E. Cohen, *Shear-Flow Properties of Concentrated-Solutions of Linear and Star Branched Polystyrenes.* Rheologica Acta, 1981. **20**(2): p. 163-178.

142. Bernreitner, K., W. Neissl, and M. Gahleitner, *Correlation between Molecular-Structure and Rheological Behavior of Polypropylene.* Polymer Testing, 1992. **11**(2): p. 89-100.

143. Kulicke, W.-M. and R. Kniewske, *The shear viscosity dependence on concentration, molecular weight and shear rate of polystyrene solutions.* Rheol. Acta, 1984. **23**: p. 75-83.

144. Cox, W.P. and E.H. Merz, *Correlation of dynamic and steady-flow viscosities.* J. Polym. Sci., 1958. **28**: p. 619-622.

145. Harrison, G.M., J. Remmelgas, and L.G. Leal, *The dynamics of ultradilute polymer solutions in transient flow: Comparison of dumbbell-based theory and experiment.* Journal of Rheology, 1998. **42**(5): p. 1039-1058.

146. Tirtaatmadja, V., G.H. McKinely, and J.J. Cooper-White, *Drop Formation and Breakup of Low Viscosity Elastic Fluids: Effects of Molecular Weight and Concentration.* Physics of Fluids, 2004. **submitted**.

147. Lindner, A., J. Vermant, and D. Bonn, *How to obtain the elongational viscosity of dilute polymer solutions?* Physica a-Statistical Mechanics and Its Applications, 2003. **319**: p. 125-133.

148. Rodd, L., et al., *Cappillary Break-up Rheometry of Low-Viscosity Elastic Fluids.* Applied Rheology, 2004. **submitted**.

149. Ressia, J.A., M.A. Villar, and E.M. Valles, *Influence of polydispersity on the viscoelastic properties of linear polydimethylsiloxanes and their binary blends.* Polymer, 2000. **41**(18): p. 6885-6894.

150. Anderssen, R.S. and D.W. Mead, *Theoretical derivation of molecular weight scaling for rheological parameters.* Journal of Non-Newtonian Fluid Mechanics, 1998. **76**(1-3): p. 299-306.

151. Doi, M. and S.F. Edwards, *The Theory of Polymer Dynamics.* Int. Series of Monographs on Physics. Vol. 73. 1989, Tokyo; Cambridge: Clarendon Press.

152. Kwan, T.C.B., N.J. Woo, and E.S.G. Shaqfeh, *An experimental and simulation study of dilute polymer solutions in exponential shear flow: Comparison to uniaxial and planar extensional flows.* Journal of Rheology, 2001. **45**(2): p. 321-349.

153. Nguyen, H. and D.V. Boger, *Kinematics and Stability of Die Entry Flows.* Journal of Non-Newtonian Fluid Mechanics, 1979. **5**(APR): p. 353-368.

154. Thielking, H., D. Roessner, and W.M. Kulicke, *Online Coupling of Flow Field-Flow Fractionation and Multiangle Laser-Light Scattering for the Characterization of Polystyrene Particles.* Analytical Chemistry, 1995. **67**(18): p. 3229-3233.

Erklärung

Der Verfasser erklärt, die vorliegende Arbeit selbständig und ohne fremde Hilfe verfasst zu haben. Andere als die angegebenen Hilfsmittel und Quellen wurden nicht benutzt und die benutzten wörtlich oder inhaltlich entnommen Stellen sind als solche kenntlich gemacht.

Diese Arbeit hat in gleicher oder ähnlicher Form noch keiner Prüfungsbehörde vorgelegen.

Hamburg, den 20.04.2005 _____

(Jan Philip Plog)

Curriculum Vitae

Name:	Jan Philip Plog
Geburtstag und -ort:	28.11.1974 in Winsen/Luhe
Staatsangehörigkeit:	deutsch
Familienstand:	ledig

Bildungsgang:

04/2003 – 04/2005	Promotionsstipendiat der wissenschaftlichen Nachwuchs-förderung Hamburg
09/2002 – 04/2005	Doktorand am Institut für Technische und Makromolekulare Chemie
01/2000 – 05/2000	ERASMUS Stipendiat, Auslandssemester Universität Sheffield, UK
10/1996 – 07/2002	Studium der Chemie mit Abschluss Diplom-Chemiker am Institut für Technische und Makromolekulare Chemie, Universität Hamburg Note: sehr gut Titel der Diplomarbeit: „*Rheologische Charakterisierung des viskoelastischen Verhaltens verschiedener Hydrokolloide in Lösung*"
09/1995 – 08/1996	Zivildienst beim Paritätischen Wohlfahrtsverband Lüneburg
09/1992 – 07/1993	Highschoolabschluss mit Auszeichnung in Los Angeles, Kalifornien, USA
08/1981 – 07/1995	Grundschule, Orientierungsstufe und Gymnasium mit Abschluss Abitur, Winsen/ Luhe und Lüneburg